Methods of Elastic-plastic Analysis of Structures

by

Tsuneyoshi Nakamura

December 1970

Methods of Elastic-plastic Analysis of Structures

BY

Tsuneyoshi Nakamura, Ph.D.
中村恒善

December 1970

TO MY PARENTS

Masatsugu and Sachiko Nakamura

ACKNOWLEDGEMENTS

The author would like to express his deep gratitude to
Professor Emeritus Dr.-Ing. Ryo Tanabashi of Kyoto University,
Professor Dr.-Ing. Yoshitsura Yokoo of Kyoto University,
Professor Dr.-Ing. Osamu Matsuoka of Nagoya University,
Professor Emeritus Dr.-Ing. W. Flügge of Stanford University and
Professor J. B. Rosen, Ph.D. of the University of Wisconsin
for suggesting the interesting topics of research and for their encouragements, advices and stimulative discussions throughout or during a part of the course of this work.

The topic of "limit analysis of structures" was suggested by Professor Yokoo in 1956 for the author's thesis for Master of Engineering. The author's attention was gradually focussed to shell analysis under the guidance of Professors Yokoo and Matsuoka. In 1958, the author was granted a University Honors Fellowship from Stanford University to start a graduate work at Stanford. Professor Flügge of Engineering Mechanics suggested there the topic,"plastic analysis of shells of revolution" for the author's dissertation. The idea developed in the dissertation has led to the results of Chapters 11 and 12 in the present work. In the summer of 1960, the author was given a chance to work under Dr. J. B. Rosen for an application of Rosen's gradient projection method of nonlinear programming to elastic-plastic analysis of trusses. When the author returned Kyoto University in 1961, Professor Tanabashi suggested him to participate in the research on elastic-plastic analysis and design of framed structures. In 1965, Professors Tanabashi and Yokoo suggested the author to promote the experimental research on energy absorption capacity and plastic fatigue of steel members. During the last few years, the author's attention has been drawn to finite-deflection analysis of elastic-plastic plates and shells under the general guidance of Professor Yokoo. The present work would not have been possible without the encouragements and advices given to the author by the five professors above.

The author would like to thank Professor M. Wakabayashi of Kyoto University for his valuable suggestions in the design of the experimental apparatus in Chapter 7. The experimental data of Chapter 7 were obtained under the cooperation of Dr. H. Kunieda, Mr.H. Matsunaga, Mr.T. Kubota and Mr.K. Isoda and

those of Chapter 8, under the cooperation of Mr.T. Kubota and Mr.A. Yamamoto. Their cooperations are gratefully acknowledged, without which the author's proposals of experimental equations in Chapter 8 and of the theory in Chapter 9 would not have been possible. The author would also like to express his sincere appreciation to Dr.T. Nonaka, associate professor of Disaster Prevention Research Institute and to Mr. H. Nagaoka, both of Kyoto University for their rigorous criticisms on the content of Chapter 4. The author is indebted to Mr.T. Matsui (Appendix to Ch.11), Mr.T. Mori (Appendix to Ch.14) and Mr.A. Kano (Ch.13) for a number of numerical results which have been obtained by applying the author's theories or by conducting numerical experiments based upon the author's suggestions. The author is also indebted to Mr.S. Ishida, assistant professor of Ritsumeikan University for a number of fruitful discussions and for his cooperation with Mr.O. Ohta in the calculation of the numerical example of Chapter 3.

Thanks are due to Mr.N. Yoshida who drew numerous figures with extreme carefulness and typed several chapters and to Miss S. Yano who typed most of the manuscript patiently.

To all of them the author is truly grateful.

CONTENTS

CHAPTER 1

INTRODUCTION

1. SIGNIFICANCE OF PLASTIC STRENGTH ANALYSIS IN PLASTIC DESIGN

The principal design criterion of the conventional "allowable stress" design method or elastic design method is the allowable stresses. The elastic designer has to select first a reasonable set of member cross-sections for a structure with the help of his design experiences, calculate stresses caused by several sets of working loads or design loads by means of elastic stress analysis and then check if the predicted stresses are all within the respective allowable stresses. The elastic designer is often inclined to believe that the predicted stresses are precisely the "absolute actual stresses" occurring in an "actual state" defined by a set of design loads. This is in many cases not true. The elastic designer is able to predict only the structural behavior under the design loads which could be superposed on a state of initial stresses if the structure were to remain entirely elastic. In any complex frame of practical interest, initial stresses such as residual stresses due to rolling and cambering, stresses induced at erection and due to imperfect fabrication and those due to foundation settlements, etc. are so great that they cannot be neglected if an "actual state of stress" is to be found. The structural behavior under subsequent external disturbances such as design loads will not in general be purely elastic and involve irreversible deformations due to local plastic deformation, slips in connections and differential settlements. It appears therefore almost endless and in many cases almost meaningless to make an effort to find "absolute actual stresses"

The requirement that the stresses calculated by means of the elastic stress analysis for the design loads must be within the respective allowable stresses does not necessarily imply that the actual absolute stresses shall be within the respective allowable stresses. Such a calculation is meaningful in the sense that it gives an estimation on the order of magnitude of stresses which would occur under the working loads if the structure were to remain purely elastic, and that it serves also for the purpose of estimating deflec-

* This has been stated in many books:Ref.[7-23]. particularly in Ref.[12]

tions and overall structural stiffnesses. Any rational design method should include these two elements but they are not sufficient for a designer to be confident of the overall safety of his structure.

The principal design criterion of the plastic design method in its simple and narrow sense is the "plastic strength based upon ductility". Not only the material but also the moment-curvature relation or the generalized stress-generalized strain relations in general need to be ductile and stable in the sense that the relation curves do not involve portions of negative slope within the usable range of a deformation measure. The well-known simple plastic theory of frames is based upon the stable rotation capacities of plastic hinges. The ductility and stability of a generalized stress-generalized strain relation may not necessarily imply that the overall behavior of a ductile structure is always stable as will be discussed in Chapter 3.

In contrast to the elastic designer making a reasonable guess in selecting member sections, the plastic designer needs to construct only one possible state of equilibrium in order to design a frame without assuming member sections.[37] From the plastic designer's point of view, the elastic moment distribution in a frame is merely another state of possible equilibrium stress distribution. A direct design of a steel frame is possible in the sense that a set of member section properties can be directly found as a solution of the problem of minimizing the structural weight written in terms of plastic moments. This problem will be discussed in Chapters 2 and 4. By constructing a reasonable state of equilibrium stress distribution for a structure under a set of loads defined by multiplying the working loads by an adequate load factor, the plastic designer can be confident how safe his structure will be under the working loads.

The value of the load factor represents the margin of the overall strength safety of the structure against the working loads. The overall strength safety of a ductile structure directly depends upon the accuracy of plastic strength analysis. In the simple plastic theory, a number of factors affecting plastic strengths are neglected. They may or may not act in favor of load-carrying behaviors. Unless their effects are estimated or at least bounded by some means, the plastic designer cannot be fully confident of the true strength safety of his structure.

2. SIGNIFICANCE OF PLASTIC STRENGTH IN STRUCTURAL TOUGHNESS

While ductility is a measure of the strain to fracture in materials engineering terminology [1] and is the term used for describing the property of a material to undergo large plastic deformation, toughness is a measure of the plastic work for fracture and is the term used for describing the capacity of a material to absorb large amount of energy Similarly, structural ductility or overall ductility is defined as the term representing the capacity of a structure to undergo large deflection involving large plastic deformation. The overall plastic strength of a structure and its overall ductility are both based upon the ductility of the material and the ductility in the generalized stress-generalized strain relations. If the overall plastic strength of a structure can be described by a single load factor and if an appropriate deformation measure is chosen so that the area under the relation curve will represent directly the work, then the total work may be analogously called the *structural toughness* or *overall toughness* representing the capacity of the structure to absorb large amount of energy in its plastic regions before the structure collapses or reaches its ultimate state. The overall toughness of a structure is therefore governed not only by the overall ductility but also by the plastic strength.

Fig.1 shows one of the numerical results presented by R. Tanabashi, S. Ishida and the present author for perfectly-plastic multi-story frames of a weak-beam strong-column type [2], [3]. The overall structural rotation θ_{ST} introduced by Ishida [3] is the deformation measure chosen so that the area under the load factor-θ_{ST} curve will represent the energy absorbed by the frame. The precise definition of θ_{ST} will be given in Chapter 3. In the coordinate system of Fig.1, the ordinate of a point on the curve represents directly the rate of work done by the horizontal loads per unit value of θ_{ST}. The overall plastic strength is therefore nothing but the rate of energy absorption.

The *strength safety* discussed in the preceding section will be appropriate only for the working loads which can be replaced by static loads. For varying dynamic disturbances such as strong motion earthquake disturbances, the direct replacement of the resulting inertia forces by some equivalent static forces may not be justified well. The significance of the overall

toughness of a ductile structure in earthquake resistant design was first pointed out by R. Tanabashi in 1935 [4],[5]. The theory now termed as "The Velocity-Potential Energy Theory" may be summarized essentially as follows: The effective intensity of the ground motion due to an earthquake disturbance acting upon a structure is proportional to the square of the maximum velocity and the resistance of a ductile structure against the earthquake is governed by the potential energy that the structure can store before it collapses. What has been called the potential energy by R. Tanabashi is the structural toughness defined above. The latter part of the Tanabashi theory may be restated in other words as that of maintaining that the appropriate measure of safety of an earthquake resistant ductile structure is the *overall toughness safety*. In the *toughness design method* defined as that method whose principal design criterion is the overall toughness safety, a ductile structure is designed so as to possess a prescribed amount of total energy absorption capacity. If a certain limit is prescribed from practical point of view not necessarily from the rotation capacities of plastic hinges, on the amount of a representative deformation measure such as θ_{ST} until up to which it is desirable for the structure to absorb all the conceivable maximum amount of input energy, then a specific value of the load factor associated with the deformation measure and hence the overall plastic strength of the structure can be determined. The ratio of the overall toughness of the structure to its energy absorption capacity prescribed represents the factor of the toughness safety. In practise, however, not only the overall toughness but also the overall plastic strength of a structure are considered to be taken as the principal design criteria.

The problem of the toughness design is thus seen to be reduced to that of plastic strength analysis in its broader sense, or in other words to the analysis of variations of load-carrying capacities. In order to evaluate the energy absorption capacity of a ductile structure, it is necessary to find load-deflection relations in the plastic range. Load-deflection relations may be affected by changes of geometry which may become more significant as deformation proceeds.

The investigations of load-carrying capacities in finite deflection ranges may be said to be of an unrealistic nature in a sense. The plastic design loads for a structure determined usually by multiplying the working

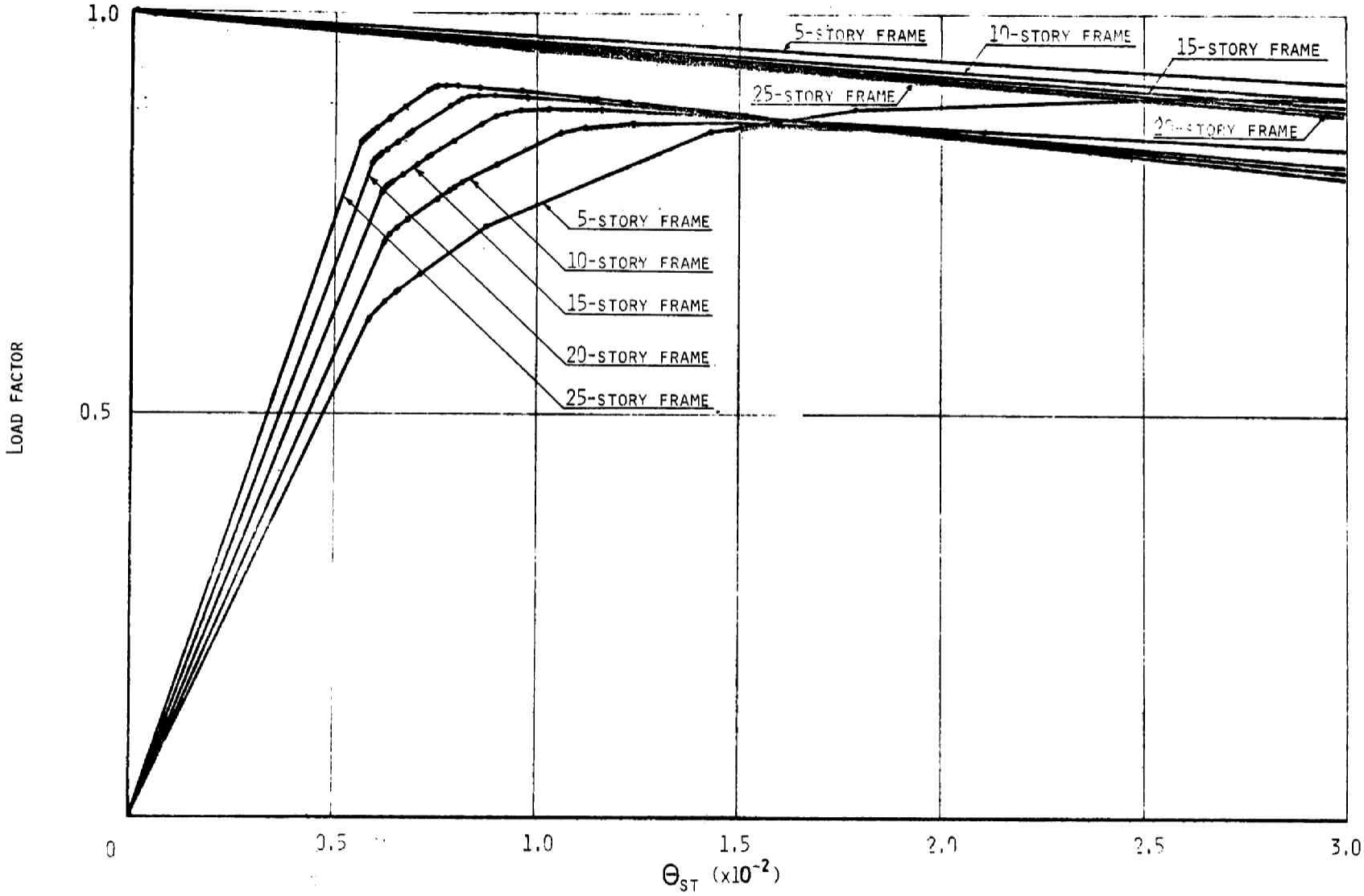

FIG. 1 LOAD-DEFLECTION CURVES AND MECHANISM CURVES FOR UNIFORM DISTRIBUTED LOADS

loads by an adequate load factor represent a conceivably worst possible combination of loads and are therefore of a hypothetical and unreal nature and not expected to occur in reality. Yet the strength safety factor of the structure under the working loads can be confirmed explicitly only after a purely hypothetical strength analysis has been made. The concepts of the strength design and of the toughness design may therefore be said to be close to the concept of the "hazard analysis". The importance of a hazard analysis in any engineering design has been emphasized by Y. Yokoo recently [6]. In summary, the safety of a structure under a working condition can be confirmed quantitatively only by investigating conceivably possible extraordinary hazardous states. The present work is devoted to methods of analysis of load-carrying capacities in the sense of the limit analysis theorems and methods of analysis of load-deflection behaviors in the plastic range and in the strain-hardening range.

3. PROBLEMS OF PLASTIC STRENGTH ANALYSIS

Useful methods and solutions of limit analysis of elementary structures have been summarized in books : Baker, Horne and Heyman [7], Neal [8], Heyman [9], Massonnet and Save [10], Tanaka [11], Baker and Heyman [12], for beams and frames; Prager [13], Hodge [14], and Tanaka [15] for more general problems including plates and/or shells; Wood [16], Sawczuk and Jaeger [17] for plates; Olszak [18], Hodge [19] and Mikeladze [20] for shells. More practical problems of elastic-plastic analysis of frame elements have been treated in detail in books by Beedle [21], Tall *et al* [22] and Galambos [23]. Several extensive surveys are also available [24, 25, 26].

With the use of electronic digital computers, the finite element and finite difference methods and mathematical programming methods are now powerful computational methods applicable not only to materially or geometrically nonlinear problems but also combined materially and geometrically nonlinear problems [27]. In spite of a great deal of previous papers concerned with methods and solutions of plastic strength analysis, several important factors affecting plastic strength analysis still need to be investigated further. Although references closely related to the problem of each chapter in the following will be cited and reviewed in the respective introductory section, a brief review on the factors affecting plastic strength analyses considered

here and related problems will be helpful for understanding the motivations and scopes of the following chapters.

The load-carrying capacity of an elastic-perfectly plastic structure subjected to proportional loading has been defined as the load intensity at which plastic deformation could occur under constant loads if all the changes in geometry of the structure were neglected. Within the limitation of the linear strain theory (infinitesimal deformation theory), the well-known theorems of limit analysis [28, 29] can be applied to the structure. So far as the load-carrying capacity and the associated stress field of a structure at plastic collapse, are of interest, Hill's theory [30, 31] on rigid-perfectly plastic structures may as well be applied. Analytical solutions have, however, been obtained only for some simpler problems and axi-symmetric problems. For practical complex structures such as shell roofs, approximate analytical solutions can only be obtained unless numerical methods are utilized. Not only numerical solutions but also approximate analytical solutions are useful for understanding the natures of problems and for ready estimates of collapse loads.

The load-carrying capacity of an elastic-perfectly plastic frame depends certainly upon the cross-sectional properties of its members. In practice, the direct plastic design of a complex frame is of great interest as well as its analysis. If the load-carrying capacity is the sole design criterion and if minimization of the structural weight is the sole design objective function, then the Foulkes theory [32] of linear minimum weight design can be applied within the limitation of infinitesimal deformation as a crude first approximation. While the linear programming techniques are directly applicable to the problem, analytical solutions for regular rectangular frames if obtained explicitly are useful for direct designs and for understanding the nature of linear minimum weight designs. More general and realistic methods of optimum design have received considerable attention during the last decade [33]. Methods of synthesizing building frames still need to be developed further in more practical formulations.

For a ductile structure subjected to varying repeated loads due, for instance, to earthquake disturbances, the structural toughness and elastic-plastic behavior under load or strain cycling need to be investigated. If the cyclic stress-strain relation is assumed, as a first approximation, to

be of a perfectly-plastic type, the stress variations in framed structures including limit analysis and shakedown problems can be traced and investigated by applying Greenberg's theorem [34] with Prager's interpretation in a stress space. Actual hysteretic stress-strain curves of structural steels subjected to strain cycling are not of a perfectly-plastic type and in general not similar to the respective virgin stress-strain curves. The idealization to the perfect-plasticity for strain cycling problems will therefore be a rather crude first approximation. A better prediction of the structural toughness of such a structure can only be made if a realistic hysteretic stress-strain relation fitting experimental results better is derived and applied. The corresponding moment-curvature relation will in general be rather complicated and not convenient for application to the analysis of structural toughness of a frame unless some simplification is considered by idealizing cross-sectional properties of the members.

The equations of equilibrium for a slender structure and its load-carrying capacity may be greatly influenced by the changes of geometry which occurs before the theoretical load-carrying capacity is attained. It is now well-known that, the so-called PΔ-effect in a structural frame decreases the load-carrying capacity predicted by an infinitesimal deformation theory, whereas the membrane action developed in a laterally loaded plate as the deflection is increased, acts in favor of the load-carrying behavior so far as in-plane displacements are restrained along the boundary. It does not appear, however, that the load-carrying behaviors of structural frames, plates and shells in the ranges of large deflection accompanying plastic deformation have been clarified well

If the effect of changes of geometry of a perfectly-plastic structure "suppresses" a load factor-deflection curve of the structure, elastic-plastic instability phenomenon will become of great importance[35]. The load-carrying capacity of such a structure may be defined by the maximum peak value of the load factor. If, on the other hand, the effect of geometrical non-linearity acts in favor of the load-carrying behavior of a structure, no maximum peak value of the load factor appears and the load-carrying capacity may be said to increase as deflections are increased The load-carrying capacity of a structure in the finite deflection range must therefore be described with respect to a state of deformation. The plastic strength analysis of structures

then necessarily means the analysis of load-deflection behaviors, The present work will include not only methods of analysis of load-deflection behaviors in the plastic range within the infinitesimal deformation theory, but also methods of analysis of some combined materially and geometrically nonlinear problems and methods of designing framed structures based upon the plastic strengths.

4. SCOPE OF THE PRESENT WORK

Table 1 shows a classification of the contents of the present work in accordance with material properties, loading conditions, types of structures, and magnitudes of deflection. Not only methods of limit analysis and design of perfectly-plastic complex structures subjected to monotonic loadings, but also methods of rigid-plastic and elastic-plastic analysis of simpler structures and structural elements involving various factors affecting plastic strengths will be presented. Most of the chapters are respectively based upon the author's papers which have been published previously. The remaining chapters also contain some new results which have not been published as yet.

Table 1 CLASSIFICATION OF THE CONTENT

(Numbers indicate Chapter numbers)

STRUCTURE / MATERIAL	DEFLECTION / LOADING	BEAMS, COLUMNS & FRAMES		PLATES & SHELLS	
		SMALL	LARGE	SMALL	LARGE
PERFECTLY PLASTIC	MONOTONIC LOADING	2, 4	3	10, 11	12
	VARIABLE REPEATED LOADING	5	—	—	
STRAIN-HARDENING	MONOTONIC LOADING	—	6		13, 14
	VARIABLE REPEATED LOADING	7, 8, 9		—	

The methods of strength analysis in the present work are based upon two common underlying principles of approximation: (1) the sandwich idealization of cross-sections not only of beams and columns but also of plates and shells and (2) the piecewise approximations to yield conditions.

The idealization of an actual moment-curvature relation in the absence of axial force for a bar member to an elastic-perfectly plastic relation corresponds in essence to the idealization of an actual H-section to an equivalent sandwich section. It will be shown in Chapter 9 that the sandwich idealization is useful also in predicting cyclic load-deflection behaviors of H-beams subjected to alternating plastic bending. Trussed or latticed plate or shell roof structures may also be idealized, to a first approximation, to anisotropic sandwich plates and shells subjected to the Kirchhoff-Love assumption [36].

The yield hypersurface for isotropic sandwich plates and shells obeying the von Mises yield criterion consists of two constituent quadratic hypersurfaces. The yield hypersurface for uniform isotropic shells obeying the Tresca yield criterion can be approximated very well by three pairs of quadratic hypersurfaces as will be shown in Chapter 10. The advantage of the piecewise approximations to the yield conditions lies in the fact that velocity equations can be uncoupled from the equations of equilibrium and that explicit general solutions can be obtained for the materially nonlinear problems. It will be shown that this advantage remains available also for geometrically nonlinear problems of rigid-plastic shells.

Part I is concerned with methods of strength design and analysis of framed structures. The problem of the linear minimum weight design is closely related to the problem of the simple plastic analysis in the sense that the latter can be regarded as a problem of restricted design in which a limit load factor and a set of fixed ratios between the members of a frame are both given. Several classes of general solutions are obtained for regular rectangular multi-story frames in Chapter 2 and for simply-supported and clamped Vierendeel frames in Chapter 4. An elaborated method in which both of the interaction yield condition and the effect of changes in geometry are taken into account will be proposed in Chapter 3.

While the assumption of the perfect plasticity simplifies load-deflection analyses and enables one to treat analytically regular frames consisting of a

large number of bar members, it is not a good approximation for problems of structures subjected to variable repeated loading in the strain-hardening range. Methods of load-deflection analysis for linear and nonlinear strain-hardening beams and for linear strain-hardening columns will be developed in Chapters 6-9 of Part II.

Part III consisting of Chapters 10-12 will be concerned with plastic analysis of axi-symmetric and non-symmetric shells. Practically useful approximate yield conditions are proposed in Chapter 10 for Axi-symmetric problems and in Chapter 11 for non-symmetric sandwich shells. It is shown in Chapter 12 that the velocity equations for finite deflection analysis are also uncoupled from the equations of equilibrium and hence that general solutions can be obtained in simple closed forms.

Two fundamental problems of numerical analysis of materially and/or geometrically nonlinear problems will be discussed in Chapters 13 and 14. It is shown in Chapter 13 that the discretization errors can be considerably reduced by using a higher-order finite difference boundary equations. The elastic-plastic stiffness matrix for a sandwich shell element is derived in Chapter 14 and its application to combined nonlinear problems will be briefly described.

REFERENCES

[1] See for instance, A. S. Tetelman and A. J. McEvily,Jr., *FRACTURE OF STRUCTURAL MATERIALS*, John Wiley & Sons, 1967, pp78-82.

[2] Ryo Tanabashi, Kiyoshi Kaneta, Tsuneyoshi Nakamura and Shuzo Ishida, "To the Final State of Rectangular Frames," 4th World Conference on Earthquake Engng., Santiago, Chile, Jan.13-18, 1969, Proc.(1970)

[3] Ryo Tanabashi, Tsuneyoshi Nakamura and Shuzo Ishida, "Overall Force-displacement Characteristics of Multi-story Frames," Proc. Symposium on Ultimate Strengths of Structures and Structural Elements,Dec.5,1969, Tokyo, pp

[4] Ryo Tanabashi, "Some Considerations on Destructive Elements of Earthquake Ground Motion and Earthquake Resistance of Structures," J. Architectural Inst. Japan, Vol.49, No.599, May 1935.

[5] Ryo Tanabashi, "On the Resistance of Structures to Earthquake Shocks," Memoirs of College of Engng., Kyoto Imperial Univ., Vol.9, No.4,1937

[6] Yoshitsura Yokoo, "A Proposal for Testing Methods of Structural Elements," An invited Lecture at the Structural Division Seminar at 1970 Annual Meeting of Architectural Inst. Japan, Tokyo, Oct. 1970.

[7] J. F. Baker, M. R. Horne and J. Heyman, *THE STEEL SKELETON, VOL.2*, Cambridge, 1956

[8] B. G. Neal, *THE PLASTIC METHODS OF STRUCTURAL ANALYSIS*, Chapman & Hall, 1956

[9] J. Heyman, *BEAMS AND FRAMED STRUCTURES*, Pergamon Press, 1964

[10] C. E. Massonnet and M. A. Save, *PLASTIC ANALYSIS AND DESIGN, VOL.1, BEAMS AND FRAMES*, Blaisdell Publishing Co., 1965

[11] H. Tanaka, 骨組の塑性力学, 建築構造講座 第5巻, コロナ社, 1963.

[12] J. Baker and J. Heyman, *PLASTIC DESIGN OF FRAMES*, Cambridge Univ Press, 1969

[13] W. Prager, *AN INTRODUCTION TO PLASTICITY*, Addison-Wesley. 1959

[14] P. G. Hodge, Jr., *PLASTIC ANALYSIS OF STRUCTURES*, McGraw-Hill, 1959.

[15] H. Tanaka, 構造物の極限解析, 建築構造学大系 9, 彰国社, 1966.

[16] R.H. Wood, *PLASTIC AND ELASTIC DESIGN OF SLABS AND PLASTES*, Thames-Hudson, 1961.

[17] A. Sawczuk und T Jaeger, *GRENZTRAGFAHIGKEITS-THEORIE DER PLATTEN*, Springer-Verlag, 1963

[18] W. Olszak and A. Sawczuk, *INELASTIC BEHAVIOR IN SHELLS*, P.Noordhoff,1967

[19] P. G. Hodge, Jr., *LIMIT ANALYSIS OF ROTATIONALLY SYMMETRIC PLATES AND SHELLS*, Prentice-Hall, 1963.

[20] M. Sh. Mikeladze, *AN INTRODUCTION TO THE TECHNICAL THEORY OF PERFECTLY PLASTIC THIN SHELLS*,(in Russian)ИЗДАТЕЛЬСТВО. «МЕЦНИЕРЕБА», ТБИЛИСИ,1969

[21] L. S. Beedle, *PLASTIC DESIGN OF STEEL FRAMES*, John-Wiley & Sons, 1958.

[22] L. Tall *et al STRUCTURAL STEEL DESIGN*, The Ronald Press, 1964.

[23] T. V. Galambos, *STRUCTURAL MEMBERS AND FRAMES*, Prentice-Hall, 1968.

[24] W. Olszak and A. Sawczuk (editors), *NON-CLASSICAL SHELL PROBLEMS*, Proc. IASS Symposium, Warszawa, 1964

[25] M. Zyczkowski, "Combined Loadings in the Theory of Plasticity," Int. J. Nonlinear Mechanics, Vol.2, pp173-205.

[26] S. S. Gill (Editor), *THE STRESS ANALYSIS OF PRESSURE VESSELS & PRESSURE VESSEL COMPONENTS*, Pergamon Press, 1970.

[27] See for instance, P. V. Marcal, "Finite Element Analysis of Combined Problems of Nonlinear Material and Geometric Behavior," *COMPUTATIONAL METHODS FOR APPLIED MECHANICS*, Proc. ASME Conference, 1969.
[28] D. C. Drucker, H. J. Greenberg and W. Prager,"The Safety Factor of an Elastic-plastic Body in Plane Strain," J. Appl. Mech..Vol.18, pp371-378, 1951.
[29] D. C. Drucker, W. Prager and H. J. Greenberg, "Extended Limit Design Theorems for Continuous Media," Quart. Appl. Math., Vol.9, pp381-389, 1952.
[30] R. Hill, "On the State of Stress in a Plastic-rigid Body at the Yield Point," Phil.Mag, Ser.7, Vol.42, pp868-875, 1951.
[31] R. Hill, "A Note on Estimating the Yield Point Loads in a Plastic-rigid Body," Phil. Mag.,Ser.7, Vol.43, pp353-355, 1952.
[32] J. Foulkes, "The Minimum-weight Design of Structural Frames," Proc. Royal Soc., London (A), Vol.223, pp482-494, 1954.
[33] See for instance, C. Y. Sheu and W. Prager, "Recent Developments in Optimal Structural Design," Appl.Mech. Rev., Vol.21, pp985-922.
[34] H. J. Greenberg, "Complementary Minimum Principles for an Elastic-plastic Material," Quart. Appl.Math. Vol.7, pp85-95, 1949.
[35] See for instance, M. R. Horne, "The Stability of Elastic-plastic Structures," *PROGRESS IN SOLID MECHANICS, VOL.2*, Chapter VIII, pp277-322, 1961.
[36] Koichiro Heki, "The Theory of Stress Analysis of Anisotropic Layered Plates, and its Applications to Some Space Structures," Trans.Archit. Inst. Japan, No.137, pp17-23, July 1967.
[37] See for instance, Ryo Tanabashi and Tsuneyoshi Nakamura, "On the Ultimate States of Rigid Frames Subjected to Earthquakes," Proc. 1962 Natn. Symp. Earthquake Engineering, pp51-56.

CHAPTER 2

THE MINIMUM WEIGHT DESIGN OF A CLASS OF TALL MULTI-STORY FRAMES SUBJECTED TO LARGE LATERAL FORCES *

1. Introduction

The minimum weight design of a broad class of tall multi-story frames subjected to a class of lateral loads which are large compared to the vertical loads on the beams is obtained in this chapter. A frame considered here consists of horizontal beams and vertical columns with uniform cross-sections between joints. Each joint is rigid enough to transmit the fully plastic moment of any member framing into it. The problem of minimum weight design may be stated as follows: Given the center line dimensions of a frame and a set of static loads acting on it as shown in Fig.1, what fully plastic moments should be assigned to the members in order that the loads may be just sustained and the material consumption is a minimum ?

This problem has been investigated in a more general form by Heyman [1], Foulkes [2], [3], Livesley [4], Heyman and Prager [5], Stone [6], Kalker [7], Tanaka [8], and Prager [9]. The principal difficulty appears to consist in the discrepancy between the structural complexity and the size of the corresponding linear programming problems stemming from the very large number of inactive constraints. Even with Heyman's and Prager's method [5], Kalker's program [7] for an IBM 704 Computer can solve, in effect, a 6-story 8-bay frame. It has not been shown how powerful and convenient Tanaka's method is for multi-story frames, compared to the former. Although these computational methods based upon the linear programming technique are quite general and automatic, they furnish a solution, problem by problem, numerically. The general qualitative features of the minimum weight designs can then hardly be studied for practical multi-story frames. Furthermore, in view of the approximate nature of the linear minimum weight design theory and the flatness of the permissible region, the exact solution of a problem may not have to be obtained for practical purposes with so much computational labor. Calladine [10] has studied the minimum weight design

---

*This chapter is based upon the author's papers, "Minimum Weight Design of a Class of Tall Multi-story Frames Subjected to Large Lateral Forces,I,II" Trans. A.I.J., No.118(Dec.1965) and No.119(Jan.1966). The papers were presented at the 15th National Congress for Applied Mechanics in 1965.

of an isolated story of a frame with equal spans. This special case appears to have revealed some interesting features of the minimum weight designs to a certain degree.

The purpose of this chapter is to establish in an extremely simple and explicit form the minimum weight design of a broad class of tall multi-story frames subjected to sufficiently large shear resultants compared to vertical loads. In view of the fact that the magnitude of vertical loads on beams hardly change from the topmost story through the first story, whereas lateral loads being accumulated downward, the proposed design may readily be modified for the case of comparatively large vertical loads in the upper stories, resulting in a good upper bound on the minimum weight. This will be illustrated by a numerical example.

The present minimum weight design should not, however, be adopted as a practically desirable design without the following modification for the effect of axial forces in twofold. First, the effect of axial forces in columns must be taken into account in the corresponding yield conditions. A practical way of augmenting the column sections will be illustrated in chapter 3. Secondly, the design must be modified for the additional moments induced by the presence of large axial forces in columns and large elastic-plastic deformation at the ultimate state of the frame. In view of the so-called Rankine formula [11], the present rigid-plastic collapse load design plays an important role as a fundamental design in establishing the real ultimate strength design [15].

Besides the customary assumptions made in the plastic analysis of structures, the following additional assumptions are made in this paper. (1) A designer has at his disposal the continuous spectrum of structural cross-sections available commercially. (2) The weight of a frame is estimated by a linearized weight function [9].

2. Frame moments and equilibrium equations

Since a frame acted upon by a set of sufficiently large lateral forces is considered here, it may be assumed that the equal extreme values of the bending moment in a member occur at its ends and any other section of the member may attain this extreme value. For the sake of simplicity, we replace here all the vertical loads on a beam by a single concentrated load acting upon its midspan [12]. The potentially critical sections of the beam are then its two ends and midspan. It should be observed that the collapse mechanisms in Foulkes'exhaustive study [4] on a portal frame must be a prototype of a more general mechanism for

a multi-story frame. The minimum weight design of internal bays of an isolated story studied by Calladine [10] must also be a special prototype which serves to suggest us a more general approach. It seems quite natural then to ask if the extreme state can exist where plastic hinges have formed at all the end sections of the members of a frame at collapse as shown in Fig.2. Some more hinges may form at some of the midspans of beams. This is the starting point of the present study. This approach is supported by the fact that, since a minimum weight design is in general represented by a vertex of a convex permissible region, it is a reasonable short cut toward the minimum weight design of the present class of frames, to minimize the weight with respect to a limited number of appropriate vertices and then to check if the corresponding mechanism satisfies the Foulkes' mechanism condition [3].

Let us consider an f-story s-bay frame. The symbols are defined in Fig.1. At such an extremely deteriorated state as mentioned above, all the end sections attain their fully plastic moments and hence the number of unknown end moments is equal to that of members if appropriate plus and minus signs are used. It is assumed here that the direction of the shear resultant in a story is always the same as that in the topmost story. Since under the above assumption the concentrated load on a beam merely determines the bending moment at its midspan, we shall first concentrate our attention to the lateral forces only. In view of the moment diagram in the elastic range, an appropriate choice of plus or minus signs may readily be made as shown in Fig.3 and we may assume the corresponding plastic hinge rotations as shown in Fig.2. The $f(s+2)$ equations of equilibrium however, do not in general suffice to determine $f(2s+1)$ plastic moments uniquely except when $s=1$. The degree of redundancy is therefore $f(s-1)$. Instead of dealing with $f(2s+1)$ plastic moments, it seems convenient to define a " frame moment ". In view of the linearity of the equations of equilibrium in terms of the plastic moments without any slope-continuity requirements, we may split or decompose the moment diagram at collapse into fs constituent elementary diagrams for the fs rectangles as shown in Fig.4., and regard the original moment diagram as the composite consisting of these elementary diagrams. It is noted that if the lower ends of the first story columns are all fixed, imaginary ground floor-beams may be supposed to exist for the frame moments of the first story rectangles. Each elementary moment distribution is such that moment equilibrium is maintained at the four corners with the same absolute value in the manner shown in Fig.4. Such an elementary moment diagram is therefore completely defined by

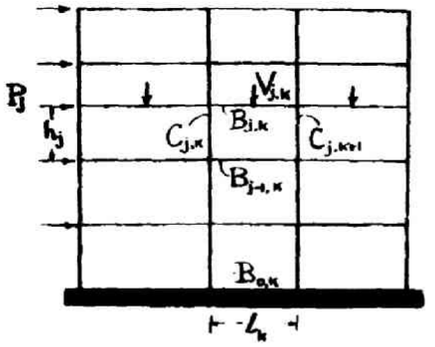

FIG. 1

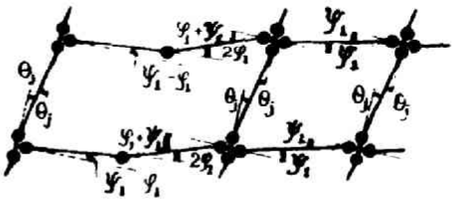

FIG. 2

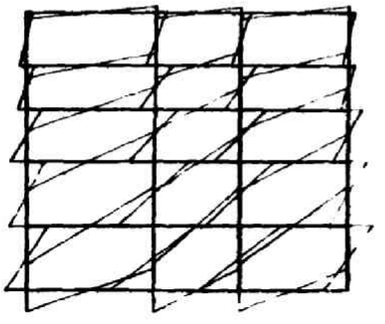

FIG. 3

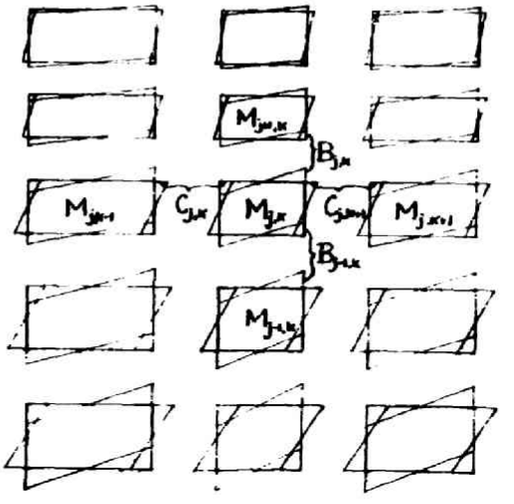

FIG 4

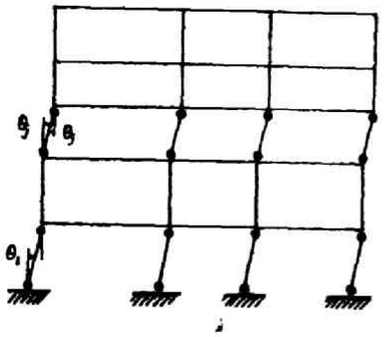

Fig.5a

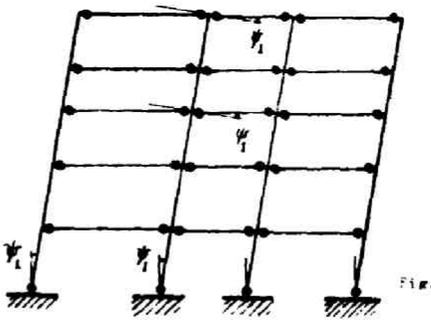

Fig.5b

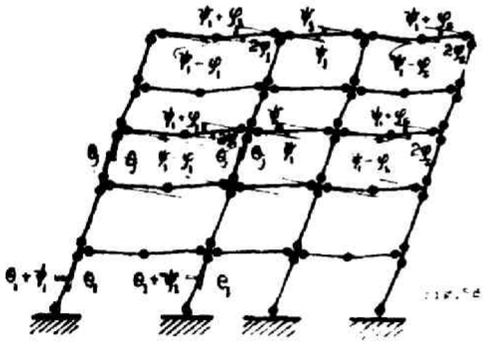

Fig.5c

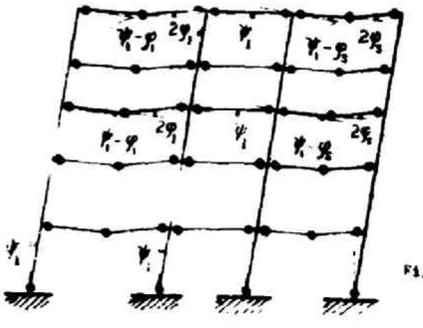

Fig.5c

this equal corner moment, which will be called a " frame moment"". The positive frame moment is defined as the one corresponding to the shear which has the same direction as that of the shear resultant in the story. The frame moments illustrated in Fig.4 are positive when the shear resultant in a story is directed from left to right. Let $M_{j,k}$ denote the frame moment of the k-th rectangle from the left in the j-th story The k-th beam and column from the left in the j-th story will be called (j,k)-beam and (j,k)-column, respectively. Let $B_{j,k}$ and $C_{j,k}$ denote the plastic moments of the (j,k)-beam and (j,k)-column, respectively. It is noted that the subscript k in $C_{j,k}$ should run from 1 through $s+1$ since there are $s+1$ columns in a story. The plastic moments of any beams and columns may be expressed in terms of these frame moments as follows.

$$\left.\begin{aligned} &B_{j,k} = M_{j,k} + M_{j+1,k} \qquad B_{f,k} = M_{f,k} \\ &C_{j,1} = M_{j,1}, \qquad C_{j,k} = M_{j,k-1} + M_{j,k}, \qquad C_{j,s+1} = M_{j,s} \\ &(j=1,2,\cdots\cdots,f;\ k=1,2,\cdots\cdots,s) \end{aligned}\right\} \quad (1)$$

If there are ground floor beams, $B_{0,k} = M_{1,k}$. The equations of equilibrium for the *assumed* moment diagram are given by

$$\left.\begin{aligned} &B_{f,1} = C_{f,1}, \qquad B_{f,k-1} + B_{f,k} = C_{f,k}, \qquad B_{f,s} = C_{f,s+1} \\ &B_{j,1} = C_{j,1} + C_{j+1,1}, \qquad B_{j,k-1} + B_{j,k} = C_{j,k} + C_{j+1,k}, \\ &B_{j,s} = C_{j,s+1} + C_{j+1,s+1} \\ &(j=1,2,3,\ldots\ldots,f-1;\ k=1,2,\ldots\ldots,s) \end{aligned}\right\} \quad (2)$$

for the $f(s+1)$ joints and are satisfied identically by these frame moments. Therefore we may only have to write down just one equation of sway equilibrium for each story In other words, f conditions of sway equilibrium for the fs unknown frame moments leave $f(s-1)$ degrees of redundancy as a whole. This reduction of the number of unknowns from $f(2s+1)$ to fs is one of the advantages of introducing the frame moments. The f equations of sway equilibrium may be written as

$$4 \sum_{k=1}^{s} M_{j,k} = h_j \sum_{i=j}^{f} P_i \qquad (j=1,2,\ldots,f) \quad (3)$$

where P_i is the lateral load applied at the i-th story beam level.

Some inequality constraints must be imposed upon the frame moments. The principal assumption in defining the frame moments has been the one that plastic hinges have formed at all the end sections of the members, no other

sections having violated the yield conditions. This assumption remains satisfied even if comparatively small vertical loads are applied together with the lateral loads. If the simple-beam bending moment diagrams are superposed on the assumed diagram in Fig.2, the resulting moment at any section of a member should not exceed the plastic moment of the member. Conversely therefore, for a specific set of vertical loads, there must exist the limiting smallest value to which the plastic moment of a beam may be decreased in order to achieve the minimum weight. Let $V_{j,k}$ denote the concentrated load acting upon the midspan of the (j,k)-beam. Then the minimum values of the plastic moment of the (j,k)-beam may be obtained as follows

$$\left.\begin{aligned} B_{f,k} &= M_{f,k} \geq (1/4)V_{f,k}l_k \\ B_{j,k} &= M_{j,k} + M_{j+1,k} \geq (1/4)V_{j,k}l_k \qquad (j=1,2,\ldots,f-1) \end{aligned}\right\} \tag{4a}$$

As far as $B_{j,k}$ and $C_{j,k}$ are all non-negative, $M_{j,k}$ does not necessarily have to be non-negative. But it is assumed that the minimum weight design satisfies the condition

$$M_{j,k} \geq 0 \tag{4b}$$

Then the problem of minimization may readily be dealt with by means of the standard techniques of linear programming parametrically [16].

3. The minimum weight design

Any moment distribution represented by a set of $M_{j,k}$ satisfying (3) and (4) provides us with a *complete solution* since it satisfies all the equilibrium equations, does not violate any yield conditions and corresponds to an overcomplete collapse mechanism. Let D denote the set of all the designs satisfying (3) and (4). Let $\overline{D}$ denote the set of all the possible designs including D and those designs which do not correspond to the present particular overcomplete collapse mechanisms. The minimum weight design may be established in the following two steps of a semi-inverse method.

(I) Assuming that the minimum weight design $D_{\min}$ in D also gives the minimum weight among all the designs in $\overline{D}$, the weight is minimized subject to the constraints (3) and (4) by means of linear programming.

(II) It is then proved that the overcomplete collapse mechanism corresponding to $D_{\min}$ indeed satisfies Foulkes' mechanism condition for the class of frames of practical interest. This proof justifies the above assumption (I) since $D_{\min}$ then satisfies all the necessary and sufficient con-

dition for the minimum weight design [3].

The linearized weight function [3], [9] may be written as

$$G = g\left[\sum_{j=1}^{f} h_j \sum_{k=1}^{s+1} C_{j,k} + \sum_{k=1}^{s} l_k \sum_{j=1}^{f} B_{j,k}\right]$$

$$= g\left[\sum_{j=1}^{f} 2h_j \sum_{k=1}^{s} M_{j,k} + \sum_{k=1}^{s} l_k \{ M_{1,k} + 2\sum_{j=2}^{f} M_{j,k} \}\right] \tag{5}$$

where g is a proportionality constant. The problem is to minimize G given by (5) subject to the constraints (3) and (4). The first step of linear programming is to convert the inequalities (4a) into equivalent equalities by introducing fs slack variables $x_{j,k}$ as follows.

$$M_{f,k} - x_{f,k} = (1/4)V_{f,k}l_k$$

$$M_{j,k} + M_{j+1,k} \quad x_{j,k} = (1/4)V_{j,k}l_k, \; x_{j,k} \geq 0 \tag{6}$$

There are now $fs+f$ constraints in $2fs$ non-negative variables. In order to choose $fs+f$ basic variables appropriately, it is helpful to consider the geometrical significance of the constraints (3) and (4) in a frame moment space of fs-dimensions whose cartesian coodinates are $M_{j,k}$. The constraints (3) define a $f(s-1)$-dimensional intersection of f hyperplanes in the fs-space. Only that part of the intersection which satisfies all the constraints in (4) is the permissible convex region. A vertex of this permissible region may be defined by a set of $f(s-1)$ equalities in (4a), provided that (4b) are also satisfied. It is noted that for a specific value of k, the f frame moments $M_{j,k}$ may be uniquely determined by the f simultaneous equalities for $M_{j,k}$ in (4a). In other words, the fs equalities in (4a) may be subdivided into s sets of those f equalities. We may then choose any $(s-1)$ out of the s sets to define a vertex. The weight function (5) represents a family of hyperplanes in this fs-space for various values of G. The minimum weight design is represented by the point or points of tangency when the weight hyperplane is tangent to the permissible region. With the help of this geometrical consideration, $x_{j,k}$ $(k \neq m)$ may be chosen as the $f(s-1)$ non-basic variables where the subscript m is defined by

$$l_m = \underset{k=1}{\overset{s}{\text{Min.}}}\{l_k\}$$

The subscript m satisfying this condition may not in general be unique. Let N denote the set of all the subscripts corresponding to the minimum beam length. Then any subscript $r \in N$ may be chosen as the subscript m. The basic variables $M_{j,k}$ and $x_{j,m}$ may readily be expressed in terms of the $f(s-1)$ non-

sic variables as follows.

$$
\begin{aligned}
M_{f,k} &= (1/4)V_{f,k}l_k + x_{f,k} \\
M_{f-1,k} &= (1/4)(V_{f-1,k} - V_{f,k})l_k + x_{f-1,k} - x_{f,k} \\
&\cdots\cdots\cdots \\
M_{j,k} &= (1/4)l_k\{V_{j,k} - V_{j+1,k} + \ldots + (-1)^{f-j}V_{f,k}\} + x_{j,k} - x_{j+1,k} + \ldots \\
&\quad \ldots + (-1)^{f-j}x_{f,k} \qquad (7) \\
M_{j,m} &= (1/4)h_j \sum_{i=j}^{f} P_i - \sum_{k\neq m} (1/4)l_k\{V_{j,k} - V_{j+1,k} + \ldots + (-1)^{f-j}V_{f,k}\} \\
&\quad - \sum_{k\neq m} \{x_{j,k} - x_{j+1,k} + \ldots + (-1)^{f-j}x_{f,k}\} \\
x_{f,m} &= (1/4)h_f P_f - (1/4)\sum_{k=1}^{s} l_k V_{f,k} - \sum_{k\neq m}^{f} x_{f,k} \\
x_{j,m} &= (1/4)h_j \sum_{i=j}^{f} P_i + (1/4)h_{j+1} \sum_{i=j+1}^{f} P_i - (1/4) \sum_{k=1}^{s} l_k V_{j,k} - \sum_{k\neq m} x_{j,k}
\end{aligned}
$$

The corresponding basic solution may immediately be obtained if we set
$_{,k}$=0. The basic solution is feasible if the following conditions are all sat-
fied.

$$
\begin{aligned}
&V_{j,k} - V_{j+1,k} + \ldots + (-1)^{f-j}V_{f,k} \geq 0 \\
&h_j \sum_{i=j}^{f} P_i - \sum_{k\neq m} l_k\{V_{j,k} - V_{j+1,k} + \ldots + (-1)^{f-j}V_{f,k}\} \geq 0 \\
&h_f P_f - \sum_{k=1}^{s} l_k V_{f,k} \geq 0, \quad h_j \sum_{i=j}^{f} P_i + h_{j+1} \sum_{i=j+1}^{f} P_i - \sum_{k=1}^{s} l_k V_{j,k} \geq 0 \qquad (8)
\end{aligned}
$$

In many practical problems where $V_{j,k}$ does not increase radically down-
ard compared to the downward increase in the shear resultant, it may readily
e found that if these conditions are satisfied at the topmost story, they will
n general be satisfied at any other story For instance, if $V_{j,k}=V_k$ for all j,
8a) is always satisfied and the remaining three conditions may be satisfied if

$$
h_j \sum_{i=j}^{f} P_i \geq \sum_{k=1}^{s} l_k V_k
$$

nly those cases in which the conditions (8) are all satisfied, will be
onsidered in the following. If equations (7) are substituted into the
cpression (5), the following expression of G may be derived:

$$G = g\Big[\sum_{j=1}^{f}(1/2)h_j^2\sum_{i=j}^{f}P_i + l_m\{(1/4)h_1\sum_{i=1}^{f}P_i + (1/2)\sum_{j=2}^{f}h_j\sum_{i=j}^{f}P_i\} + \sum_{k\neq m}^{s}(l_k-l_m)\sum_{j=1}^{f}\{(1/4)V_{j,k}l_k + x_{j,k}\}\Big] \tag{9}$$

If m is the only subscript which indicates the minimum beam length, then $l_k-l_m > 0$ for all $k\neq m$. Then the basic solution obtained above by setting $x_{j,k}=0 (k\neq m)$ in (7) is the unique minimal solution. If on the other hand, N contains more than one element, then $l_k-l_m=0$ for $k\in N$ and $l_k-l_m>0$ for $k\notin N$. In this case the coefficients of $x_{j,k}$ $(k\in N)$ become zeros. Hence the minimal basic solution obtained by setting $x_{j,k}=0$ $(k\neq m)$ in (7) is not unique and $x_{j,m}$ may be exchanged with any other $x_{j,r}$, $r\in N$, giving the same minimum weight. Any linear combination of these minimal solutions will also provide a minimum weight design. In the case where N contains the sole element m, the corresponding plastic moments may readily be obtained from equations (1).

$$\begin{aligned}
&B_{j,k} = (1/4)l_kV_{j,k} \quad (k\neq m), \qquad B_{f,m} = (1/4)h_fP_f - \sum_{k\neq m}^{s}(1/4)l_kV_{f,k}\\
&B_{j,m} = (1/4)h_j\sum_{i=j}^{f}P_i + (1/4)h_{j+1}\sum_{i=j+1}^{f}P_i - \sum_{k\neq m}^{s}(1/4)l_kV_{j,k}\\
&C_{j,k} = (1/4)l_k\sum_{t=j}^{f}(-1)^{t-j}V_{t,k} + (1/4)l_{k+1}\sum_{t=j}^{f}(-1)^{t-j}V_{t,k+1}\\
&\qquad\qquad (k\neq 1,\ m-1,\ m,\ s+1)\\
&C_{j,n} = (1/4)h_j\sum_{i=j}^{f}P_i - (1/4)\sum_{\substack{k\neq n,\\ k\neq n+1}}^{s}l_k\sum_{t=j}^{f}(-1)^{t-j}V_{t,k} \quad (n=m-1,\ m;\ m\neq 1,\ s)\\
&C_{j,e} = (1/4)l_e\sum_{t=j}^{f}(-1)^{t-j}V_{t,e} \quad (e=1,\ s+1)
\end{aligned} \tag{10}$$

Similar expressions may be obtained for the case $m=1$ or $m=s$. It is worth noticing that the $f(s-1)$ beams with length l_k's $(k\neq m)$ are to be designed to carry vertical loads in their respective spans and that the corresponding bays contribute little to supporting the lateral shear. The bay with the minimum beam length l_m, on the other hand, must then be designed to carry the remaining part of the lateral shear in each story. It should also be pointed out that in certain cases the present solution results in columns of zero plastic moments. This theoretical solution is a necessary consequence under the present assumption but appears unpractical. Although the columns may be augmented by taking into account the effect of axial forces as will be shown in Chapter 3, a more practical design may

also be obtained by imposing further restrictions on the plastic moments. Such a special class of minimum weight designs will be discussed later.

Foulkes' mechanism condition must be satisfied in Step (II) Since the present problem involves $f(2s+1)$ independent variables $B_{j,k}$ and $C_{j,k}$, a minimal design can always be found which has $f(2s+1)$ alternative collapse mechanisms. It is noted, in view of the solution obtained above, that since at least $f(s-1)$ midspans attain their fully plastic moments, plastic hinges may form not only at their end sections but also their midspans. Hence there are $f(s-1)$ independent hinge rotations at the $f(s-1)$ midspans as shown in Fig.5c. There are $f(s+1)$ independent joint rotations and f different sway mechanisms. The total number is equal to $f(2s+1)$. Foulkes' mechanism condition may be stated as follows:

A mechanism must be found by an appropriate combination of these alternative mechanisms such that, for every beam and column, $\sum$ *Hinge rotations in (j,k)-beam (or (j,k)-column) = a constant times the length of (j,k)-beam (or (j,k)-column), respectively.* ..... [A].

It should be observed that all the (j,k)-columns with a fixed number j in the j-th story have the same length h_j. Hence the condition [A] may be satisfied between all the (j,k)-columns in the j-th story if the same hinge rotations θ_j appear through all the upper and lower end sections of the j-th story columns as shown in Fig.5a. Then fs ratios between $f(s+1)$ sums of hinge rotations in the columns satisfy the condition [A], leaving only f different sums for further study. In a similar manner, the condition [A] may be satisfied between all the (j,m)-beams $(m \in N)$ if the same hinge rotations ψ_1 due to joint rotations and sways appear through all the (j,m)-beams as shown in Fig.5b. Since $l_k > l_m$, it is apparent that some more hinge rotations will be required to occur in (j,k)-beam $(k \notin N)$ As has been pointed out, a plastic hinge may appear at the midspan of any (j,k)-beam $(k \notin N)$. Hence we may consider the collapse mechanism shown in Fig.5c where the same hinge rotations $2\phi_k$ occurethrough all the hinges at the midspans of (j,k)-beams with a fixed subscript k $(k \notin N)$ A similar mechanism may be considered for every different $k \notin N$. Then the $(f-1)s$ ratios between fs sums of hinge rotations in beams satisfy the condition [A], leaving s different sums for further study. It is now shown that the condition [A] may be satisfied by a mechanism formed by an appropriate linear combination of these $f+s$ different mechanisms. Fig.5d shows the resulting overcomplete mechanism. The sums of hinge rotations for the members may be tabulated as shown in Table 1.

The condition [A] may be satisfied if the angles of rotations are deter-

Table 1

Member	Plastic moment	Length	Subscripts j	Subscripts k	Sum of hinge rotations
(j,m)-beam	$B_{j,m}$	l_m	$1,2,\cdots,f$;	m	$2\psi_1$
(j,k)-beam	$B_{j,k}$	l_k	$1,2,\cdots,f$;	$1,2,\cdots,m-1,m+1,\cdots,s$	$2\psi_1+2\phi_k$
(j,k)-column	$C_{j,k}$	h_j	$2,3,\cdots,f$;	$1,2,\cdots,s+1$	$2\theta_j$
(l,k)-column	$C_{1,k}$	h_1	1	; $1,2,\cdots,s+1$	$2\theta_1+\psi_1$

TABLE 2

Member	Plastic moment	Length	Subscripts j;	Subscripts k	Sum of hinge rotations
$(1,m)$-beam	$B_{1,m}$	l_m			$2\phi_m+2\psi_1$
$(1,k)$-beam	$B_{1,k}$	l_k		; $k\neq m$	$2\phi_k+2\psi_1$
(j,m)-beam	$B_{j,m}$	l_m	$2,\cdots, f$;		$2\psi_1+2\psi_2$
(j,k)-beam	$B_{j,k}$	l_k	$2,\cdots, f$;	$k\neq m$	$2\phi_k+2(\psi_1+\psi_2)$
$(1,k)$-column	$C_{1,k}$	h_1		; $1,2,\cdots,s+1$	ψ_1
$(2,k)$-column	$C_{2,k}$	h_2		; $1,2,\cdots,s+1$	$2\theta_2+\psi_2$
(j,k)-column	$C_{j,k}$	h_k	$3,\cdots, f$;	$1,2,\cdots,s+1$	$2\theta_j$

TABLE 3

Member	Plastic moment	Length	Sum of hinge rotations
Beam	B_j	L	$2s\psi_1$
Internal column	C_j	$(s-1)h_j$	$2(s-1)\theta_j$
	C_1	$(s-1)h_1$	$(s-1)(2\theta_1+\psi_1)$
External column	$\tilde{C}_j$	$2h_j$	$4\theta_j$
	$\tilde{C}_1$	$2h_1$	$4\theta_1+2\psi_1$

TABLE 4

Member	Plastic moment	Length	Sum of hinge rotations
Beam	B_j	L	$2s(\psi_1+\psi_2)$
	B_1	L	$2s\psi_1+2\bar{s}\psi_1$
Internal column	C_j	$(s-1)h_j$	$2(s-1)\theta_j$
	C_2	$(s-1)h_2$	$(s-1)(\psi_2+2\theta_2)$
	C_1	$(s-1)h_1$	$(s-1)\psi_1$
External column	$\tilde{C}_j$	$2h_j$	$2\theta_j$
	$\tilde{C}_2$	$2h_2$	$2\psi_2+4\theta_2$
	$\tilde{C}_1$	$2h_1$	$2\psi_1$

mined as follows.

$$\psi_1 = (1/2)l_m\Theta, \quad \phi_k = (1/2)(l_k - l_m)\Theta, \quad \theta_j = (1/2)h_j\Theta,$$
$$\theta_1 = (1/2)(h_1 - l_m/2)\Theta \tag{11}$$

where Θ is a positive constant.

Since $\psi_1 \geq \phi_k \geq 0$ and $\theta_1 \geq 0$ by assumption, the condition [A] can be satisfied by those frames which satisfy

$$2l_m \geq l_k \geq l_m \text{ and } 2h_1 \geq l_m \tag{12}$$

Thus it has been shown that the design defined by eqs.(10) for the frames satisfying the restrictions (12), indeed satisfy the three necessary and sufficient conditions for the minimum weight design. The minimum weight design for those frames which violate the latter of the restrictions (12) may be obtained by modifying the first story members of the present design.

4. A class of the minimum weight designs of the frames such that $2h_1 \leqq l_m$.

In view of the fact that the Foulkes' mechanism condition has been violated only in the first story columns and that ψ_1 is large enough to eliminate θ_1, it seems appropriate to modify the previous mechanism as shown in Fig.6, where θ_1 does not appear. (θ_j, $j \geq 2$ are not shown in Fig.6) The pattern of the mechanism shown in Fig.5 (d) is now considered only for that part of the frame which excludes the first story columns. The equal angle of rotation in the plastic hinges formed at all the lower end sections of the second story columns will be denoted by ψ_2. The equal angle of rotation of all the joints except the first story joints is equal to $\psi_1+\psi_2$. Corresponding to these modifications, a collapse mechanism of beam type will be necessary for the first story beam with the minimum span length l_m. This angle of rotation is denoted by ϕ_m. The sums of hinge rotations for the members of the frame may be tabulated as shown in Table 2.

The condition [A] may be satisfied if the angles of rotations are determined as follows.

$$\psi_1 = h_1\Theta, \qquad \psi_2 = (l_m/2 - h_1)\Theta,$$
$$\phi_m = (l_m/2 - h_1)\Theta, \quad \phi_k = (l_k/2 - h_1)\Theta, \quad \phi_k = (1/2)(l_k - l_m)\Theta,$$
$$\theta_j = (h_j/2)\Theta, \qquad \theta_2 = (1/2)(h_1 + h_2 - l_m/2)\Theta.$$

Since all the angles of hinge rotation must be non-negative, the condition [A] can be satisfied by the frames with those span lengths and story heights which satisfy

$$2l_m \geq l_k \geq l_m, \quad 4h_1 \geq l_k, \quad 2(h_1+h_2), \quad 4h_1 \geq l_m \geq 2h_1. \tag{13}$$

Corresponding to this modified overcomplete collapse mechanism, the design must be modified as follows. First, the general procedure of the previous section may be applied only to that part of the frame which excludes the first story beams and columns. Secondly, all the first story beams shall be so designed as to collapse under the vertical loads with plastic hinges formed at their midspans and both ends. Thirdly, the first story columns may be designed almost in any manner to carry the shear resultant so far as the assigned plastic moment of each column exceeds the moment at its top end in conformity with the direction of the hinge rotation. This is due to the fact that the first story columns have the same length and that the weight function is linear.

For a frame of single span, the frame moments are uniquely determined only by (3) and the solution for this case will be included in Sec.2.6.

The regions of l_m and l_k for which the minimum weight designs have been obtained, may be represented as Fig.8. The region R_1 is defined by the restriction (12), whereas R_2 by (13). In view of the restrictions in terms of h_1 and h_2, it may be well expected that a similar modification may be extended to the remaining region of $l_k \geq l_m > 0$.

5. Frames with equal span length.

Consider a special class of frames such that $l_k = l$ for all k. The linearized weight function (5) may then be written as

$$G = g[\sum_{j=1}^{f} 2h_j(\sum_{k=1}^{s} M_{j,k}) + l(\sum_{k=1}^{s} M_{1,k}) + 2l\sum_{j=2}^{f}(\sum_{k=1}^{s} M_{j,k})] \tag{14a}$$

Substitution of (3) into (14a) furnishes

$$G = g[\sum_{j=1}^{f}(1/2)h_j^2 \sum_{i=j}^{f} P_i + (1/4)lh_1 \sum_{i=1}^{f} P_i + (1/2)l\sum_{j=2}^{f} h_j \sum_{i=j}^{f} P_i] \tag{14b}$$

In order words, the weight is uniquely determined only by (3), without regard to the other constraints (4). This implies the following geometrical significance. The weight hyperplane is parallel to the intersection of f hyperplanes defined by (3). The constraints (4) truncate this intersection. G achieves the minimum weight when it coincides with this intersection bounded by (4). Unless this bounded intersection is a point, any point therein represents a minimum weight design. Even though G is unique, there exist many minimum weight designs. The corresponding overcomplete collapse mode need not include the beam type mechanism such as shown in Fig.5c. The Foulkes mechanism condition may readily be examined for both of the case $2h_1 \geq l$ and the case $2h_1 \leq l$. Included in this class of designs is the special case where

$M_{j,k} = M_j$ for all k with the same j,

satisfying all the constraints (4). This is a design such that all the beams and all the internal columns in a story have the same plastic moments, respectively and that the two external columns in a story have half the plastic moment of the internal columns in the story.

6. Frames such that $M_{j,k} = M_j$ for all k with the same j.

The aforementioned simple example leads us to the special class of designs for the case of unequal span lengths such that

$$M_{j,k} = M_j \text{ for all } k \text{ with the same } j \tag{15}$$

This implies that all the beams in a story have to be assigned the same plastic moment and altogether form a large total span with the length defined by $L = \sum_{k=1}^{g} l_k$, and that, in view of eqs. (1), the plastic moment of an internal column in a story must be twice as large as that of the external columns in the story. In view of (15), the equations of sway equilibrium (3) may be written as

$$M_j = (h_j/4s) \sum_{i=j}^{f} P_i \tag{16}$$

Substitution of eq. (16) into the weight function (5) provides

$$G = g[(1/2) \sum_{j=1}^{f} h_j^2 \sum_{i=j}^{f} P_i + (L/2s)h_1 \sum_{i=1}^{f} P_i + 2 \sum_{j=2}^{f} h_j \sum_{i=j}^{f} P_i]$$

Thus G is uniquely determined only by eq. (16) as far as the constraints (4) are all satisfied. The corresponding plastic moments are given by

$$\begin{aligned} B_j &= (1/4s)(h_j \sum_{i=j}^{f} P_i + h_{j+1} \sum_{i=j+1}^{f} P_i) \\ C_j &= (1/2s)h_j \sum_{i=j}^{f} P_i, \quad \tilde{C}_j = (1/4s)h_j \sum_{i=j}^{f} P_i \end{aligned} \tag{17}$$

where B_j, C_j and $\tilde{C}_j$ denote the plastic moments of the j-th story beam, internal column and external column, respectively.

Since there are only three different plastic moments in a story, the 3 f sums of hinge rotations for the 3 f spans must satisfy the Foulkes mechanism condition. These sums are tabulated in TABLE 3.

The Foulkes condition can be satisfied if we determine ψ_1 and θ_j as follows.

$$\psi_1 = (L/2s)\Theta, \quad \theta_j = ((1/2)h_j\Theta, \quad \theta_1 = (h_1/2 - L/4s)\Theta \tag{18}$$

In view of the limiting value of θ_1, the present design gives the minimum weight for the frames satisfying

$$2h_1 \geqq L/s \tag{19}$$

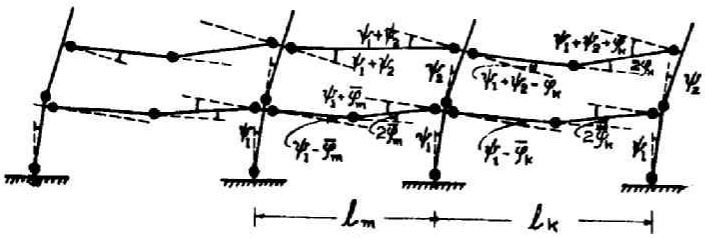

FIG. 6

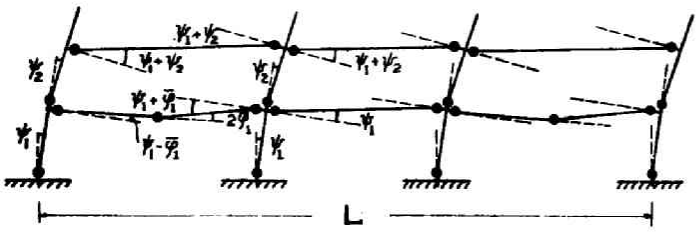

FIG. 7

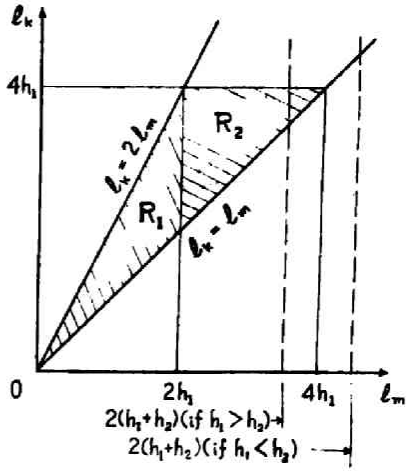

FIG. 8

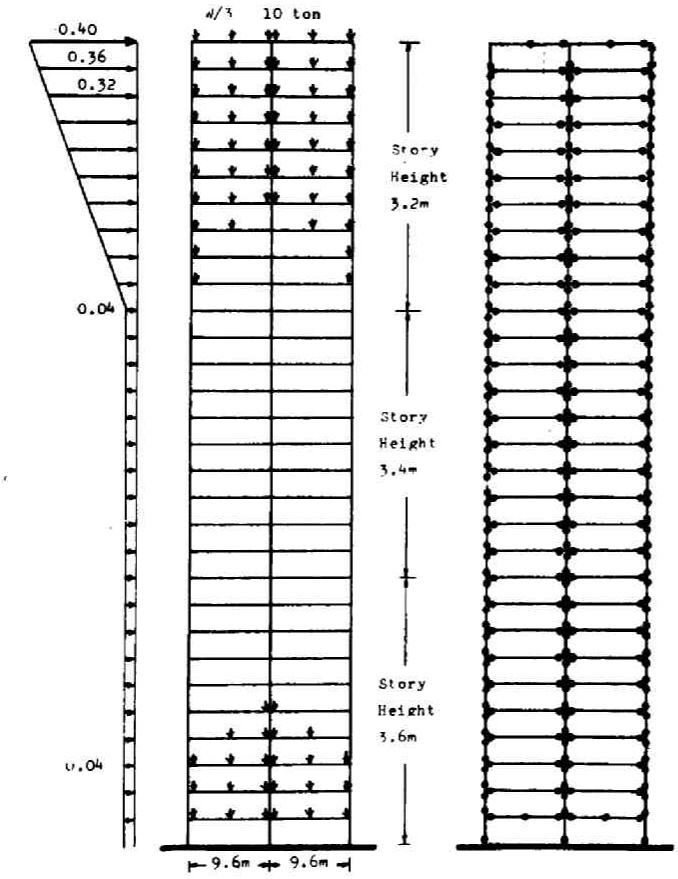

C_j	B_j	$\bar{C}_j$
28.80*	14.40*	14.40*
36.48	32.64	18.24
51.84	44.16	25.92
65.28	58.56	32.64
76.80	71.04	38.40
86.40	81.60	43.20
94.08	90.24	47.04
99.84	96.96	49.92
103.68	101.76	51.84
105.60	104.64	52.80
114.24	109.92	57.12
116.28	115.26	58.14
118.32	117.30	59.16
120.36	119.34	60.18
122.40	121.38	61.20
124.44	123.42	62.22
126.48	125.46	63.24
128.52	127.50	64.26
130.56	129.54	65.28
132.60	131.58	66.30
142.56	137.58	71.28
144.72	143.64	72.36
146.88	145.80	73.44
149.04	147.96	74.52
151.20	150.12	75.60
153.36	152.28	76.68
155.52	154.44	77.76
157.68	156.60	78.84
159.84	158.76	79.92
427.84	28.00	213.92

LATERAL LOAD DISTRIBUTION (x>w)

DIMENSIONS OF THE FRAME VERTICAL LOADS

PLASTIC HINGES

THE MINIMUM WEIGHT DESIGN

FIG.9 THE MINIMUM WEIGHT DESIGN OF A 30-STORY FRAME OF TWO EQUAL SPANS

This condition corresponds to the previous limitation (12). A slight modification is necessary for those frames in which the restriction (19) is violated. The same technique as in Section 4. may be employed again to obtain the modified mechanism shown in Fig.7. The symbols similar to those used in Fig.6 are employed here in Fig.7. Each first story beam carries a different vertical load and has the limiting smallest value to which its plastic moment may be reduced in order to achieve the minimum weight. Now that all the first story beams are to be assigned the same plastic moment here, the actual limitation is given by the largest value among all these limiting smallest values. As soon as the plastic moment of the first story beam is reduced to this largest value, there exists at least one beam at whose midspan a plastic hinge may form. Let $\bar{s}$ be the number of beams of the first story at whose midspans plastic hinges may form. Let this angle of hinge rotation be $2\,\phi_1$. The sums of hinge rotations of the members may then be tabulated as in Table 4.

In order that the Foulkes condition be satisfied, ψ_1, ψ_2, ϕ_1 and θ_j must be given by

$$\psi_1 = h_1\theta, \quad \psi_2(L/2s-h_1)\theta, \quad \phi_1 = (1/\bar{s})(L/2-sh_1)\theta,$$
$$\theta_j = (1/2)h_j\theta, \quad \theta_2 = (1/2)(h_1+h_2-L/2s)\theta. \tag{20}$$

All the hinge rotations are non-negative for the frames satisfying the conditions

$$2(h_1+h_2)\geq L/s\geq 2h_1, \quad 2(s+\bar{s})h_1/s\geq L/s \tag{21}$$

These are the restrictions corresponding to (13)

7. Example:30-story frame of 2 bays.

A 30-story frame of two bays with equal span length carrying equal vertical loads shown in Fig.9b is designed for the lateral forces distributed as shown in Fig.9a, where the base shear coefficient is 0.10. The plastic moments obtained from the general solution (17) are tabulated in Fig.9. The numbers with asterisks in the plastic moments indicate the modified design of the topmost story members by means of plastic moment distribution. In order to restrict the modification as locally as possible, plastic moment distribution has been carried out under the constraint that the lower end section of the internal column of the topmost story is to be assigned the plastic moment twice as much as that of an external column.

8. Concluding remarks.

The minimum weight design of a broad class of tall multi-story frames of

ractical interest in an extremely simple and explicit form has been established n this chapter. The theoretical solution serves to clarify the general features f the minimum weight designs of regular multi-story frames subjected to comparatively large lateral shear. It should be remarked that all the beams except hose with the minimum span length are designed to carry the vertical loads in heir respective spans, and that the corresponding bays contribute little to upporting the lateral shear. The bays with the minimum span length must then e designed to carry the remaining part of the lateral shear resultant. This esult appears to suggest, from economic point of view, the use of shear walls r bracings. It is however noted that in certain cases the present solution esults in columns of zero plastic moments. Even if the columns are to be augented by taking into account the effect of axial forces, this theoretical soution may in some cases appear to be unpractical in view of the elastic-plastic nstability just prior to collapse. Hence several special classes of restricted esigns have been obtained.

The present design must next be modified for the effect of axial forces ithin the simple plastic theory The simple plastic design so constructed must hen be augmented against the effect of additional moments induced by the large lastic-plastic deformation under the presence of large axial forces. Then the ltimate strength design within the second order theory may be established. his approach which has been suggested by the present author in Ref.[15] will e presented in the next chapter and appears to be practically useful in its implicity and directness.

EFERENCES

..Heyman, J., "Plastic Design of Beams and Plastic Frames for Minimum Material Consumption," Quart. Appl Math., Vol.8, 1951, p 373

Foulkes, J., "Minimum Weight Design and Theory of Plastic Collapse," Quart. Appl. Math., Vol.10, p 347

Foulkes, J., "The Minimum Weight Design of Structural Frames," Proc. Royal Society, Ser.A, Vol.223, 1954, p 482

Livesley, R.K., "The Automatic Design of Structural Frames," Quart. J. Mech. Appl. Math., Vol.9, 1956, p 257

. Heyman. J.,and W. Prager, "Automatic Minimum Weight Design of Steel Frames," J. Franklin Inst., Vol.226, No.5, Nov. 1958

Stone, R.L., "Automatic Minimum Weight Design of Steel Frames on the IBM 650 Computer," Brown University Tech. Rep. IBM 2038/2, 1958

7. Kalker, R.L., "Automatic Minimum Weight Design of Steel Frames on the IBM 704 Computer," Brown University Tech. Rep. IBM 2038/3, 1958
8. Tanaka, H., "Automatic Analysis and Design of Plastic Frames," Report of Inst. Indust. Sci., Univ. of Tokyo, Vol.12, No.3, 1962
9. Prager, W., "Minimum Weight Design of a Portal Frame," Proc.ASCE, Eng. Mech Div., Paper 1073, 1956
10. C.R. Calladine, Discussions on "An Approach to the Design of Tall Steel Buildings," Proc. Inst. Civil Engrs., Vol.21, 1961, p 832
11. See for instance, M.R. Horne, "The Stability of Elastic-plastic Structures," Progress in Solid Mechanics, Vol.2, Chap.VII, 1961
12. See for instance, L.S.Beedle, "Plastic Design of Steel Frames," Chap.3, 1958 p 79
13. Tanabashi, R. and T.Nakamura, "The Simplified Minimum Weight Design of Tall Multi-story Frames Subjected to Lateral Forces," Proc. of 1963 Kinki Branch Convention of A.I.J.
14. Tanabashi, R. and T.Nakamura, On the Minimum Weight Design of Tall Multi-story Frames Subjected to Lateral Forces," Proc. of 1964 Kinki Branch Convention of A.I.J.
15. Tanabashi, R. and T.Nakamura, "An Approach to the Last Hinge Point Design of Tall Multi-story Frames," Proc. 11-th Conference on Bridge and Structural Engineering, "Structural Design of Tall Multi-story Buildings and Long Span Structures," Nov. 1964, Tokyo, The Committee on Bridge and Structural Engng., Japanese Congress of Sciences
16. See for instance, S. Vajda,"The Theory of Games and Linear Programming," Methuen & Co. Ltd., 1956, (Translated into Japanese by T. Miyashita, 1959)

CHAPTER 3

OVERALL STRENGTH AND TOUGHNESS OF MULTISTORY FRAMES AS DESIGN CRITERIA*

1. INTRODUCTION

The method of linear minimum weight design in the preceding chapter is a simple but extremely idealized first approximation to more realistic plastic design methods. The quantitative results may be useful only if proper modifications are made for various factors to be taken into account in a realistic design. In plastic design methods it is usual that a plane frame is required to carry more than one set of design ultimate loads. For the overall strength safety of a plane frame designed by the linear minimum weight solutions, not only the interaction conditions in terms of bending moment and axial force but also the effect of geometry changes must be taken into account. A realistic method of design may be said to be a method of determining element sizes in a cost minimization process under practical constraints.

In previous investigations on practical design methods of a plane multistory frame or building frame, it appears that, the stronger the emphasis on the cost-minimization procedure is, the less precise the method of strength-safety analysis is [1] and that, in design methods whose primary concern is the realistic ultimate strength of a frame, the cost-minimization procedure becomes of a secondary concern [2,3,4]. The recent paper [5] by Holmes and Sinclair-Jones appears to have made an effort to incorporate both phases in a direct method which does not depend on the use of a computer analysis.

In the present chapter, the basic idea of a design method based upon the overall load-deflection curves and the overall structural toughness concept is described. The third phase of the present method makes full use of the overall load-deflection curves obtained by the well-known stiffness

---

* The basic idea of the successive modification proposed in this chapter was presented in "An Approach to the Last Hinge Point Design of Tall Multi-story Frames" *Proc. Symposium on External Forces and Structural Design of Long-span and High-rise Structures, held in Nov.1964, Japan Society for Promotion of Sciences, Tokyo, Sept.1965, pp169-179. The method of successive modification was originally proposed with respect to the last hinge point displacement for which a method of estimation without a large-capacity computer was available.*

matrix method. The significance of overall load-deflection analysis for design purpose lies in the following points:(1) An overall load-deflection curve represents the variation of the overall stiffness, the elastic-plastic stability limit, the unstable behavior after the stability limit;(2) If an appropriate second-order member stiffness matrices are used, all the possibilities of any local failure of subassemblages can be detected;(3) If the displacement axis is properly scaled as will be explained later, the overall energy absorption in a frame can be visualized as the area under the modified load-deflection curve;(4) When the second-order elastic-plastic-hinge stiffness matrices are used, all the angles of hinge rotations can be obtained as one of the computer outputs and therefore checked if they are all within their respective allowable limits of the equivalent member end rotations; and if a more elaborate member stiffness matrix is constructed, plastic strains can be evaluated. Attention is confined here only to the overall strength and toughness aspects of structural design. Although a practical design must satisfy various requirements due to architectural considerations and must be in conformity with legal design and analysis requirements, the present chapter is concerned only with an idealized bare frame consisting of idealized members without local out-of-plane member instability.

2. THE DESIGN PROBLEM AND OVERALL LOAD-DEFLECTION CURVES

The problem of ultimate strength design of a frame is usually defined in terms of several sets of design ultimate loads and the respectively corresponding sets of working loads. It has been customary to denote the states of dead, live, earthquake, snow and wind loadings symbolically by G, P, K, S and W, respectively. The same notation will be used here to represent symbolically the sets of loads. A symbol $\oplus$ will be used for denoting a set of combined loads. One of the simplest choices of the sets of design loads may be summarized as follows.

For strength design	*For deflection check*
$L^{GP} : \lambda_G\ G \oplus \lambda_P\ P$	$L_S^{GP} : G \oplus P$
$L^{K} : G \oplus P \oplus \lambda_K K$	$L_S^{K} : G \oplus P \oplus K$
$L^{W} : G \oplus P \oplus \lambda_W W$	$L_S^{W} : G \oplus P \oplus W$

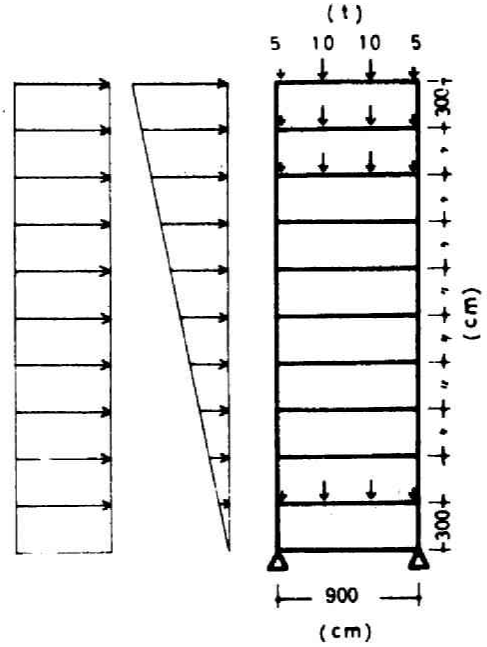

K building

M_{OVT}-θ_{ST} curves for KAa series.

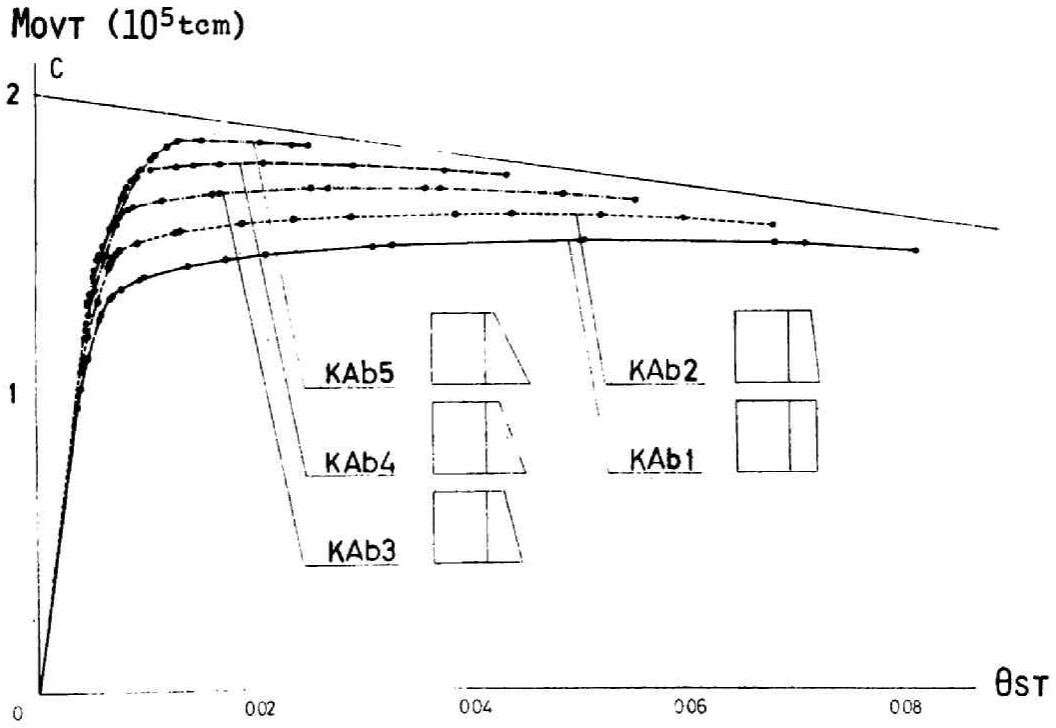

MOVT-θST CURVES FOR KAb SERIES.

Fig.1

where λ with a subscript denotes a load factor and where L and L_S denote sets of combined loads. The simplest problem of ultimate strength design may be stated as follows: *Given the centerline dimensions of a regular rectangular frame B, the three sets of design ultimate loads L^{GP}, L^K and L^W and the three sets of service loads, determine the cross-sections of the members of B so as to be able to support L^{GP}, L^K and L^W, to minimize the cost of B under the constraints due to architectural considerations and structural detail requirements and to be able to remain elastic for stresses due only to L_S^{GP}, L_S^K and L_S^W with a sufficient overall stiffness which precludes undesirable excessive deflections.*

The design procedure for a plane multistory frame subjected to a single set of loads will be described first in Section 3. The procedure will then be modified for a problem involving two load factors. A procedure of dealing with a building frame consisting of regular rectangular parallel frames will then be outlined in Sec.5.

While the interaction effect of axial forces can be taken into account without difficulty as will be stated in Sec.3, the well-known $P\Delta$-effect can be incorporated in a strength design method by defining the required strength of a frame with reference to a certain prescribed state of deformation. Since the $P\Delta$-effect can be included in elastic-plastic [6] or elastic-plastic-hinge stiffness matrices [7], it is now possible to trace the load-deflection responses of a perfectly-plastic multistory frame and in principle to trace responses of a strain-hardening multi-story frame subjected to any quasi-static loading programs.

Fig.1 shows a result of a numerical analysis of a ten-story frame subjected to a set of uniformly distributed lateral loads which are increased proportionally to a load factor [7]. The over-turning moment-top sway angle curves approach the corresponding rigid-plastic mechanism curve from below as the rate of tapering in beam stiffnesses and plastic moments is increased. The point of inception of the mechanism curve indicates the rigid-plastic collapse overturning moment and is seen to be considerably above the maxima of the elastic-plastic response curves. The mechanism curve represents a simple estimate of the $P\Delta$-effect by means of the rigid-plastic large deflection analysis by hand. The $P\Delta$-effect in a multi-story frame "suppresses" the load-deflection curves so greatly that the curves will eventually have

some negative slopes even before plastic collapse mechanisms have formed. It is also observed, however, that even after the elastic-plastic stability limit on a curve, the frame is able to support loads which are only slightly less than the maximum and is able to absorb a considerable amount of energy until up to a certain overall displacement. It is apparently natural to define the overall strength of a frame for a design purpose with respect to a certain prescribed value of the corresponding displacement scale.

For this purpose, it appears advantageous to use the concept of the overall structural rotation of a frame introduced by S.Ishida [8] Let f_i, u_i and l_i denote the lateral force acting upon the i-th floor level of a frame, the lateral displacement associated with f_i and the height of the i-th floor level from the ground, respectively. The rate of work $\dot{W}_H$ done by all the f_i's may be written as

$$\dot{W}_H = \Sigma f_i du_i = \lambda \Sigma (f_{io} l_i)(\frac{du_i}{l_i}) \tag{1}$$

where λ denotes the load factor to be multiplied on the standard state of loads $\{f_{io}\}$ The overall structural rotation is defined by

$$\theta_{ST} = \int \frac{\Sigma f_i du_i}{\Sigma f_i l_i} = \int \frac{\dot{W}_H}{R_M} \tag{2}$$

where R_M denotes the external resultant moment. The $R_M \sim \theta_{ST}$ relation visualized as a curve on a (θ_{ST}, R_M)-plane is a one-degree-of-freedom representation of the load-deflection behavior of the frame. It is then natural to consider a design problem defined by the overall strength *at a prescribed overall structural rotation.* On the (θ_{ST}, R_M)-plane, the design problem of a frame for L^W and L_S^W may be stated as that of shooting a prescribed aim (θ_D^W, R_{MD}^W) with an initial stiffness (or in other words with an initial angle of attack) which should not undershoot the deflection check point $(\theta_D^{WS}, R_{MD}^{WS})$

A typical $R_M \sim \theta_{ST}$ curve is shown as the curve *OFU* in Fig.2. The energy absorption during an overall structural rotation θ_D may now be represented by the shaded area *OFUR*. The overall strength R_M of the frame varies with respect to θ_{ST} and represents the rate of work done by R_M at θ_{ST} per unit θ_{ST}. As has been mentioned in chapter 1, the overall toughness of a frame together with the ultimate strength are considered to be the appropriate design criteria for L^K.

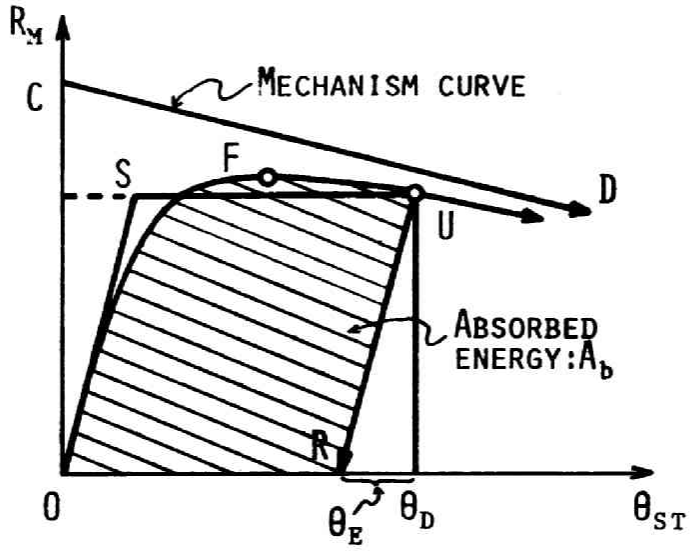

Fig.2 Energy absorption capacity of a frame.

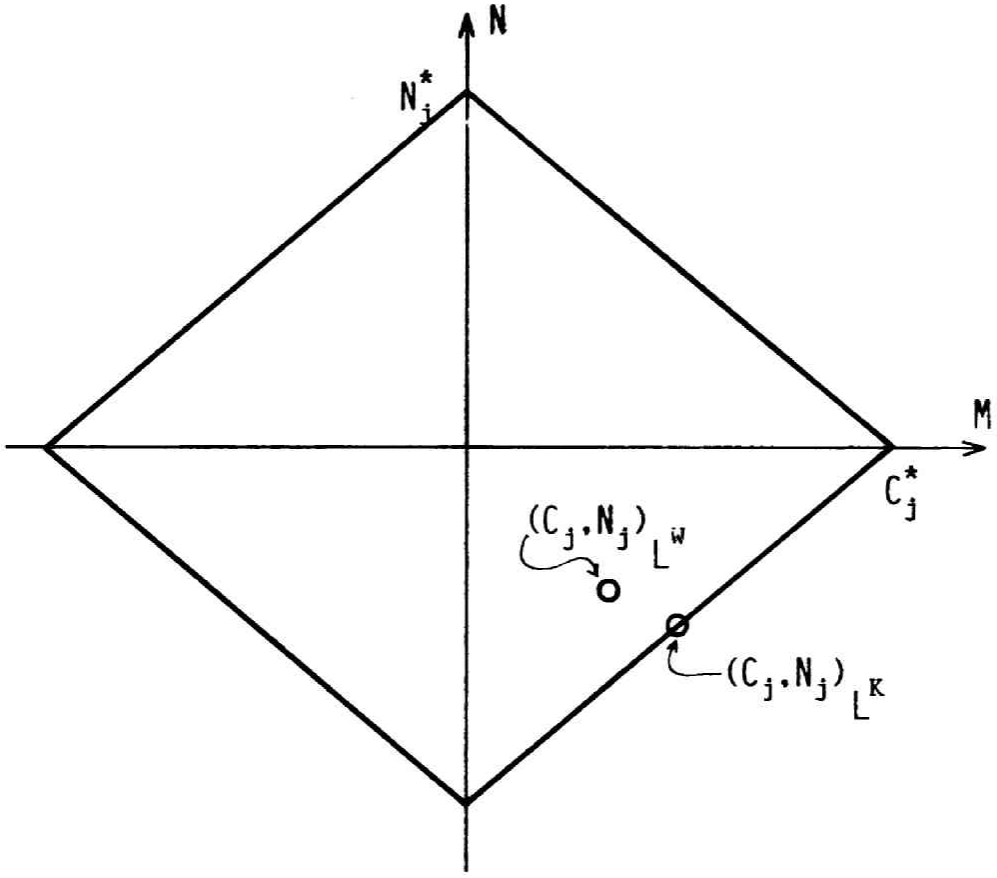

Fig.3 (M,N)-interaction yield conditions for a sandwich section.

Although the concept of "overall toughness design" appears to be fairly well-known since Tanabashi's proposal of the "Velocity-Potential Energy Theory" in 1935 [9], no practical computational procedure based upon the second-order theory has yet been proposed for multi-story frames. If a frame is designed so as to possess the energy capacity to absorb a prescribed energy A_b at a rate not less than R^K_{MD} per unit overall structural rotation at some θ_{ST} , the method of design may be called an "overall toughness design".

The energy absorption capacity may not be defined uniquely, depending upon the criterion on the deformation limit. It may be argued if it is appropriate to take into account , as serviceable energy, that portion of the area under the $R_M \sim \theta_{ST}$ curve with a negative slope as shown in Fig.2. In view of the extensive numerical results [7,8], it appears possible to design a frame so as not to possess a portion of a negative slope on the $R_M \sim \theta_{ST}$ curve within a range of a fairly small prescribed value of θ_{ST}. Furthermore, slopes observed in the extensive numerical results[7,8] are only slightly negative within a practical range of θ_{ST}, say 0.02. For these reasons, the attention in this chapter will be confined only to the shooting problems.

In practical problems, the prescription of A_b may also be written in terms of θ_{ST} if the $R_M \sim \theta_{ST}$curve can be roughly regarded as an elastic-perfectly plastic response as shown in Fig.1 and 2. For, A_b and θ_{ST} are related roughly by

$$\theta_{ST} = \frac{A_b}{R^K_{MD}} + \frac{R^K_{MD}}{S_E} \tag{3}$$

where S_E denotes the initial elastic overall stiffness of the frame. The aim of the shooting problem is then defined by (θ^K_D, R^K_{MD}). The first condition of the ultimate strength design underlined on p.34 must now be rephrased as "to support L^K at θ^K_D, L^W at θ^W_D and L^{GP}"

3. DESIGN PROCEDURE OF A PLANE FRAME FOR A SINGLE LOAD FACTOR

It has been frequently pointed out in previous investigations [1], that, although the cost of a frame B is a function of the amount of materials to be used, an exact minimization of material consumption does not necessarily result in the minimum of the cost because of other factors including fabrication and erection procedures. For instance, the columns and beams of two or three

stories of a frame are frequently designed to have the same cross-sections, respectively. Because of this circumstance, an explicit minimization of material consumption for a frame will be carried out here only in determining the starting sizes by means of the linear minimum weight design developed in Chapter 2. The starting sizes are then modified successively so as to keep the amount of augmentation minimum necessary for supporting the additional moments due to the $P\Delta$-effect.

Let the set of design ultimate loads and the corresponding overall structural rotation (L^D, θ_D) represent either (L^W, θ_D^W) or (L^K, θ_D^K). A design procedure for (L^D, θ_D) may be summarized as follows.

(i) *RIGID PLASTIC DESIGN* If a rigid-plastic multi-story frame is designed so as to collapse in a mechanism of a weak-beam strong-column type, the additional moments due to $G \oplus P$ at $\theta_{ST} = \theta_D$ can be taken into account in advance. An initial assignment of the plastic moments to the members of the frame can be made by utilizing the linear minimum weight design solutions in Chapter 2 for most stories except several stories from the topmost and by applying the "plastic moment distribution method" to the remaining stories so as to collapse in an overcomplete collapse mechanism. The load-carrying capacity of the foundation and the stability consideration will usually restrict the range of plastic moments already in this stage. The initial design so constructed will be referred to as $D^{RP}(M)$.

An assignment of the plastic moment to a member does not determine the cross-sectional dimension completely. Furthermore, the plastic moment C_j for a column in $D^{RP}(M)$ must be regarded as that plastic moment which has been reduced by the existing axial force N_j. Since $D^{RP}(M)$ is associated with an overcomplete collapse mechanism, the axial forces corresponding to the bending moment diagram at collapse may readily be found for all the members of $D^{RP}(M)$. The cross-section of each member can then be determined so that C_j and N_j will just satisfy the (M, N) interaction yield condition associated with the selected cross-sectional shape. There still remains one degree of freedom for a choice of the stiffness of the member. The set of cross-sections of all the members of B for L^D will be referred to as $D^{RP}(M, N)$.

For instance, the interaction relation for a column with an idealized H section (sandwich section) may be written as

$$C_j \pm \frac{C_j^*}{N_j^*} N_j = \pm C_j^* \qquad \text{(Fig.3)} \qquad (4)$$

where C_j^* denotes the plastic moment of the section when the axial force is absent and N_j^*, the fully plastic axial force of the section when the bending moment is zero. Since $C_j^*/N_j^* = H$ (half a depth of the sandwich section), the bending stiffness of the member may still be chosen within a certain range. The stiffnesses of all the members may be taken as independent variables with respect to which the overall elastic behavior can be controlled within a certain practical range.

It should be noted that, in the construction of $D^{RP}(M, N)$, the axial forces in the columns at collapse of the frame will be different according as the direction of the replaced static lateral forces. Two different $D^{RP}(M, N)$'s are obtained from a $D^{RP}(M)$ depending upon the lateral load directions. The larger value of C_j^* or N_j^* will be chosen for each column. The design obtained by modifying $D^{RP}(M, N)$ in this way will be referred to as $\overline{D^{RP}}(M, N)$. The frame of $\overline{D^{RP}}(M, N)$ will collapse not in the overcomplete collapse mechanism of $D^{RP}(M)$ but in a complete or incomplete collapse mechanism in which plastic hinges need not form in some columns, possibly in all the windward columns. This justifies *a posteriori* the assumption that the collapse mechanism is of a weak-beam strong-column type.

(ii) *STIFFNESS AND STRESS CHECK AT SERVICE LOADS* The design $\overline{D^{RP}}(M, N)$ has been constructed only with respect to the strength safety or to the toughness safety. A stiffness and stress check at service loads is desirable in order to preclude undesirable vibrations and excessive deflections. Such a check can be made approximately in a similar manner to the approximate stress analysis in the conventional allowable stress design.

The recent developments in the stiffness matrix methods enables one to carry out not only the elastic analysis of complex structural systems consisting of a large number of elements, but also the elastic-plastic analysis of these large systems at least by means of the elastic-plastic hinge stiffness matrices [7,8,10] and in future by means of more elaborated elastic-plastic stiffness matrices [6]. Among many advantages of the stiffness matrix method, it should be pointed out that, the method makes it possible to analyze not only the overall elastic-plastic behavior of a frame but also any possible local instability so far as the stiffness matrix including the second-order effects is used. It

Is therefore possible to assess the effect of elastic deformations of the members upon the overall behavior of the frame, which has been neglected in $\overline{D^{RP}}(M,N)$.

(iii) *SUCCESSIVE MODIFICATION FOR STRENGTH AND TOUGHNESS SAFETY* Let R_{MD} denote the external moment resultant of the design lateral loads represented either by $\lambda_K K$ or $\lambda_W W$ Let the load factor to be multiplied on R_{MD} be denoted by μ. The factor μ is used in order to represent the variation of the external moment resultant with respect to θ_{ST}. The load-factor-overall structural rotation curve ($\mu\sim\theta_{ST}$ curve) can be obtained by an elastic-plastic second-order stiffness matrix method. Due to the effect of elastic deformations of the members of a frame, a $\mu\sim\theta_{ST}$curve of the frame of $D^{RP}(M, N)$ may or may not overshoot the design aim $(\theta_{ST}, \mu) = (\theta_D, 1)$, depending upon the slendernesses of the members. If the aim is undershot by a $\mu\sim\theta_{ST}$ curve, $D^{RP}(M, N)$ must be augmented so that the curve would just shoot or overshoot the aim. The $\mu\sim\theta_{ST}$ curve overshooting $(\theta_D, 1)$ guarantees that the frame so modified and designed will be able to support the design loads at $\theta_{ST}= \theta_D$. Not only any possibility of local instability can be detected in the course of the load deflection analysis,but also the amounts of plastic hinge rotations or of plastic strains can be obtained as computer outputs. A detailed elastic-plastic analysis of a member alone can be made separately and incorporated in the design at some stage of the above procedure.

4. DESIGN PROCEDURE OF A PLANE FRAME

(i) *RIGID PLASTIC DESIGN* The additional moments due to the $P\Delta$-effect can again be evaluated in advance for the larger rotation among $\theta_D^K$and θ_D^W. $D^{RP}(M)$ must now be constructed for a lateral shear force diagram which just circumscribes both of the lateral shear force diagrams of $\lambda_K K$ and $\lambda_W W$. If, for instance, the lateral shear diagram of $\lambda_W W$ for a portion U consisting of some upper stories to the topmost circumscribes that of $\lambda_K K$, the portion U will not participate in the collapse mechanism of L^K and vice versa. It is apparent that the moment diagrams constructed for L^K alone or L^W alone are both statically admissible. The plastic moments of members in several upper stories must further be augmented so as to be able to support L^{GP} This design so modified will be referred to as $\overline{D^{RP}}(M)$ again.

The procedure of constructing $\overline{D^{RP}}(M, N)$ based upon the $\overline{D^{RP}}(M)$ remains the same as that for a single load factor in Sec.3, except that the axial forces in columns must now be evaluated from the moment diagram at collapse under the

circumscribing lateral shear force diagram. With this procedure, the stress points (N_j, C_j) of the members corresponding to the two statically admissible moment diagrams for L^k and L^W will be as shown in Fig.3.

(ii) *STIFFNESS AND STRESS CHECKS FOR WORKING LOADS* Stiffness and stress checks for L_S^{GP}, L_S^K and L_S^W can be made either by means of conventional approximate methods of elastic analysis or in the course of load-deflection analysis in (iii).

(iii) *OVERALL LOAD-DEFLECTION ANALYSIS FOR STRENGTH AND TOUGHNESS SAFETY CHECKS*

Let R_M^K and R_M^W denote the external moment resultants of the design lateral loads $\lambda_K K$ and $\lambda_W W$, respectively. Let the load factors to be multiplied on R_M^K and R_M^W be denoted by μ^K and μ^W, respectively. Both of the $\mu^K R_M^K \sim \theta_{ST}^K$ curve and $\mu^W R_M^W \sim \theta_{ST}^W$ curve can be obtained by means of an elastic-plastic second order stiffness matrix method. If the slenderness ratios of the columns are so small that the effect of elastic deformations of the members upon the overall load-deflection curves is not great and hence if no local instability phenomenon occurs, both of the $\mu^K R_M^K \sim \theta_{ST}^K$ curve and $\mu^W R_M^W \sim \theta_{ST}^W$ curve will shoot their respective aims (θ_D^K, R_M^K) and (θ_D^W, R_M^W).

For a frame consisting of members of larger slenderness ratios, both curves may undershoot their respective aims as shown in Fig.4(a) So far as the curves $S_K^{(1)}$ and $S_W^{(1)}$ have been obtained, $\max\mu^K = \mu_{(1)}^K$ and $\max\mu^W = \mu_{(1)}^W$ are known. The rigid plastic design procedure must then be repeated for the sets of magnified lateral forces $\lambda_K K/\mu_{(1)}^K$ and $\lambda_W W/\mu_{(1)}^W$.

It is in general difficult to shoot both of the aims within small errors. It suffices, however, that either of S_K or S_W shoots the corresponding aim within a small error and that the other overshoots the other aim. The successive modification procedure may be made automatic in a computer once a program is written for constructing a system stiffness matrix from a second-order elastic-plastic member stiffness matrices. Fig.4(b) illustrates the set of $\mu R_M \sim \theta_{ST}$ curves for a frame which have met the conditions stated above within a tolerance limit.

The variations of the state of stress in a member with respect to θ_{ST} are also found from computer outputs. The result may be used to check the safety of the member in view of a number of more elaborated analysis. Requirements on the cross-sectional details of a member must of course be incorporated in an earlier stage. For instance, the thickness ratio of a flange must obey a requirement obtained from a separate analysis and be checked in $\overline{D^{RP}}(M, N)$.

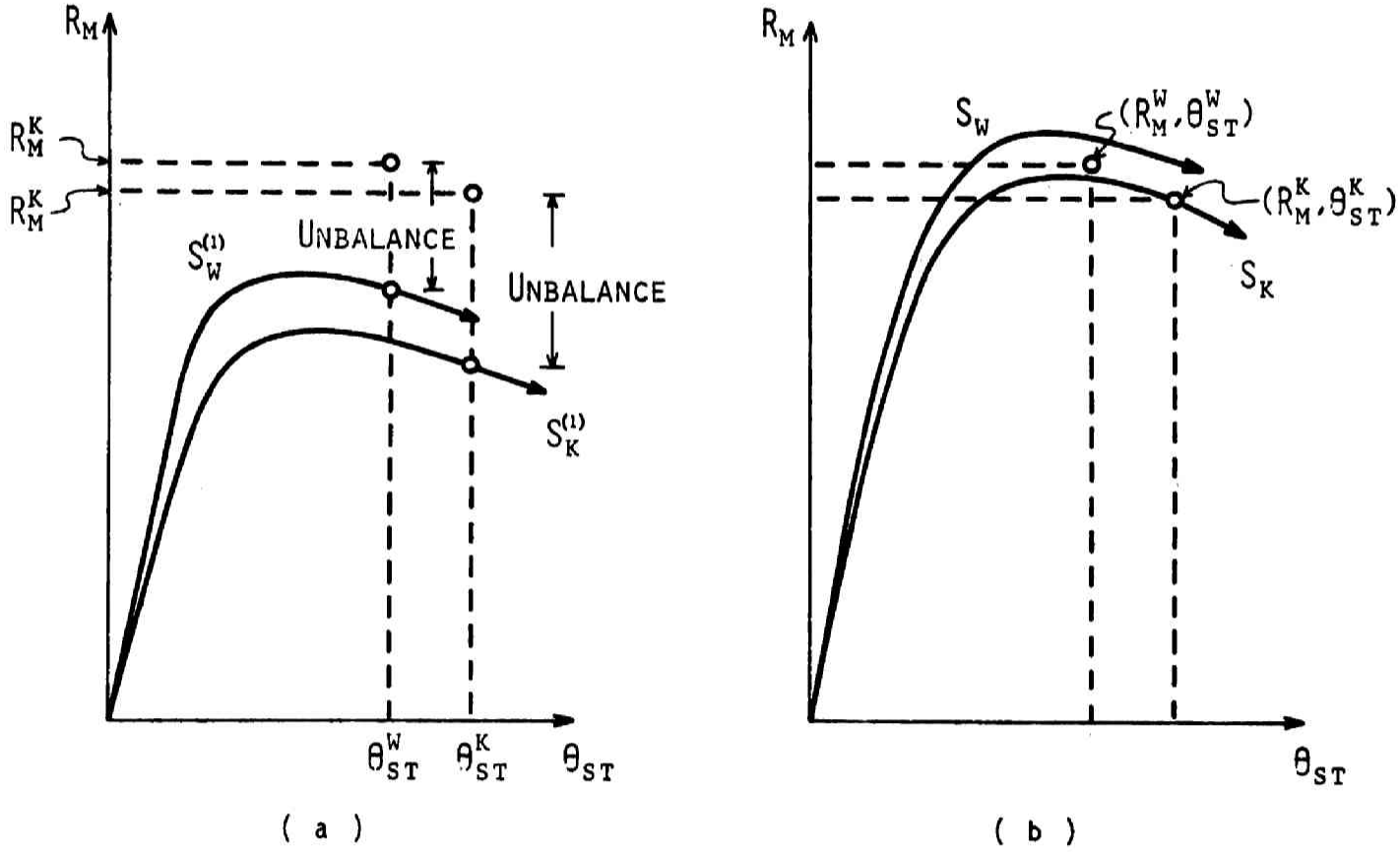

Fig.4 Successive modification of load-deflection curves.

A numerical example due to Ishida and Ohta will be shown in the Appendix to this Chapter.

5. *PROBLEMS ARISING IN BUILDING FRAME DESIGN*

The method of designing a plane frame may be extended to a three-dimensional building frame by including interaction effects between a number of parallel and intersecting plane frames. A building frame F of a rectangular parallelopiped may be considered to consist of two groups of parallel plane frames intersecting orthogonally on the plan. It is assumed that the principal directions of sidesway stiffness remain to be these two directions of the parallel plane frames even in the plastic range. The use of θ_{ST} may not be appropriate for a torsional deformation mode. Let F_α ($\alpha=1,\ldots,m$) and F_β ($\beta=1,\ldots,n$) denote the α-th plane frame of group A and the β-th plane frame of group B, respectively. Let $\{F_\alpha\}$ denote the structural system consisting of all the parallel plane frames in group A which are connected by floor slabs.

The lateral design loads must now be prescribed not only for $\{F_\alpha\}$ but also for $\{F_\beta\}$ and are denoted by (L_A^K, L_A^W) and (L_B^K, L_B^W), respectively In order to construct a $D^{RP}(M,N)$, it is necessary either to assume a set of load-carrying capacity ratios for $\{F_\alpha\}$ and for $\{F_\beta\}$ by architectural or structural consideration or to seek for appropriate ratios by means of a weight- or cost minimization procedure. $D^{RP}(M)$ can then be constructed separately for each F_α or F_β. Since a column belongs not only to a F_α but also to a F_β, it must not violate two interaction conditions of the form of equation (3).

The load-deflection analysis must be carried out on $\{F_\alpha\}$ and $\{F_\beta\}$ for μL_A^K and μL_B^K and for μL_A^W and μL_B^W, respectively by introducing connection conditions between F_α's and between F_β's in the process of constructing system stiffness matrices. If the second-order elastic-plastic hinge method is applied, the incremental analysis must be made with finer load or displacement increments due to the circumstance that the next hinge must be sought among all the members of the parallel plane frames of the respective system.

A pair of shooting problems, one for $\{F_\alpha\}$ and the other for $\{F_\beta\}$ must be solved by one and the same design. A column is subjected to a pair of modification conditions due to the unbalanced story shears in $\{F_\alpha\}$ and in $\{F_\beta\}$ and must be redesigned so as to satisfy both of the requirements.

6. CONCLUDING REMARKS

A successive modification procedure has been outlined for an ultimate strength design of a plane multi-story frame and an extention to a regular rectangular building frame has been indicated briefly. Simplifications and elaborations of various levels can be considered. For instance, if it has been investigated for a class of regular rectangular multi-story frames that $R_M \sim \theta_{ST}$ curves are mostly below the respective rigid-plastic collapse mechanism curves by a certain amount which can be bounded roughly depending upon the structural parameters, then a frame in the class can be designed by $D^{RP}(M, N)$ without load-deflection analyses so far as the $P\Delta$-effect have been included in a magnification factor on the design loads.

REFERENCES

[1] See for instance, L. A. Hill, Jr., "Automated Optimum Cost Building Design," J. Structural Div., Proc. ASCE, Vol.92,No.ST6, Dec.1966,pp247-263.

[2] L. S. Beedle *et al.* "Plastic Design of Multi-story Frames," Fritz Engng. Lab. Peport No.273.20, Dept. Civil Engng., Lehigh Univ., 1965.

[3] M. Holmes and S. N. Gandhi, "Ultimate Load Design of Tall Steel Building Frames Allowing for Instability," Proc.Instn.Civil Engrs.,Vol.30, Jan.1965, pp147-166.

[4] Yuji Nakamura, "Plastic Design Method of Multi-story Planar Frames with Deflection Constraints," Ph.D. Dissertation submitted to MIT, 1968.

[5] M. Holmes and H. W. Sinclair-Jones, "Plastic Design of Multi-story Sway Frames," Proc. Instn. Civil Engrs., Vol.47, Sep.1970, pp55-76.

[6] Y. Fujita, H. Ohtsubo and T. Yuhara, "Finite Element Analysis of Inelastic Large Deflection Behavior of Inplane Frame Structures (Plastic Design of Steel Structures, 10th Report," J.Soc.Naval Architects Japan, Vol.126 Dec.1969, pp275-294.

[7] Ryo Tanabashi, Kiyoshi Kaneta, Tsuneyoshi Nakamura and Shuzo Ishida, "To the Final State of Rectangular Frames," 4th World Conf.Earthquake Engng., Jan.1969, Santiago, Chile, Proc.1970.

[8] Ryo Tanabashi, Tsuneyoshi Nakamura and Shuzo Ishida, "Overall-Force-displacement Characteristics of multi-story Frames," Proc.Symp. Ultimate Strength of Structures and Structural Elements, Dec.5,1969, Tokyo.pp63-70.

[9] Ryo Tanabashi, "Some Considerations on Destructive Elements of Earthquake Ground Motion and Earthquake Resistance of Structures," J.Architectural Inst.Japan, Vol.49, No.599,May 1935 and also "On the Resistance of Structures to Earthquake Shocks, Memoirs, College of Engng., Kyoto Imp.Univ. Vol,9,No.4,1937

[10] Yukio Ueda, M.Matsuishi, T.Yamakawa and T.Akamatsu,"Elastic-plastic Analysis of Framed Structures using the Matrix Method,"J.Soc.Naval Arch.Japan, Vol.124,Dec.1968,pp183-199 and also PartII,Vol.126,Dec.1969,pp253-273.

DESIGN TABLE FOR A 20-STORY PLANE FRAME

Story No.	WIND			EARTHQUAKE			Design lat. shear	$D^{RP}(M)$		N_J in $D^{RP}(M)$			$D^{RP}(M, N)$						
	Lat. force	Story shear	Total shear	Lat. force	Story shear	Total shear		Beam B_j	Column C_j	Dead load	Lat. shear	Total N_j	H_c	C_j^*	$1.2C_j^*$	A_c	H_B	A_B	
	ton	*ton*	*ton*	*ton*	*ton*	*ton*	*ton*	*tm*	*tm*	*ton*	*ton*	*ton*	*cm*	*tm*	*tm*	*cm²*	*cm*	*cm²*	
20	13.12	13.12	13.52	16.33	16.33	17.13	17.13	24.50	24.50	- 28	0	28.0	21	30.38	---	---	31.0	32.9	*
								22.49	22.49	- 20	+ 1.4	- 21.4	21	26.98	32.38	64.3	---	---	#
19	12.95	26.07	26.87	15.51	31.84	33.44	33.44	51.90	29.41	- 40	- 11.2	- 51.2	21	40.24	48.29	95.8	31.0	69.8	#
18	12.78.	38.85	40.05	14.69	46.53	48.93	48.93	72.30	42.81	- 60	- 25.0	- 85.0	21	60.66	72.79	144.4	31.0	97.2	
17	12.60	51.45	53.05	13.88	60.41	63.61	63.61	98.47	55.66	- 80	- 43.8	- 123.8	23	84.13	100.96	182.9	32.0	128.2	
16	12.41	63.86	65.86	13.06	73.47	77.47	77.47	123.45	67.79	-100	- 67.3	- 167.3	23	106.27	127.52	231.0	32.0	160.7	
15	12.21	76.07	78.47	12.24	85.71	90.51	90.51	146.99	79.20	-120	- 95.3	- 215.3	23	128.72	154.46	279.8	32.0	191.4	
14	12.00	88.07	90.87	11.43	97.14	102.74	102.74	169.10	89.90	-140	-127.5	- 267.5	25	156.78	188.14	313.6	33.0	213.5	
13	11.78	99.85	103.05	10.61	107.75	114.15	114.15	189.78	99.88	-160	-163.6	- 323.6	25	180.78	216.94	361.6	33.0	239.6	
12	11.55	111.40	115.00	9.80	117.55	124.75	124.75	209.04	109.16	-180	-203.4	- 383.4	25	205.01	246.01	410.0	33.0	263.9	
11	11.30	122.70	126.70	8.98	126.53	134.53	134.53	226.87	117.71	-200	-246.6	- 446.6	26	233.83	280.60	449.7	33.5	282.2	
10	11.03	133.73	138.13	8.16	134.69	143.49	143.49	243.26	125.55	-220	-292.9	- 512.9	26	258.90	310.68	497.9	33.5	302.6	
9	10.75	144.48	149.28	7.35	142.04	151.64	151.64	258.24	132.69	-240	-342.1	- 582.1	26	284.04	340.85	546.2	33.5	321.2	
8	10.43	154.91	160.11	6.53	148.57	158.97	160.11	272.79	140.10	-260	-394.1	- 654.1	27	316.71	380.05	584.5 586.5	34.0	333.1 334.3	**
7	10.09	165.00	170.60	5.71	154.28	165.48	170.60	289.38	149.28	-280	-449.2	- 729.2	27	346.16	415.40	632.2 641.0	34.0	354.6	
6	9.71	174.71	180.71	4.90	159.18	171.18	180.71	307.40	158.12	-300	-507.8	- 807.8	27	376.23	451.47	679.8 696.7	34.0	376.7	
5	9.28	183.99	190.39	4.08	163.26	176.06	190.39	324.71	166.59	-320	-569.6	- 889.6	28	415.68	498.81	725.3 742.3	34.5	392.2	
4	8.77	192.76	199.56	3.27	166.53	180.13	199.56	341.21	174.62	-340	-634.6	- 974.6	28	447.51	537.01	782.3 799.1	34.5	412.1	
3	8.17	200.93	208.13	2.45	168.98	183.38	2o8.13	356.73	182.11	-360	-702.5	-1o62.5	28	479.61	575.53	839.5 856.5	34.5	430.8	
2	7.38	208.31	215.91	1.63	170.61	185.81	215.91	371.03	188.92	-380	-773.2	-1153.2	29	523.35	628.02	885.4 902.3	35.0	441.7	
1	6.20	214.51	222.51	0.82	171.43	187.43	222.51	383.62	194.70	-400	-846.3	-1246.3	29	556.13	667.35	941.9 958.8	35.0	456.7	
B								194.70									35.0	231.8	

*Design determined by L^{GP}, #Design by means of Plastic Moment Distribution,

** Design based upon the axial forces computed for $\lambda_K K$ and $\lambda_W W$ alone.

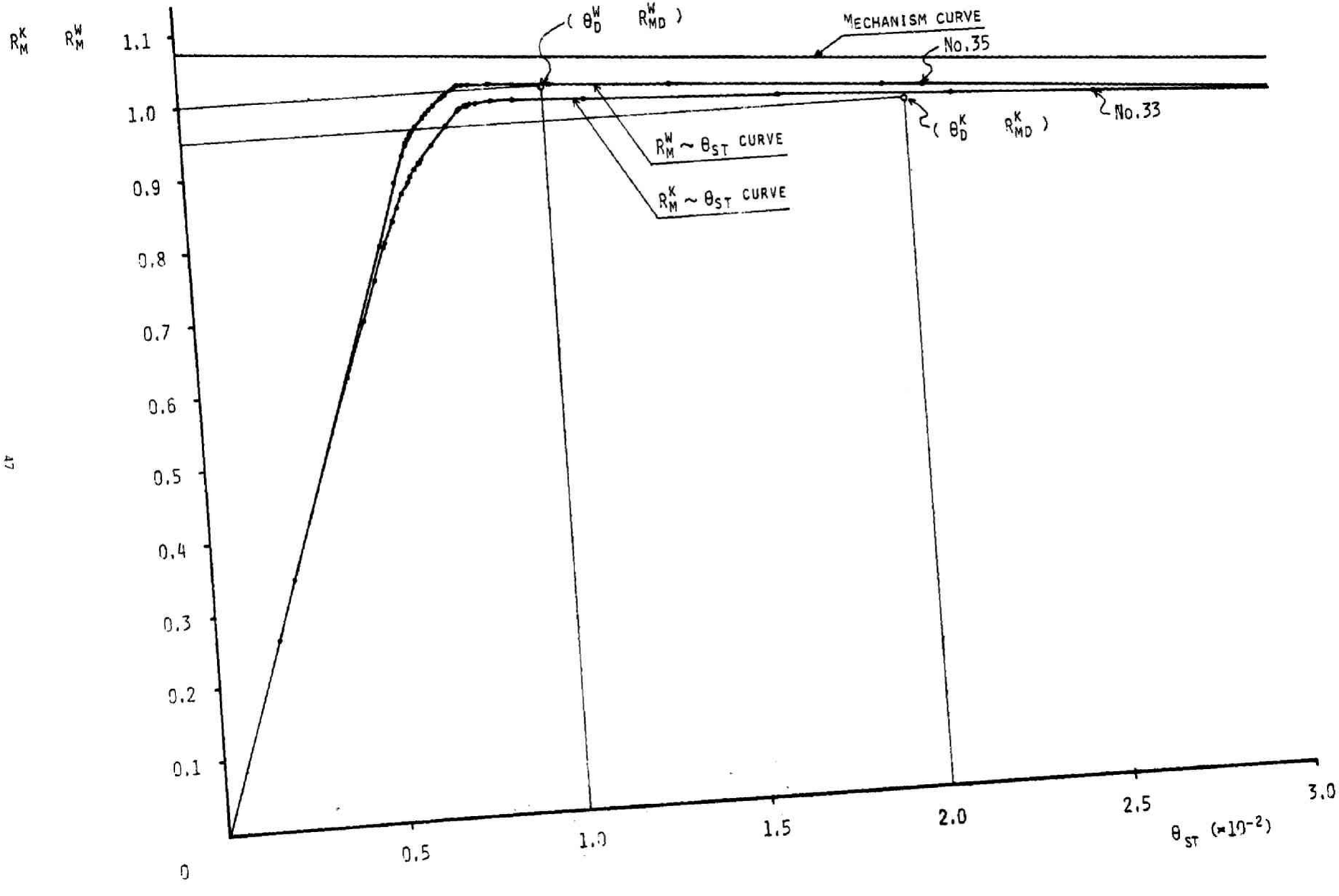
R_M^K R_M^W
1.1
1.0
0.9
0.8
0.7
0.6
0.5
0.4
0.3
0.2
0.1
0
0.5
1.0
1.5
2.0
2.5
3.0
θ_{ST} ($\times 10^{-2}$)
(θ_D^W R_{MD}^W)
MECHANISM CURVE
No.35
No.33
(θ_D^K R_{MD}^K)
$R_M^W \sim \theta_{ST}$ CURVE
$R_M^K \sim \theta_{ST}$ CURVE

CHAPTER 4

THE MINIMUM WEIGHT DESIGN OF VIERENDEEL FRAMES

1. INTRODUCTION

In this chapter, a general method of finding the linear minimum weight designs is proposed for simply-supported and clamped Vierendeel frames based upon the concept of the "frame moment", defined in chapter 2. A Vierendeel frame considered here consists of horizontal upper and lower chord members and vertical members as shown in Fig.1. Each joint is assumed to be rigid enough to transmit the fully plastic moment of any member framing into it. All the assumptions usually introduced in the linear theory of minimum weight design are also made here. The problem considered here may be stated as follows: Given the center-line dimensions of a Vierendeel frame and a set of static loads to be carried as shown in Fig.1, what fully plastic moments should be assigned to the members of uniform cross-sections in order to sustain the loads and to make the linear weight function a minimum ? For the sake of simplicity, the paper considers the case where all the external loads act only upon the joints. Some local modification may be necessary if, at some subspans, the inter-span loads are not small compared to the subspan shear.

While a multi-span multi-story frame subjected to lateral loads may be regarded as a cantilever as a whole as shown in chapter 2, a Vierendeel frame may be clamped and externally indeterminate. The weight function must therefore be minimized with respect to the unknown redundant reaction that governs the subspan shear.

2. EQUATIONS OF EQUILIBRIUM IN TERMS OF FRAME MOMENT

Consider first a simply-supported Vierendeel frame of f subspans or panels. Joints and vertical members are numbered from 0 through f from left, whereas chord members, from 1 through f as shown in Fig.1. Let l_1, l_2 ,...and l_f denote the panel lengths, respectively and h, the height of the frame. Let A_j, C_j (j = 1, 2,...,f) and B_j (j = 0, 1, 2,. .,f) denote the fully plastic moments of the jth upper and lower chord members and of the jth vertical member, respectively,,from left.

Due to the assumption that all the external loads act upon the joints

---

This chapter is based upon the author's paper,"THE MINIMUM WEIGHT DESIGN OF VIERENDEEL FRAMES," Int. J. Solids Structures, 1970, Vol. 6, pp353 to 369

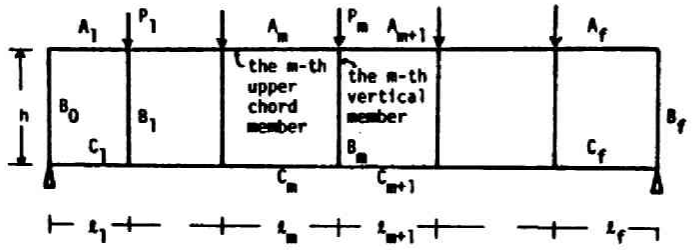

Fig.1

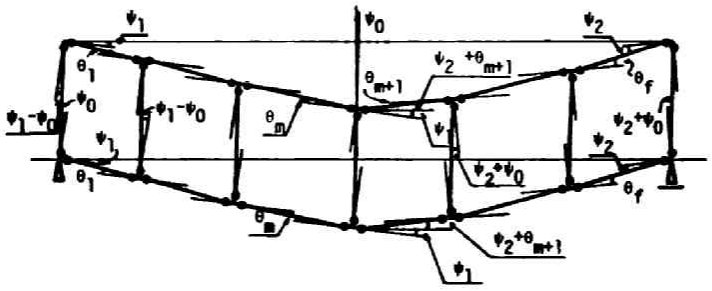

Fig.2

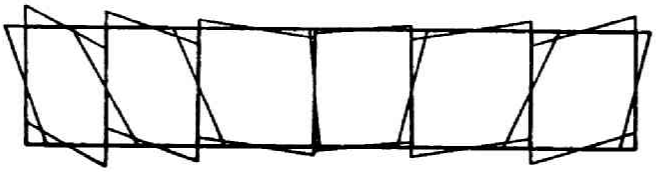

Fig.3

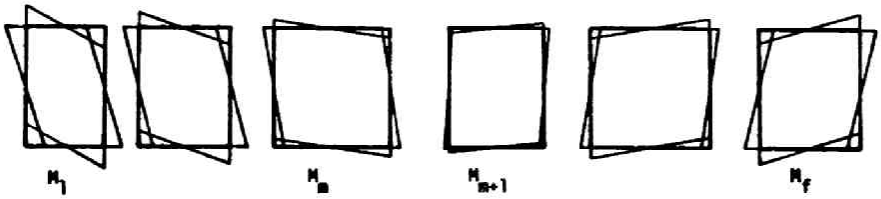

Fig.4

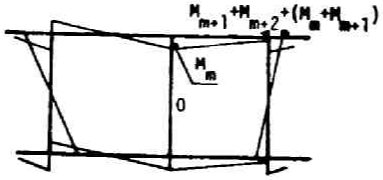

Fig.5

only, the end sections are the only potentially critical sections. In view of the overcomplete collapse mechanism for the minimum weight design of tall multi-story frames, it is natural to expect also that the minimum weight design of the Vierendeel frame be included in such a class of designs that correspond to extremely deteriorated overcomplete collapse mechanisms in which plastic hinges have formed at all the potentially critical sections as shown in Fig.2. It should then be observed that, since all the end sections attain their fully plastic moments respectively, under such a special circumstance, the number of unknown end moments is equal to the number of members, provided that their signs are properly chosen. There are then $(2f+1)$ independent equations of joint equilibrium and f equations of sway equilibrium for the $(3f+1)$ unknown fully plastic moments and the problem may be said to be statically determinate. The essential problem is then reduced to how the directions of end moments should be determined.

The concept of "frame moment" is not only useful for a proper choice of end moment signs but also convenient for understanding the simple beam character of the Vierendeel frame. In view of the linearity of the equations of equilibrium in terms of plastic moments without any slope-continuity requirements, the moment diagram at collapse may be regarded as a composite consisting of the f constituent element moment diagrams shown in Fig.3. An element diagram is to be characterized by the particular moment distribution shown in Fig.4 with the four corner values of equal magnitude. Such an element moment diagram is completely defined by this equal corner moment except the direction of the corresponding shear force. The corner moment associated with this moment distribution is called "frame moment M_i " for the ith rectangle. The positive frame moment is defined here to be the one that corresponds to a clockwise couple of vertical shear forces Q_i in analogy to the usual shear force sign convention. Then Q_i is related to M_i by

$$4M_i = l_i Q_i \tag{1}$$

The fully plastic moments may be expressed in terms of M_i as follows:

$$\begin{aligned} A_j &= C_j = M_j \qquad (j = 1,2,\ldots,f) \\ B_i &= M_i + M_{i+1} \qquad (i = 1,2,\ldots,f-1) \\ B_0 &= M_1 , \quad B_f = M_f . \end{aligned} \tag{2}$$

In the present case of externally statically determinate frame, Q_i and hence M_i are immediately determined by the external loads. If the plastic moments are

assigned to the members in accordance with equations (2), the moment distribution satisfies all the equations of equilibrium without violating any yield conditions and corresponds to the overcomplete collapse mechanism. Hence this is indeed a complete solution in the theory of limit analysis. Because of the statical determinacy in the sense stated above, there remains no further freedom for minimizing the linear weight function

$$G = 2g\Sigma\left|(l_i+h)M_i\right| = \frac{1}{2}g\Sigma\left|(l_i+h)l_iQ_i\right|, \tag{3}$$

(g: proportionality constant)

as far as the minimum weight solution is included in the assumed class of collapse mechanisms. Geometrically speaking, there is only one vertex determined by equations (1) and (2) in a $(3f+1)$-dimensional plastic moment space. In order to prove that this solution is indeed the minimum weight design, it is necessary to show that a Foulkes mechanism can be formed at this vertex. Otherwise, the minimum weight design has not been included in the assumed class of collapse mechanisms and another vertex must be sought at which the weight function can have a smaller value.

3. MECHANISM CONDITION

Since $(3f+1)$ members may be assigned different plastic moments in this problem, the Foulkes mechanism condition may be stated as follows [1]:

> A frame of minimum weight design must be able to collapse in an overcomplete collapse mechanism consisting of $(3f+1)$ independent alternative mechanisms, such that, for every member,
>
> Σ(Hinge rotations in a member) = a common constant × the length of the member.

If a frame designed for minimum weight may include a member of zero plastic moment, then that part concerned with the member in the Foulkes mechanism condition associated with the compatible statically admissible moment distribution is only sufficient but not necessary for the minimum weight design. When a Foulkes mechanism is to be constructed for a regular rectangular frame, it should first be observed that number of groups of members have the same lengths, respectively. All the vertical members of a Vierendeel frame have the same length h, whereas a pair of lower and upper chord members have the same length l_i. A pair

---

An extended sufficient condition suggested by H. Nagaoka is that the sum of hinge rotations in the member of zero plastic moment is not greater than the common constant times the length of the member

of lower and upper chord members can have the same amount of hinge rotations, if the corresponding plastic hinge rotations are the same, respectively. A pair of the same hinge rotations can be produced not only by the vertical displacement of a pair of lower and upper joints but also by the rotations of such a pair of joints of the same magnitude and direction. A joint rotation causes a hinge rotation in a vertical member framing into the joint. Since all the vertical members have the same length, the plastic hinge rotations at the ends of every vertical member must be of the same magnitude, their directions being always consistent with the moment distribution determined above. With these observations, a Foulkes mechanism may be constructed as follows:

If the given vertical loads are relatively large compared to the horizontal shear resultant, there exist a pair of adjacent chord members between which the vertical shear changes the direction. Let m denote the index of the joint and the vertical member between such a pair of chord members. The moment distribution in this mth vertical member depends upon whether $|M_m| = |M_{m+1}|$. Figure 2 shows the mechanism corresponding to the case where $|M_m| > |M_{m+1}|$. Let ψ_1 denote the angle of clockwise rotation of the $(m+1)$ joints from left and ψ_2, the angle of counterclockwise rotation of the remaining $f-(m+1)$ joints. Let ψ_0 denote the clockwise angle of horizontal sway of vertical members. Then the Foulkes condition can be satisfied through the $(f+1)$ vertical members if

$$2(\psi_1-\psi_0) = h\Theta, \quad 2(\psi_2+\psi_0) = h\Theta. \tag{4}$$

where Θ is a positive proportionality constant. Let $\theta_j (j=1,\ldots,m)$ and $\theta_k (k=m+1,\ldots,f)$ denote the angles of hinge rotation due to the vertical displacements of joints whose directions are to be consistent with the moment distribution. The Foulkes condition requires

$$2\theta_j = l_j\Theta \tag{5}$$

$$2\theta_{m+1} + \psi_1 + \psi_2 = l_{m+1}\Theta \tag{6}$$

$$2\theta_k = l_k\Theta. \tag{7}$$

The equation of compatibility of the collapse mechanism:

$$\sum_{j=1}^{m} (\theta_j + \psi_1) l_j - \sum_{k=m+1}^{f} (\theta_k + \psi_2) l_k = 0 \tag{8}$$

must further be required in order to satisfy the condition of the external supports. Equation (8) is new and was not necessary in Chapter 2 because the overall external supports of a multi-story frame may be regarded as a cantilever. The

$(f+3)$ unknown angles ψ_0, ψ_1, ψ_2, θ_j and θ_k can be determined by the $(f+3)$ equations of (4), (5), (6), (7) and (8). If the sum of the two equations in (4) is substituted into equation (6), θ_{m+1} is given by

$$\theta_{m+1} = \frac{1}{2}(l_{m+1} - h)\Theta. \tag{9}$$

Since all the hinge rotations must be non-negative in order to be consistent with the moment distribution, equation (9) requires

$$l_{m+1} \geq h. \tag{10}$$

It may now be concluded that the Foulkes condition is indeed satisfied by the assumed mechanism shown in Fig.2 for those frames where equation (10) is satisfied and hence that the minimum weight design is indeed given by equations (1) and (2).

If the vertical shear does not change its direction due to a relatively large lateral shear, then equation (6) will not be necessary and hence a simpler Foulkes mechanism may readily be constructed.

For frames with $h > l_{m+1}$, it is apparent that the assumed angles of plastic hinge rotation exceed $l_{m+1}\Theta$ even if $\theta_{m+1}=0$. In order to decrease the sum of the hinge rotation, it seems unavoidable that the angle of rotation of the mth joint be decreased from ψ_1. This change, however, would then result in violation of the Foulkes condition which had been satisfied for the mth vertical member. The latter difficulty may be resolved if the mth vertical member is assigned $B_m=0$ so that any arbitrary amount of plastic hinge rotation within the member becomes permissible. In order to maintain the equilibrium of moments about the mth joint after this change, it is necessary that the left end moment of the $(m+1)$th chord members be equal to $|M_m|$. Since the vertical shear remains the same, the moment diagram for the $(m+1)$th chord members must have the same slope as before. The right end moments must then be equal to $|M_{m+1}| - \{|M_m| - |M_{m+1}|\} = 2|M_{m+1}| - |M_m| < |M_m|$ as shown in Fig.5. The weight change may be written as

$$2\{|M_m| - |M_{m+1}|\}(l_{m+1}-h) < 0.$$

Thus the weight is indeed decreased. Let the angle of clockwise rotation of the mth joint be ψ_m. The Foulkes condition will remain satisfied if

$$(\psi_1+\theta_m-\psi_m) + \theta_m = l_m\Theta \tag{11}$$

$$\psi_2 + \psi_m = l_{m+1}\Theta \tag{12}$$

If the sum of the two equations in (4) is subtracted from the sum of equations (11) and (12), then

$$2\theta_m = (l_m+l_{m-1}-h)\Theta$$

The range of validity of this modified design is therefore given by

$$l_m+l_{m+1} \geq h. \tag{13}$$

It should be remarked that the mth vertical member in this modified design has lost the role as a bending-resistant member and simply behaves as a strut which transmits half the vertical load to the lower chord members.

4. CLAMPED VIERENDEEL FRAMES

A clamped Vierendeel frame shown in Fig.6 is characterized by its external indeterminacy together with its end constraints against lateral sway The circumstance that the vertical shear in each subspan is not statically determinate and dependent upon the redundant reaction, say R_1, in Fig.6, indicates that the weight can be minimized with respect to R_1. Because of the end constraint against sway. on the other hand, the Foulkes mechanism in Fig.2 must be so modified as to exclude the angle ψ_0.

The concept of the frame moment is again helpful for the minimization process with respect to the redundant reaction and enables one to regard the Vierendeel frame as a beam. Any moment distribution represented by a set of frame moments satisfying (1) provides a complete solution since it satisfies all the equilibrium equation, does not violate any yield conditions and corresponds to an overcomplete collapse mechanism. The corresponding design may readily be obtained from the frame moments as given by (2) Let D denote the set of all the designs that can be described by frame moments only. Assuming first that the minimum weight design $D_{\min}$ for a frame is included in D, the linear weight is minimized with respect to the redundant reaction and the necessary conditions are found. In order to prove that $D_{\min}$ is indeed the minimum weight design among all the designs including those which can not be described by the frame moments only, it must be shown that the overcomplete collapse mechanism corresponding to $D_{\min}$ satisfies the Foulkes condition. It may then be shown that the necessary conditions are violated only locally This indicates that the minimum solution for such a frame has not been included in D. Because of the local violation of the Foulkes condition, however, it is natural to expect that a local modification on $D_{\min}$ obtained as above will suffice to achieve a different minimal solution. It will be shown through three successive modifications that a local modification

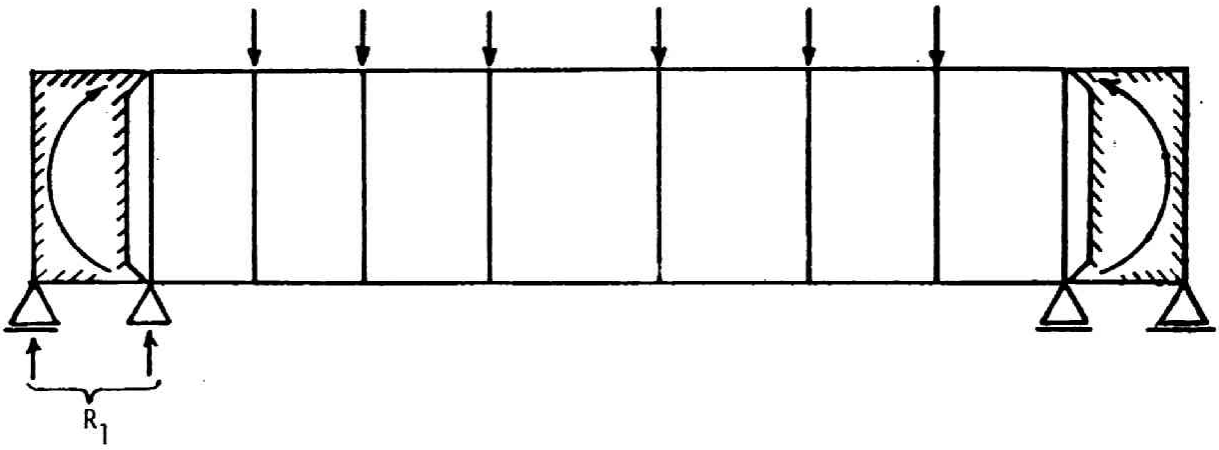
R1

Fig.6

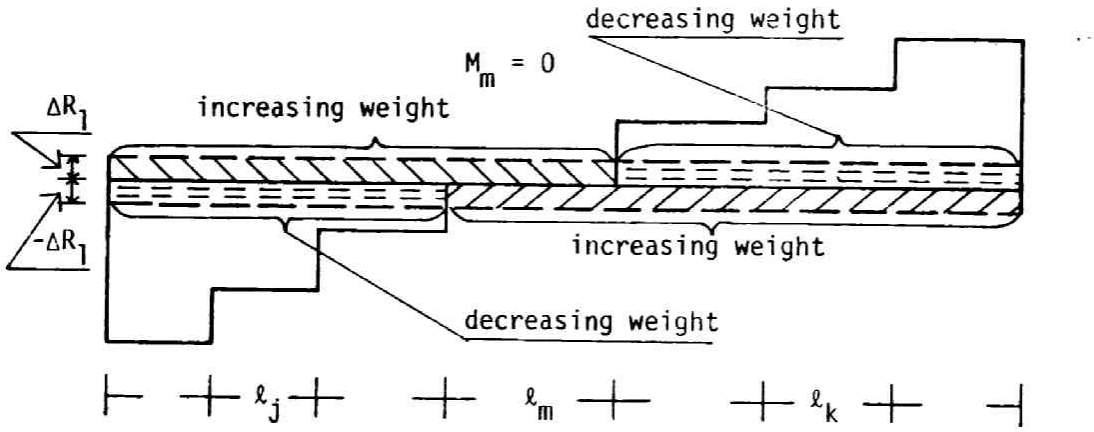
decreasing weight
Mm = 0
ΔR1
increasing weight
-ΔR1
increasing weight
decreasing weight
ℓj
ℓm
ℓk

Fig.7

on the moment diagram and the corresponding hinge pattern of the D_{min} indeed leads to a different minimal solution whose region of applicability is mutually exclusive and compensating with the previous design.

Design-I

For most practical purposes, it may be assumed that the vertical loads act only downward so that the corresponding transverse shear diagram is monotonically non-increasing with the shape as illustrated in Fig.7. The weight function given by equation (3) indicates that, for a special case of equal subspan $l_i=l$, G is proportional to the area of the $|Q_i|$ diagram. It may readily be shown that if $\int_0^x |Q(x)|\,dx$ (where $Q(0)-Q(x)$ is a given continuous monotonic function) is to be minimized with respect to the end value $Q(0)$, then $Q(l/2)=0$. Although the Q_i-diagram in the present problem is of a staircase shape, it is natural to expect that a minimizing Q_i-diagram would analogously contain a subspan with $Q_i=0$ as illustrated in Fig.7. Let n be an assumed index of the subspan for which $Q_n=0$. Then the weight may be written as

$$G = \frac{1}{2}g\{\sum_{j=1}^{n-1}(l_j+h)l_jQ_j - \sum_{k=n+1}^{f}(l_k+h)l_kQ_k\}. \tag{14}$$

In view of Fig.7 and the assumed monotonous variation of Q_i-diagram, it is apparent that G tends to decrease as n is increased from 1 in equation (14) and also decrease as n is decreased from f. There must therefore be a minimizing index number m between 1 and f

Apparently, any variation of the reaction R_1 corresponds to a simple downward or upward translation of the Q_i-diagram. An increase ΔR_1 increases Q_j $(j=1,\ldots, m-1)$ by ΔR_1, respectively and decreases $|Q_k|$ $(k=m+1,\ldots, f)$ by ΔR_1, respectively. The corresponding variation in the weight may be calculated from the variations of the moment diagram as indicated by the dashed lines in Fig.8 (a). It should be noted that since $Q_m=0$, the moment is zero through the mth chord members. Let ΔG_1 and ΔG_2 denote the weight variations for $\Delta R_1>0$ and for $-\Delta R_1$, respectively. In view of the circumstance that, since the shear direction of ΔQ_{m-1} is opposite to ΔQ_{m+1}, the weight decrease in the $(m+1)$th vertical member due to ΔQ_m just cancels with the weight increase in the mth vertical member and vice versa, the weight variations are given by

$$\Delta G_1 = \frac{1}{2}g\Delta R_1\{\sum_{j=1}^{m-1}(l_j+h)l_j + \sum_{k=m+1}^{j}(l_k+h)l_k\}$$

$$\Delta G_2 = \frac{1}{2} g \Delta R_1 \{ -\sum_{j=1}^{m-1} (l_j + h) l_j + l_m^2 + \sum_{k=m+1}^{f} (l_k + h) l_k \}.$$

If the moment diagram shown in Fig.8(a) is to correspond to the minimum weight design for a given frame, then $\Delta G_1 \geq 0$ and $\Delta G_2 \geq 0$. The necessary condition may be compactly written as

$$-l_m^2 \leq L(m) \leq l_m^2 \tag{15}$$

where

$$L(m) = \sum_{k=m+1}^{f} (l_k + h) l_k \sum_{j=1}^{m-1} (l_j + h) l_j. \tag{16}$$

$L(m)$ is a discrete-valued function of the subspan index m and is characterized by the center line dimensions of a frame. It is therefore appropriate to call it the "shape function" for the frame. Although this function has been introduced here for the convenience of describing the weight variations, it will be shown later that $L(m)$ is closely related to the angle of rotation of the mth chord members in the corresponding collapse mechanism.

The moment diagram may also be varied under the same subspan shears. The only possible variation for the mth chord members is the constant moment distribution pattern similar to Fig.9(a) This variation results in the necessary condition:

$$h \leq l_m \tag{17}$$

For those frames for which (15) and (17) are satisfied, the minimizing Q_i-diagram belonging to the index m immediately determines the design through (1) and (2). In particular, $A_m = C_m = 0$ in this case, This design will be called Design-I.

In order to prove the sufficiently of (15) and (17), it must be shown that the Foulkes condition can be satisfied in the corresponding collapse mechanism. Because of the lateral constraint, $\psi_0 = 0$ and equations(4) are reduced to

$$\psi_1 = \psi_2 = \psi = \frac{1}{2} h \Theta \tag{18}$$

The condition (5) and (7) must remain satisfied except at the mth chord members. Figures 8(b) and (c) show two of the three possible patterns of hinge formation for Design-I. The angle of clockwise rotation of the mth chord members is obtained from the equation of compatibility for the mechanism as

$$\omega = \frac{1}{2} L(m) \Theta / l_m. \tag{19}$$

The conditions of non-negative hinge rotations in the mechanism shown in Fig.8(c) are $\psi - \omega \geq 0$ and $\psi + \omega \geq 0$, from which the following inequalities are obtained.

$$-\frac{1}{2}h\Theta \leq \omega \leq \frac{1}{2}h\Theta \tag{20}$$

Similarly, the conditions $\omega + \psi \geq 0$ and $\omega - \psi \geq 0$ for the mechanism in Fig.8(b) lead to

$$\frac{1}{2}h\Theta \leq \omega \tag{21}$$

whereas the third case similar to Fig.8(b) but just reversed, leads to

$$\omega \leq -\frac{1}{2}h\Theta. \tag{22}$$

Since the particular circumstance of $A_m = C_m = 0$ permits any increase in the amount of hinge rotations by assuming arbitrary plastic hinges within the chord members, the Foulkes condition can be satisfied if the total sum Ω_m of hinge rotations for an mth chord member is not greater than $l_m\Theta$. Hence

$$\Omega_m = 2|\omega| \leq l_m\Theta, \quad \text{for Fig.8(b) and}$$

$$\Omega_m = 2\psi \leq l_m\Theta \quad \text{for Fig.8(c)}.$$

Thus the Foulkes condition can be satisfied if h and ω are within the rectangular region defined by $-\frac{1}{2}l_m\Theta \leq \omega \leq \frac{1}{2}l_m\Theta$ and $h \leq l_m$ on an (h,ω)-plane, which consists of the three subregions defined by (20), (21) and (22). These conditions obtained by the kinematical consideration precisely coincide with (15) and (17) It may therefore be concluded that the existence of the subspan index m satisfying (15) and (17) for a given set of centerline dimensions of a frame is the necessary and sufficient condition for the Design-I belonging to m to be the minimum weight design. In those frames for which $h > l_m$, Ω_m is in excess of $l_m\Theta$ and a different design must be sought.

Design-II

The state of $Q_m = 0$ does not necessarily imply $A_m = C_m = 0$ if designs other than in D may be considered. Figure 9(a) shows a constant moment distribution through the mth chord members, corresponding to the magnitude of which the plastic moments of the $(m-1)$th and the mth vertical members are decreased. This modification may be regarded as a process of shifting $\min\{B_{m-1}, B_m\}$ to the mth chord members due to the circumstance $h > l_m$ Figure 9(a) shows the case where

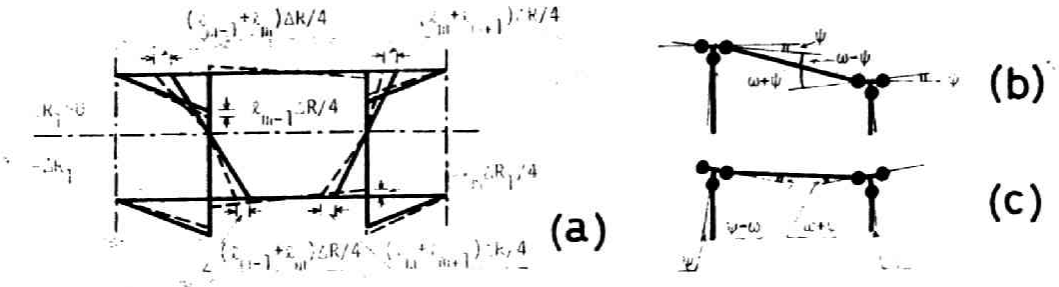

FIG.8

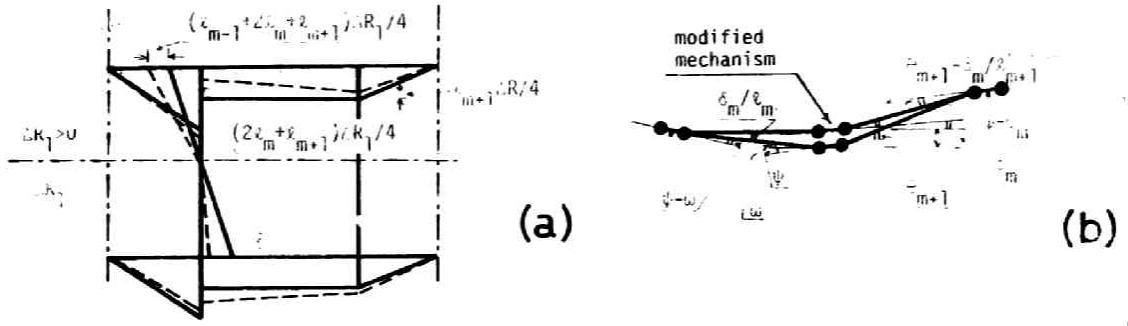

FIG.9

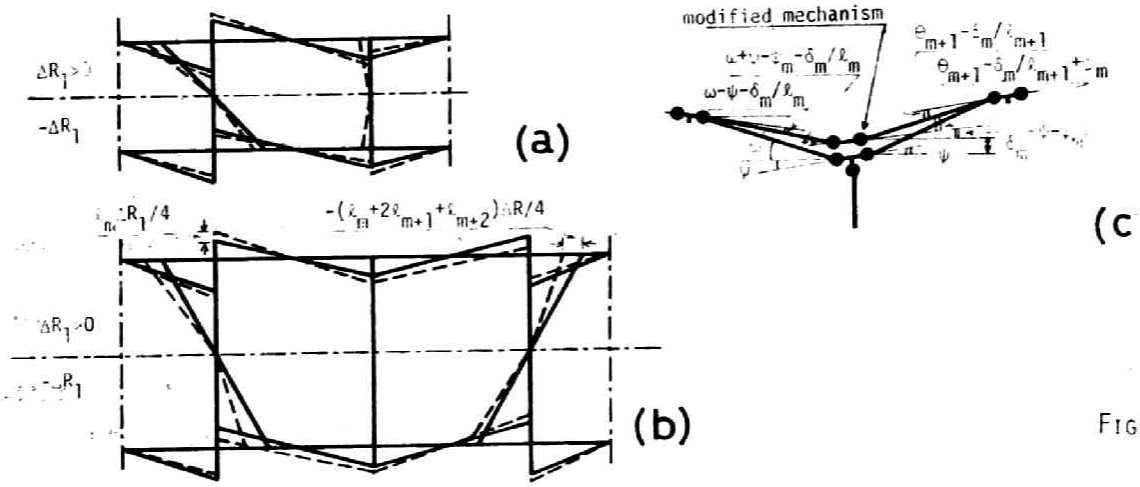

FIG.10

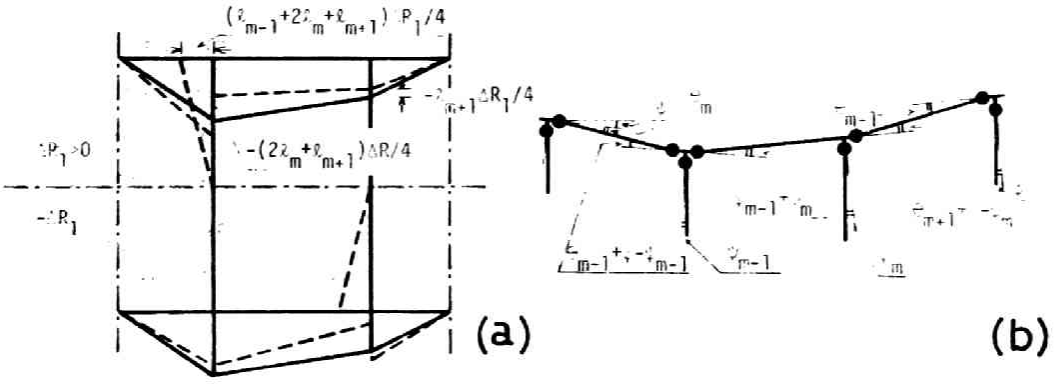

FIG.11

$\min\{B_{m-1}, B_m\} = B_m$. If the modified values of the plastic moments are indicated by a bar, the modified design may be written as

$$\overline{A}_m = \overline{C}_m = B_m, \quad \overline{B}_{m-1} = B_{m-1} - B_m, \quad \overline{B}_m = 0. \tag{23}$$

The amount of weight decrease compared to Design-I is given by $2(h-l_m)\min\{B_{m-1}, B_m\}$. This design will be called Design-II. If the moment diagram shown in Fig. 9(a) is to correspond to the minimum weight design, any change of redundant reaction R_1 must increase the weight. The smallest possible weight variations as R_1 is changed by ΔR_1 are illustrated by the dashed lines in Fig.9(a) for $\Delta R_1 \geq 0$ and $-\Delta R_1$ and may be expressed as

$$\Delta G_1 = \frac{1}{2} g \Delta R_1 \{-L(m) + h l_m + (h-l_m) l_{m+1}\}$$

$$\Delta G_2 = \frac{1}{2} g \Delta R_1 \{L(m) - (h-l_m)(l_m + l_{m+1}) + l_m^2\}$$

The necessary condition for the minimum weight is therefore given by

$$(h-l_m)(l_m+l_{m+1}) - l_m^2 \leq L(m) \leq h l_m + (h-l_m) l_{m+1}. \tag{24}$$

Variations of the moment diagram without any change in the Q_i-diagram may again be considered. The variations with respect to a simple downward translation of the moment diagram of the mth and $(m+1)$th chord members and to an upward translation of the diagram of the mth chord members lead to the following inequalities

$$l_m \leq h \leq l_m + l_{m+1}. \tag{25}$$

Since the necessary conditions have been obtained with respect to the restricted class of variations, the sufficiency must be proved by constructing a Foulkes mechanism.

In view of the moment diagram shown in Fig.9(a), the mechanism similar to the case Fig.8(c) is the only possible one. Since $\Omega_m = 2\psi = h\Theta > l_m\Theta$, Ω_m must be decreased. Ω_m can be decreased if the angles of rotation of the mth joints are decreased by ψ_m and simultaneously an additional upward displacement δ_m of the mth joints is considered as shown in Fig.9(b) This modification is permissible since the apparent decrease of the plastic hinge rotation in the mth vertical member with $\overline{B}_m = 0$ can be compensated by considering an arbitrary plastic hinge within the member. It may then be readily shown that the Foulkes condition can be satisfied if

$$\psi_m = (h-l_m)\theta \geq 0 \quad \text{and} \quad \delta_m = \frac{1}{2}(h-l_m)l_{m+1}\theta \geq 0. \tag{26}$$

Since all the hinge rotations must be non-negative, the following inequalities must be satisfied in view of Fig.9(b).

$$\psi-\omega+\delta_m/l_m \geq 0, \quad \psi-\psi_m+\omega-\delta_m/l_m \geq 0, \quad \theta_{m+1}-\delta_m/l_{m+1} \geq 0, \quad \theta_{m+1}-\delta_m/l_{m+1}+\psi_m \geq 0 \tag{27a-d}$$

(27a,b) and (27c,d) together with (26) may be shown to be reduced to (24) and (25), respectively. The existence of the subspan index m satisfying (24) and (25) for a given frame is the necessary and sufficient condition for the Design-II belonging to m to be the minimum weight design.

Design-III

A different minimizing shear diagram must be sought for a frame for which there does not exist the index m satisfying (15) and (17) or (24) and (25) It should be pointed out here that both Design-I and Design-II have included a member whose plastic moment is zero. The plastic moment of the mth vertical member may be zero not only in the case of Design-II but also if $M_m+M_{m+1}=0$ and hence if $Q_m l_m+Q_{m+1}l_{m+1}=0$. The corresponding shear force diagram to this case crosses the zero line at the position of the joint m. This condition determines the shear force diagram and the frame moment uniquely. Variation of the moment diagram depend upon whether $h \gtreqless l_m$ and $h \gtreqless l_{m+1}$ as indicated in Fig.10(a) and (b) by dashed lines for $\Delta R_1 > 0$ and for $-\Delta R_1$; respectively. If this moment diagram is to render the minimum weight, the necessary conditions may be written as

$$L(m) \geq l_m^2 \qquad \text{if } h \leq l_m$$

$$L(m) \geq h(l_m+l_{m+1})-l_m l_{m+1} \qquad \text{if } h \geq l_m$$

$$L(m) \leq h(l_m+l_{m+1})+l_m^2 \qquad \text{if } h \leq l_{m+1}$$

$$L(m) \leq l_{m+1}(l_m+l_{m+1})+l_m^2 \qquad \text{if } h \geq l_{m+1}. \tag{28a-d}$$

The collapse mechanism corresponding to the moment diagram shown in Fig.10 (a) and (b) must be similar to that shown in Fig.8(b) Since $\Omega_m = 2\omega = L(m)\theta/l_m \geq l_m\theta$, from (28a,b), however, Ω_m must be decreased With this motivation, the mechanism shown in Fig.10(c) may be considered in which the angle of rotation

of the mth joints has been decreased by ψ_m and simultaneously an additional upward displacement δ_m of the mth joint has been considered. These quantities may be so determined that the Foulkes condition is satisfied.

$$\delta_m = \frac{l_m l_{m+1}(\omega - \frac{1}{2}l_m\theta)}{l_m + l_{m+1}} \geq 0, \qquad \psi_m = \frac{2l_m(\omega - \frac{1}{2}l_m\theta)}{l_m + l_{m+1}} \geq 0. \tag{29}$$

It may readily be confirmed that the conditions of non-negative rotations on the four plastic hinges shown in Fig.10(c) and $\psi - \psi_m \geq -\frac{1}{2}h\theta$ are equivalent to the four inequalities (28a-d). The existence of the index number m satisfying (28a-d) is therefore the necessary and sufficient condition for Design-III to be the minimum weight design.

Design-IV

Design-II and Design-III have included respectively one vertical member whose plastic moment is zero. It is natural then to look for a design such that the plastic moments of two vertical members, say the $(m-1)$th and mth, are zero and such that, except in the mth subspan, the moment distribution is described by the frame moments. This condition determines the Q_i-diagram and the corresponding moment diagram uniquely as shown in Fig.11(a).

$$Q_m = \frac{l_{m+1}P_m - l_{m-1}P_{m-1}}{l_{m-1} + 2l_m + l_{m+1}}, \qquad Q_{m-1} = Q_m + P_{m-1}, \qquad Q_{m+1} = Q_m - P_m, \text{ etc} \tag{30}$$

The dashed lines in Fig.11(a) show two of the four possible variations of the moment diagram resulting in the smallest weight changes, one for $\Delta R_1 > 0$ and the other $-\Delta R_1$. It may be shown that, if this moment diagram is to correspond to the minimum weight design for a frame, the shape function must be within the following region.

$$L(m) \leq (h - l_m)(l_m + l_{m+1}) - l_m^2 \qquad \text{if } l_m + l_{m+1} \geq h$$

$$L(m) \leq l_{m+1}(l_{m-1} + 2l_m + l_{m+1}) + l_m l_{m-1} - h(l_{m-1} + l_m) \qquad \text{if } l_m + l_{m+1} \leq h$$

$$L(m) \geq -h(l_{m-1} + l_m) + l_{m-1} l_m \qquad \text{if } l_{m-1} + l_m \geq h$$

$$L(m) \geq (h - l_m)(l_m + l_{m+1}) - l_m^2 - l_{m-1}(l_{m-1} + 2l_m + l_{m+1}) \qquad \text{if } l_{m-1} + l_m \leq h. \tag{31a-d}$$

Figure 11(b) shows the corresponding Foulkes mechanism in which

$$\psi_m = \frac{-L(m)+l_{m-1}l_m+h(l_{m+1}-l_{m-1})/2}{l_{m-1}+2l_m+l_{m+1}}\,\theta, \qquad \psi_{m-1} = l_m\theta-\psi_m$$

$$2\theta_{m-1} = l_{m-1}\theta-(\psi-\psi_{m-1}), \quad 2\theta_{m+1} = l_{m+1}\theta-(\psi-\psi_m), \quad \psi = \tfrac{1}{2}h\theta \qquad (32a\text{-}e)$$

$$\psi_m \leq \psi, \quad \psi_{m-1} \leq \psi. \qquad (33)$$

The two conditions (33) are necessary for the two vertical members to satisfy the Foulkes condition and may be shown to be reduced to (31a,b), respectively. The conditions of non-negative hinge rotations: $\theta_{m-1} \geq 0$ and $\theta_{m+1} \geq 0$ are on the other hand reduced to (31c,d), respectively. It may therefore be concluded that the existence of the index m satisfying the inequalities (31) for a frame is the necessary and sufficient condition for the Design-IV to be the minimum weight design for the frame when $Q_m \leq 0$.

It is apparent that the foregoing procedures of constructing the minimum weight designs may be extended and continued to those frames which have not been covered here.

5.EXAMPLES

Consider a class of frames with equal subspan length l and with h=1.5l. The shape function $L(m)$ may readily be obtained as follows:

$L(m) = (l+h)l$ or $-(l+h)l$ if f is even, and

$L(m) = 0$ if f is odd.

Figure 12 shows the regions of applicability of the four designs for the class of frames with $l_{m-1} = l_m = l_{m+1}$. For a frame with an even number of equal subspans the line $\omega = (l+h)/2$ lies entirely within the region of Design-III as far as $0 \leq h \leq 2l$. For a frame with an odd number of equal subspans, the line $\omega = 0$ lies within the regions of Design-I, -II or -IV depending whether $h \leq l$, $l \leq h \leq 3l/2$ or $3l/2 \leq h \leq 5l/2$, respectively. The two designs for $h = 1.5l$ are indicated by the two circles in Fig.12.

Figure 13 illustrated the two moment distributions at collapse for the two minimum weight designs of a Vierendeel frame, one for simply supported ends and the other for clamped ends. In observing the difference between the two designs, it should be noted that the cost of exerting the clamping forces and the effect of axial forces have not been taken into account here.

6. EFFECT OF AXIAL FORCES

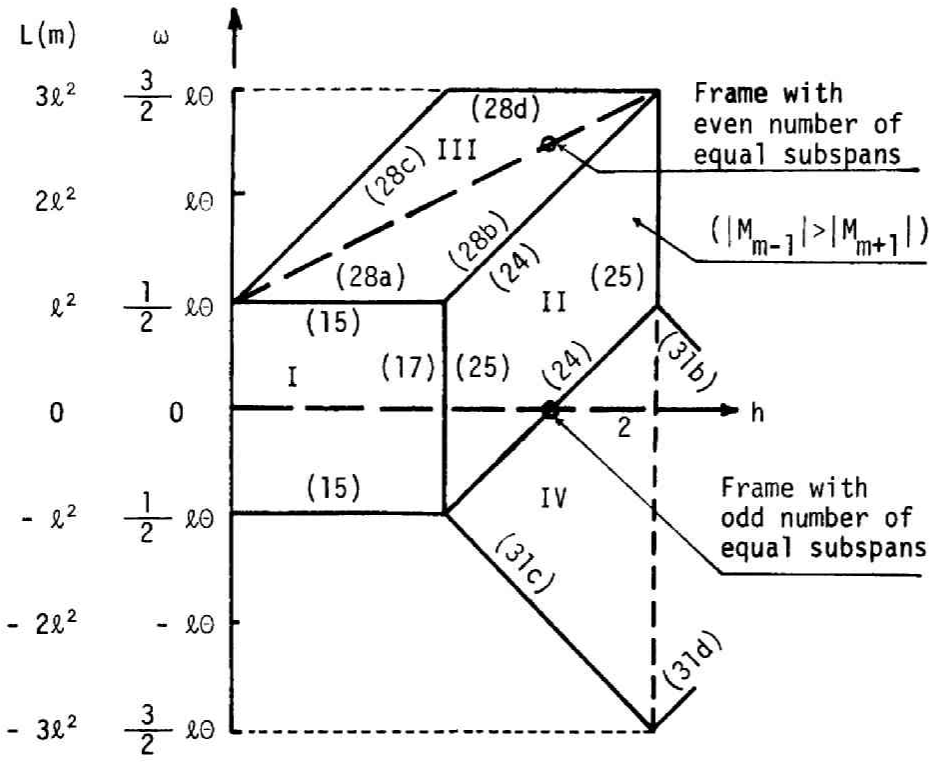
L(m)
ω
3ℓ²
2ℓ²
ℓ²
0
- ℓ²
- 2ℓ²
- 3ℓ²
3/2 ℓΘ
ℓΘ
1/2 ℓΘ
0
1/2 ℓΘ
- ℓΘ
3/2 ℓΘ
(28d)
(28c)
III
(28b)
(28a)
(24)
(25)
II
(15)
I
(17)
(25)
(24)
(31b)
h
2
(15)
IV
(31c)
(31d)
Frame with even number of equal subspans
(|M_{m-1}|>|M_{m+1}|)
Frame with odd number of equal subspans

Fig.12

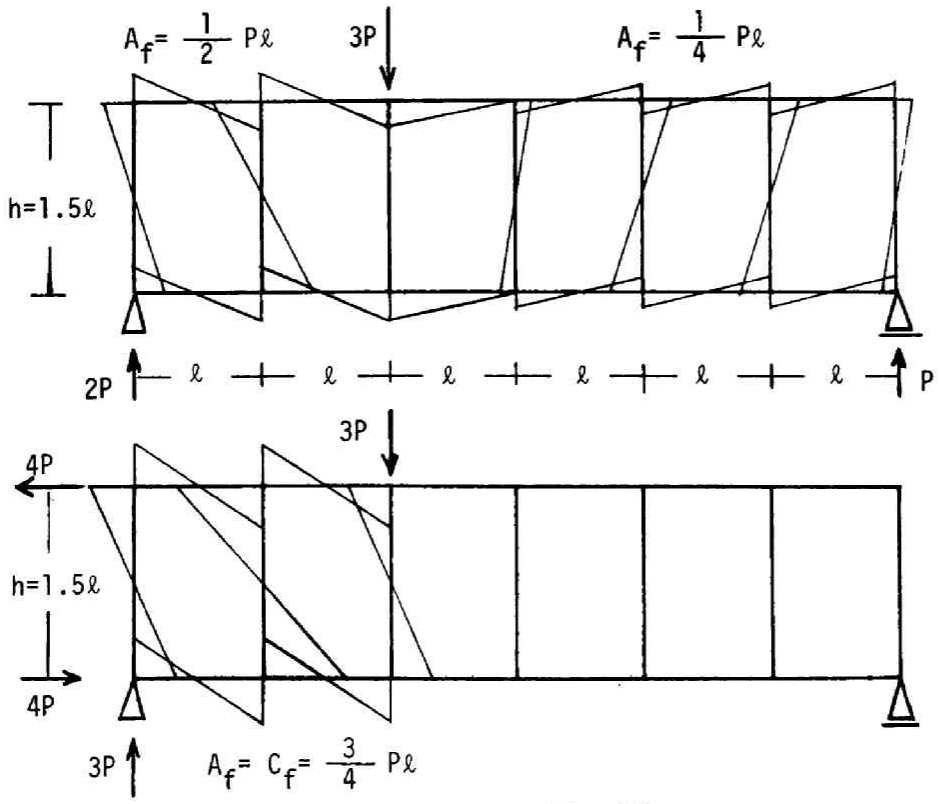
A_f= 1/2 Pℓ
3P
A_f= 1/4 Pℓ
h=1.5ℓ
2P
ℓ
ℓ
ℓ
ℓ
ℓ
ℓ
P
3P
4P
h=1.5ℓ
4P
3P
A_f= C_f= 3/4 Pℓ

Fig.13

More realistic designs may be obtained by modifying for the effect of axial forces the minimum weight designs which have been obtained in the preceding sections. The fully plastic moment M^P for a cross-section must be such that the axial force N and the bending moment M acting upon the section do not violate the interaction yield condition. For example, the yield condition for an idealized sandwich section may be represented by

$$\frac{M^{PN}}{M^P} \pm \frac{N}{N^P} \pm 1 = 0 \tag{34}$$

where M^{PN} and N^P denote the fully plastic moment under the presence of N and the fully plastic axial force under the absence of M, respectively. The plastic moments A_i, B_i and C_i obtained in the preceding sections are M^{PN} in equation (34) As soon as N_i associated with M_i^{PN} of a sandwich member is determined, M^P defining the section may be obtained from

$$M_i^P = M_i^{PN} + \frac{M_i^P}{N_i^P}|N_i| = M_i^{PN} + \frac{1}{2}H_i|N_i| \tag{35}$$

for a choice of the depth H_i of the sandwich section. The axial force distribution corresponding to the moment diagram at collapse of a simply supported frame may immediately be calculated by statics and therefore the modified design may be obtained uniquely [3].

For a clamped frame, however, the axial force distribution depends upon the remaining redundant reaction, i.e. the overall fixed end moment when the frame is regarded as a clamped-clamped beam as a whole. Consider as an example a frame in Design-I. One of the axial forces, say N_m of the mth lower chord member (m being the minimizing index in Design-I) may as well be taken as the redundant force. Then in view of the moment diagram shown in Fig.8(a), the axial force in the lower chord members at collapse may be expressed in terms of N_m as follows and is distributed as shown in Fig.14.

$$N_j = N_m - \frac{2}{h}\sum_{i=j}^{m-1}(M_i+M_{i+1}) \qquad 1 \le j \le m-1$$

$$N_k = N_m + \frac{2}{h}\sum_{i=m+1}^{k}(M_{i-1}+M_i) \qquad m+1 \le k \le f \tag{36}$$

The axial force in an upper chord member takes on the same magnitude as the corresponding lower chord member with the opposite sign. The axial force in the ith vertical member is simply given by $\frac{1}{2}P_i$. If the weight of the frame may a-

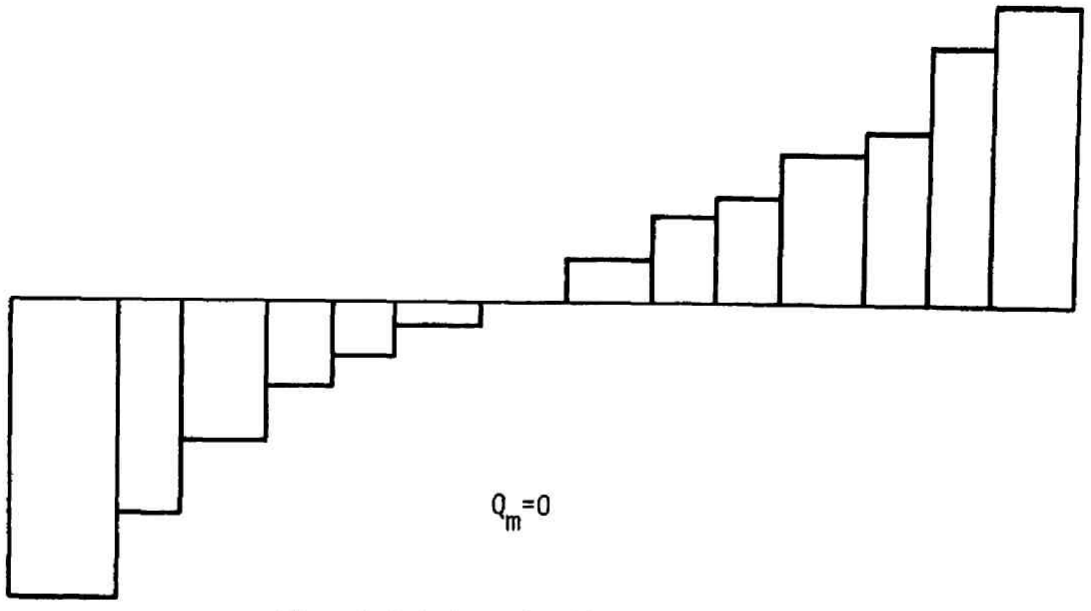

The minimizing Q_j-diagram for Design-I

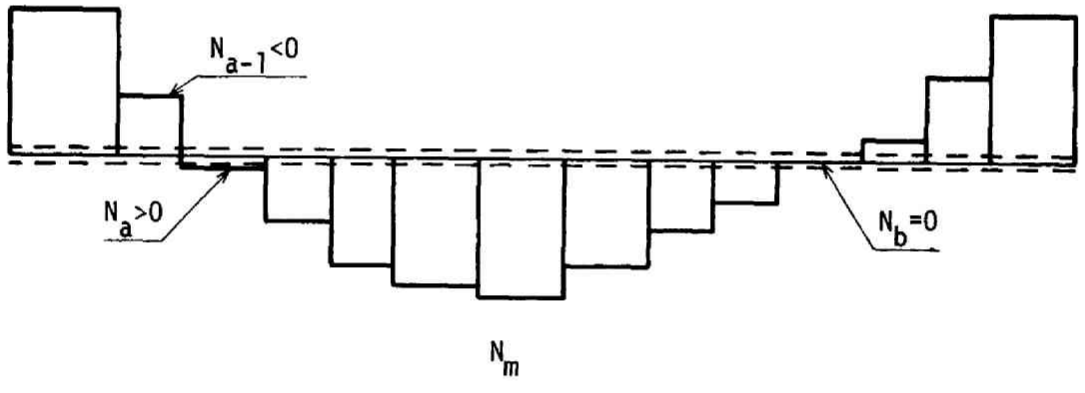

N_m

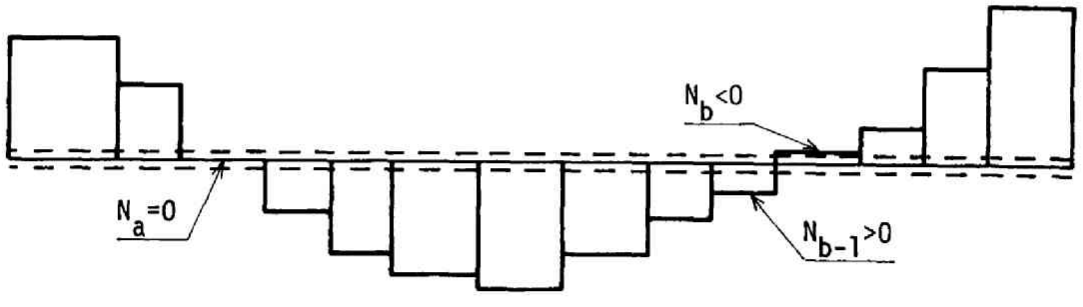

Axial Force Diagrams and their Variations

Fig.14

gain be assumed to be proportional to M^P, then N_m may be so determined, for a prescribed set of H_i's, as to minimize

$$g \sum M_i^P l_i = g\{ \sum M_i^{PN} l_i + \frac{1}{2} \sum H_i |N_i| l_i \} = G + G_{NC} + G_{NV} \tag{37}$$

where

$$G = g \sum M_i^{PN} l_i, \quad G_{NV} = g\left\{\frac{1}{2} n \sum_{s=0}^{f} P_s\right\}$$

$$G_{NC} = g\left\{ \sum_{j=1}^{m-1} H_j l_j |N_j| + H_m l_m |N_m| + \sum_{k=m+1}^{f} H_k l_k |N_k| \right\} \tag{38}$$

Since the minimum of G has already been achieved separately, it is reasonable to minimize G_{NC} alone with respect to N_m under the known set of frame moments, although the minimizations in the two separate steps may not necessarily provide the minimum of the modified weight as a whole. The minimum of G_{NC} may however be expected to provide a good upper bound on the minimum of the modified weight since the state of stress resultants so determined will satisfy all the equations of equilibrium, will determine a modified design just satisfying all the interaction yield conditions and hence may correspond again to an extremely deteriorated overcomplete collapse mechanism consisting of those plastic hinges which are governed by the plastic potential flow law associated with (34). It should be noted that the axial force diagram for chord members is of a staircase shape and coincide, when multiplied by h, with the overall moment diagram of the clamped-clamped beam only at the midspans of subspans. While Megarefs and Sidhu [4] are concerned with the minimum volume design of beams and frames with continuously varying cross-section, the present problem of modification is to minimize the absolute area of the axial force diagram of staircase shape weighted by H_r's with respect to one of the two redundant forces, or in other words, with respect to an up- or downward translation of the diagram. This is therefore quite similar to the previous problem of minimizing the absolute area of a subspan-shear diagram for G and the technique used in Section 4 may be applied, with the precaution that N_j and N_k are both monotonically nonincreasing from m toward 1 and f, respectively.

7. CONCLUSION

A general analytical method of constructing minimum weight designs has been proposed for Vierendeel frames. It has been shown that the new concept of the "frame moment" which has been introduced by Tanabashi and Nakamura [2] is useful and effective for understanding the overall beam character of a Vierendeel frame and for constructing its minimum weight design. It should be noted that the linear minimum weight design of an externally determinate Vierendeel frame is statically determinate without regard to its internal indeterminacy. The weight of an externally indeterminate frame has been minimized with respect to the external redundant forces. The four classes of designs obtained in simple and explicit analytical forms have sufficiently revealed the general intrinsic features of the linear minimum weight designs of clamped Vierendeel frames. The necessary and sufficient conditions for the minimum weight have been given in terms of the "shape function" introduced in the present paper. The minimum weight design of a clamped Vierendeel frame is almost generally such that each clamped end is to carry the vertical loads on those joints included in its respective half-span. It appears that this feature is essentially due to the circumstance that the cost of external supports has not been compared.

The present method is general enough to be extended to those clamped Vierendeel frames which have not been covered in this paper. The present approach and technique may also be applied in a fairly straightforward manner to continuous Vierendeel frames and other regular rectangular frames.

REFERENCES

[1] J. Foulkes, "The Minimum Weight Design of Structural Frames," Proc.Royal Soc., Vol.A223, pp482-494, 1954.

[2] Ryo Tanabashi and Tsuneyoshi Nakamura, "The Minimum Weight Design of a Class of Tall Multi-story Frames Subjected to Large Lateral Forces,I,II," Trans.Architectural Inst. Japan, No.118,pp10-18,Dec.1965 and No.119, pp37-44,Jan.1966. Also Proc.15th Japan Natn.Congr.Appl.Mech.,pp72-81,1965.

[3] Ryo Tanabashi and Tsuneyoshi Nakamura, "An Approach to the Last Hinge Point Design of Tall Multi-story Frames," Proc.Symposium on External Forces and Structural Design of HIgh-rise and Long-span Structures, Japan Soc.Promotion of Sciences, pp169-179, 1965.

[4] G. J. Megarefs and H. S. Sidhu,"Simplifications in Minimal Design of Frames," J.Structural Div.,Proc.ASCE, Vol94, pp2985-2998, 1968.

CHAPTER 5

ELASTIC-PLASTIC ANALYSIS OF TRUSSES AND FRAMES BY THE GRADIENT PROJECTION METHOD

1. INTRODUCTION

While the method of elastic-plastic hinge stiffness matrix (displacement method) is now well-known as has been referred to in chapter 2, it does not appear that an efficient stress method of elastic-plastic analysis of framed structures has been developed except the well-known superposition of elastic responses of successively deteriorating frames or trusses. In this chapter, the gradient projection method (GP) of nonlinear programming which has been developed by Rosen [4.5] is shown to be useful for a stress method approach to the elastic-plastic analysis. The gradient projection is a method of obtaining the global maximum of a nonlinear concave function in a convex region defined by linear or nonlinear constraints.

The geometrical representation of a state of stress given by Prager enables one to represent a change of state of stress in a truss as an infinitesimal vector in a convex yield polyhedron defined in a stress space. The minimum principle of Greenberg [1] is interpreted in this geometrical context. A more precise proof than that given in [8] is proposed for the equivalence theorem stating that the infinitesimal response vector obtained by use of the minimum principle is identical with that described by the maximization process of the gradient projection method, provided that the objective function is so chosen that the gradient vector always coincides with the direction determined by the increments of the load factors. The equivalence proof establishes the basis for the application of the computational method. The technique is first illustrated for a simple three-bar truss.

The method is then shown to be applicable to frames without modification. If the prescribed loading path is piecewise linear, the number of maximization steps is equal to the number of segments of the path, regardless

---

The present chapter is based partly upon "ELASTIC-PLASTIC ANALYSIS OF TRUSSES BY THE GRADIENT PROJECTION METHOD" by the author and J.B.Rosen, Technical Report CS11, July 17, 1964, Computer Science Division, Stanford University. (Ref.[8])

of the degrees of redundancy of a frame or a truss. It is shown that shake-down problems can be investigated readily if a loading cycle is prescribed or if it can be assumed that all the variations of the applied loads are bounded by a polyhedron or by a parallelopiped. A closed convex "safe load domain" defined by a set of all the load carrying capacities may be obtained by the GP procedure.

2. GEOMETRICAL REPRESENTATION OF STATE OF STRESS

The geometrical representation of a state of stress as given by Prager [2, 3] is introduced here in a generalized form to prepare for the ensuing discussion.

An ideal stable plane truss is composed of n bars of elastic-perfectly-plastic materials. It is assumed that the rates of settlement of the supports are all zero. Let f be the number of reactions and h the number of joints. Suppose there are s sets of loads characterized by s independent load factors $\{x_i\}$ in the form

$$\{x_1 P_{1\ell}\},\{x_2 P_{2\ell}\}, \cdots\cdots, \{x_s P_{s\ell}\} \qquad (\ell=1,2,\cdots\cdots, h) \tag{1}$$

acting upon the given ideal truss. Then the equations of equilibrium form an inhomogeneous system of linear algebraic equations of the form

$$\sum_{k=1}^{n+f} a_{\ell k} S_k = \sum_{i=1}^{s} x_i b_{i\ell} \qquad (\ell=1,2, \cdots\cdots, 2h) \tag{2}$$

where $s_1, s_2, \cdots\cdots, s_n$ denote the internal forces in the bars, $S_{n+1}, \cdots\cdots, S_{n+f}$, the reactions at supports and $b_{i\ell}, P_{i\ell}$ multiplied by a direction cosine. The coefficients $a_{\ell k}$ are essentially the direction cosines of the kth bar. Unknown quantities are $\{S_k\}$ $(k=1,2, \cdots, n+f)$.

If $n+f-2h \equiv r>0$, then the set $\{S_k\}$ is not uniquely determined by (2) and the truss has r degrees of redundancy. Let

$$\{S_{1j}\},\{S_{2j}\},\cdots\cdots,\{S_{sj}\}$$

by a set of s particular solutions of the s inhomogeneous systems the ith of which is obtained by replacing the right-hand side of (2) by the ith inhomogeneous term $\{b_{i\ell}\}$ and

$$\{R_{1j}\},\{R_{2j}\},\cdots\cdots,\{R_{rj}\},$$

a set of r linearly independent solutions of the homogeneous equation obtained

from (2). Although (2) cannot have a unique solution, any solution of (2) must be contained in the general solution given by a linear combination of s linearly independent particular solutions $\{S_{ij}\}$ and r linearly independent solutions $\{R_{kj}\}$ of the homogeneous system obtained from (2).

$$S_j = \sum_{i=1}^{s} x_i S_{ij} + \sum_{k=1}^{r} x_{s+k} R_{kj} \qquad (3)$$
$$(j=1,2,\cdots,n+f)$$

where x_{s+k}'s are arbitrary parameters. The particular solution $\{S_{ij}\}$ can be obtained by imposing r additional conditions on deformation that the truss responds elastically under the particular set of loads $\{b_i\}$ $(\ell=1,2,\cdots\cdots,2h)$ Thus $\{S_{ij}\}$ represents an elastic state of stress. $\{R_{kj}\}$ is obtained by considering the statically determinate structure which can be produced by replacing r redundant forces by a set of known forces. $\{R_{kj}\}$ then represents a state of self-stress.

It is always possible [2] by forming linear combinations of $\{S_{ij}\}$ or $\{R_{kj}\}$ to construct an orthonormal set of $(s+r)$ solutions in the sense

$$\frac{1}{2}\sum_{j=1}^{n} \alpha_j S_{kj} S_{ij} = \delta_{ki}$$

$$\frac{1}{2}\sum_{j=1}^{n} \alpha_j S_{ij} R_{\ell j} = 0 \qquad (4)$$

$$\frac{1}{2}\sum_{j=1}^{n} \alpha_j R_{\ell j} R_{mj} = \delta_{\ell m}$$

$$(k,i=1,2,\cdots\cdots,s; \qquad \ell,m=1,2,\ \cdots,r)$$

where $\alpha_j = \dfrac{\ell_j}{E_j A_j}$, ℓ_j denoting the length of bar j, A_j its cross-section and E_j its elastic modulus, and where δ_{ki} and $\delta_{\ell m}$ are Kronecker delta's. It is to be understood in the following that $\{S_{ij}\}$ and $\{R_{kj}\}$ denote elements of this orthonormalized set where j varies from 1 to n. The original load factors can then be expressed by linear combinations of the x_i's for this orthonormalized set.

The elastic strain energy corresponding to the set of internal forces $\{S_j\}$ given by (3) is defined by

$$\epsilon = \frac{1}{2}\sum_{j=1}^{n} \alpha_j S_j^2$$

$$= \frac{1}{2} \sum_{j=1}^{n} \alpha_j \left[\sum_{i=1}^{s} x_i S_{ij} + \sum_{k=1}^{r} x_{s+k} R_{kj} \right]^2 \tag{5}$$

By virtue of the orthonormality (4),(5) is reduced to

$$\epsilon = \sum_{i=1}^{s} x_i^2 + \sum_{k=1}^{r} x_{s+k}^2 \tag{6}$$

With this preparation, we can now make use of the concept of "stress space." Any solution $\{S_j\}$, and the corresponding strain energy, is completely determined by the set of parameters

$$(x_1, x_2, \cdots, x_s; \quad x_{s+1}, \quad \cdots, x_{s+r}) \tag{7}$$

as shown by (3) and (6). If we consider an $(s+r)$-dimensional stress space whose Cartesian coordinates are $(x_1, x_2, \cdots\cdots, x_s, x_{s+1}, \cdots\cdots, x_{s+r})$, then any state of stress of the truss can be represented by a point in this space. Any state of loading is then represented by the set $(x_1, x_2, \cdots\cdots, x_s)$ while any state of residual stress by $(x_{s+1}, x_{s+2}, \cdots\cdots, x_{s+r})$.

Since all the bars are assumed to be composed of perfectly-plastic materials, the corresponding yield conditions must be satisfied. The condition that the stress in any bar should not exceed the yield limit can be written as

$$c_j \leq \sum_{i=1}^{s} x_i S_{ij} + \sum_{k=1}^{r} x_{s+k} R_{kj} \leq t_j \tag{8}$$

$$(j=1,2,\cdots\cdots,n)$$

where c_j and t_j denote the yield limits of bar j in compression and in tension, respectively. Each one of the n inequalities in (8) defines a strip between two hyperplanes. The set of all the inequalities define a convex polyhedron in $(s+r)$-dimensional stress space as the common region of all the yield strips. Therefore, only the set of points on or inside the yield polyhedron can represent actual states of stress.

3. GEOMETRICAL INTERPRETATION OF THE MINIMUM PRINCIPLE.

The minimum principle of Greenberg [1] is expressed in the geometrical terms according to Prager [3] to prepare for the later use in Section 4.

In order to obtain the response of a given truss to a particular loading program, $(s-1)$ relations between s load factors must be prescribed resulting in a "loading path" in the s dimensional load factor subspace.

Let a vector

$$dq = (dx_1, dx_2, \cdots, dx_s)$$

define a set of infinitesimal changes of load factors from an instantaneous state of loading $(x_1, x_2, \cdots, x_s)$, dq being a tangent vector to the loading path. Corresponding to this change is an infinitesimal translational displacement of the r-dimensional subspace of equilibrium. The corresponding new state of stress must be represented by a point in this displaced subspace of equilibrium. If we consider a local coordinate axis q in the direction of dq at a stress point denoted by

$$\mathrm{X} = (x_1, x_2, \cdots, x_s; \quad x_{s+1}, \cdots, x_{s+r})$$

and an $(r+1)$-dimensional cross-section of the yield polyhedron spanned by q, $x_{s+1}, \cdots, x_{s+r}$ axes, then any stress change due to dq can be represented by a vector

$$d\mathrm{X} = (dq, dx_{s+1}, \cdots, dx_{s+r})$$

where $dx_{s+1}, \cdots, dx_{s+r}$ denote the variations in $x_{s+1}, \cdots, x_{s+r}$ corresponding to dq respectively. The problem is then to determine $d\mathrm{X}$ which does not violate the yield conditions (8)

The stress rate intensity may be written as

$$\begin{aligned} \Delta\varepsilon &= dq^2 + dx_{s+1}^2 + \cdots + dx_{s+r}^2 \\ &= \|d\mathrm{X}\|^2 \end{aligned} \tag{9}$$

Since the new stress point must lie in the displaced subspace of equilibrium and in the yield polyhedron, a vector $d\mathrm{X}$ is said to be admissible if the point $\mathrm{X}+d\mathrm{X}$ is in the displaced hyperplane of equilibrium bounded by the yield polyhedron. Admissible vectors form a family any one of which can represent an admissible stress change. The minimum principle can be stated as follows: For a given dq, the actual stress change is given by the vector which minimizes the absolute value of $d\mathrm{X}$ among all the admissible vectors. In other words, we wish to obtain the shortest distance from an initial point to the intersection of the equilibrium hyperplane and the yield polyhedron.

It may be helpful to consider a two-dimensional illustrative example. A truss consisting of three bars shown in Figure 1 is subjected to a vertical varying load P. Let the internal forces transmitted by the

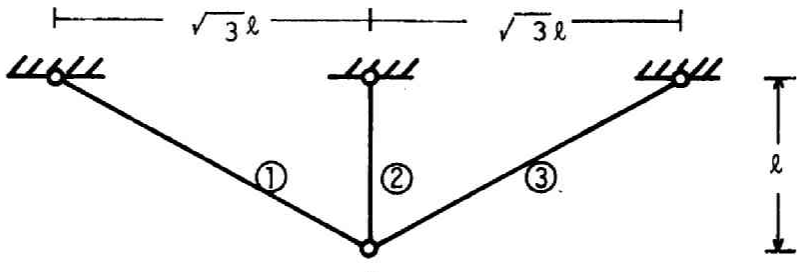

Fig.1(a) Three-bar truss.

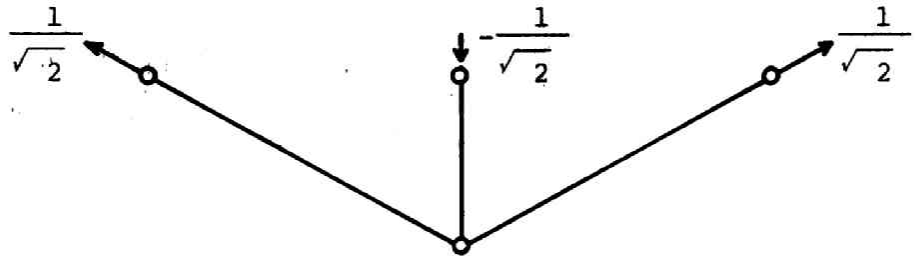

Fig.1(b) State of self-stress.

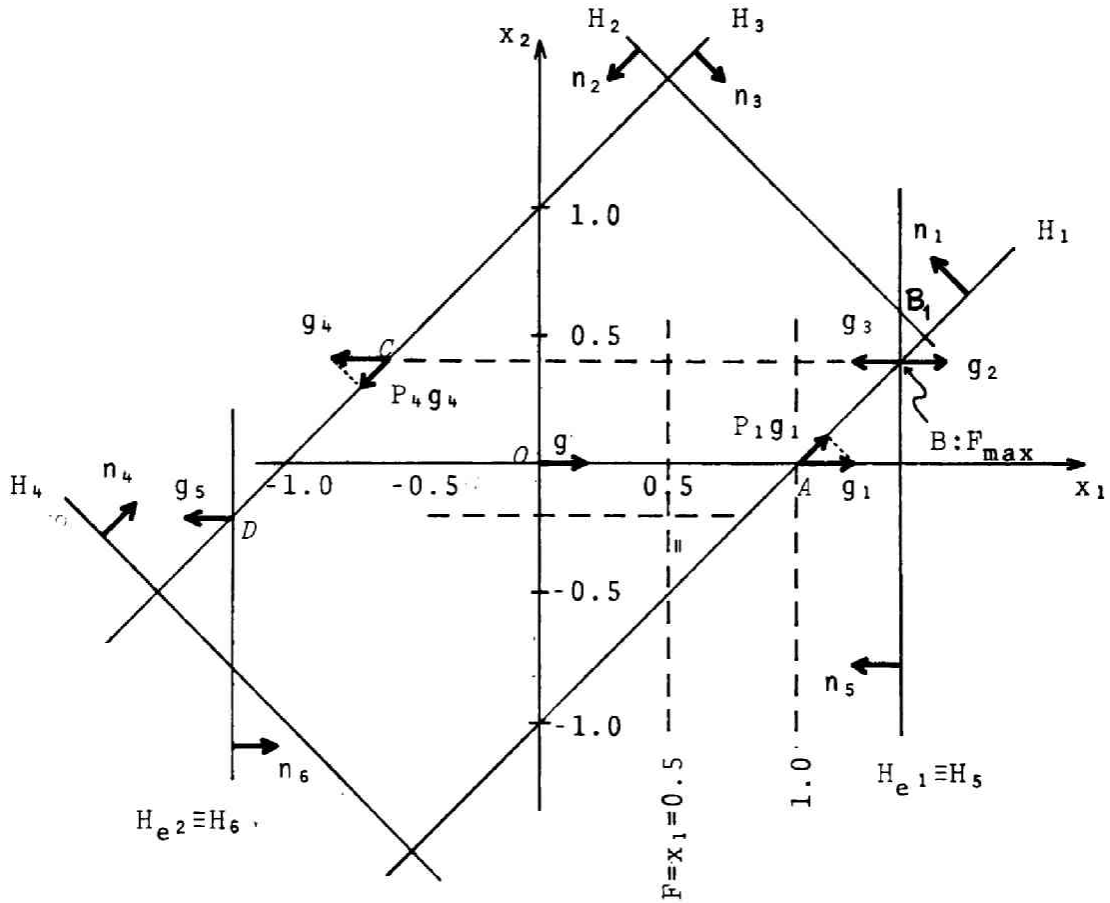

Fig.2 The yield polygon.

bars 1 (or 3) and 2 be S_1 and S_2, and $2\ell_1/A_1E=\ell_2/A_2E$.

The equation of equilibrium is written as

$$S_1 + S_2 = P \tag{10}$$

and the compatibility equation

$$2S_2 = 2S_1 \tag{11}$$

The solution of (10) and (11) is

$$S_1 = \frac{P}{2}, \quad S_2 = \frac{P}{2}$$

the normalized set is

$$\{S_{11}, S_{12}\} = \{\frac{1}{\sqrt{2}}, \frac{1}{\sqrt{2}}\} \tag{12}$$

The state of self-stress is shown in Figure 2. The normalized set is given by

$$\{R_{11}, R_{12}\} = \{\frac{1}{\sqrt{2}}, -\frac{1}{\sqrt{2}}\} \tag{13}$$

Thus a typical state of stress can be written

$$\begin{aligned} S_1 &= \frac{x_1}{\sqrt{2}} + \frac{x_2}{\sqrt{2}} \\ S_2 &= \frac{x_1}{\sqrt{2}} - \frac{x_2}{\sqrt{2}} \end{aligned} \tag{14}$$

For the sake of simlicity, let the yield limits of the bars 1(3) and 2 be $\pm\sqrt{2}$ and $\pm\frac{1}{\sqrt{2}}$ respectively Then the yield conditions are

$$\left.\begin{aligned} -2 < x_1 + x_2 \leq 2 \\ -1 \leq x_1 - x_2 \leq 1 \end{aligned}\right\} \tag{15}$$

Figure 2 shows the yield polygon defined by the four straight lines of (15) The dashed lines x_1=constant represent lines of equilibrium.

Consider a loading program: x_1=0 → 1.4 As the load factor x_1 is increased and hence the line of equilibrium x_1=constant is displaced, the stress point moves from O toward A. As soon as the stress point hits the yield line H_1, the subsequent response cannot be along the x_1-axis in order not to violate the yield condition. If, for instance, the load increment from A is 0.4, the equilibrium line located at x_1=1.4 is bounded by the yield line H_1 and H_2 as indicated in Figure 2 by $\overline{BB_1}$. A line which connects A and any point on the line segment $\overline{BB_1}$ represents an admissible vector. The problem of response analysis at this stage is then to find the vector which has the minimum absolute value among all the admissible vectors.

4. APPLICATION OF THE GRADIENT PROJECTION METHOD

The problem of incremental response analysis described in geometrical terms in the preceding sections can be solved numerically by the gradient projection method (GP). The applicability of the method is based essentially on the fact that, in GP the global maximum is sought by cutting across the interior of the convex region of definition, if possible. The stress change dx determined by the minimum peinciple stated above exactly coincides with the vector determined by GP. provided that the objective function F is chosen so that the gradient vector is always in the di ection of the tangent to a prescribed loading path.

Suppose if a stress point x lies in an intersection Γ of γ yield hyperplanes $\{H_i\}$ Corresponding to each hyperplane H_i, a unit vector n_i is defined

$$n_i \equiv \{n_{i1}, n_{i2}, \cdots\cdots, n_{im}\}$$
$$(m=r+1,\ i=1,\ \cdots\cdots,\gamma)$$

which is orthogonal to H_i and is directed so that it points "into" the region bounded by $\{H_i\}$. It is convenient to write the desired stress change dx in the form $dx=y\ dq$ by considering a local coordinate system at x. The convex cone defined by the γ yield hyperplanes can be written as

$$N_\gamma^T\ y \geq 0 \qquad (16)$$

where

$$N_\gamma \equiv [n_1, n_2, \cdots\cdots, n_\gamma]$$

The remaining yield inequalities can be written as

$$N_\beta^T\ y - b_\beta \geq 0 \qquad (17)$$

Let g be a unit normal vector from x to the displaced hyperplane of equilibrium H_e.

The problem of incremental response analysis defined by the minimum principle can be stated as that of finding a vector y which satisfies the following quadratic programming problem

$$min\ \{y^T y \mid N_\gamma^T y \geq 0\ ,\quad N_\beta^T y \quad b_\beta \geq 0\ ,\quad g^T y = 1\} \qquad (18)$$

This problem can be solved by the gradient projection method provided that the objective function F is so chosen that

$$\text{grad}F = g \quad \text{at} \quad x. \tag{19}$$

Let the finite set $\{N_j\}$ represent all the submatrices which can be formed with linearly independent columns of N_γ. Because of the choice of the linearly independent columns of N_γ, the $j \times j$ symmetric matrix $N_j^T N_j$ is non-singular. The $m \times m$ matrix

$$P_j \equiv I - N_j (N_j^T N_j)^{-1} N_j^T \tag{20}$$

which takes any m-dimensional vector into the space orthogonal to that spanned by the columns of N_j, can be formed and is called a "*projection matrix*". Let $P=\{P_j, I\}$ be the finite set of all P_j and the $m \times m$ identity matrix. The gradient projection algorithm will form the projection matrix $P_\ell \in P$, such that

$$|P_\ell g| = \max_{P_j \in P} \{|P_j g| \mid N_\gamma^T P_j g \geq 0\} \tag{21}$$

as shown by Rosen in [4] and [5]. It has been shown that an appropriate basis change is made whenever such a change will increase the norm of the projected gradient, subject to the feasibility restriction.

The equivalence theorem can now be stated in the form given by Rosen [8].

EQUIVALENCE THEOREM

If $P_\ell g$ is the solution of (21), then $y=\alpha P_\ell g$ is the solution of (18), where $\alpha>0$ is a scalar.

The proof given by Rosen in [8] is not complete and must be supplemented as follows:*

PROOF It is first shown in accordance with Rosen [8] that the maximization process of the problem (21) corresponds to the minimization process of the problem (18). Consider a set of $y_j=\alpha_j P_j g$ for all the possible projection matrices $P_j \in P$. In order to satisfy $g^T y=1$,

$$\alpha_j g^T P_j g = \alpha_j |P_j g|^2 = 1 \quad \text{or} \quad \alpha_j = |P_j g|^{-2}$$

Then $y^T y=|P_j g|^{-2}$ Hence if $|P_\ell g|=\max|P_j g|$, $P_j \in P$, then

$$y \equiv \frac{P_\ell g}{|P_\ell g|^2} \tag{22}$$

---

* This was proposed in a private communication from the author to J.B.Rosen (May 4, 1965) and admitted by him (July 7, 1965).

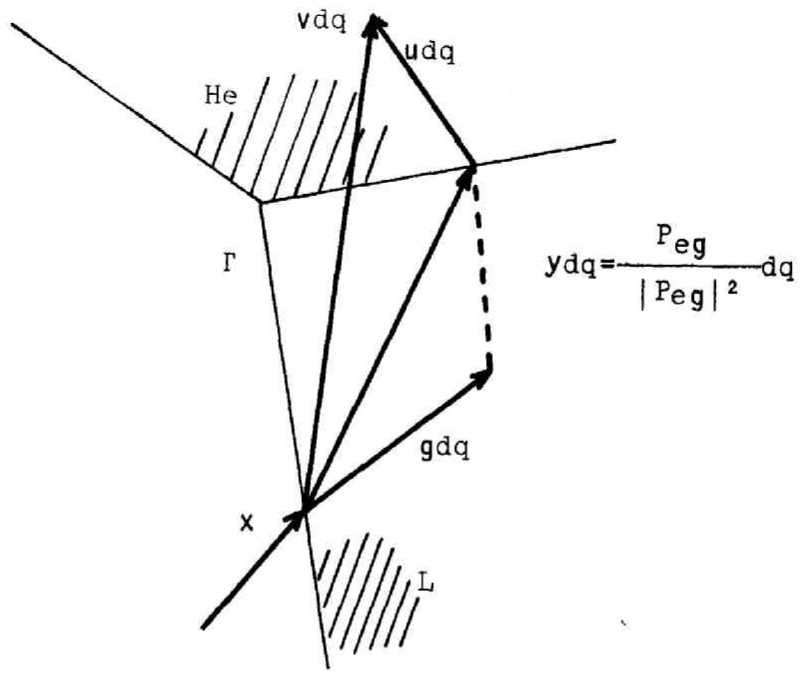

Fig.3 The minimizing vector.

gives a minimum in the problem (18).

If must still be shown that the vector y given by (22) is indeed the minimum among *all* the admissible vectors. Let u be any vector in H_e such that

$$v = y + u \tag{23}$$

will be in H_e bounded by all the yield hyperplanes as shown in Figure 3, *i.e*

$$N_\beta^T v - b_\beta \geq 0, \quad N_\gamma^T v \geq 0, \quad g^T v = 1$$

Since $g^T u=0$, it is evident that $g^T v=1$. A vector v is called an admissible vector. Apparently all the admissible vectors can be given by (23) as u exhausts all the points in H_e bounded by all the yield hyperplanes. The objective function of (18) can be written as

$$v^T v = |y|^2 + 2u^T y + |u|^2 \tag{24}$$

and is minimized with respect to u.

By lemma 3 of [4], $u^T n_k \geq 0$, $k=1,2,\cdots\cdots,\ell$. Furthermore g can be written as

$$g = P_\ell g + \sum_{k=1}^{\ell} \gamma_k n_k \tag{25}$$

Since $P_\ell g$ is the solution of (21), the basis actually selected for this step of the gradient projection procedure is such that all $\gamma_k \leq 0$. As has been indicated in [5], if for any basis being considered there is at least one $\gamma_q > 0$, then the vector n_q is dropped from the basis. This is continued until all $\gamma_k \leq 0$. If (25) is premultiplied by u^T and if $g^T u=0$ is used, the second term of (24) may be written as

$$u^T y = \frac{u^T P_\ell g}{|P_\ell g|^2} = \frac{1}{|P_\ell g|^2} \Sigma (-\gamma_k) u^T n_k \geq 0$$

Hence

$$v^T v \geq |y|^2 = \frac{1}{|P_\ell g|^2}$$

and y given by (22) is indeed the minimum among all the admissible vectors.

If the unit normal vector g to H_e is inside the yield polyhedron it is obvious that $g\,dq$ gives the desired minimum of (18), coinciding with the gradient vector since no constraints are active.

The gradient projection procedure of the incremental elastic-plastic analysis is now illustrated for the example of the three-bar truss in the

preceding section. The feasible region R is determined by the yield conditions (15) and the lines of equilibrium. Inward drawn unit vectors n_i (i= 1,2,$\cdots$,6) to the yield lines H_1,H_2,H_3,H_4,H_5,H_6, are shown in Figure 2. The objective function is $F=x_1$ whose contour lines are a family of equally-spaced parallel dotted lines which are the lines of equilibrium themselves.

Consider the loading and unloading process given by

$$x_1: \quad 0 \to 1.4 \to 0 \to -1.2 \to 0 \to 1.4 \tag{26}$$

The initial point is the origin with the gradient $|g|=1.0$. The largest permitted step length in the direction of g without leaving R is to H_1. The projection P_1g_1 is shown in the Figure 2, where P_1 is the corresponding projection matrix to H_1. Since $P_1g_1=(\frac{1}{2},\frac{1}{2})$ the new direction $z_1=P_1g_1/|P_1g_1|$ is $\overrightarrow{AB}$. The largest step length is to H_2 giving $g_2=g_0$ as shown. At this point B, the projection of g_2 on H_5 becomes zero because H_5 is one of the contour lines. Thus at B the maximum of $F=x_1$ is achieved first.
The computer describes exactly the path $\overrightarrow{OA}$, $\overrightarrow{AB}$, which represent the actual response of the truss. It should by noted that the computer stops at the point B where the maximum first achieved although there are an infinite number of points of maxima along H_5.

For the unloading process, x_1: 1.4→0→-1.2, the program must be started with the new initial point B. The corresponding mathematical problem is stated as follows:

Maximize $F=-x_1$
subject to the constraints $x_1 \geq -1.2$, $-x_1 \geq -1.4$ and (15) with the new initial point B.

Tables 1 & 2 show the results obtained by *GP*. They demonstrate that the actual response of the truss to the prescribed variation of x_1 is exactly traced by the computer within the round-off errors in the last digit.

5. MULTI-STORY FRAMES*

The elastic-plastic analysis by the gradient projection method is not restricted to trusses but can be extended to multi-story frames. For the sake of illustration, a symmetric multi-story frame of a single span is

---

* An abstract of this section was presented at 1962 Annual Meeting of A.I.J. (Kanazawa), Summaries of Technical Papers of 1962 Annual Meeting of A.I.J. P.56

Table 1. Response I. No shakedown.

X_1	X_2		Loading
0	0	0	+
1	0	A	Loading
1.40000000	0.39999997	B	
-0.60000002	0.39999997	C	-
-1.20000000	-0.19999997	D	Unloading
0.80000003	-0.19999997	E	+
1.40000000	0.39999997	B	Loading

Table 2. Response II. Shakedown.

X_1	X_2		Loading
0	0	0	+
1	0	A	Loading
1.40000000	0.39999997	B	
-0.59999999	0.39999997	C	Unloading
1.40000000	0.39999997	B	Loading
-0.59999999	0.39999997	C	Unloading

considered here. If the effect of axial forces and elongations can be neglected, a half of the frame has only to be considered where all the mid-points of the beams are supported by rollers. The degree of redundancy is therefore equal to the number of stories. Let r be the number of stories. Let the end moments be denoted by

$$M_1, M_2, \cdots, M_{3r}$$

as shown in Figure 4. If we write the equations of equilibrium in terms of these end moments, we obtain $2r$ linear algebraic equations for $3r$ unknowns; r equations of moment equilibriun about r joints and r sway equilibrium equations. In matrix form it may be written as

$$AM = x_1 B_1 + x_2 B_2 + \cdots + x_s B_s \tag{27}$$

where A is a $3r \times 2r$ matrix, M a column vector with $3r$ components and B_i a column vector with $2r$ components representing the inhomogeneous term due to the i-th set of external loads.

Owing to the redundancy of r degrees, the solution of (27) is not uniquely determined by (27) only, but any state of moment distribution must be a solution included in the general solution of (27) For the later use, the general solution of (27) is written as follows. Let M^{Ei} be a particular solution of the inhomogeneous system of (27) when $x_i=1$, and $x_1=x_2=\cdots\cdots=x_{i-1}=x_{i+1}=\cdots=x_s=0$. Let M^{R1}, M^{R2}, $\cdots$, M^{Rr} be any r linearly independent solutions of the homogeneous system obtained from (27). Then the general solution of (27) may be written as

$$M = \sum_{i=1}^{s} x_i M^{Ei} + \sum_{j=1}^{r} x_{s+j} M^{Rj} \tag{28}$$

where x_{s+1}, x_{s+2}, $\cdots$, x_{s+r} are arbitrary parameters to be determined later. Physically, M^{Rj} ($j=1,2,\cdots$,r) represents a state of self-stress or residual moment distribution, since there is no external force for these cases. The quantities M^{Ei} and M^{Rj} in Eq.(28) are all column vectors whose components are $3r$ end moments. If all the $3r$ end moments are known, the moment distribution is completely specified throughout the frame. Therefore Eq.(28) may also be interpreted as that representing a moment distribution throughout the frame where M, M^{Ei}, M^{Rj} are then functions of position along the members of the frame. Let z denote the independent variable representing the position.

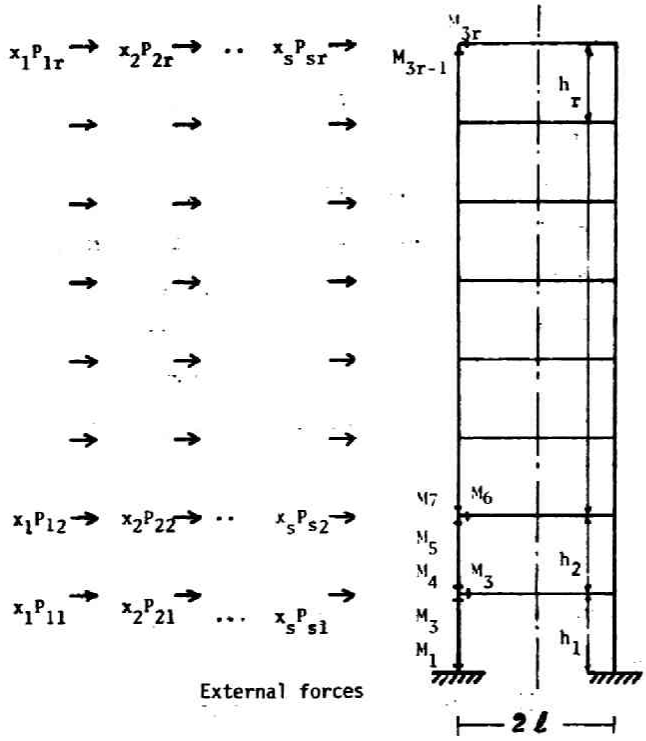

Fig.4 MULTISTORY FRAME OF ONE _SPAN

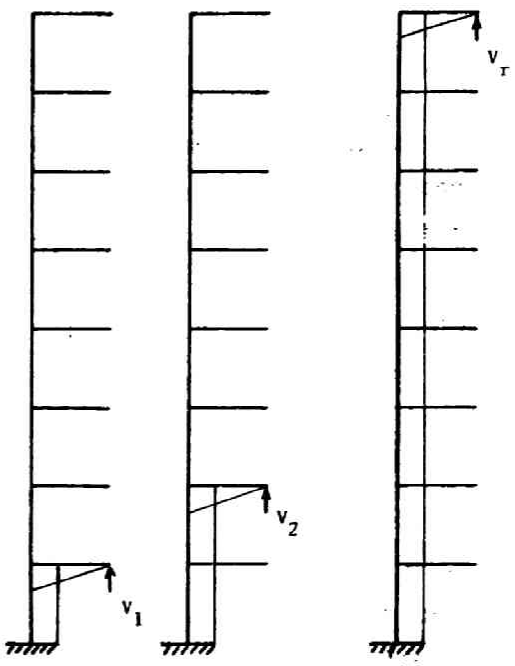

Fig.5 RESIDUAL MOMENT DISTRIBUTIONS

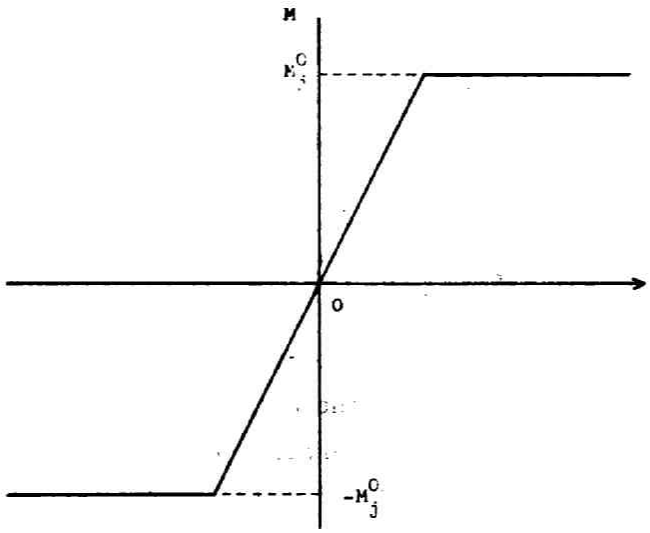

Fig.6 THE MOMENT CURVATURE DIAGRAM OF AN IDEALIZED CROSS-SECTION

In order to construct these states of residual moment distribution it is convenient to consider the statically determinate basic system by removing the r roller supports and then to apply r vertical forces one by one separately as shown in Figure 5. In the elastic analysis of the frame, these f forces may be regarded as redundant forces and the principle of virtual work may be applied on these moment distributions and the actual displacements of the original frame. Let M^{Li} denote the moment distribution in the basic determinate system due to the i-th set of external loads only. Then the corresponding M^{Ei} may be written as

$$M^{Ei} = M^{Li} + \sum_{j=1}^{f} x_{s+j} M^{Rj}$$

It is assumed that the rates of settlement of the supports are all zero. Then the virtual work of each vertical force on the displacements of the elastic moment distribution M^{Ei} vanishes. The equations of virtual work explicitly represent the orhtogonality relationships between M^{Ei} and M^{Rj} in the sense

$$\int \frac{M^{Ei}(z)M^{Rj}(z)}{EI}\, dz = 0 \quad (i=1,2,\cdots\cdots,s;\ \ j=1,2,\cdots\cdots,r) \tag{29}$$

where the integral is to be taken throughout the half frame.

In dealing with the stress rate intensity obtained from Eq.(28) later, the orthogonality between M^{Ei} and M^{Ek} $(i \neq k)$ and between M^{Rj} and M^{Rh} $(j \neq h)$ enables one to interpret the stress rate intensity in geometrical terms in a stress space. The residual moment distribution M^{Rj} is not in general orthogonal to any other M^{Rh} $(j \neq h)$. It is always possible to form an orthogonal set $\{\bar{M}^{Rj}\}$ from the original set $\{M^{Rj}\}$ in the following way.

$$\bar{M}^{Rj} = M^{Rj} - \sum_{t=1}^{j-1} \bar{M}^{Rt} \frac{\int \frac{M^{Rt} M^{Rj}}{EI}\, dy}{\int \frac{(\bar{M}^{Rt})^2}{EI}\, dy} \qquad (j=1,2,\cdots\cdots,r) \tag{30}$$

In a similar manner, it is also possible to form an orthogonal set $\{\bar{M}^{Ei}\}$ It should be noted however that each of the mutually orthogonal moment distributions would then be produced by certain linear combination of the original sets of external forces. Conversely therefore, the original sets of external forces may be represented by linear combinations of the sets of external forces corresponding to the orthogonal set.

The orthogonal set of moment distributions $\{\bar{M}^{Ei};\ \bar{M}^{Rj}\}$ is now

normalized in the following sense. A state of moment distribution with unit strain energy is called "standard". Each one of the n parameters of load factor type associated with M^{Ei} shall be so chosen that when it is unity, the corresponding moment distribution is standard. Similarly, the vertical forces at the roller supports are so chosen that each M^{Rj} is standardized. The orthonormal set of moment distributions is denoted by

$$\{m^{E1}, m^{E2}, \cdots\cdots, m^{Es}; \; m^{R1}, m^{R2}, \cdots\cdots, m^{Rr}\}$$

The orthonormality of this set may be compactly written as

$$\frac{1}{2}\int \frac{m^{Ei}\, m^{Ek}}{EI}\, dy = \delta_{ik}, \quad \frac{1}{2}\int \frac{m^{Ei}\, m^{Rj}}{EI}\, dy = 0, \quad \frac{1}{2}\int \frac{m^{Rj}\, m^{Rh}}{EI}\, dy = \delta_{jh}$$

where δ_{ik} and δ_{jh} denote Kronecher delta's. The $(s+r)$ parameters associated with this orthonormal set will again be denoted by $x_1, x_2, \cdots\cdots, x_{s+r}$ in the following. Any state of moment distribution may now be written as

$$M = \sum_{i=1}^{s} x_i\, m^{Ei} + \sum_{j=1}^{r} x_{s+j}\, m^{Rj} \tag{32}$$

The elastic strain energy corresponding to the moment distribution may then be represented as

$$\varepsilon = \frac{1}{2}\int \frac{(M)^2}{EI}\, dz = \sum_{i=1}^{s+r} x_i^{\,2} \tag{33}$$

by virtue of (31).

Once the orthonormal set $\{m^{Ei}; \; m^{Rj}\}$ is obtained for a frame, any moment distribution may be completely specified by the set of parameters $(x_1, x_2, \cdots\cdots, x_{s+r})$ as given by Eq.(32). This implies that if we consider an $(s+r)$-dimensional stress space whose Cartesian coordinates are $x_1, x_2, \cdots\cdots, x_{s+r}$, any moment distribution in the frame may be represented by a point in this stress space. The first n parameters are load factors and any state of loading may be defined by the set $(x_1, x_2, \cdots\cdots, x_s)$. Any loading path may then be conceived as a curve in this load factor subspace. The rest of the parameters $(x_{s+1}, \cdots\cdots, x_{s+r})$ define a state of residual moment distribution. The elastic strain energy ε is given by the square of the absolute value of the vector $(x_1, x_2, \cdots\cdots, x_{s+r})$

It is assumed that each member of the frame obeys the elastic-perfectly-plastic moment-curvature relationship as shown in Figure 6. If we denote the plastic moment of the j-th member by M_j^{ρ}, then the yield condition may be written as

$$-M_j^o \le M_j \le M_j^o \qquad (j=1,2,\cdots\cdots,2r) \tag{34}$$

where M_j is in general a function of position. In the present case, however, the possible hinge locations are, from the loading condition, the $3r$ ends of the $2r$ uniform members. It suffices therefore to write the yield inequalities only for these $3r$ end sections. Let $\mathbf{M}^o$ denote a column vector with $3r$ components representing the plastic moments of the $3r$ end sections. Then the yield inequalities may be written as

$$-\mathbf{M}^o \le \sum_{i=1}^{s} x_i \, \mathbf{m}^{Ei} + \sum_{j=1}^{r} x_{s+j} \, \mathbf{m}^{Rj} \le \mathbf{M}^o \tag{35}$$

where $\mathbf{m}^{Ei}$ and $\mathbf{m}^{Rj}$ are also column vectors of $3r$ elements, respectively. Geometrically, each one of the inequalities in (35) defines a strip between two hyperplanes in the stress space. The set of all the inequalities define a convex polyhedron as the common region of all the yield strips. Therefore any actual moment distribution must be represented by a point on or inside this yield polyhedron.

The remaining treatment of the problem is the same as for a truss. For a piecewisely linear loading path, the following linear programming problem in *GP* for the problem of incremental analysis may be formulated;

Maximize $F = \sum_{i=1}^{s} b_i \, x_i$

subject to the inequalities (35) and the bounds representing the length of a linear loading path.

As an example, the computational procedure and the numerical results are shown for a three-story frame of one span. The end moments and the bending stiffness ratios of the members are denoted as shown in Figure 7. The orthonormalized residual moment distributions $\mathbf{m}^{R1}$, $\mathbf{m}^{R2}$ and $\mathbf{m}^{R3}$ are shown in Figure 8. The end moments are as follows;

$$\mathbf{m}^{R1} = \begin{pmatrix} 0.894 \\ -0.894 \\ 0.894 \\ 0 \\ 0 \\ 0 \\ 0 \\ 0 \\ 0 \end{pmatrix} \quad \mathbf{m}^{R2} = \begin{pmatrix} 0.062 \\ -0.062 \\ -0.529 \\ 0.591 \\ -0.591 \\ 0.591 \\ 0 \\ 0 \\ 0 \end{pmatrix} \quad \mathbf{m}^{R3} = \begin{pmatrix} 0.018 \\ -0.018 \\ -0.073 \\ 0.091 \\ -0.091 \\ -0.299 \\ 0.414 \\ -0.414 \\ 0.414 \end{pmatrix}$$

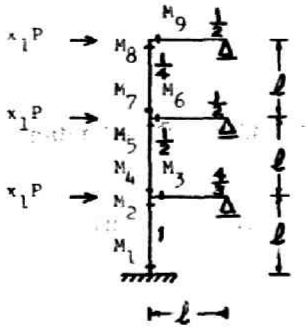

Fig.7 THREE-STORY FRAME

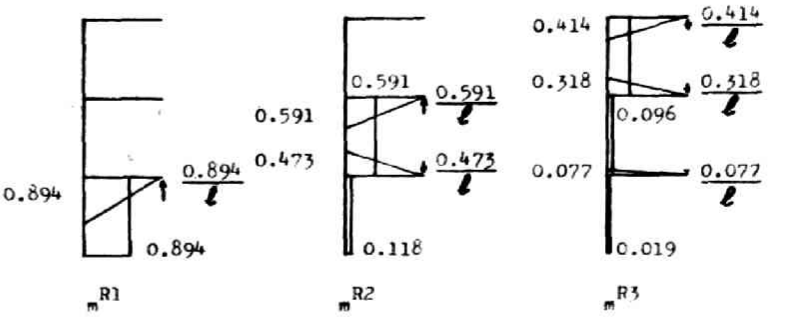

Fig.8 THE ORTHONORMAL SET OF RESIDUAL MOMENT DISTRIBUTIONS (Unit: $\sqrt{2EI_1/\ell}$)

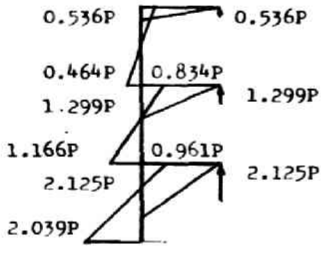

Fig.9a ELASTIC MOMENT DISTRIBUTION (x_1=1)

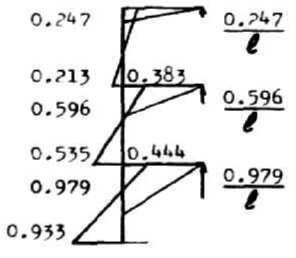

Fig.9b THE STANDARD ELASTIC MOMENT DISTRIBUTION (Unit: $\sqrt{2EI_1/\ell}$)

Table 3 ELASTIC-PLASTIC RESPONSE OF THE FRAME WITH THE PLASTIC MOMENTS M^{01}

Step	Hyperplanes added	x-vector x_1	x_2	x_3	x_4	F
0	(Initail)	0	0	0	0	0
1	H6	5.0000000	0	0	0	5.0000000
2	H12	5.0059617	- 0.0050713	0.0026831	0.0004366	5.0059617
3	H18	5.0289878	0.0357124	0.0105833	0.0189372	5.0289878
4	H1	5.1288566	- 0.2204569	- 0.1433572	- 0.0406463	5.1288566

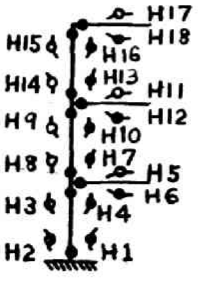

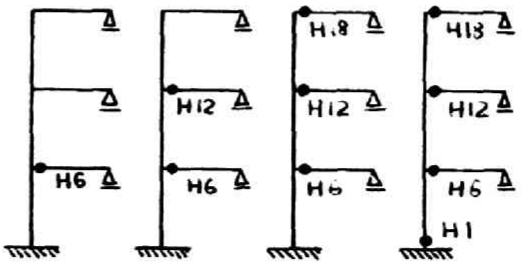

Fig.10

Since the elastic moment distribution may be written as

$$M^E = M^L + v_1\, \mathbb{m}^{R1} + v_2\, \mathbb{m}^{R2} + v_3\, \mathbb{m}^{R3}$$

where v_1, v_2, and v_3 are parameters representing the magnitudes of redundant forces, respectively. The equations of virtual work between the states of stress $\mathbb{m}^{Rj}$ and the j-th vertical force and the state of elastic deformation vanish, respectively. Figure 9a shows the elastic moment distribution. The corresponding standardized elastic moment distribution $\mathbb{m}^E$ is shown in Figure 9b. The corresponding set of end moments is

$$\mathbb{m}^E = \begin{pmatrix} -0.933 \\ -0.444 \\ 0.979 \\ -0.535 \\ -0.383 \\ 0.596 \\ -0.213 \\ -0.247 \\ 0.247 \end{pmatrix}$$

Any moment distribution may now be written as

$$M = x_1\, m^E + x_2\, m^{R1} + x_3\, m^{R2} + x_4\, m^{R3}$$

The plastic moments must next be prescribed. It should be noted that as far as the frame is in the elastic range starting from the virgin state, the parameters x_2, x_3 and x_4 are all zero and that it may readily be found which end moments reach their yield limits first. In order to illustrate two different cases, the plastic moments are prescribed in the following two ways.

$$\mathbb{M}^{O1} = \begin{pmatrix} 5.000 \\ 5.000 \\ 4.895 \\ 3.000 \\ 3.000 \\ 2.985 \\ 1.500 \\ 1.500 \\ 1.250 \end{pmatrix} \qquad \mathbb{M}^{O2} = \begin{pmatrix} 5.000 \\ 5.000 \\ 4.895 \\ 3.000 \\ 3.000 \\ 2.980 \\ 1.500 \\ 1.500 \\ 1.235 \end{pmatrix}$$

$\mathbb{M}^{O1}$ is the case where plastic hinges form one by one successively, whereas $\mathbb{M}^{O2}$ the case where three plastic hinges form at once at the ends of the three beams. The linear constraint inequalities may be written as

$$
\begin{array}{ll}
\text{H 1} & \begin{pmatrix} -0.933 & +0.894 & +0.118 & +0.019 \end{pmatrix} \\
\text{H 2} & \begin{pmatrix} 0.933 & -0.894 & -0.118 & -0.019 \end{pmatrix} \\
\text{H 3} & \begin{pmatrix} 0.444 & 0.894 & 0.118 & 0.019 \end{pmatrix} \\
\text{H 4} & \begin{pmatrix} -0.444 & -0.894 & -0.118 & -0.019 \end{pmatrix} \\
\text{H 5} & \begin{pmatrix} 0.979 & 0.894 & -0.473 & -0.077 \end{pmatrix} \\
\text{H 6} & \begin{pmatrix} -0.979 & -0.894 & 0.473 & 0.077 \end{pmatrix} \\
\text{H 7} & \begin{pmatrix} -0.535 & & 0.591 & 0.096 \end{pmatrix} \\
\text{H 8} & \begin{pmatrix} 0.535 & & -0.591 & -0.096 \end{pmatrix} \\
\text{H 9} & \begin{pmatrix} 0.383 & & 0.591 & 0.096 \end{pmatrix} \\
\text{H10} & \begin{pmatrix} -0.383 & & -0.591 & -0.096 \end{pmatrix} \\
\text{H11} & \begin{pmatrix} 0.596 & & 0.591 & 0.096 \end{pmatrix} \\
\text{H12} & \begin{pmatrix} -0.596 & & -0.591 & -0.096 \end{pmatrix} \\
\text{H13} & \begin{pmatrix} -0.213 & & & 0.414 \end{pmatrix} \\
\text{H14} & \begin{pmatrix} 0.213 & & & -0.414 \end{pmatrix} \\
\text{H15} & \begin{pmatrix} 0.247 & & & 0.414 \end{pmatrix} \\
\text{H16} & \begin{pmatrix} -0.247 & & & -0.414 \end{pmatrix} \\
\text{H17} & \begin{pmatrix} 0.247 & & & 0.414 \end{pmatrix} \\
\text{H18} & \begin{pmatrix} -0.247 & & & -0.414 \end{pmatrix}
\end{array}
\begin{pmatrix} x_1 \\ x_2 \\ x_3 \\ x_4 \end{pmatrix} \geq M^{O1}, M^{O2}
$$

Problems of finding load carrying capacities and quasi-static responses to various loading and unloading programs may now be formulated. The initial points may be chosen in any way so far as they are inside the yield polyhedron.

Problem 1. The load carrying capacity of the frame with M^{O1}

Maximize $F=x_1$ starting with $(x_1,x_2,x_3,x_4)=(0,0,0,0)$
subject to the inequalities (36) with the right hand side M^{O1}

Problem 2. The load carrying capacity of the frame with M^{O2}

Maximize $F=x_1$ starting with (2.5836821,0,0,-1.5414721)
subject to the inequalities (36) with the right hand side M^{O2}

The result computed by the *GP* procedure on an IBM 7090 are shown in Table 3 and 4 and Figure 10 and 11. The response obtained for the Problem 2 exhibits that if the initial state is an arbitrary residual moment distribution, some of the hinges once formed have been unloaded under monotonically increasing loads. Figure 11 shows how the hinges have formed and been unloaded in each step of the *GP* procedure.

Any loading and unloading programs may now be prescribed within the limits of the load carrying capacity of the Problem 2. Problem 3 is to illustrate the case of alternating plasticity, whereas Problem 4 the case of shakedown.

Table 4 ELASTIC-PLASTIC RESPONSE OF THE FRAME WITH THE PLASTIC MOMENTS M^{02}

Step	Hyperplanes	x-vector x_1	x_2	x_3	x_4	F
0	(Initial)	2.5836821	0	0	1.5414721	
1	H13 added	3.7308683	0	0	1.5414721	3.7308683
2	H12 added	4.3668848	0	0	1.1865934	4.3668848
3	H 6 added	4.7826516	0	0.29445948	0.95460749	4.7826516
4	H 7 added H13 dropped	4.9777778	0.27741756	- 0.43265416	0.84573270	4.9777778
5	H 1 added H 7 dropped	5.0072622	0.29556868	0.41904746	0.76518461	5.0072622
6	H18 added	5.1215968	0.22493897	0.16166107	0.072546869	5.1215968

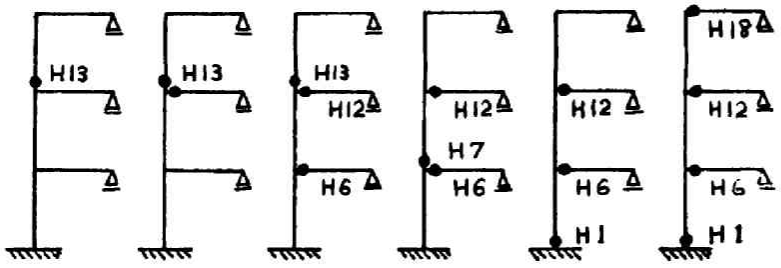

Fig.11

Table 5 ALTERNATING PLASTICITY

Step	Hyperplanes added	x-vector x_1	x_2	x_3	x_4	F
0	(Initial)	0	0	0	0	0
1.1	H 6, H12, H18	5.0000000	0	0	0	5.0000000
1.2	B 2	5.1199999	0.22198449	0.15953793	- 0.071594172	5.1199999
2.1	H 5, H11, H17	-4.8799999	0.22198449	- 0.15953793	0.071594172	-4.8799999
2.2	B1	-5.1199999	0.22198482	0.15953817	0.071594278	-5.1199999
3.1	H 6, H12, H18	4.8799998	0.22198482	0.15953817	0.071594278	4.8799998
3.2	B 2	5.1199999	0.22198471	0.15953809	- 0.071594243	5.1199999

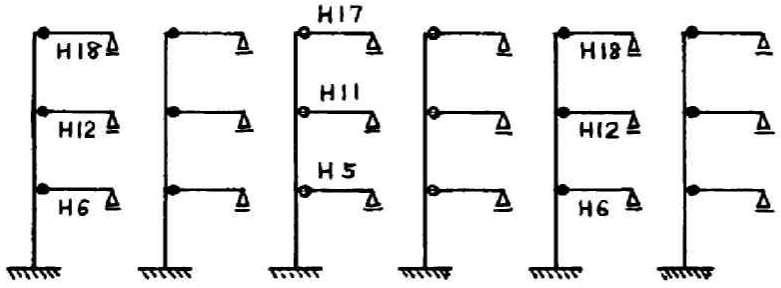

Fig.12

Table 6 SHAKEDOWN

Step	Hyperplanes added	x-vector x_1	x_2	x_3	x_4	F
0	(Initial)	0	0	0	0	0
1.1	H6, H12, H18	5.0000000	0	0	0	5.0000000
1.2	B2	5.0999999	0.18498709	0.13294829	- 0.059661816	5.0999999
2	B1	3.0000000	0.18498709	0.13294829	- 0.059661816	-3.0000000
3	B2	5.0999998	0.18498709	0.13294829	- 0.059661816	5.0999998

Problem 3. Alternating plasticity

Step 1. Maximize $F=x_1$ starting with $(x_1,x_2,x_3,x_4)=(0,0,0,0)$ subject to the inequalities (36) with the right hand side M^{02} and to the bounds $-5.120\leq x_1\leq 5.120$.

Step 2. Maximize $F=-x_1$ starting with the previous maximum subject to the same constraints.

Step 3. Maximize $F=x_1$ starting with the previous maximum subject to the same constraints.

Problem 4. Shakedown

Repeat precisely the same three steps of maximization process with the different bounds $-3.000\leq x_1\leq 5.100$

The results are shown in Table 5 and 6 and in Figure 12. $B1$ and $B2$ in Table 5 denote the bounds $x_1\geq -5.120$ and $-x_1\geq -5.120$, while $B1$ and $B2$ in Table 4 denote the bounds $x_1\geq -3.000$ and $-x_1\geq -5.100$. It should be noted that x_2-, x_3- and x_4-coordinates do not vary in Table 6. This implies that shakedown indeed occurs for this loading cycle.

6. SHAKEDOWN

In many practical cases, the precise variations of the loads applied to a structure are not known or are so complicated that it is difficult to prescribe them. For the purpose of designing structures, certain bounds on the working loads can be assumed which may be based on statistical data. The shakedown problem may be stated as follows; Given a structure subjected to a set of periodically varying loads, whose bounds of variations are prescribed, determine whether the structure will shakedown to a state of self-stress after a finite number of cycles of loading and unloading processes such that its response to all further cycles becomes purely elastic.

An example will be considered first. Figure 13(a) shows a simply redundant ideal truss of 8 bars with 5 joints subjected to a vertical load P and a hoeizontal load Q which vary independently. The elements $\{S_{1j}\}$, $\{S_{2j}\}$ and $\{R_j\}$ of the orthonormal stress set for the present example are shown in Figure 13(f) and in Table 7. The original varying loads P and Q may then be written as

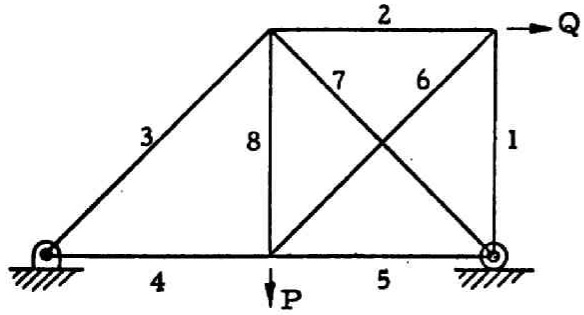

(a) The Truss

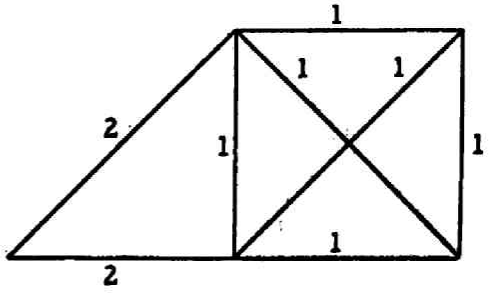

(e) The Yield Limits of Bars

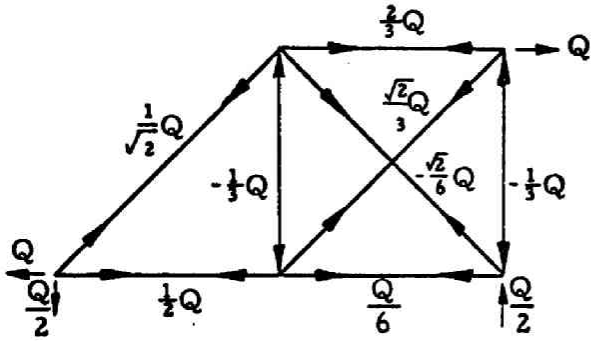

(b) The Stresses due to Q

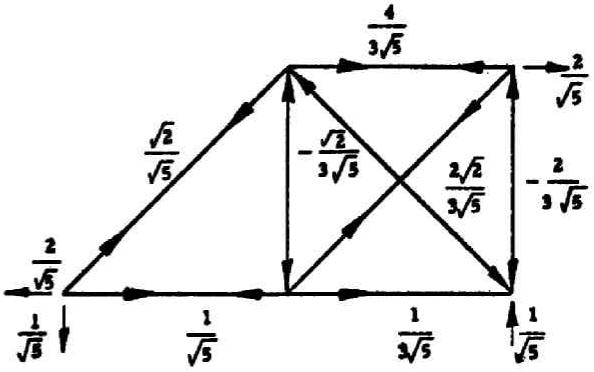

(f_1) $\{S_{1j}\}$

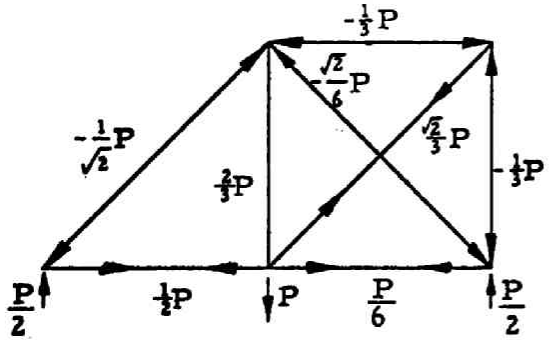

(c) The Stresses due to P

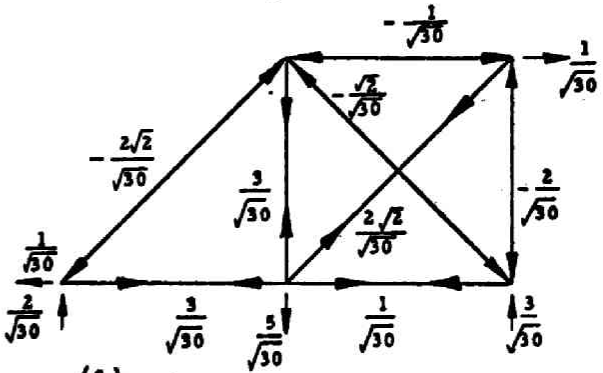

(f_2) $\{S_{2j}\}$

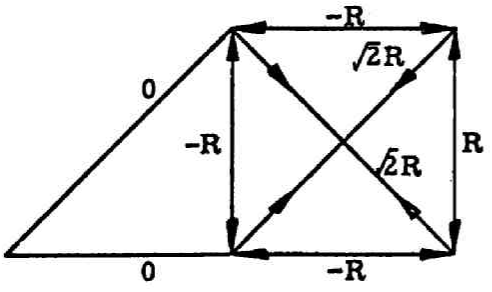

(d) A State of Residual Stress

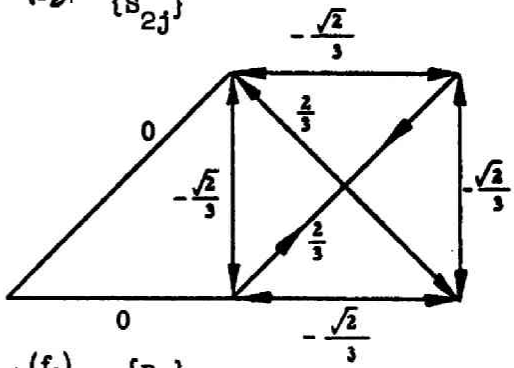

(f_3) $\{R_j\}$

Figure 13

Table 7. THE ORTHONORMAL SET OF STRESS SETS

j	ρ_j	S_{1j}	S_{2j}	R_j
1	1	$-\frac{2}{3\sqrt{5}}$	$-\frac{2}{\sqrt{30}}$	$-\frac{\sqrt{2}}{3}$
2	1	$\frac{4}{3\sqrt{5}}$	$\frac{1}{\sqrt{30}}$	$\frac{\sqrt{2}}{3}$
3	2	$\frac{\sqrt{2}}{\sqrt{5}}$	$-\frac{2}{\sqrt{30}}$	0
4	2	$\frac{1}{\sqrt{5}}$	$\frac{3}{\sqrt{30}}$	0
5	2	$\frac{1}{3\sqrt{5}}$	$\frac{1}{\sqrt{30}}$	$-\frac{\sqrt{2}}{3}$
6	1	$\frac{2\sqrt{2}}{3\sqrt{5}}$	$\frac{2\sqrt{2}}{\sqrt{30}}$	$\frac{2}{3}$
7	1	$\frac{\sqrt{2}}{3\sqrt{5}}$	$-\frac{\sqrt{2}}{\sqrt{30}}$	$\frac{2}{3}$
8	1	$-\frac{2}{3\sqrt{5}}$	$\frac{3}{\sqrt{30}}$	$-\frac{\sqrt{2}}{3}$

$$P = \frac{5}{\sqrt{30}} x_2$$

$$Q = \frac{2}{\sqrt{5}} x_1 + \frac{1}{\sqrt{30}} x_2$$

The yield conditions for the eight members may be expressed as

$$\left.\begin{aligned}
-1 \le \frac{2}{3\sqrt{5}} x_1 \quad & \frac{2}{\sqrt{30}} x_2 \quad \frac{\sqrt{2}}{3} x_3 \le 1 \\
-1 \le \frac{4}{3\sqrt{5}} x_1 \quad & \frac{1}{\sqrt{30}} x_2 - \frac{\sqrt{2}}{3} x_3 \le 1 \\
-2 \le \frac{\sqrt{2}}{\sqrt{5}} x_1 \quad & \frac{2\sqrt{2}}{\sqrt{30}} x_2 \qquad\quad \le 2 \\
-2 \le \frac{1}{\sqrt{5}} x_1 + & \frac{3}{\sqrt{30}} x_2 \qquad\quad \le 2 \\
-1 \le \frac{1}{3\sqrt{5}} x_1 + & \frac{1}{\sqrt{30}} x_2 \quad \frac{\sqrt{2}}{3} x_3 \le 1 \\
-1 \le \frac{2\sqrt{2}}{3\sqrt{5}} x_1 + & \frac{2\sqrt{2}}{\sqrt{30}} x_2 + \frac{2}{3} x_3 \le 1 \\
-1 \le -\frac{\sqrt{2}}{3\sqrt{5}} x_1 - & \frac{\sqrt{2}}{\sqrt{30}} x_2 + \frac{2}{3} x_3 \le 1 \\
-1 < -\frac{2}{3\sqrt{5}} x_1 + & \frac{3}{\sqrt{30}} x_2 \quad \frac{\sqrt{2}}{3} x_3 < 1
\end{aligned}\right\} \qquad (37)$$

where the yield limits of the bars have been chosen as

$$\begin{aligned} t_j = |c_j| &= 1 \quad \text{for } j = 1,2,5,6,7,8, \\ &= 2 \quad \text{for } j = 3,4 \end{aligned}$$

This choice of t_j and c_j prevents the truss from collapsing due to yielding of the bars 3 and 4 in an incomplete mode. The yield polyhedron for this truss is shown in Figures 14 and 15. Suppose a complicated periodical loading path is entirely contained in a rectangular region given by

$$\left.\begin{aligned} -1.5 \le x_1 \le 0.5 \\ -1.2 \le x_2 \le 0.1 \end{aligned}\right\} \qquad (38)$$

According to the general shakedown theorem, if there exists any state of self-stress which would enable the truss to respond in a purely elastic manner to all further cycles of loading, then it will shakedown. In order to show that the truss will shakedown, it suffices therefore to find only one state of residual stress to which it might shake down. Any purely

elastic response is characterized by the fact that the response curve is entirely on a plane parallel to x_1 x_2-plane. Then the problem may be conceived geometrically as that of imbedding the prescribed region of loading program into the yield polyhedron by a translational displacement normal to itself only [3]. This leads us to investigate the possibility of imbedding the rectangular region defined by (38) into the yield polyhedron. The imbedding can be achieved if the fictitious response to the worst possible loading cycle, which consists of the circumference of the rectangle, shows that x_3 becomes a constant eventually.

In the yield polyhedron shown in Figure 14, the response to the piecewise linear cycle: 0→1→2→3→4→5→2

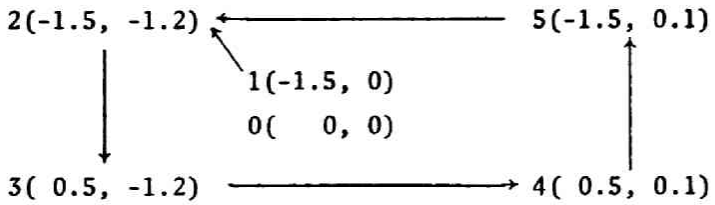

is constructed as shown by the arrows

$$\vec{1};\ \vec{2}',\ \vec{2};\ \vec{3};\ \vec{4};\ \vec{5}',\ \vec{5};\ \vec{6}',\ \vec{6}$$

the corresponding stepwise formulation of the problem in terms of GP is given in Table 8. The result given in Table 9 shows the coincidence with that obtained graphically. The steps 5 and 6 require plastic deformation so that the truss will not shake down if all possible arbitrary loading cycles in the rectangular region must be taken into account.

In order to illustrate the case where shakedown actually occurs, the response to the small rectangular region

$$\begin{aligned} -1.3 &\le \xi_1 \le 0.5 \\ -1.2 &\le \xi_2 \le 0.1 \end{aligned} \tag{39}$$

has been obtained as shown in Table 10. The result illustrated in Figure 15 shows that this smaller rectangular region is indeed imbedded in the polyhedron.

This procedure can easily be generalized. If a truss of r degrees of redundancy is subjected to s sets of loads characterized by s load factors whose bounds are prescribed by

$$L_i \le x_i \le U_i \qquad (i=1,2,\cdots\cdots,s) \tag{40}$$

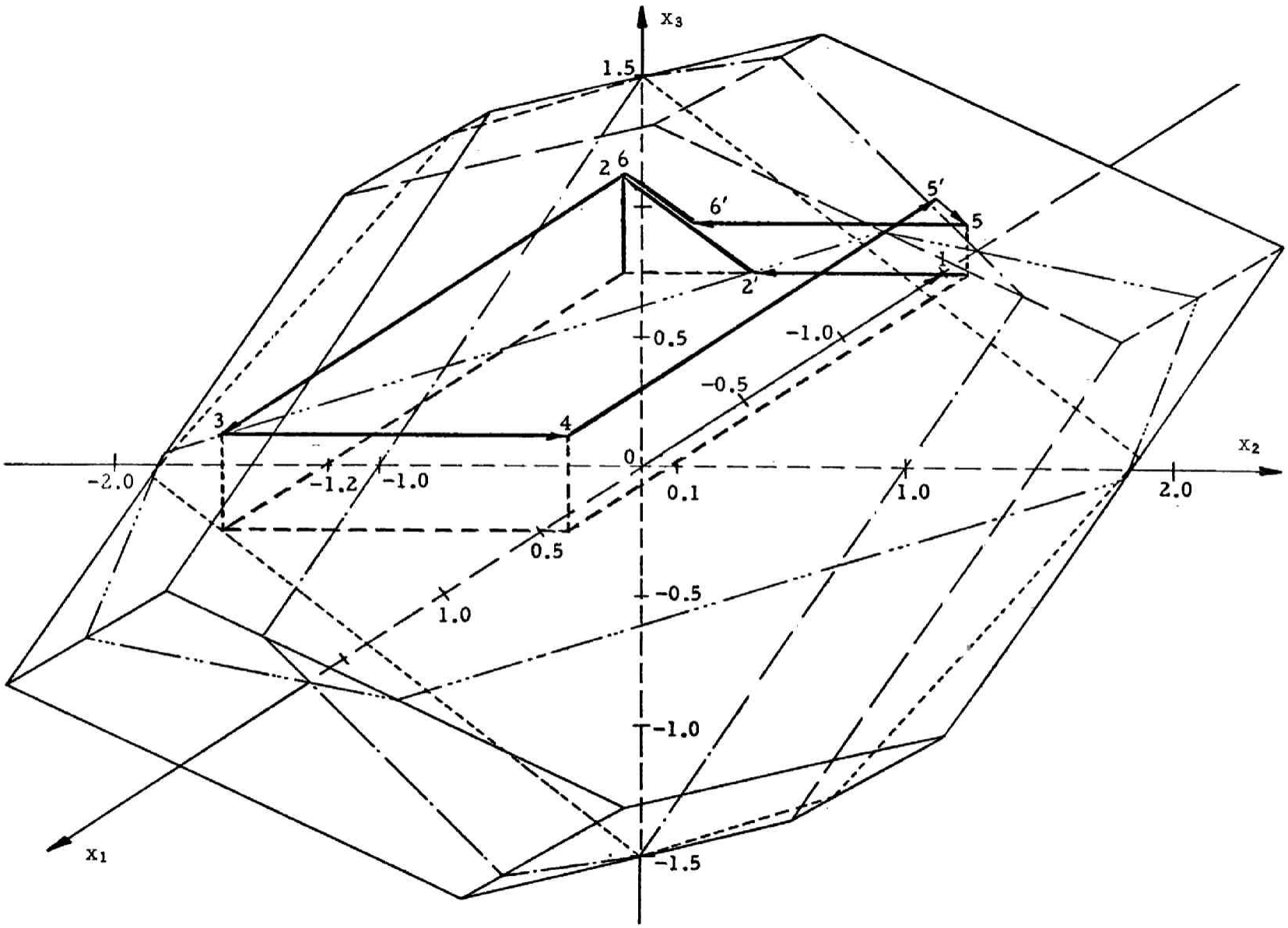

Figure 14. NON-SHAKEDOWN CYCLE

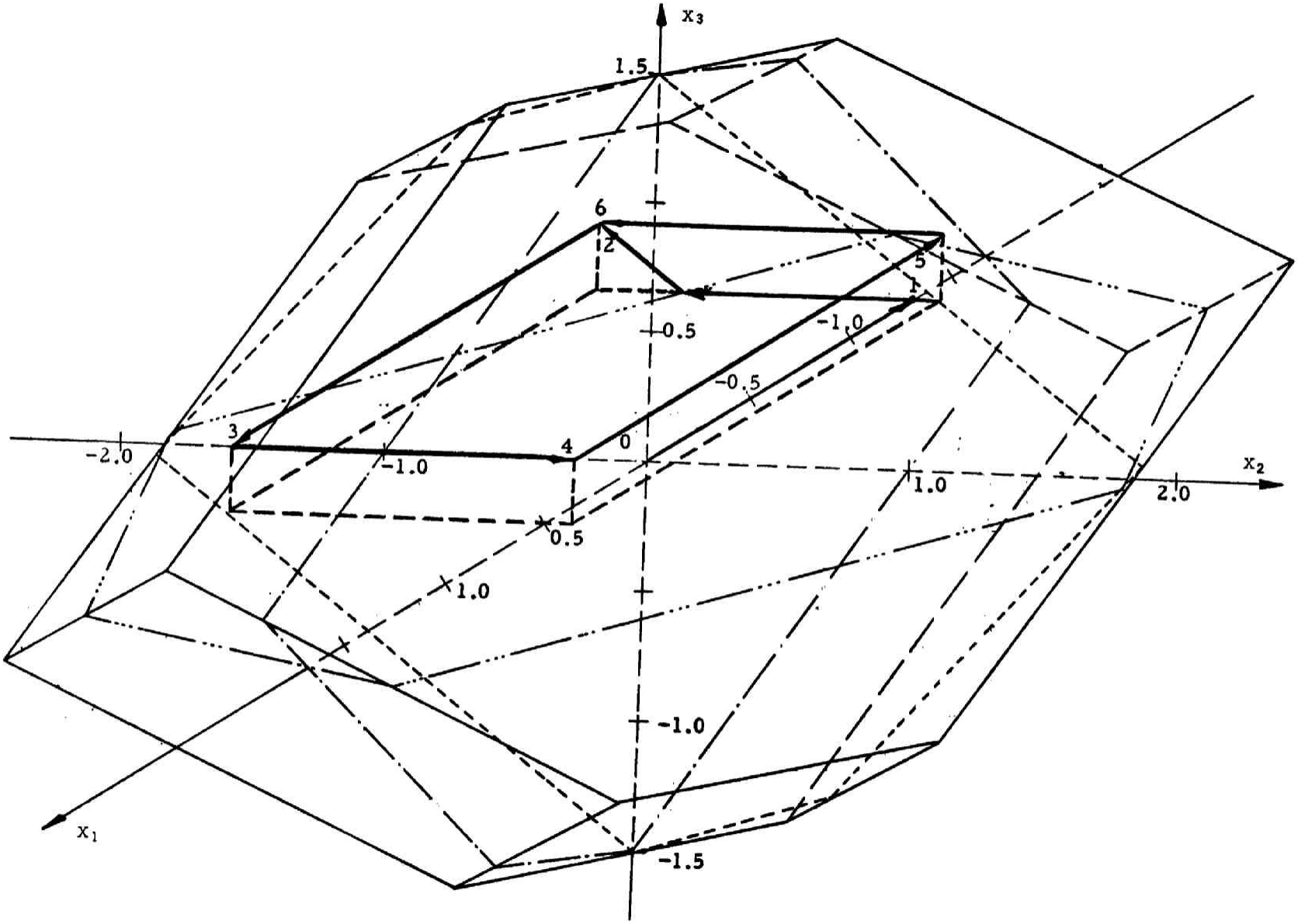

Figure 15. SHAKEDOWN

where L_i and U_i denote the lower and upper bounds on x_i, respectively, then any conceivable variation of the set x_i is contained in the parallelopiped defined by (40). Let x_{s+1}, ..., x_{s+r} denote r parameters for r independent states of self-stress. A yield polyhedron is then considered in an $(s+r)$-dimensional stress space. Shakedown will occur under any loading cycle contained in the parallelipiped if it can be imbedded in the yield polyhedron by translation normal to itself only. By virture of the convexity of the yield polyhedron, it is sufficient to consider a fictitious response of the truss to that loading cycle which passes through all the corners of the parallelopiped. If this response shows that all the x_{s+k}'s $(k=1,2,\cdots\cdots,r)$ become constant after a finite number of cycles, then the imbedding of the parallilopiped is indeed achieved and shakedown occurs. The loading cycle may be piecewise linear from one corner to another. Hence the *GP* program can be applied. On this basis it appears that the number of steps required to show the shakedown will be at least 2^s and at most 2×2^s In the case of the example, $s=2$. The number of steps N required should be

$$4 \leq N \leq 8$$

Six steps were necessary for the loading path chosen as above.

Table 8 FORMULATION FOR THE NON-SHAKEDOWN CYCLE

Step	Maximize F =	Subject to: Bounds		Yield Ineq.	Path
1	$-x_1$	$x_1 \geq -1.5$	$-x_1 \geq -0.5$	(6.1) (6.16)	$x_2 = 0$
2	$-x_2$	$x_2 \geq -1.2$	$-x_2 \geq -0.1$	"	$x_1 = -1.5$
3	x_1	$x_1 \geq -1.5$	$-x_1 \geq -0.5$	"	$x_2 = -1.2$
4	x_2	$x_2 \geq -1.2$	$-x_2 \geq -0.1$	"	$x_1 = 0.5$
5	$-x_1$	$x_1 \geq -1.5$	$-x_1 \geq -0.5$	"	$x_2 = 0.1$
6	$-x_2$	$x_2 \geq -1.2$	$-x_2 \geq -0.1$	"	$x_1 = -1.5$

To investigate more extensively under what kind of loading cycles the given truss will shake down, it is necessary to know the shapes of the elastic subspaces defined by x_3=const. i.e., cross-sections of the yield polyhedron parallel to x_1 x_2 plane. Responses of the truss are characterized by a family of an infinite number of elastic subspaces to which the truss could shake down. Since the original yield polyhedron is convex, these elastic subspaces are convex polygons, Any of these polygons will be called

Table 9. THE RESPONSE TO THE NON-SHAKEDOWN CYCLE

Step	Maximum F	x_1	x_2	x_3
1	1.50000000	-1.5000000	0	0
2		-1.5000000	-0.71174686	0
2	1.20000000	-1.5000000	-1.20000000	0.37819923
3	0.50000000	0.50000000	-1.20000000	0.37819923
4	0.09999994	0.50000000	0.09999999	0.37819923
5		-1.3474396	0.09999999	0.37819923
5	1.50000000	-1.50000000	0.09999999	0.18522390
6		-1.50000000	-0.95086989	0.18522390
6	1.20000000	-1.50000000	-1.20000000	0.37819923

Table 10. FORMULATION FOR A SHAKEDOWN CYCLE

Step	Maximize F =	Subject to: Bounds		Yield Ineq.	Path
1	$-x_1$	$x_1 \geq -1.3$	$-x_1 \geq -0.5$	(6.1) ~ (6.16)	$x_2 = 0$
2	$-x_2$	$x_2 \geq -1.2$	$-x_2 \geq -0.1$	"	$x_1 = -1.5$
3	x_1	$x_1 \geq -1.3$	$-x_1 \geq -0.5$	"	$x_2 = -1.2$
4	x_2	$x_2 \geq -1.2$	$-x_2 \geq -0.1$	"	$x_1 = 0.5$
5	$-x_1$	$x_1 \geq -1.3$	$-x_1 \geq -0.5$	"	$x_2 = 0.1$
6	$-x_2$	$x_2 \geq -1.2$	$-x_2 \geq -0.1$	"	$x_1 = -1.5$

Table 11. THE RESPONSE TO THE SHAKEDOWN CYCLE

Step	Maximum F	x_1	x_2	x_3
1	1.30000000	-1.30000000	0	0
2	1.20000000	-1.30000000	-1.20000000	0.25170814
3	0.50000000	0.50000000	-1.20000000	0.25170814
4	0.09999999	0.50000000	0.09999999	0.25170814
5	1.30000000	-1.30000000	0.09999999	0.25170814
6	1.20000000	-1.30000000	-1.20000000	0.25170814

tentatively a *shakedown polygon*. Any loading cycle under which the given truss will shakedown must therefore be contained in one of this family of an infinite number of shakedown polygons. For practical purposes, several shakedown polygons will be sufficient for revealing shakedown characteristics of a truss. If they can be drawn by some means, it can be immediately inspected whether or not a given loading cycle can be imbedded into the yield polyhedron or how it may be enlarged or should be shrunk, if the truss is to shake down.

These shakedown polygons can easily be obtained by use of the *GP* as follows. Since any shakedown polygon is convex, it is always possible to circumscribe it by a rectangle as shown in Figure 16. There are, in general, four points of contact with the rectangle or some of the sides of the polygon may coincide with those of the rectangle. Then it is obvious that the following five steps of maximization suffice to describe the polygon completely.

1:	max.	$F_1 = x_1$	with the initial point	0
1 → 2:	max.	$F_2 = x_2$	"	1
2 → 3:	max	$F_3 = -x_1$	"	2
3 → 4:	max.	$F_4 = -x_2$	"	3
4 → 1:	max.	$F_5 = x_1$	"	4

In the present example it is not difficult to obtain these shakedown polygons graphically since there are only eight inequalities as given by (37). However, as the number of bars increases, the graphical solution becomes cumbersome. Furthermore, if the truss has r degrees of redundancy then a shakedown polygon is an intersection of the yield polyhedron of $(r+2)$-dimension and r hyperplanes given by

$$x_{s+1} = \text{const.}, \quad x_{s+2} = \text{const.}, \cdots, x_{s+r} = \text{const.}$$

where the truss is subjected to two independently varying sets of loads. As long as the truss is subjected only to two independently varying loads, $F_1, F_2, \cdots\cdots, F_5$ remain the same through all the shakedown polygons of the family. Only the right-hand sides of r equality constraints $\{x_{s+k}=\text{const.}\}$ are changed. The results from the *GP* program give all the vertices of the polygons. If the number of independent load factors is greater than two, then this technique cannot be used because it is very difficult to describe all the vertices of a complicated polyhedron by means of *GP*.

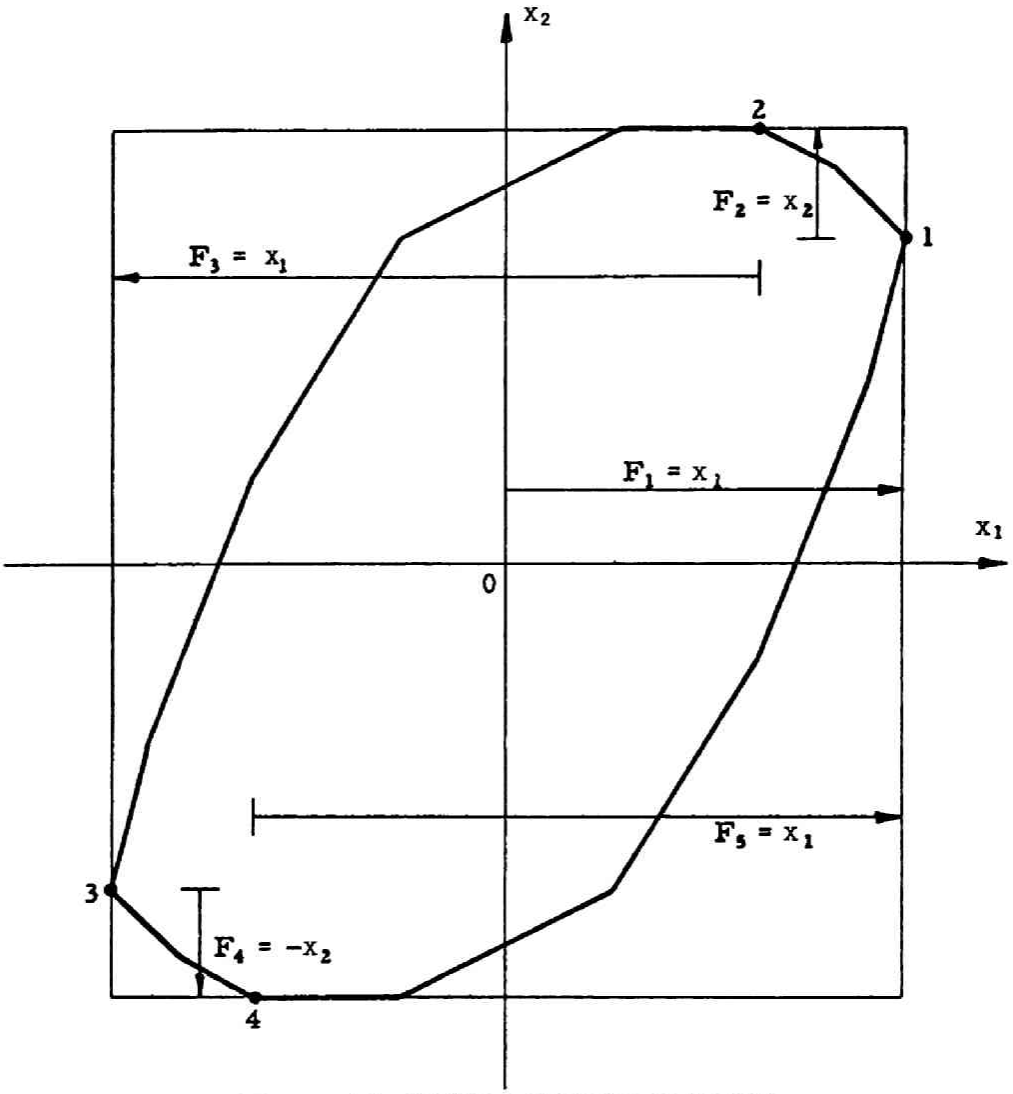

Figure 16. SHAKEDOWN POLYGON

7. LOAD CARRYING CAPACITY AND SAFE LOAD DOMAIN

If a structure is subjected to a set of loads characterized by only one load factor, then the corresponding load carrying capacity is uniquely defined. However, if it is subjected to s sets of loads characterized by s independently varying load factors $\{x_i\}$, then the set $\{x_i\}$ at collapse will reveal the load-carrying capacity characteristics. In order to obtain all the sets $\{x_i\}$ at collapse. it suffices to consider a family of straight line paths defined by

$$\frac{x_1}{m_1} = \frac{x_2}{m_2} = \cdots = \frac{x_s}{m_s}$$

where $(m_1, m_2, \cdots, m_s)$ is a set of numbers which determine the ratios between x_i's. This family covers the s-dimensional load factor subspace completely. To every one of these paths there corresponds a set $(x_1, x_2, \cdots, x_s)$ at collapse. All these sets $(x_1, x_2, \cdots, x_s)$ form a closed hypersurface in the s-dimensional load factor subspace. Since this hypersurface can be regarded as a projection of the yield polyhedron into the s-dimensional load factor subspace, it must be a convex polyhedron in s-space. This will be called the "safe load domain". This domain is characterized by the property that any combination of the s sets of loads represented by a point interior to it does not cause collapse if the loads are monotonically increased from zero. This can easily be obtained by the *GP* method since some equality constraints have only to be added.

It should be noted that if we denote an infinite number of regions of shakedown polygons by $D_1, D_2, \cdots, D_m, \cdots$ then the union $D_1 \cup D_2 \cup \cdots \cup D_m \cup \cdots$ gives a safe load domain approximated from inside *i.e.*, from safe side.

In the case of the example, since there are two load factors all the ratios x_1/x_2 must be considered. By virtue of the symmetry of the yield polyhedron, we have only to consider a family of straight line paths originating from the origin which cover a half x_1 x_2 plane completely. The safe load domain in this case is a polygon and practically several straight line paths suffice to draw the polygon. The result is shown in Figure 17.

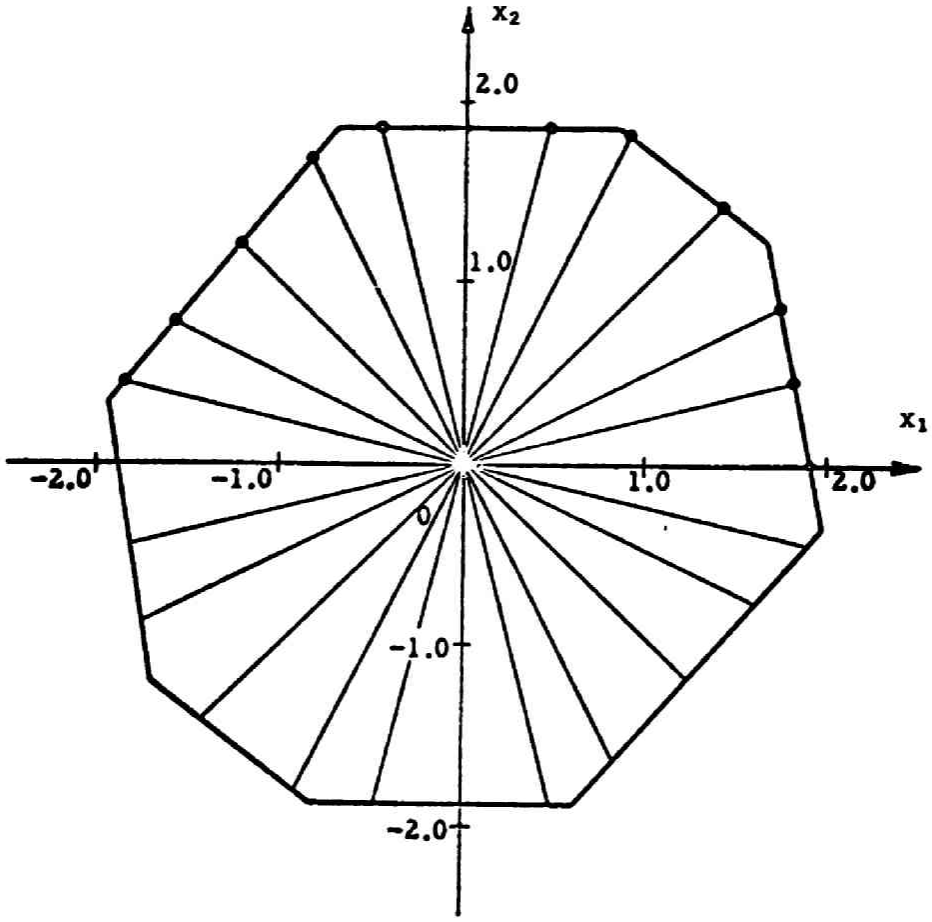

Figure 17. SAFE LOAD DOMAIN

8. CONCLUDING REMARKS

The procedure of applying the gradient projection method of nonlinear programming to the elastic-plastic analysis of trusses has been shown in considerable detail. It should be emphasized that as long as loading paths are piecewise linear, *GP* automatically gives integral results for every segment of the paths and the exact elastic-plastic responses of multiply redundant trusses to several independently varying loads can readily be obtained by *GP*.

It has also been shown that the gradient projection method is useful and powerful to investigate shakedown and load carrying capacities of trusses and that frames can be treated in the same manner as trusses without modification. Since most of the collapse modes of a frame of uniform prismatic members contain a finite number of plastic hinges, yield polyhedrons rather than smooth convex hypersurfaces are again obtained and the application of *GP* is precisely the same as for trusses.

REFERENCES

1. Greenberg, H. J., "Complementary minimum principles for an elastic-plastic material", Q. Appl. Math. Vol. 7, pp. 85-95 1949.

2. Prager, W., "Introduction to plasticity", Addison-Wesley, 1959.

3. Prager, W., "Stress analysis in the plastic range", Brown University Tech. Rept. C11-52. October 1959.

4. Rosen, J. B., "The gradient projection method for nonlinear programming". I. Linear Constraints. J.Soc. Indust. Appl. Math. 8, pp. 181-217 (1960).

5. Rosen, J. B., "The gradient projection method for nonlinear programming. Part II. Nonlinear constraints". J. Soc. Indust. Appl. Math. 9, pp. 514-532 (1961).

6. Neal, B. G., "The plastic methods of structural analysis", J. Wiley, 1956.

7. Koiter, W. T., "General theorems for elastic-plastic solids". Progress in Solid Mechanics. Vol. 1, Interscience Pub. Inc. 1960.

8. Tsuneyoshi Nakamura and J. B. Rosen, "Elastic-plastic Analysis of Trusses by the Gradient Projection Method", Tech. Rept. CS11 July 17, 1964. Computer Science Division, Stanford University

CHAPTER 6

A LINEAR STRAIN-HARDENING IDEALIZED COLUMN SUBJECTED TO COMBINED LOADING

1. INTRODUCTION

The plastic collapse strength of a frame subjected to a set of monotonic loads can be estimated considerably well by the plastic-hinge method of the simple plastic theory or of the second-order theory provided that the plastic deformation in the members at collapse is so small that the effect of strain-hardening may be neglected and so far as the members have been designed so as not to exhibit any local instability phenomenon. If, however, the frame is subjected to variable repeated loads, the effect of strain-hardening and the Bauschinger effect must be taken into consideration and the assumption of perfect-plasticity will not be appropriate.

No systematic method, such as an incremental member-stiffness matrix method, of analyzing a frame characterized by a complicated hysteretic stress-strain relation has yet been proposed except for beams and beam-columns. Among more realistic idealizations than that of perfect-plasticity, the bilinear hysteretic stress-strain relation is the simplest. The author has presented an analytical method of solution to the bilinear hysteretic strain-hardening column problem based upon a 2-material-point model in 1966 [1]. whereas Yamada *et al* [2] proposed moment-curvature relations based upon 3- and 4-point models at the same Meetings of A.I.J, and subsequently proposed a numerical solution [3]. Kato *et al* [4] described an approximate analysis based upon an assumed rigid-plastic moment-curvature relation. Since then, a number of refined treatments have been proposed [8].

This chapter is concerned with a detailed presentation of the result of Ref.[1],[5],[6] but is not limited to the case of constant axial forces which have been assumed in all the previous works. Analytical solutions to a cantilever column subjected to combined varying axial and lateral forces will be obtained. The constituent solutions may also be applied to other various practical cases. It will be illustrated that the concept of the "stress line" is useful for examing all the possible responses from a previous state. While stress-trajectory in Chapter 10 is the stress space representation of only the state of stress at plastic collapse of a structure, the "stress line" here may vary as the external loads are varied.

2. BILINEAR HYSTERETIC STRESS-STRAIN RELATION

Although the experimental hysteretic and skeleton stress-strain relations in Chapter 8 suggest a bilinear hysteretic stress-strain relation with variable strain-hardening modulus as shown in Fig.1, the one with a constant modulus without regard to the stress or strain amplitudes is the simplest even if slightly less realistic. It is shown that many of the essential features of the inelastic behavior of a beam-column can be disclosed with the use of the stress-strain relation with a constant strain-hardening modulus and that the resulting analytical solutions are explicit, in closed form and much simpler than if otherwise. The procedure described in the following may, however, be applied to any bilinear hysteretic stress-strain relations.

Let α, E, ε_y and σ_y denote the constant linear strain-hardening coefficient, the modulus of elasticity, the yield strain and stress, respectively as shown in Fig.2. For later convenience, the dimensionless strain and stress are defined by

$$\frac{\varepsilon}{\varepsilon_y} = e \quad , \quad \frac{\sigma}{\sigma_y} = s \tag{1}$$

The virgin stress-strain relation may then be defined by

$$s = e \quad , \quad -1 \leq e \leq 1$$

$$s-1 = \alpha(e-1) \quad 1 \leq e$$

$$s+1 = \alpha(e+1) \quad e \leq -1 \tag{2a-c}$$

Let the state of strain and stress at the end of the j-th step be $(e^{(j)}, s^{(j)})$. The subsequent stress-strain relations are given in the incremental form by

$$\dot{s} = \dot{e} \quad \text{if} \quad -2+s^{(j)} < s < s^{(j)} \tag{3a}$$

$$\text{or if} \quad s = s^{(j)} \text{ and } \dot{s} < 0 \tag{3b}$$

$$\text{or if} \quad s = s^{(j)}-2 \text{ and } \dot{s} > 0 \quad \text{and} \tag{3c}$$

$$\dot{s} = \alpha\dot{e} \quad \text{if} \quad s = s^{(j)} \text{ and } \dot{s} > 0 \tag{3d}$$

$$\text{or if} \quad s = s^{(j)}-2 \text{ and } \dot{s} < 0 \tag{3e}$$

for $e^{(j)}, s^{(j)} > 1$, and

$$\dot{s} = \dot{e} \quad \text{if} \quad s^{(j)} < s < s^{(j)}+2 \tag{4a}$$

$$\text{or if} \quad s = s^{(j)} \text{ and } \dot{s} > 0 \tag{4b}$$

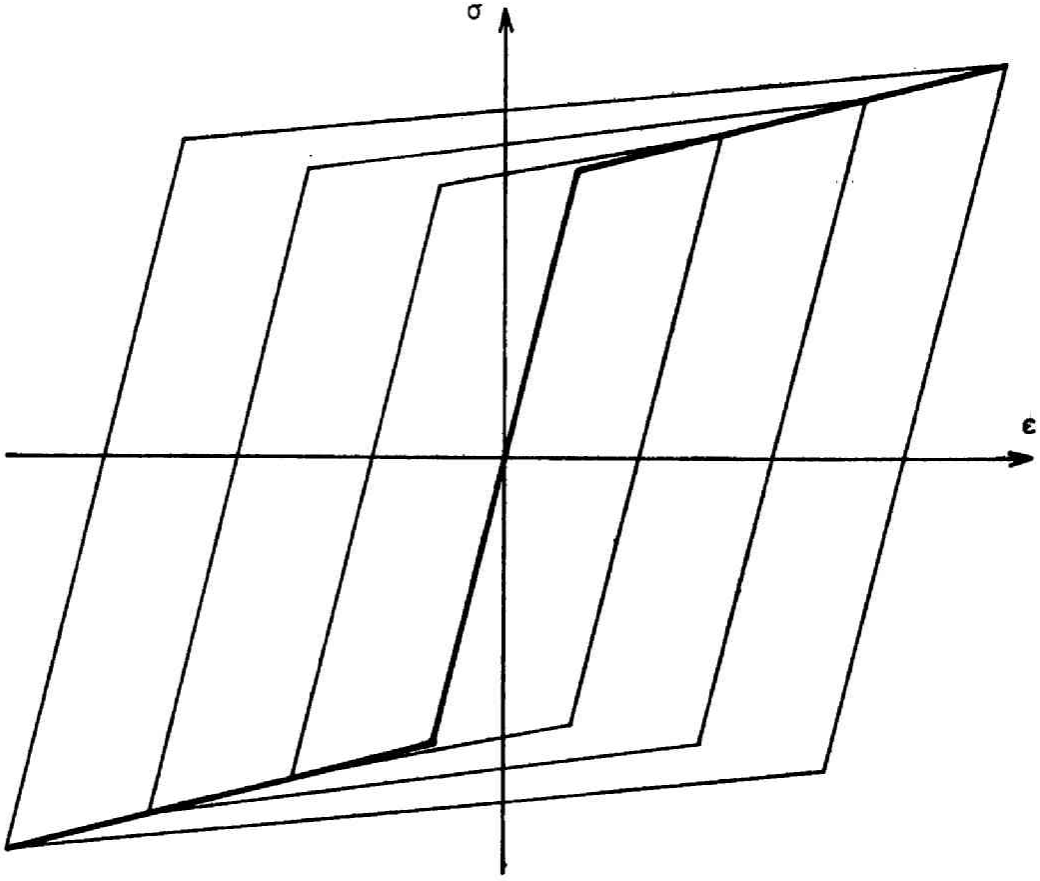

Fig.1 Bilinear hysteretic stress-strain relation with variable strain-hardening modulus.

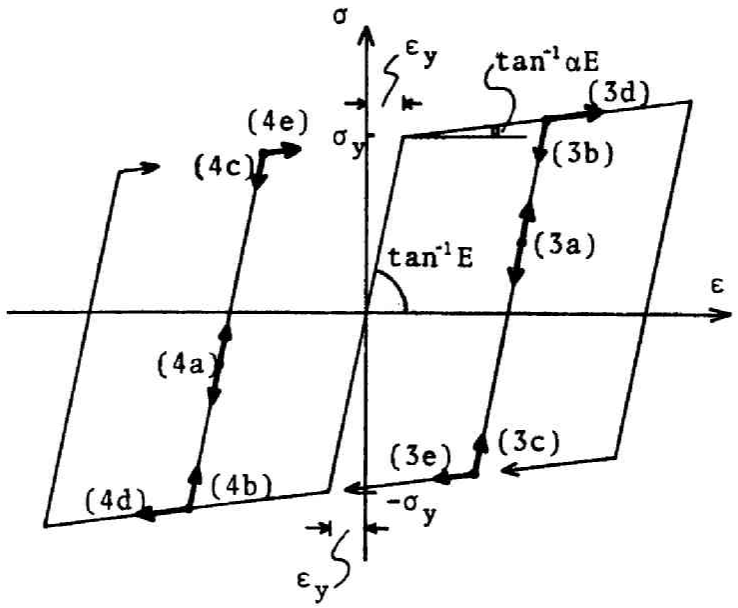

Fig. 2 Bilinear hysteretic stress-strain relation with a constant strain-hardening modulus.

$$\text{or if} \quad s = s^{(j)}+2 \text{ and } s < 0 \qquad \text{and} \tag{4c}$$

$$\dot{s} = \alpha\dot{e} \quad \text{if} \quad s = s^{(j)} \text{ and } \dot{s} < 0 \tag{4d}$$

$$\text{or if} \quad s = s^{(j)}+2 \text{ and } \dot{s} > 0 \tag{4e}$$

$$\text{for } e^{(j)},\ s^{(j)} < -1,$$

where the dot denotes an increment with respect to some appropriate time scale. The ten cases (3a-e) and (4a-e) are indicated by arrows in Fig.2. These relations may be written in a finite form if $\dot{s}$ and $\dot{e}$ are known or may be assumed to be definite, positive or negative, throughout a step.

$$s-s^{(j)} = e-e^{(j)} \quad \text{if } -2+s^{(j)} < s < s^{(j)}, \quad \text{and} \tag{5a}$$

$$s-(s^{(j)}-2) = \alpha\{e-(e^{(j)}-2)\} \quad \text{if} \quad s < -2+s^{(j)} \tag{5b}$$

$$\text{where} \quad s^{(j)}-1 = \alpha(e^{(j)}-1) \quad \text{and}$$

$$s-s^{(j)} = e-e^{(j)} \quad \text{if} \quad s^{(j)} < s < s^{(j)}+2, \text{ and} \tag{6a}$$

$$s-(s^{(j)}+2) = \alpha\{e-(e^{(j)}+2)\} \quad \text{if} \quad s^{(j)}+2 < s \tag{6b}$$

$$\text{where} \quad s^{(j)}+1 = \alpha(e^{(j)}+1).$$

3. IDEALIZED SANDWICH SECTION

Besides the idealization of the stress-strain relation, the idealization of the cross-sectional properties of a column is indispensable for the purpose of extracting most of the essential features of its inelastic behavior in an explicit and analytical form. The idealized sandwich section consists of sufficiently thin cover sheets or flanges of equal area and the core in between, which carries the shear stress only without any extensional stiffness. The real cross-section of a column and an associated sandwich section are defined here to be equivalent if the extensional and bending stiffnesses are the same in the elastic range. Let the cross-sectional area and the moment of inertia of the real section be A and I, respectively. Let A_e and h denote the cross-sectional area and the depth of the equivalent sandwich section, respectively. The equivalence is defined by

$$A_e = A \tag{7a}$$

$$I_e = A_e(H_e/2)^2 = I, \text{ or } \quad \frac{1}{2} H_e = \sqrt{\frac{I}{A}} = r \tag{7b}$$

The equivalence in the elastic range does not necessarily imply the equivalence in the strain-hardening range, except some special cases.*

The interaction yield condition for the idealized sandwich section may

*An assessment of the accuracy of the approximation is given in the Appendix.

be derived as follows. The bending moment M and axial force N acting upon a section are given by

$$M = \frac{1}{4} A_e H_e (\sigma_L \quad \sigma_U), \quad N = \frac{1}{2} A_e (\sigma_L + \sigma_U) \tag{8}$$

where σ_L and σ_U denotes the normal stresses in the two flanges, referred to as the lower flange and the upper flange shown in Fig.4, respectively. If the first and second equations of (8) are divided by the yield moment $M_y = \frac{1}{2} \sigma_y A_e H_e$ and the yield axial force $N_y = \sigma_y A_e$, respectively, the following expressions may be obtained.

$$S_L = m + n, \quad S_U = -m + n \tag{9}$$

where

$$m = M/M_y, \quad n = N/N_y, \quad S_L = \sigma_L/\sigma_y, \quad S_U = \sigma_U/\sigma_y. \tag{10}$$

The initial yield condition is given by

$$S_L = m + n = \pm 1, \quad \text{and/or} \quad S_U = -m + n = \pm 1 \tag{11}$$

Eqs.(11) represent a square on the (m, n)-plane or (S_L, S_U)-plane as shown in Fig.5 which will be referred to as the yield square. The region inside the initial yield square is called the initial elastic region. If some strain-hardening limits are to be considered, the corresponding limit square may be drawn as shown in Fig.5 by dashed lines. As the strain-hardening proceeds in a flange, say $\dot{S}_L > 0$ and $S_L > 1$, the yield square is translated in the positive direction of the S_L-axis inside the limit square. This observation is useful for a deeper insight into the nature of the moment-curvature relationship in the following section. It should also be noted that, in view of the stress-strain relation shown in Fig.2, an unloading elastic region from a strain-hardening state is always represented by a square of the same size.

4. MOMENT CURVATURE RELATIONS

Since the stress-strain relations are bilinear hysteretic as given by Eqs.(2), (3),and (4), the moment-curvature relations must also be derived piecewisely for each linear branch. Let ε_L and ε_U be the longitudinal strains in the lower and upper flanges, respectively. Corresponding to S_L and S_U, the following reduced strains will be used

$$\frac{\varepsilon_L}{\varepsilon_y} = e_L, \qquad \frac{\varepsilon_U}{\varepsilon_y} = e_U \tag{12}$$

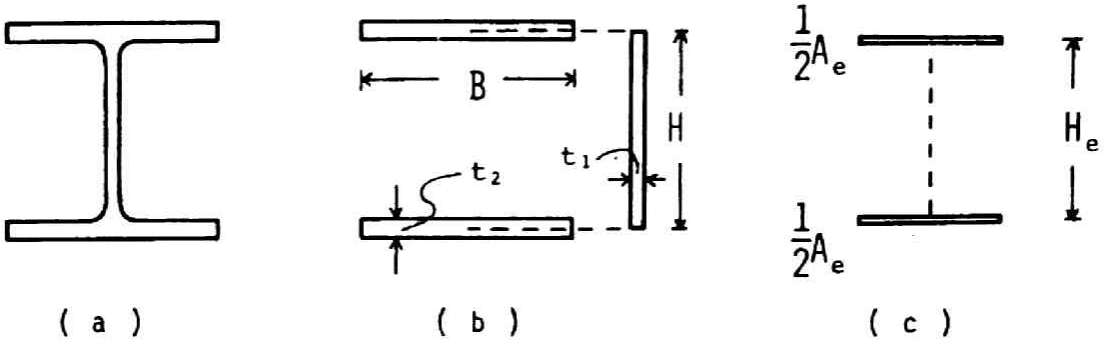

Fig.3 Equivalent sandwich section.

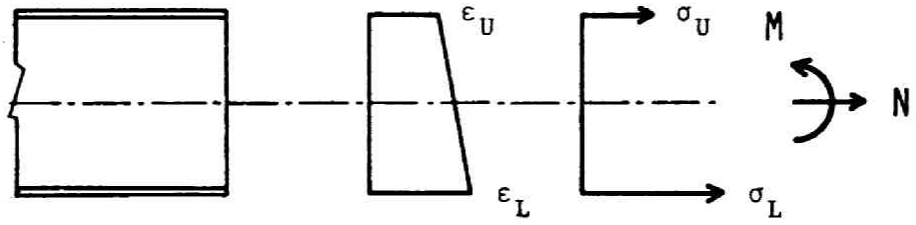

Fig.4 Stresses and strains at a section.

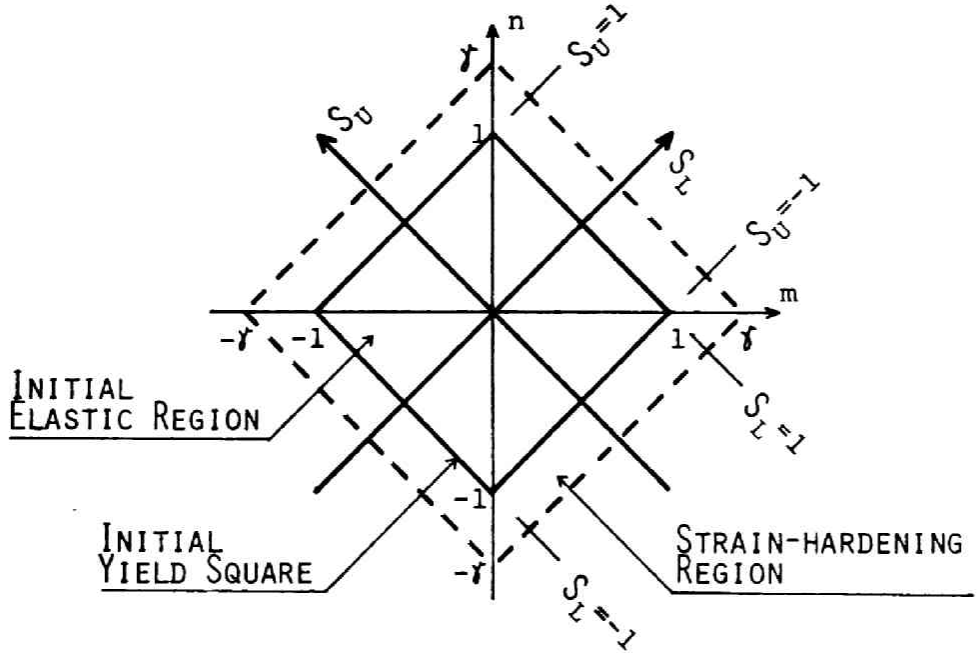

Fig.5 Initial yield square on (m,n)-plane.

The dimensionless curvature is defined by

$$\kappa = \frac{K}{K_y} = \frac{1}{2}(e_L \quad e_U), \qquad \text{where} \quad K_y = \frac{2\varepsilon_y}{H_e} = \frac{M_y}{EI_e} \tag{13}$$

The moment-curvature-rate relations based upon Eqs.(3) and (4) may be summarized as shown in Table 1, where

$$\beta_1 = \frac{1-\alpha}{1+\alpha} \tag{14}$$

TABLE 1

lower flange	upper flange	Moment-curvature rate relations
Elastic	Elastic	$\dot{\kappa} = \dot{m}$ (15)
Elastic	Strain-hardening	$\dot{\kappa} = \frac{1+\alpha}{2\alpha}(\dot{m}-\beta_1\dot{n})$ (16)
Strain-hardening	Elastic	$\dot{\kappa} = \frac{1+\alpha}{2\alpha}(\dot{m}+\beta_1\dot{n})$ (17)
Strain-hardening	Strain-hardening	$\dot{\kappa} = \frac{1}{\alpha}\dot{m}$ (18)

If a response step is such that Eqs.(5) and (6) are applicable, then the moment-curvature relations may be written in finite forms. For this purpose, it is helpful to represent the process of stress variation as a locus on the (S_L, S_U)-plane superposed on the (m, n)-plane. Fig.6 shows some examples of such stress loci from an initial state in which the axial force only acts upon a section. In order to identify a stress locus of a cross-section, it is convenient to use a symbol which indicates the states of stress in both flanges. A stress locus is denoted by $R_j[T_i, T_k]$, where j denotes the (j)-th response stop and

$$T_i = \begin{cases} E_i & \text{if } S_L \text{ is in the } i\text{-th unloading elastic region,} \\ L_i^+ & \text{if } S_L \text{ is in the } i\text{-th strain-hardening region with } \dot{S}_U > 0 \text{ and} \\ L_i^- & \text{if } S_L \text{ is in the } i\text{-th strain-hardening region with } \dot{S}_U < 0, \text{ and} \end{cases}$$

$$T_k = \begin{cases} E_k & \text{if } S_U \text{ is in the } k\text{-th unloading elastic region,} \\ U_k^+ & \text{if } S_U \text{ is in the } k\text{-th strain-hardening region with } \dot{S}_L > 0 \text{ and} \\ U_k^- & \text{if } S_U \text{ is in the } k\text{-th strain-hardening region with } \dot{S}_L < 0 \end{cases}$$

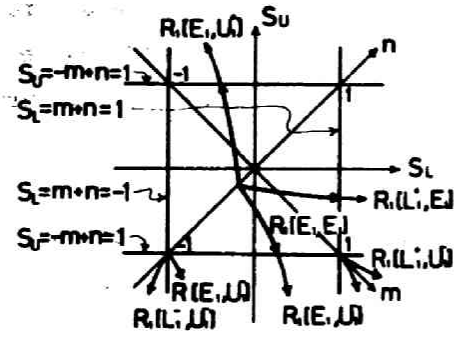

Fig.6

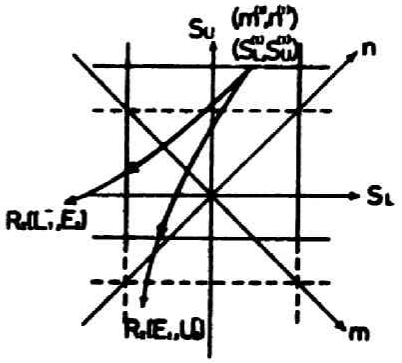

Fig.7(a)

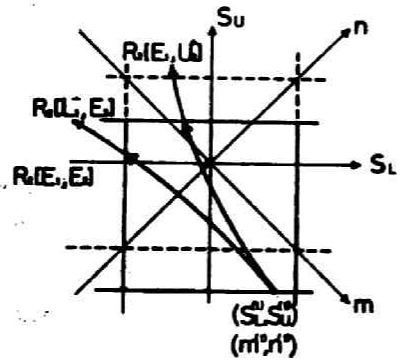

Fig.7(b)

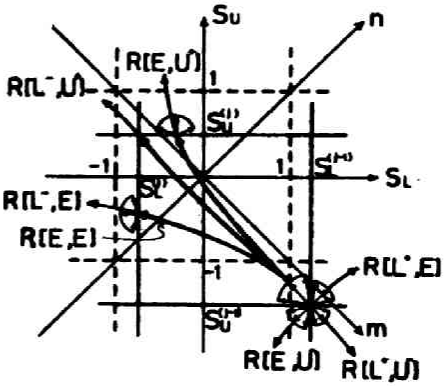

Fig.7(c)

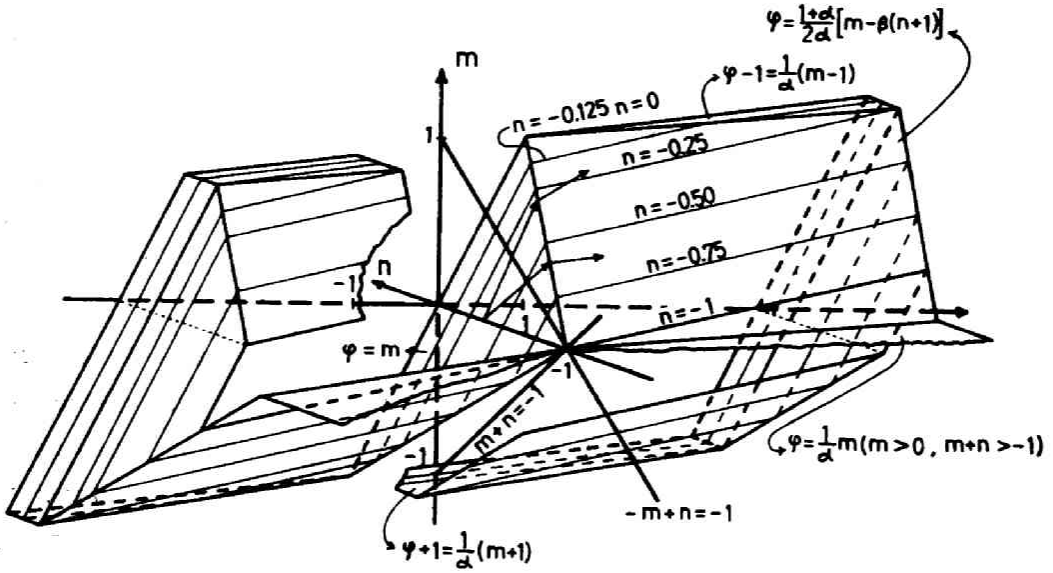

Fig.8

The moment-curvature relations have been summarized in Tables 2 and 3 for several typical stress loci of practical interest in the 1st and 2nd response steps shown in Fig.6 and 7, respectively. The family of the moment-curvature lines form a polyhedron in (m, n, κ)-space as shown in Fig.8.

5. CANTILEVER COLUMN PROBLEM

A cantilever column with the idealized sandwich section composed of the bilinear hysteretic strain-hardening material is subjected to a vertical force N and a lateral force Q as shown in Fig.9. N and Q are varied under a given loading program which is independent of the deformation history of the column. The dimensionless lateral force is defined by $q = Q/N_y$. If a rectangular cartesian coordinate system whose axes are n and q is considered, a point (n, q) moving in accordance with the given loading program describes a "loading path" on the (n, q)-plane.

A static rsponse of the cantilever column to a complicated loading path is characterized by its dependence upon its strain- or deformation history that the column experiences. A representive displacement is usually taken as the primary overall response quantity. Let Δ denote the horizontal displacement of the top of the column. The dimensionless displacement is defined by $\delta = \Delta/\ell$, where ℓ is the length of the column. If δ-axis is considered to form a rectangular cartesian (n, q, δ)-space, then the overall elastic-plastic behavior may be geometrically visualized as a "response curve". The essential features of the present problem are that the one-to-one correspondance between (n, q) and δ is lost after a stability limit even under monotonically increasing δ, that a response curve to a prescribed alternating loading path may describe hysteresis loops and that a stability limit is deformation-history dependent.

Since the $m \sim \kappa$ relation for the idealized section is trilinear hysteretic, an inelastic deflection curve of the column consists in general of different portions governed by different $m \sim \kappa$ relations. In order to identify constituent solutions, it is helpful to visualize the state of stress in the column at any state of loading (n, q) on the (S_L, S_U)- and (m, n)-planes. A set of stress points corresponding to a state of loading (n, q) form in general a curve and in the present problem a line if the slope of the column is small. For instance, suppose if the column with a small slenderness ratio is first subjected to an initial axial force $-1 \leq n_0 < 0$ which is small compared to the Euler load, and then to a proportionally varying set of axial and lateral forces. All the stress points corresponding to the load point $(n_0, 0)$ are at

TABLE 2 Moment-curvature relations for the 1st loading step

Response Symbol	Range of Stress path	Stress-strain Relations	Moment-curvature Relation
$R_1[E_1,E_1]$	$-1\le -m+n\le 1$	$e_u=S_u$	$\kappa=\frac{1}{2}(e_L-e_u)=\frac{1}{2}(S_L-S_u)$
	$-1\le m+n\le 1$	$e_L=S_L$	$=m$ (19)
$R_1[E_1,U_1^-]$	$-m+n<-1$ $-\dot{m}+\dot{n}<0$	$e_u=\frac{1}{\alpha}(S_u+1)-1$	$\kappa=\frac{1}{2}[S_L-\frac{1}{\alpha}(S_u+1)-1]$
	$-1\le m+n\le 1$	$e_L=S_L$	$\kappa=\frac{1+\alpha}{2\alpha}[m-\beta_1(n+1)]$ (20)
$R_1[L_1^+,U_1^-]$	$m+n<-1$ $-\dot{m}+\dot{n}<0$	$e_u=\frac{1}{\alpha}(S_u+1)-1$	$\kappa=\frac{1}{2}[\frac{1}{\alpha}(S_L-1)-\frac{1}{\alpha}(S_u+1)+2]$
	$1<m+n$ $0<m+n$	$e_L=\frac{1}{\alpha}(S_L-1)+1$	$\kappa-1=\frac{1}{\alpha}(m-1)$ (21)
$R_1[L_1^-,U_1^-]$	$-m+n\le -1$ $-\dot{m}+\dot{n}\le 0$	$e_u=\frac{1}{\alpha}(S_u+1)-1$	$\kappa=\frac{1}{2}[\frac{1}{\alpha}(S_L+1)-\frac{1}{\alpha}(S_u+1)]$
	$m+n\le -1$ $\dot{m}+\dot{n}\le 0$	$e_L=\frac{1}{\alpha}(S_L+1)-1$	$=\frac{1}{\alpha}m$ (22)
$R_1[L_1^+,E_1]$	$-1\le -m+n\le 1$	$e_u=S_u$	$\kappa=\frac{1}{2}[\frac{1}{\alpha}(S_L-1)+1-S_u]$
	$1<m+n$ $0<\dot{m}+\dot{n}$	$e_L=\frac{1}{\alpha}(S_L-1)+1$	$=\frac{1+\alpha}{2\alpha}[m-\beta_1(1-n)]$ (23)
$R_1[E_1,U_1^+]$	$1<-m+n$ $0<-\dot{m}+\dot{n}$	$e_u=\frac{1}{\alpha}(S_u-1)+1$	$\kappa=\frac{1}{2}[S_L-\frac{1}{\alpha}(S_u-1)-1]$
	$-1\le m+n\le 1$	$e_L=S_L$	$=\frac{1+\alpha}{2\alpha}[m+\beta_1(1-n)]$ (24)

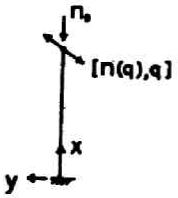

Fig.9

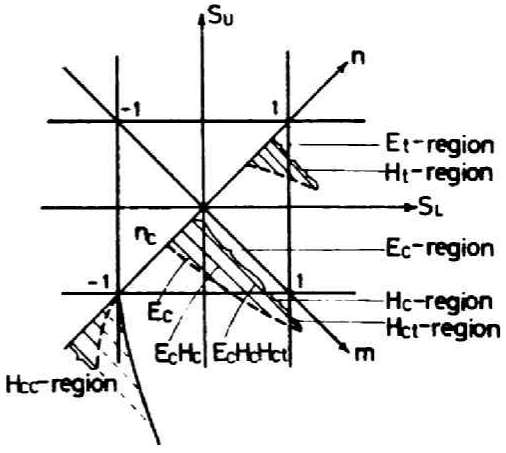

Fig.10

TABLE 3 Moment-curvature relations for the 2nd loading step

Response Symbol	Range of Stress path	Stress-strain Relations	Moment-curvature Relation
$R_1[E_1, U_1^-]$	$-m+n \le -m^{(1)}+n^{(1)}+2$	$e_u - e_u^{(1)} = S_u - S_u^{(1)}$	$\kappa - \kappa^{(1)} = m - m^{(1)}$
		$e_u^{(1)} = \frac{1}{\alpha}(S_u^{(1)}+1)-1$	
$R_2[E_1, E_2]$	$-1 \le m+n \le 1$	$e_L = S_L$	(25)
$R_1[E_1, U_1^-]$	$-m+n \le -m^{(1)}+n^{(1)}+2$	$e_u - e^{(1)} = S_u - S^{(1)}$	$\kappa = \frac{1+\alpha}{2\alpha}\{m+\beta_1(n+m^{(1)}-n^{(1)})\}$
		$e_u^{(1)} = \frac{1}{\alpha}(S_u^{(1)}+1)-1$	
$R_2[L_1^-, E_2]$	$m+n < -1$ $\dot{m}+\dot{n} < 0$	$e_L = \frac{1}{\alpha}(S_L+1)-1$	(26)
$R_1[E_1, U_1^-]$	$-m^{(1)}+n^{(1)}+2 < -m+n$ $0 < -\dot{m}+\dot{n}$	$e_u = e_u^{(1)}+2 + \frac{1}{\alpha}(S_u - S_u^{(1)}-2)$	$\kappa = \frac{1+\alpha}{2\alpha}\{m-\beta_1(n-1)\}$
		$e_u^{(1)} = \frac{1}{\alpha}(S_u^{(1)}+1)-1$	
$R_2[E_1, U_2^+]$	$-1 \le m+n \le 1$	$e_L = S_L$	(27)
$R_1[E_1, U_1^+]$	$-m+n < -m^{(1)}+n^{(1)}-2$ $-\dot{m}+\dot{n} < 0$	$e_u = e_u^{(1)}-2 + \frac{1}{\alpha}(S_u - S_u^{(1)}+2)$	$\kappa = \frac{1+\alpha}{2\alpha}\{m-\beta_1(n+1)\}$
		$e_u^{(1)} = \frac{1}{\alpha}(S_u^{(1)}-1)+1$	
$R_2[E_1, U_2^-]$	$-1 \le m+n \le 1$	$e_L = S_L$	(28)
$R_1[E_1, U_1^+]$	$-m^{(1)}+n^{(1)}-2 \le -m+n$	$e_u = S_u - S_u^{(1)}+e_u^{(1)}$	$\kappa = \frac{1+\alpha}{2\alpha}\{m+\beta_1(n+m^{(1)}+n^{(1)}+2)\}$
		$e_u^{(1)} = \frac{1}{\alpha}(S_u^{(1)}-1)+1$	
$R_2[L_1^-, E_2]$	$m+n < -1$ $\dot{m}+\dot{n} < 0$	$e_L = \frac{1}{\alpha}(S_L+1)-1$	(29)

$(m, n) = (0, n_0)$. At any state of loading (n, q), the state of stress throughout the column may be visualized as a straight line parallel to the m-axis on the (m, n)-plane. As (n, q) is varied, the straight line may grow parallel to the m-axis moving in the n-direction as shown in Fig.10. The straight line will henceforth be called a "stress line". If q and n are sufficiently small, the corresponding stress line will be entirely within the initial elastic region. The symbol E_c is used for identifying an elastic portion of the column governed by the elastic moment curvature relation (19) under compression As q and n are increased proportionally, the stress line will eventually contain the portion beyond the line $S_U = -m + n = -1$ as indicated by E_cH_c in Fig.10. The portion of the column in strain-hardening is referred to as a H_c-region, where the subscript c represents that one of the flanges are in the strain-hardening range in compression. The deflection curve and $q/(-n)\sim\delta$ relation for this state of stress will be called the E_cH_c-solution. If q and n are increased further, the tension flange may also start strain-hardening. In this case the stress line will include a portion beyond the line $S_L = m + n = 1$. The portion of the column for which $S_U = -m + n < -1$ and $S_L = m + n > 1$ will be called a H_{ct}-region. The double subscripts c and t denote that one flange is in strain-hardening state in compression, the other being in strain-hardening state in tension. The solution to this case will be referred to as the $E_cH_cH_{ct}$-solution. Fig.10 illustrates two other cases of the growing processes of stress lines. The boundaries of these different regions will be denoted by E_cH_c-boundary, H_cH_{ct}-boundary and so forth.

6. VIRGIN LOAD-DEFLECTION BEHAVIOR

6.1 E_cH_c-solution

Fig.9 shows the coordinates chosen for the column. The following dimensionless quantities will be used:

$$\frac{X}{l} = \xi, \quad \frac{Y}{l} = \eta, \quad \bar{\eta} = lK = lK_y\kappa = \frac{M_p l}{EI}\kappa = k^2\frac{h}{2}\kappa$$

$$\frac{H_e}{l} = h, \quad \frac{N_y l^2}{EI} = \frac{\sigma_y A_e l^2}{A_e H_e^2 E/4} = \left(\frac{\sigma_y}{E}\right)\left(\frac{h}{2}\right)^2 \equiv k^2 \qquad (30)$$

The deflection curves of the E_c-, H_c- and H_{ct}-regions are denoted by $\eta_e(\xi)$, $\eta_c(\xi)$, and $\eta_{ct}(\xi)$, respectively.

The dimensionless expression of the bending moment distribution is given by

$$m=\frac{Ny\ell}{My}\,[q(1-\xi)-n(\delta-\eta(\xi))]=\frac{2}{h}\,(-n)\{\frac{q}{-n}\,(1-\xi)+\delta-\eta\} \tag{31}$$

The governing differential equation for E_c-region is given by

$$\ddot{\eta}_e(\xi)=k^2(-n)\{\frac{q}{-n}\,(1-\xi)+\delta-\eta_e\} \tag{32}$$

where dots denote differentiation with respect to ξ. The general solution of (32) may be written as

$$\eta_e(\xi)=C_1\sin k_e\xi+C_2\cos k_e\xi+\frac{q}{-n}\,(1-\xi)+\delta \tag{33}$$

where $k_e=k\sqrt{(-n)}\quad(-n\geq 0)$.

The boundary condition $\eta_e(1)=\delta$ at the free end determines C_2 in terms of C_1 and (33) may be reduced to

$$\eta_e(\xi)=-C_1\,\frac{\sin k_e(1-\xi)}{\cos k_e}+\frac{q}{-n}\,(1-\xi)+\delta \tag{34}$$

The boundary conditions at the fixed end $\eta_e(0)=0$ and $\dot{\eta}_e(0)=0$ determine the elastic $\frac{q}{-n}\sim\delta$ relation as follows.

$$\delta=\frac{\tan k_e-k_e}{k_e}\,(\frac{q}{-n}) \tag{35}$$

The expression (35) is valid if $m(0)=\frac{2}{h}\,(q-n\delta)\leq 1+n$. Let $\frac{h}{2}\,(1+\frac{1}{n})\equiv\mu$. Then the (35) is valid if

$$\frac{q}{-n}+\delta\leq-\mu \tag{36}$$

If (3.6) is violated, then H_c solution must be combined with (34). The differential equation for $\eta_c(\xi)$ may be obtained by introducing (31) into (20) as follows

$$\ddot{\eta}_c=k^2(\frac{1+\alpha}{2\alpha})(-n)\{\frac{q}{-n}\,(1-\xi)+\delta-\eta_c+\beta_1\mu\} \tag{37}$$

The general solution of (37) may be readily found as

$$\eta_c(\xi)=C_3\sin k_c\xi+C_4\cos k_c\xi+\frac{q}{-n}\,(1-\xi)+\delta+\beta_1\mu \tag{38}$$

where

$$k_c=k\sqrt{\frac{1+\alpha}{2\alpha}\,(-n)}=k_e\sqrt{\frac{1+\alpha}{2\alpha}} \tag{39}$$

The E_cH_c-boundary is characteriged by the yield condition

$$m(\lambda_c)=\frac{2}{h}\,(-n)\{\frac{q}{-n}(1-\lambda_c)+\delta-\eta(\lambda_c)\}=1+n \tag{40}$$

where λ_c denotes the location of the E_cH_c-boundary. The continuity conditions between (34) and (38) and the yield condition (40) may be written in the following form.

$$-C_1\,\frac{\sin k_e(1-\lambda_c)}{\cos k_e}=\mu=C_3\sin k_c\lambda_c+C_4\cos k_c\lambda_c+\beta\mu$$

$$C_1k_e\,\frac{\cos k_e(1-\lambda_c)}{\cos k_e}=C_3k_c\cos k_c\lambda_c-C_4k_c\sin k_c\lambda_c$$

It is convenient to define the following functions

$$\left.\begin{aligned} C_c[\tau;u,v]&=\tau\mu\{\tau\cos(u)+\sin(u)\cot(v)\}\\ S_c[\tau;u,v]&=\tau\mu\{\tau\sin(u)-\cos(u)\cot(v)\}\end{aligned}\right\} \quad (41)$$

Then the constants may be written as

$$\left.\begin{aligned} C_1&=-\mu\,\frac{\cos k_e}{\sin k_e(1-\lambda_c)}\\ C_3&=S_c[\beta_2;k_c\lambda_c,k_e(1-\lambda_c)]\ ,\ C_4=C_c[\beta_2;k_c\lambda_c,k_e(1-\lambda_c)]\end{aligned}\right\} \quad (42)$$

where $k_e^2/k_c^2=1-\beta_1=\beta_2^2$ has been used. Substitution of (42) into (34) and (3 8) furnishes

$$\left.\begin{aligned} \eta_e(\xi)&=\mu\,\frac{\sin k_e(1-\xi)}{\sin k_e(1-\lambda_c)}+\frac{q}{-n}\,(1-\xi)+\delta \qquad (\lambda_c\le\xi\le 1)\\ \eta_c(\xi)&=C_c[\beta_2;k_c(\lambda_c-\xi),k_e(1-\lambda_c)]+\frac{q}{-n}\,(1-\xi)+\delta+\beta_1\mu \qquad (0\le\xi\le\lambda_c)\end{aligned}\right\} \quad (43)$$

The boundary conditions $\eta_c(0)=0$ and $\dot{\eta}_c(0)=0$ at the fixed end provide the following parametric representation of $\frac{q}{-n}\sim\delta$ relation.

$$\left.\begin{aligned} \frac{q}{-n}&=k_cS_c[\beta_2;k_c\lambda_c,k_e(1-\lambda_c)]\\ \frac{q}{-n}+\delta&=-\beta_1\mu-C_c[\beta_2;k_c\lambda_c,k_e(1-\lambda_c)]\end{aligned}\right\} \quad (44)$$

Eqs. (44) is applicable if $m(\xi)\le m(0)\le 1-n$ and $n\ge -1$,

or $$\frac{q}{-n}+\delta\le\frac{h}{2}\left(1-\frac{1}{n}\right)\equiv-\nu \text{ and } n\ge -1 \quad (45)$$

Fig.11 shows several $q\sim\delta$ curves for constant n. Fig.12 is a bird-eye view of several families of $q\sim\delta$ curves for varying n, spanning a load-displacement surface in a (q,n,δ)-space.

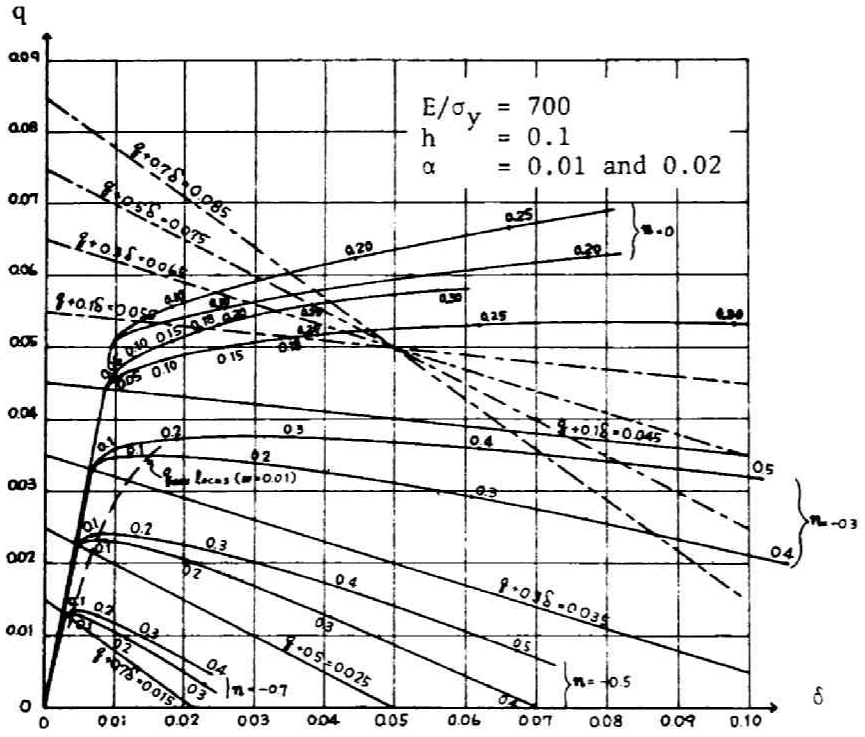

Fig.11

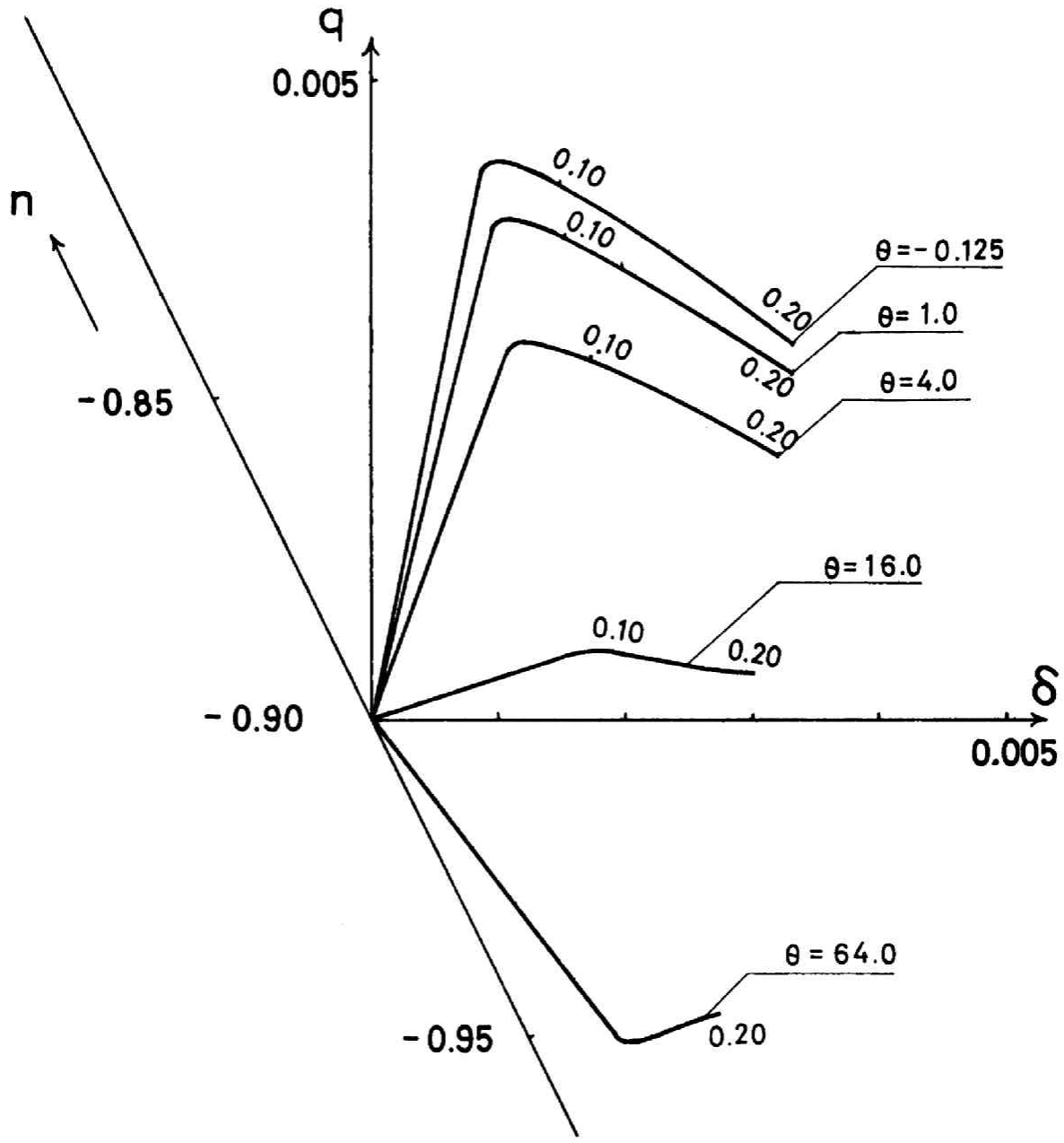
q
0.005
n
-0.85
-0.90
-0.95
0.10
0.10
0.10
0.20
0.20
0.20
θ=-0.125
θ=1.0
θ=4.0
θ=16.0
0.10
0.20
θ=64.0
0.20
δ
0.005

Fig.12

6.2 $E_cH_cH_{ct}$-solution

The solutions $\eta_e(\xi)$ and $\eta_c(\xi)$ for the E_c and H_c-regions as given by (43) are still applicable in the $E_cH_cH_{ct}$-solution. The differentical equation for $\eta_{ct}(\xi)$ of the H_{ct}-region may be obtained by introducing (31) into (21)

$$\ddot{\eta}_{ct}=\frac{h}{2}k^2\{1+\frac{1}{\alpha}\frac{2}{h}(-n)[\frac{q}{-n}(1-\xi)+\delta-\eta_{ct}(\xi)]-\frac{1}{\alpha}\}$$

Let $(-n)k^2/\alpha\equiv k_e^2/\alpha\equiv k_{ct}^2$ Then

$$\ddot{\eta}_{ct}+k_{ct}^2\eta_{ct}=k_{ct}^2\{\frac{q}{-n}(1-\xi)+\delta+\frac{1-\alpha}{n}\frac{h}{2}\} \tag{46}$$

The general solution of (46) is given by

$$\eta_{ct}=C_5\sin k_{ct}\xi+C_6\cos k_{ct}\xi+(\frac{q}{-n})(1-\xi)+\delta+(1-\alpha)(\mu+\nu)/2 \tag{47}$$

The H_cH_{ct}-boundary is characterized by the condition

$$m(\lambda_{ct})=\frac{2}{h}[q(1-\lambda_{ct})-n(\delta-\eta(\lambda_{ct}))]=1-n \tag{48}$$

The continuity conditions and (48) may be written as

$$C_5\sin k_{ct}\lambda_{ct}+C_6\cos k_{ct}\lambda_{ct}+(\frac{1-\alpha}{2})(\mu+\nu)=+\nu$$

$$=\beta_1\mu+C_c[\beta_2;k_c(\lambda_c-\lambda_{ct}),k_e(1-\lambda_c)]$$

$$C_5\cos k_{ct}\lambda_{ct}-C_6\sin k_{ct}\lambda_{ct}=\frac{k_c}{k_{ct}}S_c[\beta_2;k_c(\lambda_c-\lambda_{ct}),k_e(1-\lambda_c)]$$

The determined constants may be substituted into (47) and one obtains

$$\eta_{ct}(\xi)=\frac{h}{2}(\frac{\alpha}{n}-1)\cos k_{ct}(\lambda_{ct}-\xi)$$
$$-\frac{1}{\beta_3}S_c[\beta_2;k_c(\lambda_c-\lambda_{ct}),k_e(1-\lambda_c)]\sin k_{ct}(\lambda_{ct}-\xi)$$
$$+(\frac{q}{-n})(1-\xi)+\delta+\frac{1-\alpha}{2}(\mu+\nu) \tag{49}$$

where

$$\beta_3=\sqrt{\frac{2}{1+\alpha}}=\frac{k_{ct}}{k_c}$$

The remaining condition is the $\lambda_c\sim\lambda_{ct}$ relation;

$$C_c[\beta_2:k_c(\lambda_c-\lambda_{ct}),k_e(1-\lambda_c)]+\beta_1\mu-\nu=0 \tag{50}$$

The boundary conditions at the fixed end furnish the $\frac{q}{-n}\sim\delta$ relation.

$$\frac{1}{k_{ct}}(\frac{q}{-n})=\frac{h}{2}(\frac{\alpha}{n}-1)\sin k_{ct}\lambda_{ct}$$
$$+\frac{1}{\beta_3}S_c[\beta_2;k_c(\lambda_c-\lambda_{ct}),k_e(1-\lambda_c)]\cos k_{ct}\lambda_{ct}$$
$$\frac{q}{-n}+\delta=(\frac{1-\alpha}{-n})\frac{h}{2}-(\frac{\alpha}{n}-1)\frac{h}{2}\cos k_{ct}\lambda_{ct}$$
$$+\frac{1}{\beta_3}S_c[\beta_2;k_c(\lambda_c-\lambda_{ct}),k_e(1-\lambda_c)]\sin k_{ct}\lambda_{ct} \tag{51}$$

As λ_c is varied, λ_{ct} varies in accordance with (50) and the corresponding values of $\frac{q}{-n}$ and δ may be determined from (51) Fig.11 contains a portion of the $q\sim\delta$ curve governed by (51) for n=-0.1.

6.3 Mechanism surface

An elastic-perfectly plastic column may be regarded as a limiting case of the linear strain-hardening column as $\alpha \to 0$. If the two equations of (44) are respectively squared and then added, the following expression may be obtained.

$$\mu^2\beta_2^2\{\beta_2^2+\cot^2 k_e(1-\lambda_c)\} = \frac{1}{k_c^2}\left(\frac{q}{-n}\right)^2 + \left\{\frac{q}{-n}+\delta+\beta_1\mu\right\}^2$$

When α lends to zero, $\beta_2 \to 0$, $\beta_1 \to 1$ and $k_c \to \infty$ while $\cot k_e(1-\lambda_c)$ remains finite. Then $\frac{q}{-n} \sim \delta$ relation approaches the straight line

$$q-n\delta-n\mu=0 \qquad (52)$$

Eq.(52) represents a possible equilibrium path as a collapse mechanism of a rigid perfectly plastic column and may also be directly obtained from its equilibrium condition.

The smaller the value of α is, the smaller the possibility of attaining the validity limit (45) will be. As $\alpha \to 0$, Eq.(52) will always be below the limit of (45) except when $n \to 0$ and hence the $E_cH_cH_{ct}$-solution will not be applicable. When $n \to 0$, Eq.(52) becomes coincident with Eq.(45).

In the (q,n,δ)-space, Eq.(52) describes a surface any point on which also represents a possible equilibrium state as a collapse mechanism of a rigid-perfectly plastic column. This surface will be called a "mechanism surface". Fig.13 shows the mechanism surface. The solid lines on the surface indicate the mechanism curves when n=constant. It is apparent that the magnitude of negative slope representing how instable the equilibrium state is, depends upon the loading path (q,n) along which the equilibrium state is varied. The arrows at a point P indicates the possible slopes depending upon the loading path.

A similar mechanism surface may be continued over to the case $n>0$. The equation of the surface is given by

$$q-n\delta-n\nu=0 \qquad (53)$$

This portion of the mechanism surface has also been included in Fig.13.

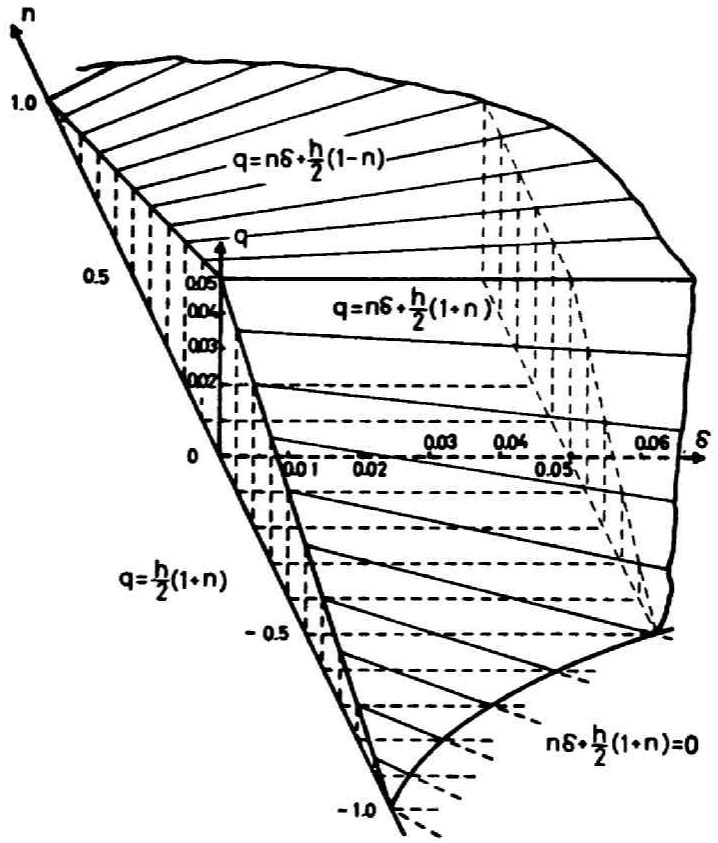
n
1.0
0.5
0
- 0.5
- 1.0
q
q=nδ+h/2(1-n)
q=nδ+h/2(1+n)
q=h/2(1+n)
nδ+h/2(1+n)=0
0.005
0.004
0.003
0.002
0.001
0.002
0.003
0.004
0.005
0.006
δ

Fig.13

7. EH_t-SOLUTION

The governing differential equation for the elastic state in tensile bending may be written as

$$\ddot{\eta}=k^2[q(1-\xi)-n(\delta-\eta)] \tag{54}$$

Let $\kappa_e=k\sqrt{n}$ $(n\geq 0)$. Then the general solution to (54) may be written as

$$\eta=C_1\sinh\kappa_e\xi+C_2\cosh\kappa_e\xi-\frac{q}{n}(1-\xi)+\delta \tag{55}$$

The boundary conditions are

$$\left.\begin{aligned} &\eta(1)=\delta \;:\; C_1\sinh\kappa_e+C_2\cosh\kappa_e=0\\ &\eta(0)=0 \;:\; C_2-\frac{q}{n}+\delta=0\\ &\dot{\eta}(0)=0 \;:\; C_1\kappa_e+\frac{q}{n}=0 \end{aligned}\right\} \tag{56}$$

Elimination of C_1 and C_2 from (56) furnishes the $q/n\sim\delta$ relation as follows

$$\frac{q}{n}=\frac{\kappa_e}{\kappa_e-\tanh\kappa_e}\delta \tag{57}$$

The equation (57) is valid until a strain-hardening region appears. The extent of validity is given by

$$1-n\geq m(0)=\frac{2}{h}(q-n\delta) \quad \text{or} \quad \frac{q}{n}-\delta\leqq\nu$$

An EH_t-solution consists of an elastic solution and a strain-hardening solution. The elastic solution satisfying the boundary condition (56a) may be wrtten as

$$\eta_e=-C_1\frac{\sinh\kappa_e(1-\xi)}{\cosh\kappa_e}-\frac{q}{n}(1-\xi)+\delta. \tag{58}$$

The differential equation for the strain-hardening region is given by

$$\ddot{\eta}_t=k^2\frac{h}{2}\frac{1+\alpha}{2\alpha}\left\{\frac{2}{h}[q(1-\xi)-n(\delta-\eta)-\beta_1(1-n)\right\} \tag{59}$$

Let $\kappa_t\equiv k\sqrt{\frac{1+\alpha}{2\alpha}n}$ Then the general solution to (59) is given by

$$\eta_t=C_3\sinh\kappa_t\xi+C_4\cosh\kappa_t\xi-\frac{q}{n}(1-\xi)+\delta+\beta\nu. \tag{60}$$

Let the boundary between two regions be at $\xi=\lambda t$. The yield condition and the continuity conditions must be satisfied at $\xi=\lambda_t$.

$$\left.\begin{aligned} &m(\lambda_t)=\frac{2}{h}[q(1-\lambda_t)-n(\delta-\eta(\lambda_t))]=1-n\\ &\eta_e(\lambda_t)=\eta_t(\lambda_t)\\ &\dot{\eta}_e(\lambda_t)=\dot{\eta}_t(\lambda_t) \end{aligned}\right\} \tag{61}$$

Substitution of (58) and (59) into (61) yields the following conditions.is.

$$-C_1\frac{\sinh\kappa_e(1-\lambda_t)}{\cosh\kappa_e}=\nu=C_3\sinh\kappa_t\lambda_t+C_4\cosh\kappa_t\lambda_t+\beta_1\nu$$

$$C_1\kappa_e\frac{\cosh\kappa_e(1-\lambda_t)}{\cosh\kappa_e}=C_3\kappa_t\cosh\kappa_t\lambda_t+C_4\kappa_t\sinh\kappa_t\lambda_t$$

Taking into account the relations

$$1-\beta_1=\beta_2^2\ , \qquad \frac{\kappa_e}{\kappa_t}=\beta_2$$

one obtains the following expressions for the constants:

$$\left.\begin{aligned} C_1 &= -\frac{\nu\cosh\kappa_e}{\sinh\kappa_e(1-\lambda_t)} \\ C_3 &= -\nu\beta_2\{\beta_2\sinh\kappa_t\lambda_t+\cosh\kappa_t\lambda_t\coth\kappa_e(1-\lambda_t)\} \\ C_4 &= \nu\beta_2\{\beta_2\cosh\kappa_t\lambda_t+\sinh\kappa_t\lambda_t\coth\kappa_e(1-\lambda_t)\} \end{aligned}\right\} \quad (62)$$

Again, the following functions are defined in analogy to (41)

$$\left.\begin{aligned} C_t[\tau;u,v] &\equiv \tau\nu\{\tau\cosh(u)+\sinh(u)\coth(v)\} \\ S_t[\tau;u,v] &\equiv \tau\nu\{\tau\sinh(u)+\cosh(u)\coth(v)\} \end{aligned}\right\} \quad (63)$$

Then substitution of (62) into (58) and (60) provides

$$\left.\begin{aligned} \eta_e &= \nu\frac{\sinh\kappa_e(1-\xi)}{\sinh\kappa_e(1-\lambda_t)}\ \frac{q}{n}(1-\xi)+\delta \\ \eta_t &= C_t[\beta_2;\kappa_t(\lambda_t-\xi),\kappa_e(1-\lambda_t)]-\frac{q}{n}(1-\xi)+\delta+\beta\nu \end{aligned}\right\} \quad (64)$$

Finally the boundary conditions at the fixed end are assigned.

$$\eta_t(0)=0 \ : \ C_t[\beta_2;\kappa_t\lambda_t,\kappa_e(1-\lambda_t)]-\frac{q}{n}+\delta+\beta\nu=0$$

$$\dot{\eta}_t(0)=0 \ : \ -\kappa_t S_t[\beta_2;\kappa_t\lambda_t,\kappa_e(1-\lambda_t)]+\frac{q}{n}=0$$

The $\frac{q}{n}\sim\delta$ relation is given parametrically by

$$\left.\begin{aligned} \frac{q}{n} &= \kappa_t S_t[\beta_2;\kappa_t\lambda_t,\kappa_e(1-\lambda_t)] \\ \frac{q}{n}-\delta &= \beta\nu+C_t[\beta_2;\kappa_t\lambda_t,\kappa_e(1-\lambda_t)] \end{aligned}\right\} \quad (65)$$

The validity limits are given by

$$\left.\begin{aligned} &n\le 1 \\ &m(0)=\frac{2}{h}[q-n\delta]\le n+1 \end{aligned}\right\} \quad (66)$$

8. $E_c^{(\alpha)}H_c^{(\alpha)}$-$E_c^{(\alpha)}H_c^{(\alpha)}$-SOLUTION IN THE SECOND DISPLACEMENT PATH WITH VARIABLE N

A displacement path is called the second if the displacement direction is reversed. The inelastic behavior in the second displacement path depends in general upon the deformation history in the first step. If the displacement path is reversed after an inelastic stability limit is attained in the first loading step, the unloading elastic response will occur that is different from the unstable equilibrium path which would have been obtained for the same loading path if the first displacement direction were continued. In other words, the characteristic behavior of the beam-column is that, at any point on that portion of a load displacement curve with a negative slope, there exist two different possible equilibrium paths for one and the same load decrement: one along the first load displacement curve with a negative slope and another for the reversed displacement direction.

If the displacement path is reversed and the loads in the reverse direction is increased, another inelastic response will occur and another inelastic stability limit may appear.

8.1 $E_c^{(1)}H_c^{(1)}$-E_c solution

The superscript (j) will be attached to a quantity or to a symbol to denote its terminal value or state in the j-th displacement step. The elastic solution for the second displacement step from an $E_c^{(1)}H_c^{(1)}$-state is denoted by $E_c^{(1)}H_c^{(1)}$-E_c-solution. The $m\sim\kappa$ relation is given by (25)

$$\kappa(\xi)-\kappa^{(1)}(\xi)=m(\xi)-m^{(1)}(\xi) \qquad ((67)$$

where $\kappa^{(1)}(\xi)=m^{(1)}(\xi)$ for $E^{(1)}$-region: $\lambda_c^{(1)}\le\xi\le 1$ and

$$\kappa^{(1)}(\xi)-m^{(1)}(\xi)=\frac{1-\alpha}{2\alpha}\{m^{(1)}(\xi)-(n^{(1)}+1)\} \text{ for } H_c^{(1)} \text{ region: } 0\le\xi\le\lambda_c^{(1)}$$

The governing differential equations may be written as

$$\ddot{\eta}_{e/e}=k_e^2\{(\frac{q}{-n})(1-\xi)+\delta-\eta_{e/e}\} \qquad \lambda_c^{(1)}\le\xi\le 1$$

$$\ddot{\eta}_{c/e}=k_e^2\{(\frac{q}{-n})(1-\xi)+\delta-\eta_{c/e}\}+\beta_1(k_c^{(1)})^2\{(\frac{q^{(1)}}{-n^{(1)}})(1-\xi)+\delta^{(1)}-\eta_c^{(1)}+\mu^{(1)}\} \qquad 0\le\xi\le\lambda_c^{(1)} \qquad (68a,b)$$

where $\eta_c^{(1)}$ is given by (43b). The general solution (68b) may be reduced to

$$\eta_{c/e}=D_3\sin k_e\xi+D_4\cos k_e\xi+(\frac{q}{-n})(1-\xi)+\delta$$
$$+\beta_1(k_c^{(1)})^2\{\frac{C_c[\beta_2;k_c^{(1)}(\lambda_c^{(1)}-\xi),k_e^{(1)}(1-\lambda_c^{(1)})]}{(k_c^{(1)})^2-k_e^2}+\frac{\beta_2^2}{k_e^2}\mu^{(1)}\} \qquad (69)$$

The solution to (68a) after assigning the boundary condition $\eta(1)=\delta$, may be given by Eq.(34). The continuity conditions that must be maintained at $\xi=\lambda_c^{(1)}$ determine the constants D_3 and D_4 in terms of the constant in Eg.(3.4), which is here denoted by D_1 in stead of C_1.

$$-D_1\frac{\sin k_e(1-\lambda_c^{(1)})}{\cos k_e}=D_3\sin k_e\lambda_c^{(1)}+D_4\cos k_e\lambda_c^{(1)}+\frac{\beta_1\gamma^2\mu^{(1)}}{\gamma^2-\beta_2^2}\gamma^2$$

$$D_1\frac{\cos k_e(1-\lambda_c^{(1)})}{\cos k_e}=D_3\cos k_e\lambda_c^{(1)}-D_4\sin k_e\lambda_c^{(1)}-\frac{\beta_1\gamma^2\mu^{(1)}}{\gamma^2-\beta_2^2}\gamma\cot k_e^{(1)}(1-\lambda_c^{(1)})$$

where $\gamma\equiv n^{(1)}/n=k_c^{(1)}/k_c=k_e^{(1)}/k_e$

$$D_3=D_1-\frac{\beta_1\gamma^2}{\gamma^2-\beta_2^2}S_c[\gamma;k_e\lambda_c^{(1)},k_e^{(1)}(1-\lambda_c^{(1)})]$$
$$D_4=-D_1\tan k_e-\frac{\beta_1\gamma^2}{\gamma^2-\beta_2^2}C_c[\gamma;k_e\lambda_c^{(1)},k_e^{(1)}(1-\lambda_c^{(1)})] \qquad (70a,b)$$

Hence (69) may be reduced to

$$\eta_{c/e}=(\frac{q}{-n})(1-\xi)+\delta-D_1\frac{\sin k_e(1-\xi)}{\cos k_e}$$
$$+\beta_1\gamma^2\mu^{(1)}-\frac{\beta_1\gamma^2}{\gamma^2-\beta_2^2}\{C_c[\gamma;k_e(\lambda_c^{(1)}-\xi),k_e^{(1)}(1-\lambda_c^{(1)})]-C_c[\beta_2;k_e^{(1)}(\lambda_c^{(1)}-\xi),k_e^{(1)}(1-\lambda_c^{(1)})]\} \qquad (71)$$

The boundary conditions at the fixed end require

$$(\frac{q}{-n})+\delta-D_1\tan k_e$$
$$+\beta_1\gamma^2\mu^{(1)}-\frac{\beta_1\gamma^2}{\gamma^2-\beta_2^2}\{C_c[\gamma;k_e\lambda_c^{(1)}k_e^{(1)}(1-\lambda_c^{(1)})]-C_c[\beta_2;k_c^{(1)}\lambda_c^{(1)},k_e^{(1)}(1-\lambda_c^{(1)})]\}=0$$

$$-(\frac{q}{-n})+D_1k_e$$
$$\frac{\beta_1\gamma^2}{\gamma^2-\beta_2^2}\{k_eS_c[\gamma;k_e\lambda_c^{(1)},k_e^{(1)}(1-\lambda_c^{(1)})]-k_c^{(1)}S_c[\beta_2;k_c^{(1)}\lambda_c^{(1)},k_e^{(1)}(1-\lambda_c^{(1)})]\}=0$$

from which one finds

$$D_1=\frac{1}{k_e}\frac{q}{-n}+\frac{\beta_1\gamma^2}{\gamma^2-\beta_2^2}\{S_c[\gamma;k_e\lambda_c^{(1)},k_e^{(1)}(1-\lambda_c^{(1)})]-\frac{\gamma}{\beta_2}S_c[\beta_2;k_c^{(1)}\lambda_c^{(1)},k_e^{(1)}(1-\lambda_c^{(1)})]\}$$

$$(1-\frac{\tanh_e}{k_e})(\frac{q}{-n})+\delta+\beta_1\gamma^2\mu^{(1)}$$

$$-\frac{\beta_1\gamma^2}{\gamma^2-\beta_2^2}\{C_c[\gamma;-k_e(1-\lambda_c^{(1)}),k_e^{(1)}(1-\lambda_c^{(1)})]/\cosh_e$$

$$-C_c[\beta_2;k_c^{(1)}\lambda_c^{(1)},k_e^{(1)}(1-\lambda_c^{(1)})]-\frac{\gamma}{\beta_2}\tanh_e S_c[\beta_2;k_c^{(1)}\lambda_c^{(1)},k_e^{(1)}(1-\lambda_c^{(1)})]\}=0 \qquad (72a,b)$$

The validity limit is given by

$$m(0)=\frac{2}{h}(q-n\delta)\geq-(1+n) \quad \text{or} \quad q-n\delta\geq\mu \qquad (73)$$

8.2 $E_c^{(1)}H_c^{(1)}/E_cH_c$-solution $(\lambda_c\leq\lambda_c^{(1)})$

The new E_c-region consists of the $E_c^{(1)}E_c$-region and the $H_c^{(1)}E_c$-region. The solution to the latter is given by (71). The m-κ relation for the $H_c^{(1)}H_c$-region is given by (26). The governing differentical equation may then be written as

$$\ddot{\eta}_{c/c}+k_c^2\eta_{c/c}=k_c^2\{(\frac{q}{-n})(1-\xi)+\delta-\beta\mu\}-\beta_1(k_c^{(1)})^2\{C_c[\beta_2;k_c^{(1)}(\lambda_c^{(1)}-\xi),k_e^{(1)}(1-\lambda_c^{(1)})]-\beta_2^2\mu^{(1)}\} \qquad (74)$$

The general solution for $\gamma\neq1$ is given by

$$\eta_{c/c}=D_5\sin k_c\xi+D_6\cos k_c\xi+(\frac{q}{-n})(1-\xi)+\delta-\beta_1\mu$$

$$+\frac{\beta_1\gamma^2}{\gamma^2-1}C_c[\beta_2;k_c^{(1)}(\lambda_c^{(1)}-\xi),k_e^{(1)}(1-\lambda_c^{(1)})]+\beta_1\gamma^2\beta_2^2\mu^{(1)} \qquad (75)$$

The continuity conditions and the yield condition $m=-(1+n)$ at $\xi=\lambda_c$ may be expressed in the following form:

$$-D_1\frac{\sin k_e(1-\lambda_c)}{\cos k_e}-\frac{\beta_1\gamma^2}{\gamma^2-\beta_2^2}(C_{c\gamma}^{(1)}-C_{c\beta}^{(1)})+\beta_1\gamma^2\mu^{(1)}=-\mu$$

$$=D_5\sin k_c\lambda_c+D_6\cos k_c\lambda_c-\beta\mu+\frac{\beta_1\gamma^2}{\gamma^2-1}C_{c\beta}^{(1)}+\beta_1\gamma^2\beta_2^2\mu^{(1)}$$

$$D_1\beta_2\frac{\cos k_e(1-\lambda_c)}{\cos k_e}-\frac{\beta_1\gamma^2}{\gamma^2-\beta_2^2}(\beta_2S_{c\gamma}^{(1)}-\gamma S_{c\beta}^{(1)})=D_5\cos k_c\lambda_c-D_6\sin k_c\lambda_c+\frac{\beta_1\gamma^2}{\gamma^2-1}\gamma S_{c\beta}^{(1)} \qquad (76a,b)$$

where $C_{c\gamma}^{(1)}\equiv C_c[\gamma;k_e(\lambda_c^{(1)}-\lambda_c),k_e^{(1)}(1-\lambda_c^{(1)})]$, $S_{c\gamma}^{(1)}\equiv S_c[\gamma;k_e(\lambda_c^{(1)}-\lambda_c),k_e^{(1)}(1-\lambda_c^{(1)})]$

$C_{c\beta}^{(1)}\equiv C_c[\beta_2;k_c^{(1)}(\lambda_c^{(1)}-\lambda_c),k_e^{(1)}(1-\lambda_c^{(1)})]$, $S_{c\beta}^{(1)}\equiv S_c[\beta_2;k_c^{(1)}(\lambda_c^{(1)}-\lambda_c),k_e^{(1)}(1-\lambda_c^{(1)})]$

The constants may then be determined as follows:

$$D_1=\frac{\cos k_e}{\sin k_e(1-\lambda_c)}\{\mu+\beta_1\mu^{(1)}\gamma^2-\frac{\beta_1\gamma^2}{\gamma^2-\beta_2^2}(C_{c\gamma}^{(1)}-C_{c\beta}^{(1)})\}$$

$$D_5=-(1+\beta_1\gamma^2\frac{\mu^{(1)}}{\mu})S_c[\beta_2;k_c\lambda_c;k_e(1-\lambda_c)]-\frac{\beta_1\gamma^2}{\gamma^2-1}(C_{c\beta}^{(1)}\sin k_c\lambda_c+\gamma S_{c\beta}^{(1)}\cos k_c\lambda_c)$$

$$\frac{\beta_1\gamma^2}{\gamma^2-\beta_2^2}\{\beta_2S_{c\gamma}^{(1)}-\gamma S_{c\beta}^{(1)}+\beta_2(C_{c\gamma}^{(1)}-C_{c\beta}^{(1)})\cot k_e(1-\lambda_c)\}\cos k_c\lambda_c$$

$$D_6=-(1+\beta_1\gamma^2\frac{\mu^{(1)}}{\mu})C_c[\beta_2;k_c\lambda_c,k_e(1-\lambda_c)]-\frac{\beta_1\gamma^2}{\gamma^2-1}(C_{c\beta}^{(1)}\cos k_c\lambda_c-\gamma S_{c\beta}^{(1)}\sin k_c\lambda_c)$$

$$+\frac{\beta_1\gamma^2}{\gamma^2-\beta_2^2}\{\beta_2S_{c\gamma}^{(1)}-\gamma S_{c\beta}^{(1)}+\beta_2(C_{c\gamma}^{(1)}-C_{c\beta}^{(1)})\cot k_e(1-\lambda_c)\}\sin k_c\lambda_c \qquad (77a,b,c)$$

The boundary conditions at the fixed end require:

$$\left.\begin{aligned} &D_5-\frac{1}{k_c}\left(\frac{q}{-n}\right)+\frac{\beta_1\gamma^3}{\gamma^2-1}S_c[\beta_2;k_c^{(1)}\lambda_c^{(1)},k_e^{(1)}(1-\lambda_c^{(1)})]=0\\ &D_6+\frac{q}{-n}+\delta-\beta_1\mu+\frac{\beta_1\gamma^2}{\gamma^2-1}C_c[\beta_2;k_c^{(1)}\lambda_c^{(1)},k_e^{(1)}(1-\lambda_c^{(1)})]+\beta_1\gamma^2\beta_2^2\mu^{(1)}=0\end{aligned}\right\}\quad(78)$$

8.3 $E_c^{(1)}H_c^{(1)}/E_cH_c$ solution $(\lambda_c\geq\lambda_c^{(1)})$

In this case, the beam-column consists of the three regions: $E_c^{(1)}E_c$, $E_c^{(1)}H_c$ and $H_c^{(1)}H_c$. The continuity conditions at λ_c between $E_c^{(1)}E_c$-region and $E_c^{(1)}H_c$-region take on the same form as in the first displacement step except that the middle term μ must change its sign corresponding to the bending in the reversed direction. Hence the solution for $\lambda_c^{(1)}\leq\xi\leq1$ may be written as

$$\eta_{e/c}=-C_c[\beta_2;k_c(\lambda_c-\xi),k_e(1-\lambda_c)]+\left(\frac{q}{-n}\right)(1-\xi)+\delta-\beta_1\mu \qquad (79)$$

The general solution for the $H_c^{(1)}H_c$-region is given by (75). The continuity conditions at $\lambda_c^{(1)}$ may be written as

$$\begin{aligned}-C_c[\beta_2,k_c(\lambda_c-\lambda_c^{(1)}),k_e(1-\lambda_c)]&=D_5\sin k_c\lambda_c^{(1)}+D_6\cos k_c\lambda_c^{(1)}\\ &\quad+\beta_1\gamma^2\beta_2^2\mu^{(1)}+\frac{\beta_1\gamma^2}{\gamma^2-1}C_c[\beta_2;0,k_e^{(1)}(1-\lambda_c^{(1)})]\\ -S_c[\beta_2,k_c(\lambda_c-\lambda_c^{(1)}),k_e(1-\lambda_c)]&=D_5\cos k_c\lambda_c^{(1)}-D_6\sin k_c\lambda_c^{(1)}\\ &\quad+\frac{\beta_1\gamma^2}{\gamma^2-1}\gamma S_c[\beta_2;0,k_e^{(1)}(1-\lambda_c^{(1)})]\end{aligned}$$

from which D_5 and D_6 may be determined as

$$\left.\begin{aligned} D_5&=-S_c[\beta_2;k_c\lambda_c,k_e(1-\lambda_c)]-\frac{\beta_1\gamma^2}{\gamma^2-1}S_c[\beta_2\gamma;k_c\lambda_c^{(1)},k_e^{(1)}(1-\lambda_c^{(1)})]\\ D_6&=-C_c[\beta_2;k_c\lambda_c,k_e(1-\lambda_c)]-\frac{\beta_1\gamma^2}{\gamma^2-1}C_c[\beta_2\gamma;k_c\lambda_c^{(1)},k_e^{(1)}(1-\lambda_c^{(1)})]\end{aligned}\right\}\quad(80)$$

If $\lambda_c=\lambda_c^{(1)}$ in (5.11), then

$$C_{c\gamma}^{(1)}=C_c[\gamma;0,k_e^{(1)}(1-\lambda_c^{(1)})]=\gamma^2\mu^{(1)},\quad S_{c\gamma}^{(1)}=S_c[\gamma;0,k_e^{(1)}(1-\lambda_c^{(1)})]=-\gamma\mu^{(1)}\cot k_e^{(1)}(1-\lambda_c^{(1)})$$
$$C_{c\beta}^{(1)}=C_c[\beta_2;0,k_e^{(1)}(1-\lambda_c^{(1)})]=\beta_2^2\mu^{(1)},\quad S_{c\beta}^{(1)}=S_c[\beta_2;0,k_e^{(1)}(1-\lambda_c^{(1)})]=-\beta_2^{(1)}\mu\cot k_e^{(1)}(1-\lambda_c^{(1)})$$

and it may readily be confirmed that D_5 and D_6 in (77) are reduced to the expressions given by (80) The boundary conditions at the fixed end require

$$\begin{aligned} &D_5-\frac{1}{k_c}\left(\frac{q}{-n}\right)+\frac{\beta_1\gamma^3}{\gamma^2-1}S_c[\beta_2;k_c^{(1)}\lambda_c^{(1)},k_e^{(1)}(1-\lambda_c^{(1)})]=0\\ &D_6+\left(\frac{q}{-n}\right)+\delta-\beta_1\mu+\frac{\beta_1\gamma^2}{\gamma^2-1}C_c[\beta_2;k_c^{(1)}\lambda_c^{(1)},k_e^{(1)}(1-\lambda_c^{(1)})]+\beta_1\gamma^2\beta_2^2\mu^{(1)}=0\end{aligned}$$

Hence

$$\left(\frac{q}{-n}\right)\mp k_c\left\{-S_c[\beta_2;k_c\lambda_c,k_e(1-\lambda_c)]-\frac{\beta_1\gamma^2}{\gamma^2-1}\{S_c[\beta_2\gamma;k_c\lambda_c^{(1)},k_e^{(1)}(1-\lambda_c^{(1)})]-\gamma S_c[\beta_2;k_c^{(1)}\lambda_c^{(1)},k_e^{(1)}(1-\lambda_c^{(1)})]\}\right\}$$

$$\left(\frac{q}{-n}\right)+\delta=\beta_1\mu+C_c[\beta_2;k_c\lambda_c,k_e(1-\lambda_c)]+\frac{\beta_1\gamma^2}{\gamma^2-1}\{C_c[\beta_2\gamma;k_c\lambda_c^{(1)},k_e^{(1)}(1-\lambda_c^{(1)})]-C_c[\beta_2;k_c^{(1)}\lambda_c^{(1)},k_e^{(1)}(1-\lambda_c^{(1)})]\}-\beta_1\gamma^2\beta_2^2\mu^{(1)} \qquad (81)$$

Fig.14 shows an example of the computed $q\sim\delta$ curves.

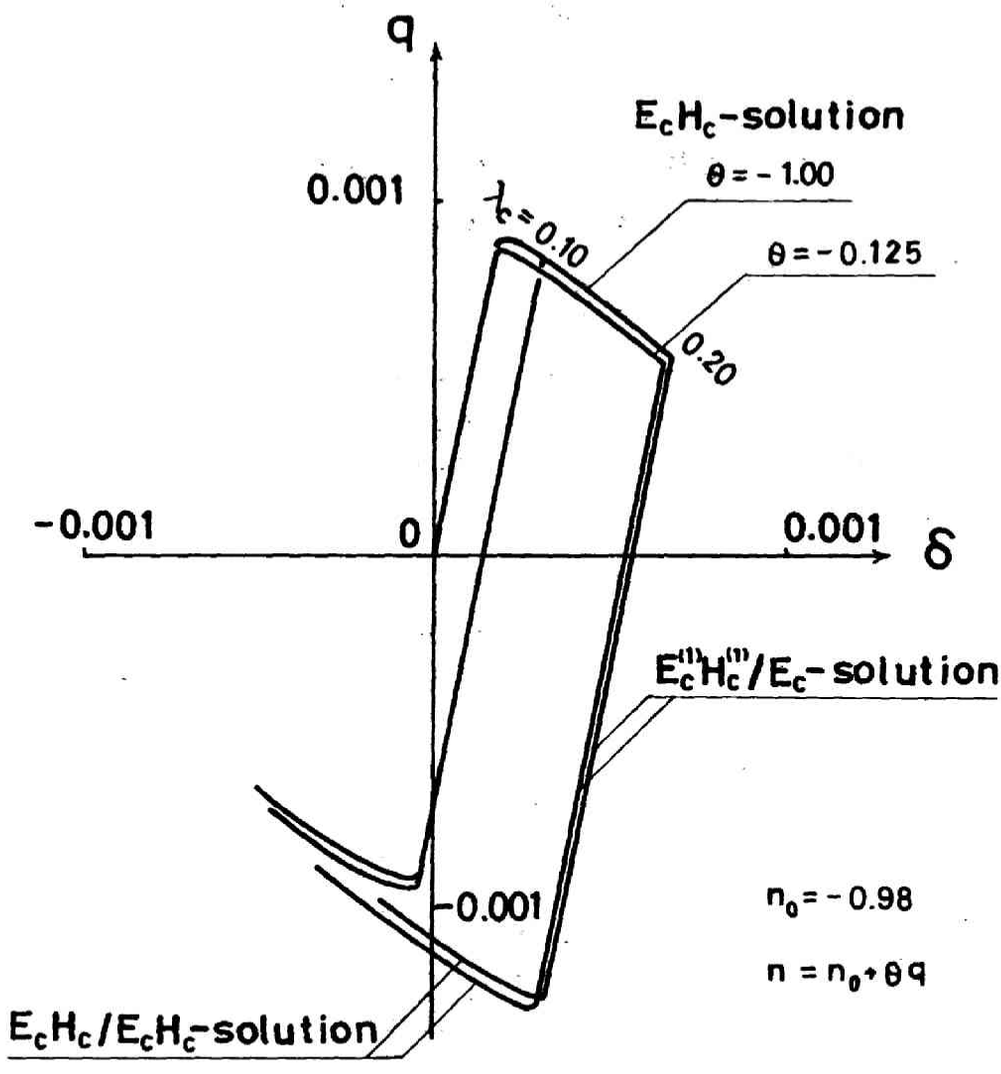
q
0.001
-0.001
0
0.001
δ
E_cH_c-solution
θ = - 1.00
θ = - 0.125
λ_c = 0.10
0.20
$E_c^{(1)}H_c^{(1)}/E_c$-solution
-0.001
n_0 = - 0.98
$n = n_0 + \theta q$
E_cH_c/E_cH_c-solution

Fig.14

9. $E_c^{(1)}H_c^{(1)}/E_cH_c$-SOLUTION IN THE SECOND DISPLACEMENT PATH WITH CONSTANT N.

9.1 $E_c^{(1)}H_c^{(1)}/E_c$-solution

If q is varied under a constant n, then Eq.(67) may be written as

$$\ddot{\eta}_{/e}(\xi)-\ddot{\eta}^{(1)}(\xi)=(k_e^{(1)})^2\{(\frac{q-q^{(1)}}{-\pi^{(1)}})(1-\xi)+\delta-\delta^{(1)}-(\eta(\xi)-\eta^{(1)}(\xi))\} \qquad (82)$$

without regard to $E_c^{(1)}E_c$ or $H_c^{(1)}E_c$. The solution to (82) satisfyingg $\eta_{/e}(1)=\delta$ may be expressed as

$$\eta_{/e}-\eta^{(1)}=-G_1\frac{\sin k_e^{(1)}(1-\xi)}{\cos k_e^{(1)}}+(\frac{q-q^{(1)}}{-\pi^{(1)}})(1-\xi)+\delta-\delta^{(1)} \qquad (83)$$

The $q\sim\delta$ relationship may readily be found from the boundary conditions at the fixed end.

$$\delta-\delta^{(1)}=\frac{\tan k_e^{(1)}-k_e^{(1)}}{k_e^{(1)}}(\frac{q-q^{(1)}}{-\pi^{(1)}}) \qquad (84)$$

Eq.(6.3) is applicable with in the limit given by (73). It is apparent that a similar expression to Eq.(84) may be obtained for the (j)-th displacement step as for as n is constant.

9.2 $E_c^{(1)}H_c^{(1)}/E_cH_c$-solution $\quad(\lambda_c\le\lambda_c^{(1)})$

Since n is kept constant, the $m\sim\psi$ relation (26) is simplified and the differential equation for $\eta_{c/c}$ of the $H_c^{(1)}H_c$-region may be reduced to

$$\ddot{\eta}_{c/c}+(k_c^{(1)})^2\eta_{c/c}=(k_c^{(1)})^2\{(\frac{q}{-\pi^{(1)}})(1-\xi)+\delta-\beta_1C_c[\beta_2;k_c^{(1)}(\lambda_c^{(1)}-\xi),k_e^{(1)}(1-\lambda_c^{(1)})]-\beta_1^2\mu^{(1)}\} \qquad (85)$$

The general solution to Eq.(85) is given by

$$\eta_{c/c}=G_3\sin k_c^{(1)}\xi+G_4\cos k_c^{(1)}\xi+(\frac{q}{-\pi^{(1)}})(1-\xi)+\delta-\beta_1^2\mu^{(1)}+\frac{1}{2}\beta_1k_c^{(1)}\xi S_c[\beta_2;k_c^{(1)}(\lambda_c^{(1)}-\xi),k_e^{(1)}(1-\lambda_c^{(1)})] \qquad (86)$$

Eq.(86) must be continued to Eq.(83) through the continuity conditionsis and the yield condition $m(\lambda_c)=-(1+\pi^{(1)})$, which may be written as

$$C_c[\beta_2;k_c^{(1)}(\lambda_c^{(1)}-\lambda_c),k_e^{(1)}(1-\lambda_c^{(1)})]-G_1\frac{\sin k_e^{(1)}(1-\lambda_c)}{\cos k_e^{(1)}}+\beta_1\mu^{(1)}=-\mu^{(1)}$$

$$=G_3\sin k_c^{(1)}\lambda_c+G_4\cos k_c^{(1)}\lambda_c-\beta_1^2\mu^{(1)}+\frac{1}{2}\beta_1k_c^{(1)}\lambda_cS_c[\beta_2;k_c^{(1)}(\lambda_c^{(1)}-\lambda_c),k_e^{(1)}(1-\lambda_c^{(1)})]$$

$$S_c[\beta_2;k_c^{(1)}(\lambda_c^{(1)}-\lambda_c),k_e^{(1)}(1-\lambda_c^{(1)})]+G_1\beta_2\frac{\cos k_e^{(1)}(1-\lambda_c)}{\cos k_e^{(1)}}$$

$$=G_3\cos k_c^{(1)}\lambda_c-G_4\sin k_c^{(1)}\lambda_c+\frac{1}{2}\beta\{S_c[\beta_2;k_c^{(1)}(\lambda_c^{(1)}-\lambda_c),k_e^{(1)}(1-\lambda_c^{(1)})]-k_c^{(1)}\lambda_cC_c[\beta_2;k_c^{(1)}(\lambda_c^{(1)}-\lambda_c),k_e^{(1)}(1-\lambda_c^{(1)})]\}$$

The constants may be expressed as

$$G_1=\frac{\cos k_e^{(1)}}{\sin k_e^{(1)}(1-\lambda_c)}\{\beta_3^2\mu^{(1)}+C_c[\beta_2;k_c^{(1)}(\lambda_c^{(1)}-\lambda_c),k_e^{(1)}(1-\lambda_c^{(1)})]\}$$

$$G_3=-\{\beta_3^2+C_c[\beta_2;k_c^{(1)}(\lambda_c^{(1)}-\lambda_c),k_e^{(1)}(1-\lambda_c^{(1)})]/\mu\}Sc[\beta_2;k_c^{(1)}\lambda_c,k_e^{(1)}(1-\lambda_c)]$$

$$+\beta_2^2S_c[\beta_2;k_c^{(1)}\lambda_c^{(1)},k_e^{(1)}(1-\lambda_c^{(1)})]+\frac{1}{2}\beta_1k_c^{(1)}\lambda_cC_c[\beta_2;k_c^{(1)}\lambda_c^{(1)},k_e^{(1)}(1-\lambda_c^{(1)})]$$

$$+\frac{1}{2}\beta_1S_c[\beta_2;k_c^{(1)}(\lambda_c^{(1)}-\lambda_c),k_e(1-\lambda_c^{(1)})]\cos k_c^{(1)}\lambda_c$$

$$G_4=-\{\beta_3^2+C_c[\beta_2;k_c^{(1)}(\lambda_c^{(1)}-\lambda_c),k_e^{(1)}(1-\lambda_c^{(1)})]/\mu\}C_c[\beta_2;k_c^{(1)}\lambda_c,k_e^{(1)}(1-\lambda_c)]$$
$$+\beta_2^2C_c[\beta_2;k_c^{(1)}\lambda_c^{(1)},k_e^{(1)}(1-\lambda_c^{(1)})]-\frac{1}{2}\beta_1k_c^{(1)}S_c[\beta_2;k_c^{(1)}\lambda_c^{(1)},k_e^{(1)}(1-\lambda_c^{(1)})]$$
$$-\frac{1}{2}\beta_1S_c[\beta_2;k_c^{(1)}(\lambda_c^{(1)}-\lambda_c),k_e(1-\lambda_c^{(1)})]\sin k_c^{(1)}\lambda_c \qquad (87a,b,c)$$

With these expressions for G_3 and G_4, the $q\sim\delta$ relation is given by

$$\left.\begin{aligned}\frac{q}{-\pi^{(1)}}&=G_3k_c^{(1)}+\frac{1}{2}\beta_1k_c^{(1)}S_c[\beta_2;k_c^{(1)}\lambda_c^{(1)},k_e^{(1)}(1-\lambda_c^{(1)})]\\ \frac{q}{-\pi^{(1)}}&+\delta=\beta_1^2\mu^{(1)}-G_4\end{aligned}\right\} \qquad (88a,b)$$

9.3 $E_c^{(1)}H_c^{(1)}/E_cH_c$-solution $\quad(\lambda_c\geq\lambda_c^{(1)})$

If the H_c-region prevails over the $E_c^{(1)}$-region and hence $\lambda_c\geq\lambda_c^{(1)}$, the solution must be obtained separately. The $E_c^{(1)}H_c$-solution takes on the same form as Eq. (43b) except that μ must be replaced by $-\mu$ due to the yield condition $m(\lambda_c)=-(1+n)$. Hence

$$\eta_{e/c}=-C_c[\beta_2;k_c^{(1)}(\lambda_c-\xi),k_e^{(1)}(1-\lambda_c)]+\left(\frac{q}{-\pi^{(1)}}\right)(1-\xi)+\delta-\beta_1\mu^{(1)}$$
$$(\lambda_c^{(1)}\leq\xi\leq\lambda_c) \qquad (89)$$

The $H_c^{(1)}H_c$-solution is the same as (86). The continuity conditions for (89) and (86) are $\eta_{c/c}(\lambda_c^{(1)})=\eta_{e/c}(\lambda_c^{(1)})$ and $\dot{\eta}_{c/c}(\lambda_c^{(1)})=\dot{\eta}_{e/c}(\lambda_c^{(1)})$, which may be reduced to

$$G_5\sin k_c^{(1)}\lambda_c^{(1)}+G_6\cos k_c^{(1)}\lambda_c^{(1)}=-\beta_1\beta_2^2\mu^{(1)}-C_c[\beta_2;k_c^{(1)}(\lambda_c-\lambda_c^{(1)}),k_e^{(1)}(1-\lambda_c)]$$
$$+\frac{1}{2}\beta_1k_c^{(1)}\lambda_c^{(1)}\beta_2\mu^{(1)}\cot k_e^{(1)}(1-\lambda_c^{(1)})$$
$$G_5\cos k_c^{(1)}\lambda_c^{(1)}-G_6\sin k_c^{(1)}\lambda_c^{(1)}=-S_c[\beta_2;k_c^{(1)}(\lambda_c-\lambda_c^{(1)}),k_e^{(1)}(1-\lambda_c)]$$
$$+\frac{1}{2}\beta_1\beta_2\mu[\beta_2k_c^{(1)}\lambda_c^{(1)}+\cot k_e^{(1)}(1-\lambda_c^{(1)})]$$

G_5 and G_6 may be expressed as

$$G_5=-S_c[\beta_2;k_c^{(1)}\lambda_c,k_e^{(1)}(1-\lambda_c)]+\frac{1}{2}\beta_1k_c^{(1)}\lambda_c^{(1)}C_c[\beta_2;k_c^{(1)}\lambda_c^{(1)},k_e^{(1)}(1-\lambda_c^{(1)})]$$
$$-\beta_1S_c[\beta_2;k_c^{(1)}\lambda_c^{(1)},k_e^{(1)}(1-\lambda_c^{(1)})]+\frac{1}{2}\beta_1S_c[\beta_2;0,k_e^{(1)}(1-\lambda_c^{(1)})]\cos k_c^{(1)}\lambda_c^{(1)}$$
$$G_6=-C_c[\beta_2;k_c^{(1)}\lambda_c,k_e^{(1)}(1-\lambda_c)]-\frac{1}{2}\beta_1k_c^{(1)}\lambda_c^{(1)}S_c[\beta_2;k_c^{(1)}\lambda_c^{(1)},k_e^{(1)}(1-\lambda_c^{(1)})]$$
$$-\beta_1C_c[\beta_2;k_c^{(1)}\lambda_c^{(1)},k_e^{(1)}(1-\lambda_c^{(1)})]-\frac{1}{2}\beta_1S_c[\beta_2;0,k_e^{(1)}(1-\lambda_c^{(1)})]\sin k_c^{(1)}\lambda_c^{(1)} \qquad (90)$$

With these expressions for G_5 and G_6, the $q\sim\delta$ relation is given by

$$\left.\begin{aligned}\frac{q}{-\pi^{(1)}}&=G_5k_c^{(1)}+\frac{1}{2}\beta_1k_c^{(1)}S_c[\beta_2;k_c^{(1)}\lambda_c^{(1)},k_e^{(1)}(1-\lambda_c^{(1)})]\\ \frac{q}{-\pi^{(1)}}&+\delta=\beta_1^2\mu^{(1)}-G_6\end{aligned}\right\} \qquad (91)$$

Fig.15 shows an example of the computed $q\sim\delta$ curves.

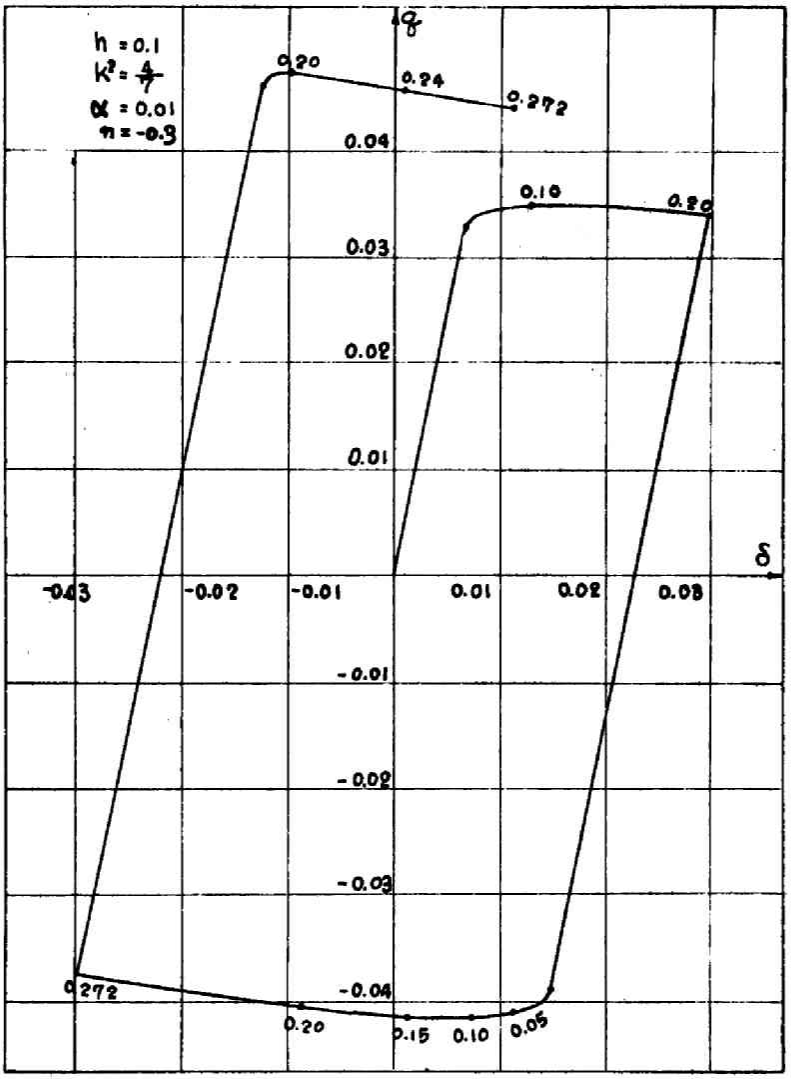
h = 0.1
$k^2 = \frac{4}{7}$
α = 0.01
η = -0.3
q
δ
0.20
0.24
0.272
0.10
0.20
0.04
0.03
0.02
0.01
-0.03
-0.02
-0.01
0.01
0.02
0.03
-0.01
-0.02
-0.03
-0.04
0.272
0.20
0.15
0.10
0.05

Fig.15

10. ALTERNATING BENDING WITHOUT AXIAL FORCE

For the case n=0, the differential equations become simple and may be treated separately.

10.1 EH_{ct}-solution

for the elastic po tion (E-region) satisfying the boundary condition $\eta(1)=\delta$ may be reduced to

$$\eta_e=k^2q\{\frac{1}{2}\xi^2-\frac{1}{6}\xi^3-\frac{1}{3}\}+\delta-C_1(1-\xi). \tag{92}$$

The differntial equation:

$$\ddot{\eta}_p=k^2\{\frac{q}{\alpha}(1-\xi)-\frac{h}{2}(\frac{1-\alpha}{\alpha})\} \tag{93}$$

for the H_{ct}-region may readily be solved. The H_{ct}-solution must then be matched with the E-solution (92) by the continuity conditions and yield condition at the EH_{ct}-boundary $\xi=\lambda$. A parametric representation of the virgin $q\sim\delta$ curves may be reduced to the following:

$$\begin{aligned} q&=\frac{h}{2}\frac{1}{1-\lambda}\\ \delta&=k^2\{\frac{1}{3}q+\lambda^2(\frac{1-\alpha}{\alpha})(\frac{1}{3}q\lambda+\frac{1}{4}h)\} \end{aligned} \tag{94}$$

10.2 $E^{(1)}H^{(1)}_{ct}/EH_{ct}$-solution

The moment-curvature relations for the unloading elastic and strain-hardening regions are given, respectively, by

$$\kappa-\kappa^{(1)}=m-m^{(1)} \tag{95}$$

$$\kappa=-1+\frac{1}{\alpha}(m-1). \tag{96}$$

If the $E^{(1)}H^{(1)}_{ct}$/E-solution and $E^{(1)}H^{(1)}_{c}/H_{ct}$-solution are matched by the continuity conditions and the yield condition which is given by

$$m(\lambda)-m^{(1)}(\lambda)=-2, \tag{97}$$

the following equations of the $E^{(1)}H^{(1)}_{ct}/EH_{ct}$-solution are obtained:

$$\begin{aligned} q-q^{(1)}&=-\frac{h}{1-\lambda}\\ \delta-\delta^{(1)}&=k^2\{\frac{1}{3}(q-q^{(1)})+\lambda^2(\frac{1-\alpha}{\alpha})[\frac{1}{3}(q-q^{(1)})\lambda-\frac{h}{2}]\} \end{aligned} \tag{98}$$

If the second loading step is terminated at $\lambda=\lambda$, then it may be readily be shown that

$$(\delta^{(2)}, q^{(2)})=(-\delta^{(1)}, -q^{(1)}) \tag{99}$$

and consequently that

$$\eta_p^{(2)}(\xi)=-\eta_p^{(1)}(\xi) \tag{100}$$

The deflected shape at the end of the second loading step of the same load or deflection amplitude in the opposite direction is precisely the same as that at the end of the virgin loading step and hence a closed hysteresis loop is obtained as shown in Fig.16. This feature is not due to the piecewise linearity of the stress-strain relation but will also be observed in beams governed by

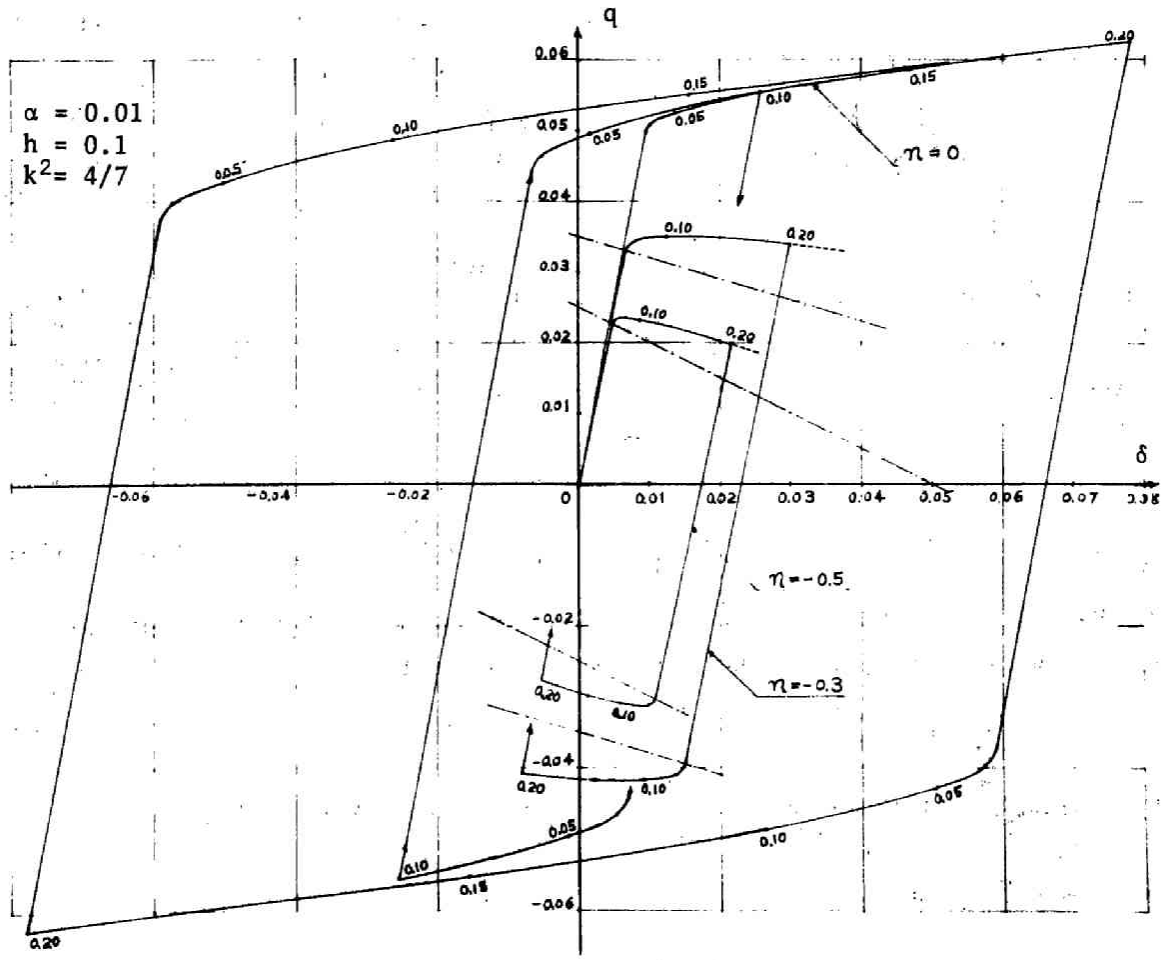

Fig.16

the nonlinear hysteretic stress-strain relation in chapter 9.

11. CONCLIDING REMARKS

The bilinear hysteretic stress-strain relation and the sandwich idealization have enabled one to obtain explicit and piecewisely analytical solutions to the column problem. The geometrical representation of the varying states of stress and the stress line concept have been shown to be useful for finding appropriate constituent solutions. The method of matching constituent solutions is not restricted to the case of a cantilever column but may be applied to various other cases. For instance, the result of Duberg and Wilder [9] which has proved mathematically the existence of the Shanley tangent modulus load, may be discussed from wider point of view. The disadvantage of the method is the labor of matching constituent solutions which is inherent to any piecewise linear approximation. A more realistic hysteretic stress-strain relation will be proposed in a more restricted manner for the problem of alternating plastic bending in chapter 8.

REFERENCES

[1] T. Nakamura, "Elastic-plastic Behavior of a Linear Strain-hardening Idealized Column Subjected to a Repeated Lateral Force, PartII," Proc. 1966 Annual Meeting of the Kinki Branch of A. I. J. at Osaka Univ., May 1966, pp121-124, and also Summaries of Technical Papers of 1966 Annual Meeting of A. I. J. at Univ. of Tokyo, Oct.1966, p285.

[2] M. Yamada, *et al*, "Study on the Elasto-plastic Flexural Behaviors of Wide-Flange Members subjected to Axial load, Part I, II and III," Proc. 1966 Annual Meeting of the Kinki Branch of A. I.JJ. at Osaka Univ., May 1966, pp161-168, and also Summaries of Technical Papers of 1966 Annual Meeting of A. I. J. at Univ. of Tokyo, Oct. 1966, pp282-284.

[3] M. Yamada and K. Shirakawa, "Elasto-plastic Bending Deformation of Wide-Flange Beam-Columns under Axial Compression," Trans. A. I. J., No.141, Nov.1967.

[4] B. Kato, *et al*, "Ultimate Strength of Steel Short Column subjected to Reciprocal load," Summaries of Technical Papers of 1966 Annual Meeting of A. I. J. at Univ. of Tokyo, Oct. 1966, pp281, and B. Kato and H. Akiyama, "The Ultimate Strength of the Steel Beam-Column Part IV," Trans. A. I. J., No.151, Sept. 1968, pp

[5] T. Nakamura and T. Terabayashi, "Elastic-plastic Behavior of a Linear Strain-hardening Idealized Column Subjected to a Repeated Lateral Force, Part II," Proc. 1967 Annual Meeting of the Kinki Branch of A. I. J. at Osaka City Univ., 1967, pp.117-120.

[6] T.Nakamura and T. Kubota, "Elastic-plastic Bhavior of a Linear Strain-hardening Portal Frame Subjected to Repeated Lateral Forces," Proc. 1967 Annual Meeting of the Kinki Branch of A. I. J. at Osaka City Univ., 1967, pp.113-116.

[7] M. Fujimoto, H. Hagura and Y. Matsumoto, "Resarch on the Elasto-plastic Analysis of Steel Structures Subjected to Alternative Lateral Load," Trans. A. I. J., No.145, Mar. 1968

[8] See for instance, S.Igarashi and C.Matsui, "Elastic-plastic Behaviors of Steel Members Subjected to Repeated Combined Stresses,"(Part I,II) Summaries of Technical Papers of the 1969 Annual Meeting of A.I.J., pp1057-1060.

[9] J. E. Duberg, and T. W. Wilder III, "Inelastic Column Behavior", NACA Report 1072, 1952. Also J. E. Duberg, "Inelastic Buckling" Handbook of Engineering Mechanics(Edited by W. Flügge), Chapter 52,pp52-1-9.

APPENDIX

A simple estimate of the error involved in the sandwich approximation can be made by finding asymptots to which the moment-curvature relations would approach if the curvature were increased.. Since the strain-hardening modulus αE is of the order $10^{-2}E$, the relation between a "real" asymptot and the corresponding "sandwich" asymptot for $\alpha \neq 0$ may be considered to be fairly close to that for $\alpha = 0$. A good accuracy of the sandwich approximation when $\alpha = 0$ is a necessary condition, even if not sufficient, of the good accuracy for $\alpha \neq 0$.

The figure below shows the yield curves for a real H section and for the equivalent sandwich section. The maximum deviation for a constant n is about 7%. For a thinner walled H section, the maximum deviation may amount to 9%.

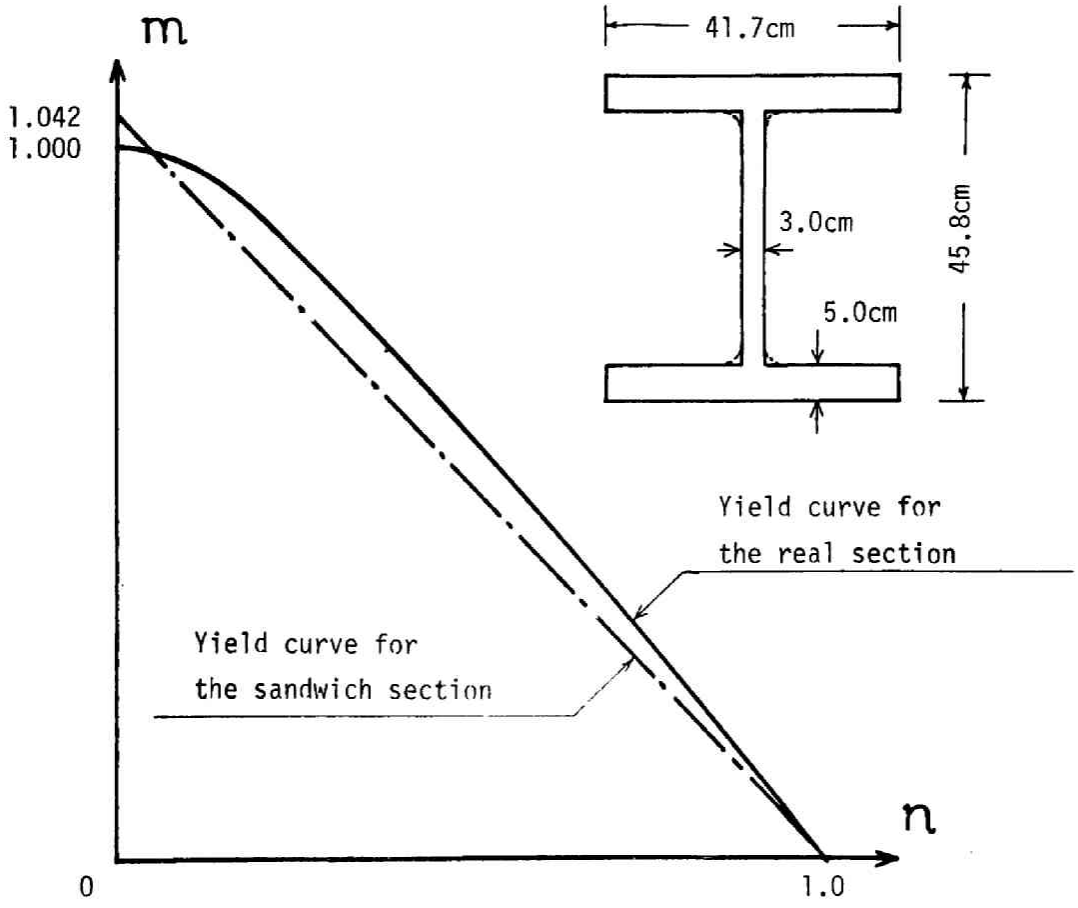

CHAPTER 7

EXPERIMENTAL INVESTIGATION ON THE LOAD DEFLECTION BEHAVIORS AND PLASTIC FATIGUE OF WIDE FLANGE BEAMS SUBJECTED TO ALTERNATING PLASTIC BENDING*

1. INTRODUCTION

As has been mentioned in Ch.3,Sec.2, the importance of the energy absorption capacity as one of the most essential measures representing the overall earthquake resistance of a ductile structure was first pointed out by R.Tanabashi [1] for a one-degree-of-freedom system subjected to a single monotonic load. For varying external disturbances, however, the load-deflection behavior and the plastic energy absorption capacity of a ductile structure under varying loads or forced displacements need also to be investigated. It is then necessary that the cyclic load-deflection behavior and energy absorption capacity of constituent members as well as subassemblages can be predicted on the basis of the behavior of structural steel under varying stresses and strains.

Since R. Tanabashi [2] investigated the behaviors of welded and riveted joints of steel members under alternating bending, a considerable amount of experimental investigations have been done on overall elastic-plastic behaviors of beam-to-column joints subjected to alternating bending with or without axial forces. As for beams, Sidebottom and Chang [3] derived a moment-strain relation for reversed bending based upon a bilinear stress-strain relation to compare with their experimental result. Fujimoto and Hagura's detailed investigations [4] on the behaviors of rectangular and wide-flange

*The results contained in Ch.7,8, and 9 have been published as a series of three papers:"LOAD-DEFLECTION BEHAVIORS AND PLASTIC FATIGUE OF WIDE-FLANGE BEAMS SUBJECTED TO ALTERNATING PLASTIC BENDING," Part I Experimental Investigation by R.Tanabashi,Y.Yokoo,M.Wakabayashi,T.Nakamura,H.Kunieda,H.Matsunaga & T.Kubota; Part II HYSTERETIC AND SKELETON STRESS-STRAIN RELATIONS AND PLASTIC FATIGUE OF FLANGES, BY R.Tanabashi,Y.Yokoo,T.Nakamura,T.Kubota & A.Yamamoto;PartIII STEADY-STATE THEORY, by R.Tanabashi,Y.Yokoo & T.Nakamura;Trans.A.I.J., No.175(pp17-29), No.176(pp25-36),No.177(pp17-28), 1970. The experimental data were obtained in cooperation with junior coauthors.

sections and columns subjected to alternating plastic bending under the presence of axial force were based upon the perfectly-plastic stress-strain relation and subsequently [5] extended to include the effect of strain-hardening in the form of bilinear and trilinear stress-strain relations. Nakamura [6] Yamada *et al* [7] and Kato *et al* [8] have also proposed approximate theories based upon various discrete material point models and bilinear and/or trilinear hysteretic stress-strain relations as first-order approximations. Igarashi and Taga [9] have shown that the experimental skeleton load-deflection curve of a portal frame may be represented by a Ramberg-Osgood equation considerably well and that a similar representation is possible also for hysteretic load-deflection curves. The more realistic hysteresis model for moment-curvature relation represented by a Ramberg-Osgood equation has been applied to inelastic earthquake response analysis by Goel and Berg [10]. The experimental investigation by Wakabayashi and Tsuji [11] revealed more complex load-deflection behaviors of three-story frames with or without bracing under repeated horizontal loads. Carpenter and Lu [12] have shown that the hysteresis loops of a single-story single-bay frame and a three-story single-bay frame subjected to cyclic lateral displacements are very stable even for deformations greater than those corresponding to the maximum lateral loads. While the afore-mentioned works are concerned more with initial transient elastic-plastic behaviors of steel members and frames, Bertero and Popov [13] investigated the plastic fatigue limits of cantilever I-beams subjected to alternating plastic bending in strain-controlled loadings. The plastic fatigue limits of small size metal specimens in bending have been investigated by several researchers [14] but it appears that no effort has yet been made to correlate the result with that of uni-axial tests. On the other hand, it has been shown by Kasiraj and Yao [15] that, when the yield strength of a ductile structure is so small as to

cause more inelastic deformations, the low cycle fatigue damage factor becomes a better indication of structural failure due to earthquake loads.

From this brief survey of the literature, it is apparent that the following problems have not been investigated in detail: (1)The bilinear and trilinear hysteretic stress-strain relations which have been assumed by a number of Japanese authors should be derived quantitatively from experimental stress-strain relations. As no author mentioned above has referred to any experimental hysteretic stress-strain law for structural steel, it does not appear that the hysteretic and skeleton stress-strain relations for SS41 have been derived. Although cyclic stress-strain relations for various metals have been investigated by Morrow[16][17], Serensen and Schneiderovitch [18], Blatherwick and Mowbray[19], Shiratori and Obataya[20], and Davidenkov[21], the hysteretic and skeleton stress-strain relations must be derived from experimental result in a form applicable to the analysis of plastic bending. (2) It is desirable to establish a theory which is able to predict quantitatively the load-deflection behaviors and energy absorption capacity of a member based upon a more realistic stress-strain relation. (3) The afore-mentioned papers on frames and members [3-13] are primarily concerned with load-deflection behaviors but not particularly with the energy absorption capacity characteristics except [9]. One of the most basic tests for the energy absorption capacity characteristics may be that of constant strain or displacement amplitudes. Although Bertero and Popov [13] investigated the plastic fatigue limits of cantilever I-beams under constant bending strain amplitudes, it has not been clarified how the energy absorption capacity of a beam is deteriorated as local and lateral torsional deformations grow. (4) The low-cycle fatigue data applicable to structural members directly are needed. No attempt has been made to correlate the result of

plastic bending fatigue tests of structural members with that of uni-axial tests on the material.

The present chapter and the two succeeding chapters are concerned with these problems. The result of an experimental investigation on the cyclic load-deflection behavior, energy absorption capacity and plastic fatigue limit of SS41 rolled wide-flange beams subjected to alternating plastic bending with constant deflection amplitudes will be presented in this chapter. The test under constant deflection amplitudes was considered to be one of the most basic tests before any other tests of varying amplitudes were attempted. It will be shown that, in spite of complex local buckling and lateral torsional deformations developed during deflection cycling in specimens subjected to larger deflection amplitudes, a load-deflection curve converges in general to a steady-state hysteresis loop. In view of the flange strains measured, it was considered appropriate to assume as a first-order approximation that a flange was essentially subjected to alternating tension and compression of a constant strain amplitude. Plate specimens taken from flanges with surfaces as rolled were therefore subjected to alternating tension and compression of constant strain amplitudes. The experimental result will be presented in chapter 8. The propose of chapter 8 is to derive the hysteretic and skeleton stress-strain relations from the test result and to find the energy absorption capacity and plastic fatigue characteristics of the flange steel. Based upon the hysteretic and skeleton stress-strain relations, a theory of steady-state response will be proposed in chapter 9, which is able to predict the steady-state load-deflection behaviors, the energy dissipated during a steady-state hysteretic cycle and the flange strains. The numerical results in chapter 9 based upon the material data in chapter 8 are compared with the bending test result in chapter 7.

2. TEST SPECIMENS

The test specimens were SS41 wide-flange members of H100x100 as rolled. Fig.1(a) shows a general description of the test. A specimen of length 400cm was subjected to an alternating concentrated load at the midspan with the half-span length 180cm. Since it was anticipated that local plastic buckling deformation will be developed in the course of alternating plastic bending, three stiffners were inserted as shown in Fig.1(b) in the vicinity of the midspan.* Since the present work is concerned not only with hysteretic load-deflection behaviors but also with the energy absorption capacity characteristics up to the plastic fatigue limits of wide-flange members themselves, the stiffners were simply inserted and cemented with epoxy resin to exclude an influence of welding. All the specimens were tested as rolled without any machining for straightening except a saw cut at ends. The test result includes therefore the effect of residual stresses and surface effect. The dimensions of the cross-sections of all the specimens were measured by vernier calipers and micrometers for later use in the analysis in Chapter 9. The tests were carried out on 11 specimens of two series A and B which were manufactured in 1966 and 1967, respectively. Table 1 shows a description of the materials. The data for Series B was taken from the mill sheet whereas the data for Series A are the result of a check analysis on a piece of a flange. The mechanical properties of the materials investigated on flange plate specimens with surfaces as rolled will be presented in Chapter 8.

---

* The result of several preliminary tests for determining the shape of the three stiffners were reported at the 1967 Annual Convention of A.I.J. and is shown in Summaries of Technical Papers of Annual Meeting of A.I.J., 1967, pp413-415.

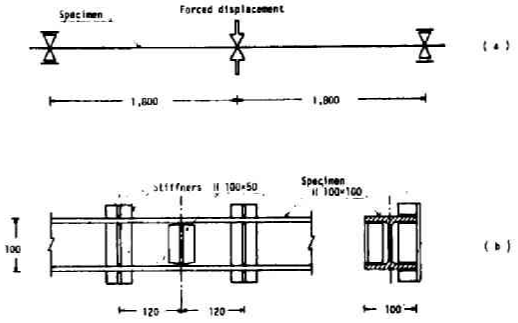

Fig. 1 (a) Specimen and supports. (b) Stiffners

Fig. 1

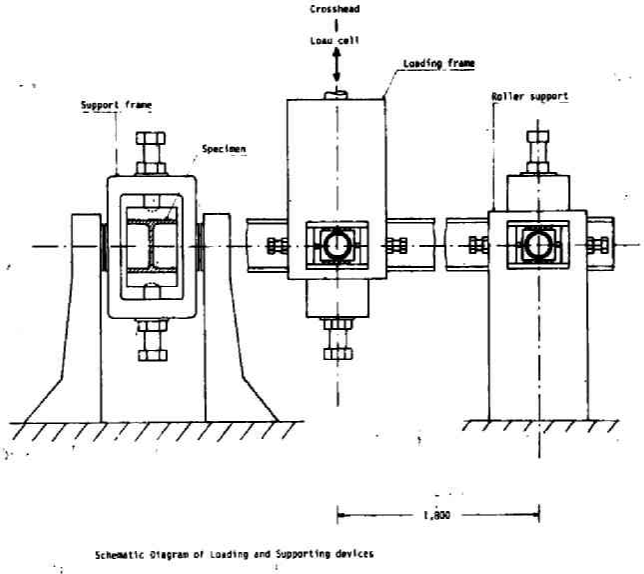

Schematic Diagram of Loading and Supporting devices

Fig.2

TABLE 1 Materials

Series	Lower yield stress (ton/cm^2)	Chemical composition (%)				
		C	S_i	M_n	P	S
A	2.86	0.16	0.09	0.54	0.009	0.018
B	2.84	0.22	0.08	0.50	0.012	0.019

Table 2

Series A		Series B		Control conditions	
Specimen No.	Fully-plastic moment	Specimen No.	Fully-plastic moment	Deflection amplitude	Cross-head speed
11	264 (tcm)	21	251 (tcm)	± 50 (mm)	200 (mm/min)
12	258	20	251	± 60	300
13	265	17	256	± 75	300
14	258			± 80	300
15	268	18	249	± 90	300
16	238	19	254	±100	300

3. TEST SETUP

METHOD OF LOADING Fig.2 shows a schematic diagram of the loading and supporting frames and a specimen inserted. Load is applied through the cross-head of an electronic universal testing machine (AUTOGRAPH) of capacity 10tons and is sensed by a load-cell of tension-compression type inserted between the loading frame and the cross-head. The supporting device which has been designed for the present tests is able to transmit only a vertical reaction under alternating bending without restraining rotation and horizontal displacement. The horizontal displacement of a specimen was restrained only at the central loading frame. A specimen was also able to rotate about the vertical axis which coincided with the axis of loading. Lateral torsional deformation of an S-shape with an inflection point at the midspan was not restrained.

CONTROLL CONDITIONS A constant forced displacement of an equal amplitude in downward and upward bending was assigned at the midspan of a specimen. The crosshead was displaced at a constant speed so that the prescribed displacement pattern was of a triangular one. The testing machine is able to reverse its crosshead motion within 0.5second after a turn signal is automatically operated at the prescribed maximum and minimum displacement positions. Table 2 shows specimen numbers and the control conditions. During first several cycles, the crosshead was stopped at the maximum and minimum displacement positions for several minutes for strain readings.

MEASUREMENT SYSTEM Since the crosshead of the testing machine has been designed to move at a constant speed prescribed within the range 0.05-500mm/min, the displacement of the crosshead may be synchronized with the displacement of the T-axis of the XY(T) recorder of the testing machine. The total elastic deformation of the testing machine in the direction of loading

does not amount to 1% of the smallest prescribed deflection amplitude. The displacement of the crosshead as recorded on the XY(T) recorder may therefore be considered to represent the deflection of a specimen at the midspan.

The output of the load-cell was fed into the X-axis and load-deflection curves were continuously obtained. Since the crosshead speed of 300mm/min was chosen as the standard speed, the test frequencies were different from specimen to specimen with different deflection amplitudes and ranged from 0.75 to 1.25 cpm. At this speed, a potensiometric recorder is satisfactory to record hysteresis loops. All the hysteresis loops for every specimen was recorded up to the cycle at which one of the flanges fractured in tension. The area of a hysteresis loop representing the energy dissipated during one cycle was integrated automatically by an electric integrator and the result was recorded digitally by a printer.

The number of cycles was counted by an electric counter. It was not easy to detect the number of cycles N_c at which a crack visible with naked eyes was initiated in a flange of a specimen partly because of the surfaces as rolled, although numerous hair cracks had been observed long before a deep crack with 2-3cm width penerated through a flange in the thickness direction. An obvious definition of the fatigue life is that number of cycles at which one of the flanges of a specimen fractured throughout in tension. This is denoted by N_{HF}.

On four specimens in Series B, strains at a cross-section between two adjacent stiffners were measured by precalibrated clip gauges of a portal frame shape. Eight clip gauges on each of which two wire strain gauges were mounted, were cemented with epoxy resin to both sides of the two flanges of a specimen. Two wire strain gauges were mounted directly on the midweb where strains must be small.

4. TEST RESULT AND DISCUSSION

(1) Load-deflection Behavior and Hysteresis Loops Fig.3(a) and (b) show typical load-deflection curves recorded on the XY(T)-recorder. The perfectly plastic behavior of a specimen appears only in the virgin loading and the subsequent load-deflection curve rapidly converges to a steady-state hysteresis loop within a few cycles. The shape of the steady-state hysteresis loop varies very slightly with deflection cycling for a specimen subjected to a smaller deflection amplitude, whereas the height which represents the load amplitude is decreased gradually for a specimen subjected to a larger deflection amplitude due to gradual deterioration of the stiffness caused by the development of local buckling deformation accompanied by lateral torsional deformation. Table 2 includes the measured fully-plastic moments.

A steady-state hysteresis loop may be represented by an equation consisting of a linear function and a power function in a similar manner to that used by Morrow[16] for materials. The hysteretic hardening exponents may readily be found from log-log plots of load-plastic deflection relations. A comparison of log-log plots for different specimens must be made after a normalization of the load axis and will be presented in Chapter 9 together with a comparison with a theoretical prediction of loop curves. The hysteretic hardening exponents were found to be close to $\frac{1}{8}$ for both of Series A and B. It is interesting to compare the value with the hysteretic hardening exponents of $\frac{1}{8}$ or $\frac{1}{9}$ recommended for connections by Popov and Pinkney[13].

(2) Deformation In specimens No.11 and 21 subjected to deflection amplitude 50mm, local buckling was not observed and lateral deformation was very slight up to their fracture limits. In specimens No.12 and 20 (60mm), very slight local buckling deformation and small lateral torsional deformation

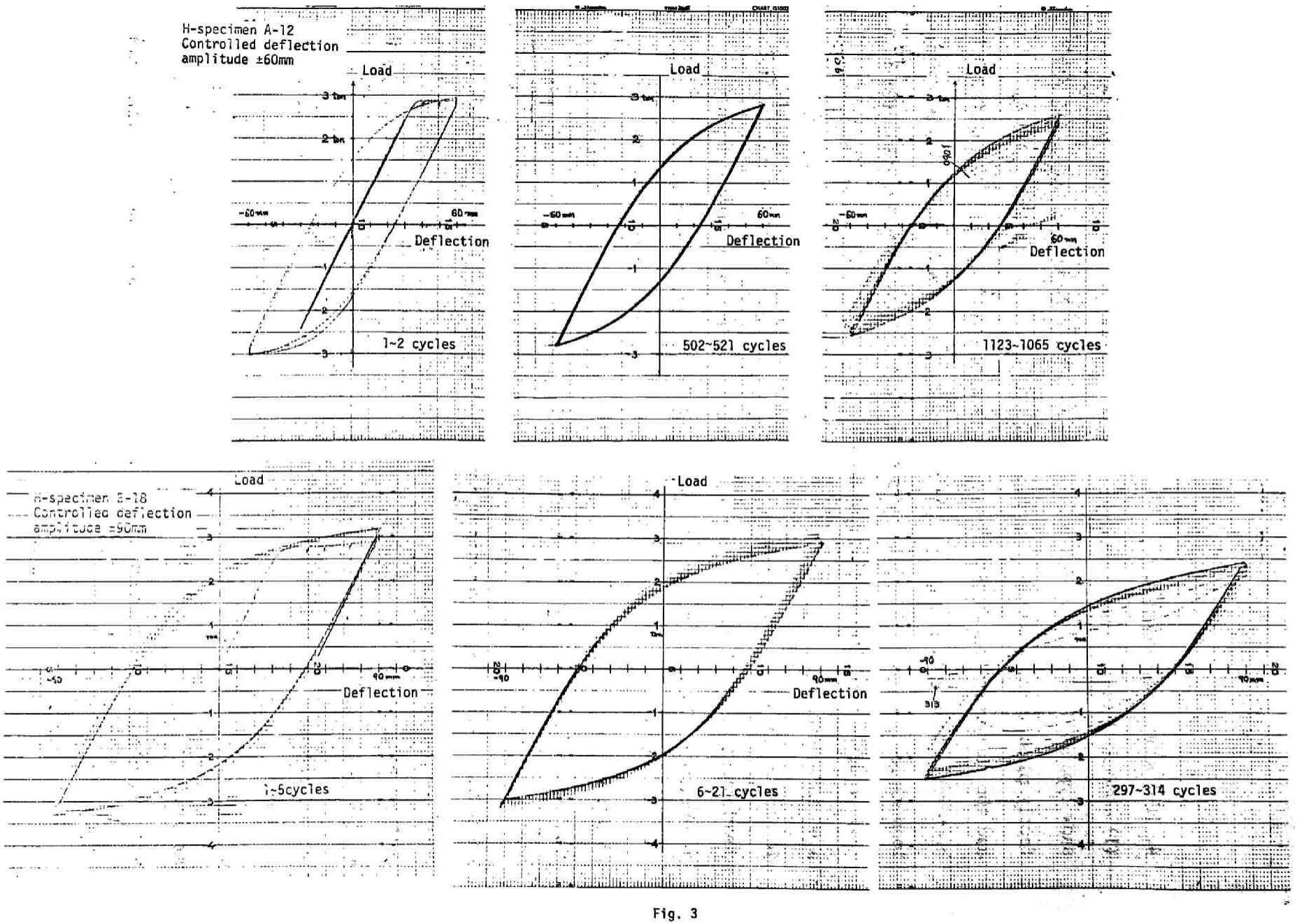
H-specimen A-12
Controlled deflection
amplitude ±60mm
Load
Deflection
1~2 cycles
502~521 cycles
1123~1065 cycles
H-specimen B-18
Controlled deflection
amplitude ±90mm
1~5cycles
6~21 cycles
297~314 cycles

Fig. 3

were gradually developed after several hundred cycles. In a specimen subjected to a greater deflection amplitude than 60mm, lateral torsional deformation of a S-shape with its inflection point at the midspan was developed within a few cycles together with small local buckling waves. A number of buckling waves were developed before crack initiation as shown in Fig.4 for specimen No.15 with the deflection amplitude 90mm. The amplitude of the largest local buckling wave was more than twice as large as the flange thickness.

(3) Strain Distribution Fig.5 shows the strain distributions over the cross-sections located at 6cm from the midspan . Each strain value for a flange is an average over four strain readings on the four wire strain gauges (two in each clip gauge) on the same level from the centroidal axis. D and U denote the distributions at the downward and upward maximum deflection configurations, respectively. The numbers following D and U indicate the number of cycles. Fig.6 shows the variations of extreme fibre strains with respect to the number of cycles. It is apparent from Fig.5 and 6 that the strain distribution in a specimen also converges to a steady state corresponding to the steady-state hysteresis loop. In specimens subjected to smaller deflection amplitudes, the strain distributions did not alter greatly even after several hundred cycles. In specimens subjected to greater deflection amplitudes, the steady-state strain distributions were gradually disturbed after initial several cycles primarily due to the development of local and lateral torsional deformations. As a first-order approximation applicable better to initial steady-state responses than to later cycles, it seems reasonable to assume that both flanges in a specimen are subjected to alternating tension and compression of a constant equal strain amplitude. Although plastic deformation is in general loading and strain history dependent, this assumption neglects the influence of the initial perfectly-plastic response

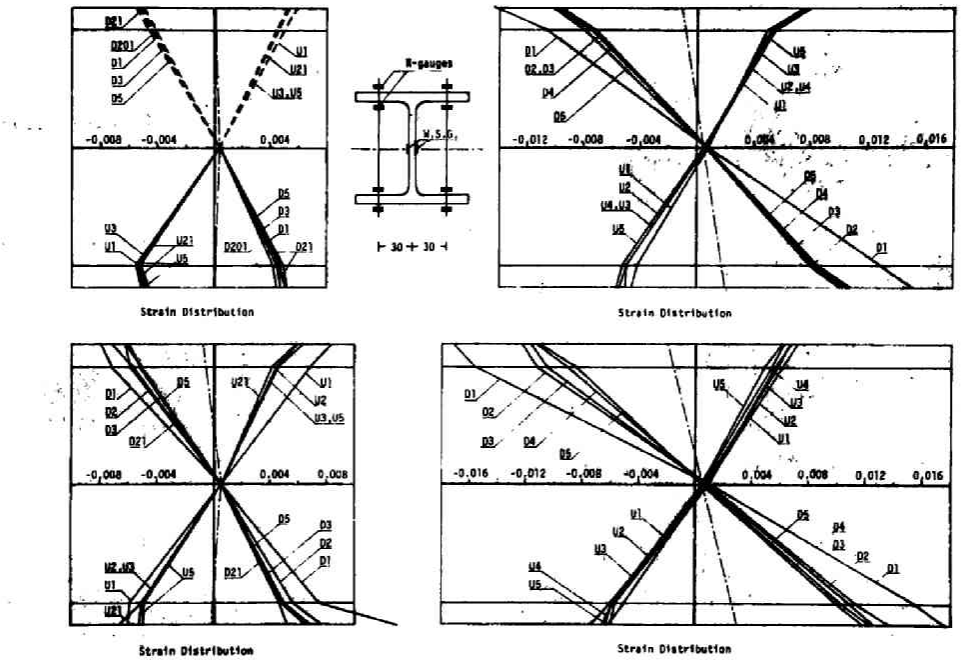
R-gauges
W.S.G.
30 + 30
Strain Distribution
Strain Distribution
Strain Distribution
Strain Distribution

Fig. 5

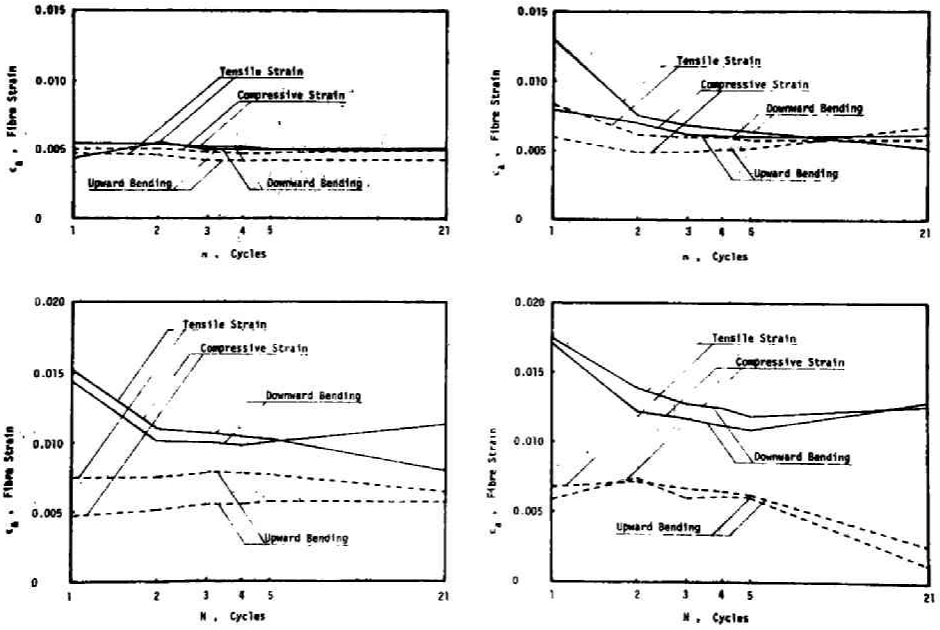
Tensile Strain
Compressive Strain
Upward Bending
Downward Bending
n , Cycles
N , Cycles
Fibre Strain

Fig. 6

Fig.4

Fig.7

on the subsequent responses. The strain at midweb was caused in the initial perfectly plastic response and remained almost constant during the subsequent cycles.

(4) Crack Propagation Numerous hair cracks had been observed long before a deep crack penetrated through the thickness of a flange. A deep crack was mostly initiated from an edge of a flange at the concave side of the largest local buckling wave. After it penetrated through the thickness of the flange with a fracture surface normal to the member axis, it propagated rapidly to the flange-to-web intersection and after several cycles it penetrated through the other half of the flange and through a substantial part of the web with an irregular inclined fracture surface. Fig.7 shows the fracture surface for Specimen No.11. A fracture surface in a web generally made roughly 45° with the web surface and some of the surfaces were of an irregular saw-tooth shape.

(5) δ_{ap}- N_{HF} relation Fig.8 shows a log-log plot of the steady-state dimensionless plastic deflection amplitude δ_{ap} (= Δ_{ap}/L) versus the fatigue life N_{HF}, where Δ_{ap} denotes the plastic component of the deflection amplitude of a specimen and L, the constant half-span length, 180cm. For the sake of brevity, Δ_{ap} will be called the plastic deflection amplitude hereafter. The plot resulted in two bands of points for the two series of specimens. The two straight lines given by

$$\delta_{ap} N_{HF}^{\gamma_i} = \delta_{ai} \qquad (1)$$

where γ_1 =0.45 and δ_{a1} = 0.31 for Series A and γ_2 =0.43 and δ_{a2} =0.35 for Series B, appear to represent the tendency of the test result. It is interesting to observe that similar rolled H-specimens with the same stiffners but from different manufacturing lots have resulted in apparently different fatigue

ductility properties. The tips of the arrows in Fig. 8 indicate the numbers of cycles at which hair cracks were observable.

(6) Energy Dissipation per Cycle, d_p Fig.9 shows the variations of energy dissipation per cycle d_p with respect to number of cycles. While the energy absorption capacity of a specimen subjected to a smaller deflection amplitude is almost constant up to initiation of a deep crack, the deterioration of the energy capacity is apparently considerable in a specimen subjected to a larger deflection amplitude due to gradual development of local buckling and lateral torsional deformations. Fig.9 may also be regarded to show a relation between the dissipated energy d_p and the fatigue life N_{HF}. Although a log-log plot of the energy dissipation per cycle versus the fatigue life for the steel under tension and compression results in a straight line as will be shown in Part II, it is apparently difficult to consider a similar relation for the present case due to the variation of d_p with respect to N,the number of cycles, and also due to the circumstance that local buckling deformation must have influenced on the magnitude of N_{HF}. The energy dissipation per cycle during the initial several cycles must have been less influenced by the disturbances than that in later cycles. Fig.10 is a log-log plot of $d_p^{(3)}$ (toncm) of the third cycle versus the corresponding plastic deflection amplitude Δ_{ap} (cm) The two straight lines fitting the experimental points may be represented by

$$d_p^{(3)} = c_i(\Delta_{ap})^{\lambda_i} \qquad (2)$$

where c_1 = 7.3 (toncm) and λ_1 =1.2 for Series A and c_2 =8.3(toncm) and λ_2=1.1 for Series B.

(7) Total Energy Dissipation Capacity. D_p Because of the scatter in δ_{ap}-N_{HF} relation, it is anticipated that the total energy dissipation capacity D_p will also show some scatter when plotted with respect to Δ_{ap}. Yet the

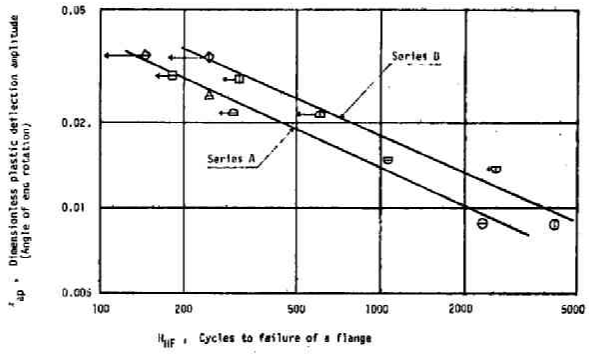

Fig.8

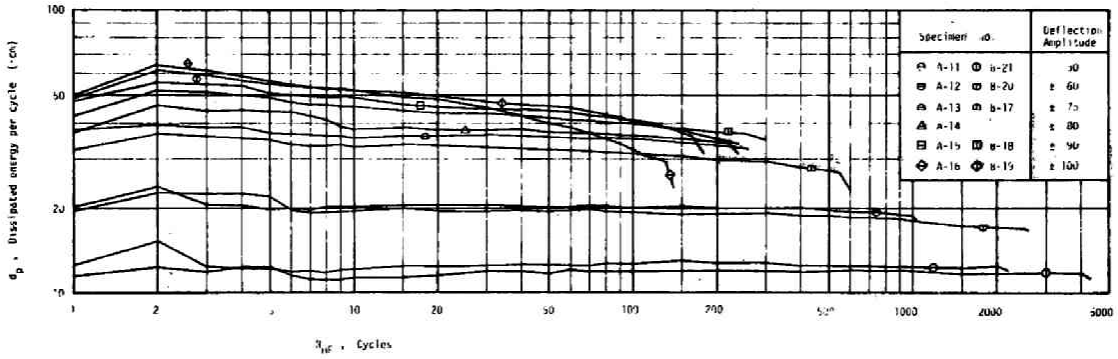

Fig.9

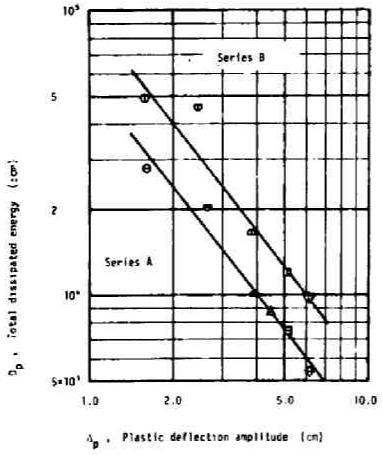

Fig.11

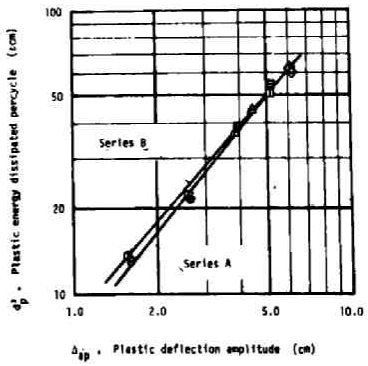

Fig.10

tendency of the experimental result observed in the log-log plots in Fig.10 may be represented by

$$D_p \, \Delta_{ap}^{1.25} = D_i \qquad (3)$$

where $D_1 = 5.7 \times 10^4 (ton\text{cm})$ and $D_2 = 9.7 \times 10^4 (ton\text{cm})$, for Series A and B, respectively.

5. CONCLUSION

The cyclic load-deflection behavior, energy absorption capacity and plastic fatigue limit of SS41 rolled wide-flange members subjected to alternating plastic bending with constant deflection amplitudes have been investigated experimentally. Although the specimens of the same nominal size have been tested, a normalization with respect to the cross-sectional dimensions and the mechanical properties of the material will be necessary for a more accurate quantitative treatment of the test result to be compared with a theoretical prediction as will be shown in Chapter 9. The following features may however be pointed out:

(1) The load-deflection curve for a specimen and the corresponding strain distribution rapidly converges to a steady-state response and the flanges may, as a first-order approximation, be regarded as being subjected to alternating tension and compression of a constant and almost equal strain amplitude.

(2) Since the cross-sectional properties of a specimen is deteriorated as local buckling and lateral torsional deformations are developed,particularly when subjected to forced displacement of a larger deflection amplitude, Eq.(1) which is apparently similar to the well-known Manson-Coffin relation includes the effect of the deterioration upon the fatigue life. If the largest flange strains in the steady-state of an idealized specimen without local buckling and lateral torsional deformations can be estimated and may be assumed to obey

a Manson-Coffin relation to be derived in Part II, then the fatigue life of the idealized specimen can be predicted with respect to which the effect of deterioration in the corresponding real member may be evaluated approximately. It is noticed that similar SS41 wide-flange specimens from different manufacturing lots have exhibited apparently different fatigue ductility properties.

(3) The energy dissipated in a specimen during one cycle of the initial steady state is clearly related to the plastic deflection amplitude by a linear law on the log-log scale as given by Eq.(2).

(4) While the energy dissipated during one cycle of the initial steady state increases with the plastic deflection amplitude, the total energy dissipation capacity decreases with the plastic deflection amplitude. This feature is similar to that of metals subjected to strain cycling as has been shown by Morrow [16].

REFERENCES

[1] R.Tanabashi,"Some Considerations on Destructive Elements of Earthquake Ground Motion and Earthquake Resistance of Structures", J. Architectural Inst. Japan, Vol.49, No.599, May 1935
R.Tanabashi, "On the Resistance of Structures to Earthquake Shocks", Memoirs, College of Engng., Kyoto Imp.Univ., Vol.9,No.4, 1937

[2] R.Tanabashi, "Alternating Bending Test of Welded Beam-to column Joints", J.Japanese Welding Soc., Vol.9, No.12, pp587-598, 1937
R.Tanabashi, "Test to Determine the Behavior of Riveted Joints of Steel Structure under Alternate Bending Moment", Memoirs College of Engng., Kyoto Imp.Univ., Vol.8, No.4, Kyoto, 1936

[3] O. M. Sidebottom and C. T. Chang, "Influence of the Bauschinger Effect on Inelastic Bending of Beams", Proc.First U.S. Nat'l. Congr.Appl.Mech., 1951, pp631-639

[4] M. Fujimoto and H. Hagura, "Research on the Elasto-plastic Analysis of Steel Section Subjected to Alternative Load", Trans.A.I.J., Part I, No.117, Nov.1965, Part II, No.121, Mar.1966, Part III, No.122, Apr.1966, Part IV, No.125, Jul.1966

[5] M. Fujimoto, H. Hagura and Y. Matsumoto, "Research on the Elasto-plastic Analysis of Steel Structures Subjected to Alternative lateral Load", Trans.A.I.J., No.145,Mar.1968

[6] Tsuneyoshi Nakamura, "Elastic-plastic behavior of a Linear Strain-hardening Sandwich Column Subjected to an Alternating Lateral Force", Summaries of Technical Papers of Annual Meeting of A.I.J.,1966, p285

[7] M. Yamada and K. Shirakawa, "Elasto-plastic Bending Deformation of Wide-flange Beam-columns under Axial Compression", Trans.A.I.J, No.141 Nov.1967,

[8] B. Kato and H. Akiyama, "The Ultimate Strength of the Steel Beam-column", Part IV, Trans.A.I.J.,No.151, Sept.1968

[9] S. Igarashi and N. Taga, "Hysteretic Characteristics and Structural Damping of Steel Structures under Alternate Lateral Loading", Trans.A.T.J. No.120, Feb.1966
S. Igarashi, N. Taga, S. Takada and Y. Koyanagi, "Plastic Behavior of Steel Frames under Cyclic Loadings", Trans.A.I.J., No.130, Dec.1966

[10] S. C. Goel and G. V. Berg, "Inelastic Earthquake Response of Tall Steel Frames", J. Structural Div ,Proc.ASCE,Vol.94, No.ST8, Aug.1968

[11] M. Wakabayashi and B. Tsuji, "Experimental Investigation on the Behavior of Frames with and without Bracing under Horizontal Loading", Bull. Disaster Prev. Res. Inst., Kyoto Univ., Vol.16, Part II, No.112,Jan.1967, "Experimental Studies on the Frames under Horizontal Loading", Annuals Disaster Prev.Res.Inst., Kyoto Univ.,No 10A, 1967

[12] L. D. Carpenter and Le-Wu Lu, "Behavior of Steel Fames Subjected to Repeated and Reversed Loads", Preliminary Publications of the 8th Congr. of IABSE

[13] V. V. Bertero and E. P. Popov, "Effect of Large Alternating Strains of Steel Beams", J.Structural Div.,Proc.ASCE, Vol.91, ST1,Feb.1965, pp1-12
Also E. P. Popov and R. B. Pinkney,"Reliability of Steel Beam-to-column Connections under Cyclic Loading", 4th World Conf. Earthquake Engng., Santiago, Chile, Jan.1969

[14] See for instance, W. Johnson, J. H. Lamble and M. Safdar Ali, "Low Cycle High Strain Bending Fatigue Tests on Ductile Metals", Int. J. Mech. Sci, Vol.7 1965, pp1-13

[15] I. Kasiraj and J. T. P. Yao, "Fatigue Damage in Seismic Structures", J.Structural Div., Proc. ASCE, Vol.95, No.ST8, Aug.1969

[16] JoDean Morrow, "Cyclic Plastic Strain Energy and Fatigue of Metals", INTERNAL FRICTION, DAMPING, AND CYCLIC PLASTICITY, ASTM STP378, 1964 pp45-87

[17] JoDean Morrow, "Low Cycle Fatigue Evaluation of Inconel 713C and Waspaloy", J.Basic Engng., Jan.1965, pp275-289

[18] S. V. Serensen and R. M. Schneiderovitch, "Elasto-plastic Cyclic Deformation", Proc.ASTM, Vol61,1961, pp789-799

[19] A. A. Bratherwick and D. F. Mowbray,"Stress-strain Relationships in Low and Intermediate Cycle Fatigue", Proc.ASTM, Vol.64, pp561-580

[20] E. Shiratori and Y. Obataya, "Shape of the Cyclic Stress-strain Loop in the Low Cycle Fatigue Tests", Trans. Japan Soc. Mech. Engrs, Vol.35, No.272, Apr.1969, pp705-710

[21] B. J. Lazan, "DAMPING OF MATERIALS AND MEMBERS IN STRUCTURAL MECHANICS", Pergamon Press, 1968, pp97-100

CHAPTER 8

HYSTERETIC AND SKELETON STRESS-STRAIN RELATIONS AND PLASTIC FATIGUE OF FLANGES

1. INTRODUCTION

The cyclic stress-strain relations are the fundamental relations based upon which a theory can be established, as will be shown in chapter 9, that is able to predict the cyclic load-deflection behaviors and energy dissipation of rolled wide-flange members subjected to alternating plastic bending of constant deflection amplitudes. Cyclic stress-strain relations for various metals have been investigated by a number of researchers [chapter 7-16~21]. Morrow [Ch.7-16, 17] has shown that the plastic component of the hysteretic strain measured from a tip of a hysteresis loop may be represented by a power function of the stress measured from the tip and proposed a hysteretic stress-strain relation in the form of the Ramberg-Osgood equation. In the Davidenkov equations shown in Lazan's book [Ch.7-21], the stress has been expressed as a sum of a linear and nonlinear terms of strain. Shiratori and Obataya [Ch.7-20] have shown that the hysteretic stress-strain relations in constant load-amplitude tests may be regarded to consist of three piecewisely applicable power laws. Ilda *et al* [1] have recently shown that the strain hardening exponent for a tempered and quenched 60kg/mm^2 high tensile steel depends upon strain wave patterns and amplitudes of strain cycling.

In this chapter, the hysteretic and skeleton stress-strain relations for SS41 rolled wide-flange members which, to the authors' knowledge, have not been obtained in forms applicable readily to the analysis of plastic bending, will be derived in Morrow's approach. In order that the present test

result may be directly applicable to the analysis of wide-flange members subjected to alternating plastic bending, plate specimens cut out of the flanges of wide-flange specimens with surfaces as rolled, have been preferred to other types of specimens in order to include the surface effect but exclude the size effect as far as possible. Contrary to Morrow's first approximation it will be shown that the hysteretic strain-hardening exponent is greatly different from the skeleton strain-hardening exponent. A modified hysteretic stress-strain relation will be derived which takes this difference into account. The energy absorption capacity of the specimens will also be investigated up to the plastic fatigue limit. The derived stress-strain relations may be used as a lead to bilinear or trilinear approximation, if desired.

2. SPECIMEN

Fig.1 shows the shape and size of the plate specimens. A specimen was manufactured by shapering from a half flange of 40mm width, so that the uniform reduced test section was entirely within the portion of the flange with a uniform thickness. The shapered surface was finished with abrasive cloth (AA320) in the direction of loading. The plate surfaces of a specimen were left as rolled to include the surface effect. No heat treatment was applied to the specimens. The size of a finished specimen was measured on a flat surface by a travelling microscope. The plate thickness was measured by a micrometer. The cross-sectional areas of test sections were within 0.78~0.82 cm^2. Plate specimens were taken from two different wide-flange specimens; P-4 and B-17. The H-specimen B-17 appeared already in Chapter 7 and P-4 is one of the members in the same lot as Series A of Chpter 7 and was subjected to a preliminary test. The chemical composition of the steels are therefore as shown in Table 1 of Chapter 7.

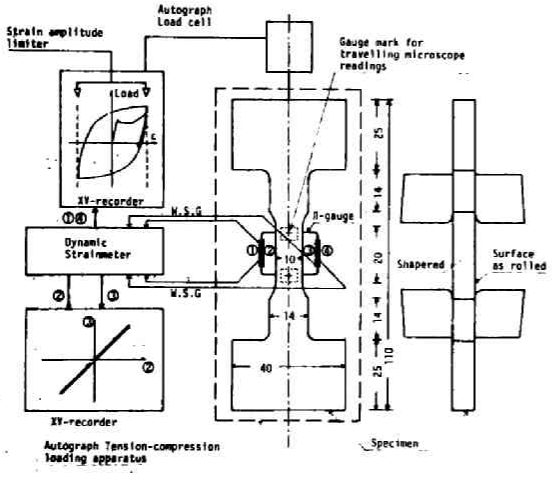

Fig.1

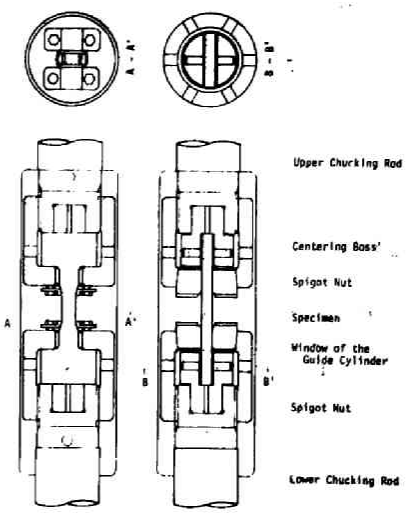

Fig.2

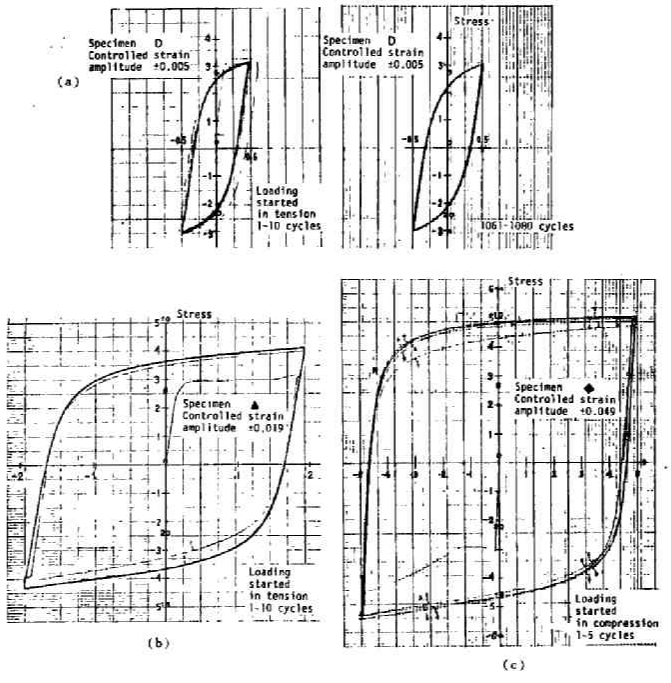

Fig.3

3. TEST SETUP

GRIPPING AND LOADING APPARATUS The tension-compression gripping and loading apparatus which had been designed* originally for typical solid cylindrical specimens was modified#partially for a plate specimen as shown in Fig.2. A specimen is inserted into a spigot nut through its keyhole and then turned around by 90° so that the shoulders of the specimen support the spigot nut. A pair of wedges are then inserted into the keyhole not only for clamping the specimen and for reducing the buckling length but also for reducing misalignment as small as possible. After the specimen is turned upside down, an adjusting boss is placed at the end of the specimen and then the spigot nut is screwed onto the upper chucking rod. After the lower spigot nut is fixed to the other end of the specimen in a similar manner, the lower chucking rod is screwed into the lower spigot nut. Both chucking rods are contained in a guide cylinder which is fixed to the york. Load was applied by the universal testing machine of capacity 10 tons (AUTOGRAPH) and sensed by a load-cell of tension-compression type.

MEASUREMENT SYSTEM Fig.1 shows a schematic diagram of the measurement system. Strain was measured by a pair of precalibrated clip gauges mounted on a specimen symmetrically with epoxy resin as shown in Fig.1. Two wire strain gauges were mounted on each clip gauge. A care had to be taken to mount and use clip gauges under almost the same temperature as at calibration. Some of the calibrations of clip gauges for specimens were modified by the readings of a pair of travelling microscopes. The output of the load cell and the output of a pair of strain gauges were fed into the XY-recorder of the testing machine. All the hysteresis loops were recorded up to fracture. Cracks were detected

---

*Designed by Shimadzu for an AUTOGRAPH universal testing machine.
#The modified design is due to the present author.

by continuous observations with naked eyes from both sides of a specimen. The numbers of cycles to crack initiation were not of a uniform accuracy.

CONTROL CONDITIONS The X-axis of the XY-recorder of the testing machine is equipped with a pair of amplitude limiter. All the tests were completely reversed cyclic strain-controlled tests under zero mean strain. Tests were conducted mostly at a constant crosshead speed of 2mm/min. The strain-rates in the elastic and plastic ranges were considerably different. The frequencies were different from specimen to specimen and were within the range from 0.2 1.0 cpm, which was considered to result in the strain-rates of the same order as in the alternating bending of Chapter 7. Strain cycling was continued up to fracture. A specimen was able to dissipate some more energy during more than several cycles after the initiation of a crack visible with naked eyes.

4. HYSTERETIC AND SKELETON STRESS-STRAIN RELATIONS

4.1 STEADY STATE HYSTERESIS LOOPS Fig.3(a-c) show some of the recorded hysteresis curves for the SS41 steel subjected to cyclic tension-compression of equal strain amplitudes. The steel exhibits the perfectly-plastic behavior only under a virgin loading and the initial yield point disappears in the cyclic state. It is observed apparently that the stress-strain curve of a specimen converges within a few cycles to a steady-state hysteresis loop under the strain cycling of zero mean strain. A collection of steady-state hysteresis loops for different strain amplitudes indicates the existence of a skeleton curve as has already been discussed by Morrow[Ch.7-16, 17]. A "skeleton curve" is defined as that curve obtained by connecting the tips of hysteresis loops for different strain amplitudes.

The converging process to a steady-state loop may be idealized as shown schematically in Fig.4. The straight lines $\overline{OY}$ and $\overline{YR}_A$ represent the virgin elastic-perfectly plastic behavior. Let P denote the point on the skeleton curve for which $\sigma = \sigma_y$. Let the plastic strain at P be denoted by ε_{py}. If the steel is subjected to cyclic tension-compression of an equal strain amplitude which is less than $\varepsilon_y + \varepsilon_{py}$, then the stress-strain curve after the virgin response may be represented by $R_A \rightarrow A_1 \rightarrow A_2 \rightarrow etc.$ and apparently converges in a few cycles to a steady-state loop the tips of which are below the yield stress σ_y. If, on the other hand, the strain amplitude is greater than $\varepsilon_y + \varepsilon_{py}$, then the stress-strain curve takes on the converging process $R_B \rightarrow B_1 \rightarrow B_2 \rightarrow etc.$

A steady-state hysteresis loop after the third cycle remain almost unchanged during most of its fatigue life except those of the three specimens subjected to larger strain amplitudes in which some buckling deformation had been accumulated when fractured. As has been pointed out by Morrow[Ch.7-16], the steel has indeed exhibited cyclic softening behavior when subjected to strain

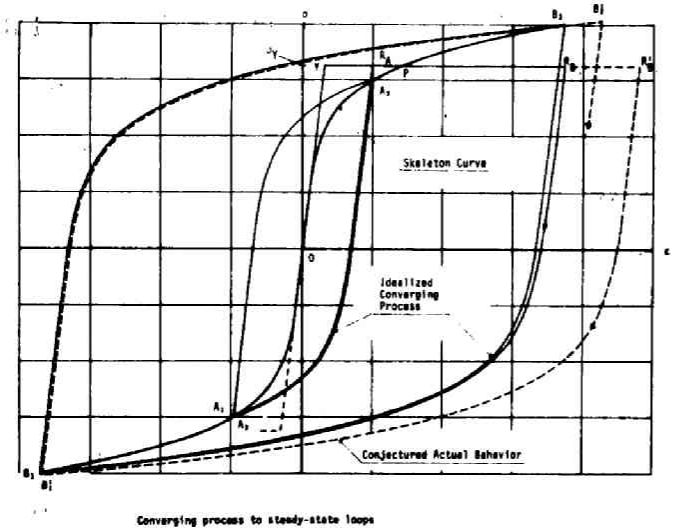

Converging process to steady-state loops

Fig.4

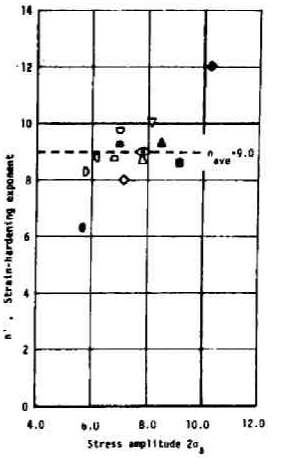

Hysteretic strain hardening exponents

Fig.6

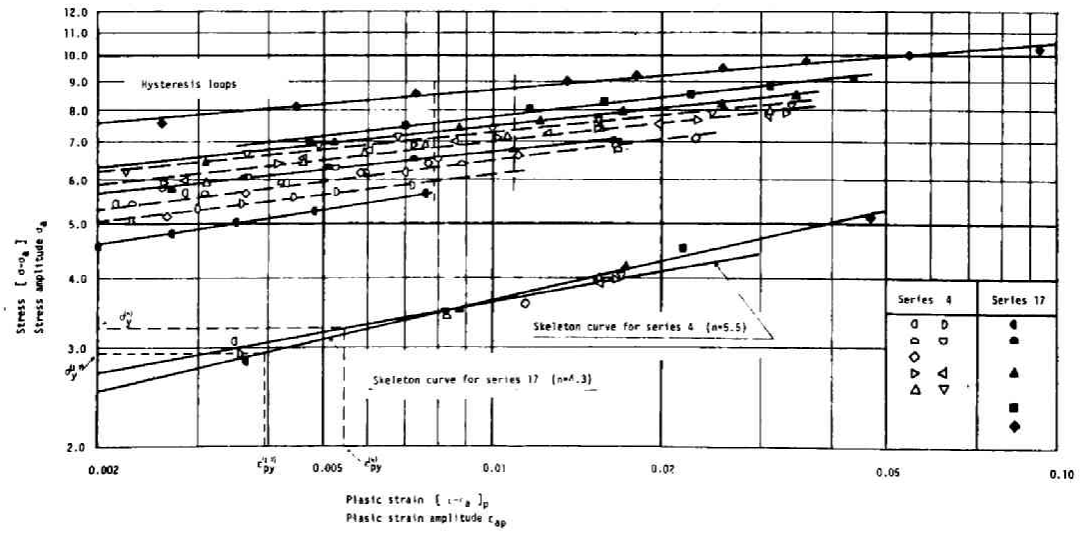

Fig.5

cycling of ±0.5%, whereas it has cyclically hardened for larger strain amplitudes than =±0.5%. The variation may also be represented in terms of the plastic energy dissipation capacity as will be shown later.

4.2 HYSTERETIC AND SKELETON STRAIN-HARDENING EXPONENTS A steady-state hysteresis loop which may be considered to have reached in the third or fourth cycle consists of a pair of smooth curves which are almost symmetric with respect to the origin in the plane of the nominal stress and the engineering strain. Each half of such a curve may be represented as the sum of the linear (elastic) part and the plastic part governed by a power law [Ch.7-16]. The origin is first displaced to a tip of a steady-state loop. Two straight lines are then drawn with the virgin elastic slope $\tan^{-1}E$ at the tips. Although an experimental steady-state loop appears to have a slightly smaller elastic slope than $\tan^{-1}E$ and the two straight lines are therefore not strictly tangent to the curve at the tips, the nominal virgin elastic slope with E=2,100 t/cm² was used. The strain measured with respect to one of these straight lines is the plastic strain $[\varepsilon \pm \varepsilon_a]_p$, where ε_a denotes the total strain amplitude. The total strain range is therefore $2\varepsilon_a$. A simple average of two plastic strain values for the same stress level $[\sigma + \sigma_a^-]$ and $[\sigma_a^+ - \sigma]$ measured from the displaced origins $(-\varepsilon_a, -\sigma_a^-)$ and $(\varepsilon_a, \sigma_a^+)$, respectively, has been used to make a symmetric fitting, where σ_a^+ and σ_a^- denote the stress amplitudes in tension and compression, respectively. Fig.5 shows a log-log plot of the average plastic strain versus the stress values $|\sigma \pm \sigma_a|$ for all the specimens. Plate specimens from P-4 and B-17 are identified by white and black figures, respectively. It is apparent that most of the straight lines to be fit have almost the same slope. The slope is called the "hysteretic strain-hardening exponent" and is denoted, for the later convenience, by $\frac{1}{n'}$. The

values of n' have been plotted with respect to the stress amplitude in Fig.6. Although Fig.6 appears to indicate some dependence of n' on the stress or strain amplitude [1], the exponent may be regarded to be constant to the first-order approximation within the range of strain amplitude ±0.03. A simple average n' = 9.0 will be used for the later analysis of alternating plastic bending of wide-flange beams.

A similar procedure may also be applied to the skeleton curves. A simple average, $\frac{1}{2}$ [$\sigma_a^+ + \sigma_a$] has been regarded as the stress amplitude σ_a and plotted with respect to the plastic strain amplitude ε_{ap} in Fig.5. The log-log plots have resulted in two straight lines with different slopes for specimens of Series 4 and 17. The slope is called the "skeleton strain-hardening exponent" and is denoted by $\frac{1}{n}$. The values of n for Series 4 and 17 obtained from the plot were 5.5 and 4.3, respectively. Although Morrow[I-16] states that n may be taken to be approximately equal to n', the present result apparently indicates a definite difference between n and n'

4.3 SKELETON AND HYSTERETIC STRESS-STRAIN RELATIONS A skeleton curve may be represented, as is well-known ,by

$$\frac{\varepsilon}{\varepsilon_y} = \frac{\sigma}{\sigma_y} \{1 + \frac{\varepsilon_{py}}{\varepsilon_y} \left|\frac{\sigma}{\sigma_y}\right|^{n-1}\} \qquad (1)$$

The value of ε_{py} may be read from Fig.5 if σ_y is found from the virgin stress strain curve.

If the skeleton and hysteretic strain-hardening exponents are to be distinguished, a modified analytic representation slightly different from the form of Eq.(1) must be sought for hysteresis loops. Corresponding to the previous symmetric fitting, a symmetrized stress-strain relation will be derived for steady-state loops. The symmetric half of an averaged hysteresis

loop starting at the tip $(-\varepsilon_a, -\sigma_a)$ on the skeleton curve must terminate at the symmetric tip $(\varepsilon_a, \sigma_a)$ on the same skeleton curve and vice versa. It is appropriate to assume that a hysteresis loop with the strain amplitude ε_a and the stress amplitude σ_a be represented by

$$\frac{\varepsilon \pm \varepsilon_a}{2\varepsilon_y} = \frac{\sigma \pm \sigma_a}{2\sigma_y}\left\{1 + \left(\frac{\varepsilon_{py}}{\varepsilon_y}\right) f\left[\frac{\sigma_a}{\sigma_y}\right]\left|\frac{\sigma \pm \sigma_a}{2\sigma_y}\right|^{n'-1}\right\} \qquad (2)$$

For $\sigma = \pm \sigma_a$ and $\varepsilon = \pm \varepsilon_a$, Eq.(2) must give rise to the same expression as Eq.(1). Hence

$$f\left[\frac{\sigma_a}{\sigma_y}\right] = \left|\frac{\sigma_a}{\sigma_y}\right|^{n-n'}$$

Eq.(2) may then be written as

$$\frac{\varepsilon \pm \varepsilon_a}{2\varepsilon_y} = \frac{\sigma \pm \sigma_a}{2\sigma_y}\left\{1 + \left(\frac{\varepsilon_{py}}{\varepsilon_y}\right)\left|\frac{\sigma_a}{\sigma_y}\right|^{n-n'}\left|\frac{\sigma \pm \sigma_a}{2\sigma_y}\right|^{n'-1}\right\} \qquad (3)$$

The symmetrized hysteresis loops described by Eq.(3) have been drawn for ε_a = 0.005, 0.010, and 0.0186 in Fig.7 to compare with the experimental loops. Apparently Eq.(3) fit the experimental loops considerably well. In order to testify the role of the factor $|\sigma_a/\sigma_y|^{n-n'}$ in Eq.(3) more explicitly, $|(\sigma + \sigma_a)/2\sigma_y|$ at $[\varepsilon + \varepsilon_a]_p = 2\varepsilon_{py}$ has been plotted with respect to $|\sigma_a/\sigma_y|$ in Fig.8. In this case , Eq.(3) may be reduced to

$$\log\left|\frac{\sigma_a}{\sigma_y}\right| = \frac{n'}{n'-n}\log\left|\frac{\sigma + \sigma_a}{2\sigma_y}\right|_{[\varepsilon+\varepsilon_a]_p=2\varepsilon_{py}} \qquad (4)$$

The straight lines given by Eq.(4) in log-log scale fit the test result fairly well for both cases.

4.4 SKELETON YIELD POINT If the skeleton stress-strain relation (1) is to be applied not only to the plastic region but also to the elastic region, it implies that the steel has been assumed to exhibit cyclic softening in the elastic region in a few cycles from test initiation. Although no specimen was

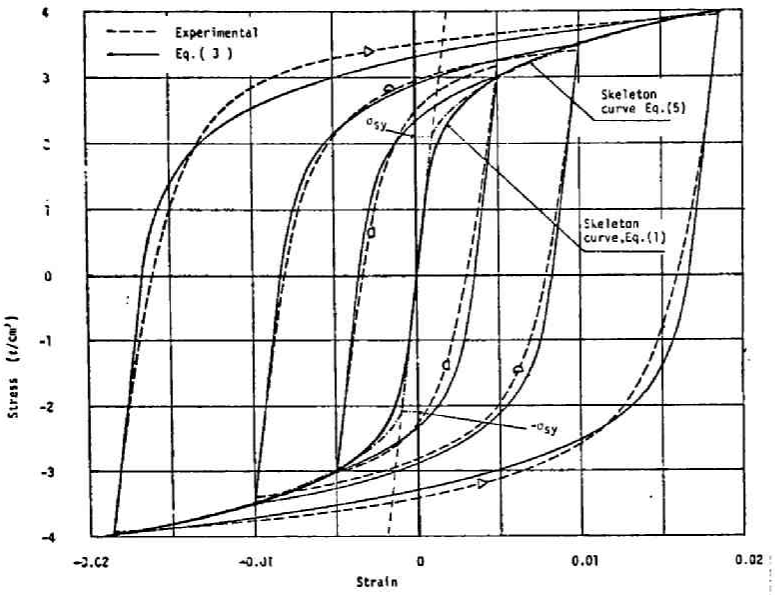

Fig. 7

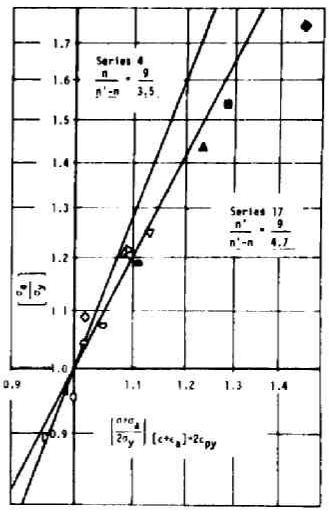

Fig.8 Another justification of the idealized stress-strain relation

Fig.8

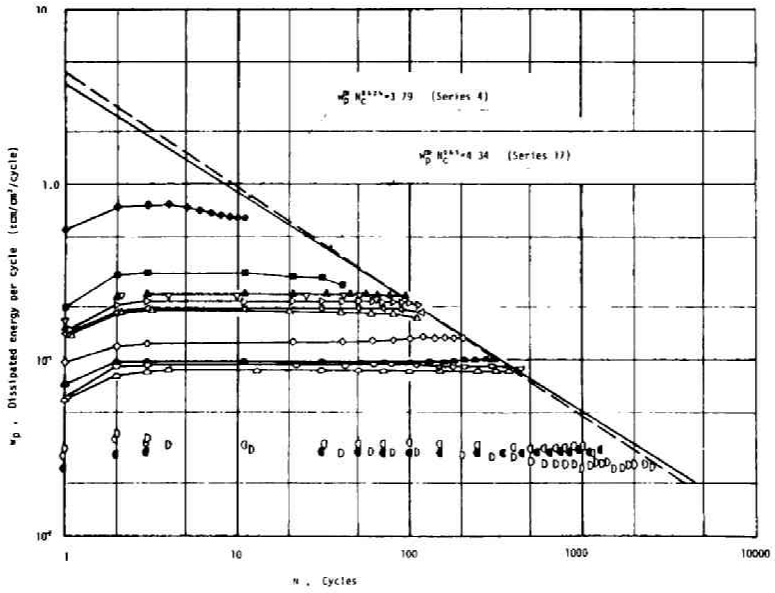

Fig.9

tested at a strain amplitude less than 0.005 in the present work, previous experimental evidences [2,3] on other metals appear to indicate that a skeleton stress-strain curve coincides with the virgin elastic stress-strain curve up to a certain branch point below the yield stress without exhibiting cyclic softening and obeys a power law in the plastic region beyond the branch point. The branch point will henceforth be called the "skeleton yield point". While the previous skeleton stress-strain relation (1) will be shown to be useful for the analysis of hysteretic load-deflection behaviors, the following skeleton stress-strain relation will also be plausible as far as it is applied only to the analysis of the skeleton load-deflection behaviors.

If the stress amplitude is plotted with respect to the total strain amplitude in log-log scale, another skeleton strain hardening exponent denoted by $\frac{1}{\bar{n}}$ may be found which is different from $\frac{1}{n}$. The values of $\bar{n}$ for Series 4 and 17 were about 4.5 and 3.8, respectively. The total strain may then be represented by

$$\frac{\varepsilon}{\varepsilon_y} = (1 + r)\left(\frac{\sigma}{\sigma_y}\right)\left|\frac{\sigma}{\sigma_y}\right|^{\bar{n}-1} \qquad (5)$$

where $r = \varepsilon_{py}/\varepsilon_y$. The skeleton curve given by Eq.(5) for the plastic region intersects with the virgin elastic stress-strain line at the skeleton yield point denoted by $(\varepsilon_{sy}, \sigma_{sy})$. If the ratio $\varepsilon_{sy}/\varepsilon_y = \sigma_{sy}/\sigma_y$ is denoted by r_s, then ε_{sy} may be found from the solution of

$$r_s^{\bar{n}-1}(1 + r) = 1$$

The values of r_s for Series 4 and 17 were found to be 0.730 and 0.644, respectively. The skeleton curves for Series 4 represented by Eq.(1) and Eq.(5) have been plotted in Fig.7 by a solid line and a dot-dash line, respectively.

5. ENERGY DISSIPATION CAPACITY AND PLASTIC FATIGUE TOUGHNESS

5.1 ENERGY DISSIPATION PER CYCLE The area of a hysteresis loop represents the energy dissipated during one cycle. All the areas of hysteresis loops were measured by a planimeter. The energy dissipation per cycle denoted by w_p has been plotted in Fig.9 with respect to the number of cycles, N up to the respective plastic fatigue limit N_c. N_c is defined as that cycle at which a crack has just become visible with naked eyes. Although $w_p^{(N)}$ of the N-th cycle of a specimen varies within the first three cycles and after N_c, $w_p^{(N)}$ may be regarded as almost constant from the third cycle up to N_c except those of the two specimens subjected to larger strain amplitudes in which some buckling deformation had been accumulated very slowly before N_c.

Fig.10 shows a log-log plot of $w_p^{(3)}$ versus ε_{ap}. It is apparent that there exists a linear relationship between $\log w_p^{(3)}$ and $\log \varepsilon_{ap}$. Since the skeleton and hysteretic stress-strain relations have been determined in the preceding section, $w_p^{(3)}$ may readily be expressed in terms of ε_{ap} by a simple integration as follows:

$$w_p^{(3)} = 4\sigma_y \varepsilon_{py} \left(\frac{n'-1}{n'+1}\right) \left(\frac{\varepsilon_{ap}}{\varepsilon_{py}}\right)^{1+\frac{1}{n}} \qquad (6)$$

The two straight lines drawn in Fig.10 in accordance with Eq.(6) fit the experimental data very well. This agreement is another justification of the previous determination of n and n'.

5.2 PLASTIC FATIGUE LIMIT In order to evaluate the total energy dissipation capacity of a specimen, the relation between ε_{ap} and N_c must be found. Fig.11 shows a log-log plot of ε_{ap} versus N_c. It appears difficult to find any difference between the ε_{ap}~N_c relations for Series 4 and 17. The straight line

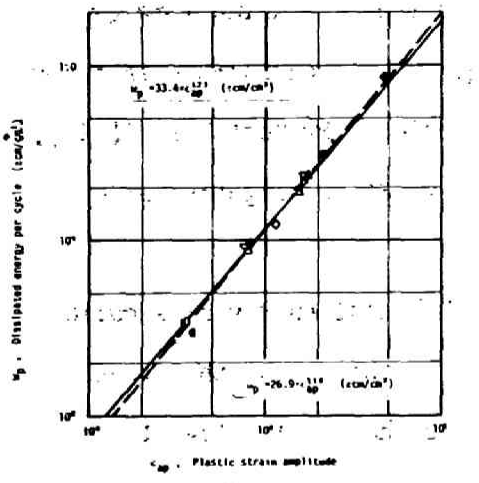

Fig.10

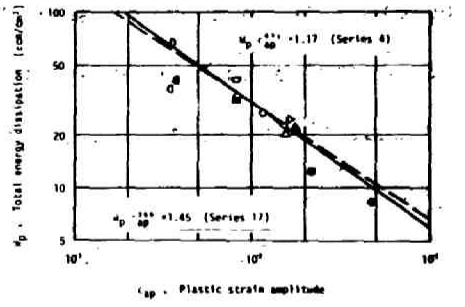

Fig.12

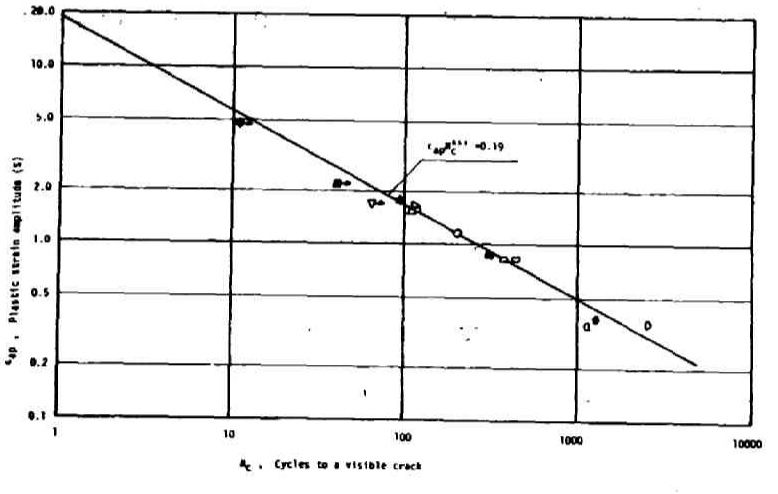

Fig.11

$$\varepsilon_{ap} N_c^{\alpha} = \frac{1}{2^{\alpha}} \{\varepsilon_{ap}(\tfrac{1}{2})\} \quad \text{where } \alpha = 0.53 \text{ and } \varepsilon_{ap}(\tfrac{1}{2}) = 0.27 \qquad (7)$$

appears to fit the experimental points as is well-known for various metals[2,3] where $\varepsilon_{ap}(\frac{1}{2})$ denotes Morrow's fatigue ductility coefficient. The three specimens with arrows indicating longer lives are those in which some gradual buckling deformations had been observed. If Eq.(7) is compared with the recent experimental result on SS41 hour-glass specimens by Hotta *et al*[4], it is found that the present result $(2\varepsilon_{ap})N_c^{0.53} = 0.38$ is slightly below $\varepsilon_p^L N_c^{0.535} = 0.44$.

5.3 TOTAL ENERGY DISSIPATION CAPACITY The total energy dissipation during N_c cycles of a specimen has been computed as the sum of the areas of hysteresis loops measured by a planimeter. Fig.12 shows a log-log plot of the total energy dissipation W_p versus ε_{ap}. Although the experimental result shows considerable scatter, it is apparent that W_p decreases with respect to ε_{ap}. The relation between W_p and ε_{ap} may be found from Eqs.(6) and (7). Since $w_p^{(N)}$ may be regarded roughly as a constant for a prescribed ε_{ap} as given by Eq.(6) from the third cycle up to N_c, the total energy dissipation during N_c cycles may be evaluated approximately by

$$W_p = w_p^{(3)} N_c \qquad (8)$$

Eq.(6) may be written as

$$w_p = C\, \varepsilon_{ap}^{1+\frac{1}{n}} \quad (C: \text{constant}) \qquad (9)$$

Upon substitution of Eq.(9), Eq.(8) may be reduced to

$$W_p = C(\varepsilon_{ap} N_c^{\alpha})^{1/\alpha}\ \varepsilon_{ap}^{1+\frac{1}{n}-\frac{1}{\alpha}} \qquad (10)$$

Substitution of Eq.(7) into Eq.(10) provides

$$W_p = 1.17\ \varepsilon_{ap}^{-0.71}\ (\text{ton cm/cm}^3) \quad \text{for Series 4 and}$$
$$W_p = 1.45\ \varepsilon_{ap}^{-0.66}\ (\text{ton cm/cm}^3) \quad \text{for Series 17} \qquad (11)$$

The two straight lines given by Eqs.(11) have been drawn in Fig.12 and appear to represent the tendency considerably well.

5.4 $w_p \sim N_c$ RELATION AND $W_p \sim N_c$ RELATION When ε_{ap} in Eq.(9) is replaced by N_c by means of Eq.(7), w_p may be expressed in terms of N_c as

$$w_p = \gamma N_c^{\beta} \quad \textit{where } \beta = -\alpha(1+\frac{1}{n}) \textit{ and } \gamma = C\left\{\varepsilon_{ap}(\frac{1}{2})/2^{\alpha}\right\}^{1+\frac{1}{n}} \quad (12)$$

The values of the constants are $\beta_4 = -0.624, \gamma_4 = 3.79 (ton\ cm/cm^3)$ for Series 4 and $\beta_{17} = -0.65$, *and* $\gamma_{17} = 4.34 (ton\ cm/cm^3)$ for Series 17. The two straight lines given by Eq.(12) have been drawn in Fig.9 and fit the experimental result fairly closely. W_p may also be represented by N_c alone. Substitution of Eq.(12) into Eq.(8) furnishes

$$W_p = \gamma N_c^{1+\beta} \quad (13)$$

where $1+\beta = 0.376$ and 0.350 for Series 4 and 17, respectively. Since β does not contain n', both series have almost the same exponents as those due to Morrow's theory and Halford's compilation of more than 1200 individual tests.

6. CONCLUSION

From the completely reversed strain cycling tests of the plate specimens taken from flanges of SS41 wide-flange members, the following conclusions may be drawn:

(1) The skeleton strain-hardening exponent $\frac{1}{n}$ should be distinguished from the hysteretic strain-hardening exponent $\frac{1}{n'}$ for SS41 even to the first approximation contrary to Morrow's treatment [Ch.7-16], the modified hysteretic stress-strain relation which takes into account the difference between n and n', has been shown to agree well with the experimental hysteresis loops and result in an accurate evaluation of the plastic energy dissipated per cycle.

(2) The other representation, Eq.(5), of the skeleton curves in terms of the total strain amplitudes is another realistic approximation, implying that the

cyclic softening does not occur in the elastic range up to the skeleton yield point.

(3) It has been shown in Chapter 7 that the H-specimens of Series A and B have different plastic bending fatigue toughness. While it was difficult to detect any significant difference in n' and in ε_{ap}~N_c relation between the two Series, the experimental points indicated definitely different skeleton strain-hardening exponents $\frac{1}{n}$ and $\frac{1}{\bar{n}}$. This difference in n or $\bar{n}$ appears therefore to be one of the factors affecting the difference in the plastic bending fatigue toughness.

(4) The constants and exponents which characterize the relations between the energy dissipation per cycle, the total energy dissipation, the plastic strain amplitude, and the number of cycles to a crack visible with naked eyes have been determined for the SS41 flange steel. It was reconfirmed that the exponents of N_c in the W_p~N_c relations for the two series are both close to the value found by Morrow and Halford.

REFERENCES

[1] K. Iida, H. Inoue, Y. Kobayashi, and T. Miyamoto, "Effect of Waveform of Controlled Strain in the Diametral Strain Controlled Low Cycle Fatigue", J.Soc. Naval Architects of Japan, Vol.125, June 1969, pp217-225

[2] S. S. Manson, "THERMAL STRESS AND LOW CYCLE FATIGUE" McGraw-Hill, 1966

[3] R. W. Smith, M. H. Hirschberg and S. S. Manson, "Fatigue Behavior of Materials under Strain Cycling in Low and Intermediate Life Range", NASA Tech. Note D.1574, April 1963.

[4] T. Hotta, J.Muraki, T. Ishiguro, N. Ishii and S. Sekiguchi, "Further Investigation of Estimation on Low Cycle Fatigue Strength of Steels (1st Report)", J.Soc.Naval Architects of Japan, Vol.124, Dec.1968, p346

CHAPTER 9

STEADY-STATE THEORY

1 INTRODUCTION

Previous theoretical predictions of load-deflection behaviors of wide-flange beams, columns and frames are mostly based upon bilinear or polylinear hysteretic stress-strain relations assumed without sufficient quantitative evidences and concerned primarily with initial transient behaviors [chapter 7-3~10]. Nonlinear stress-strain relations have been applied only to virgin response [1], [2]. The use of modern electronic computers and of the finite difference or finite element method enables one to obtain numerical solutions to the load-deflection behaviors of members subjected to alternating plastic bending under the presence of an axial force [3], [4]. In this chapter, however, an approximate but analytical solution to the steady-state load-deflection behaviors and energy absorption capacity based upon the concept of the steady-state alternating plastic bending and the concept of an approximately equivalent sandwich cross-section will be derived. In view of the experimental evidence in chapter 7, the flanges of the idealized sandwich section of a specimen may be assumed, to the first-order approximation, to be subjected to alternating tension and compression of an equal strain amplitude in steady-state alternating bending. The skeleton and hysteretic stress-strain relations in chapter 8 are therefore applied. It will be shown that the numerical result obtained from the present theory predicts the experimental load-deflection curves, energy absorption per cycle considerably well. Since the maximum absolute strain amplitudes can also be estimated by the present theory, a prediction on the plastic bending fatigue ductility relation will also be made on the assumption that the tension-compression fatigue ductility relation derived in chapter 8 may be applied to flanges of wide-flange specimens.

2. ASSUMPTIONS FOR APPROXIMATE ANALYSIS

The bending strain distributions shown in Figs.5 and 6 of Part I have clearly indicated the existence of steady-state bending strain distributions. It should be noted, however, that the steady-state bending strain distributions in specimens subjected to larger deflection amplitudes are the results which include the effect of local and lateral deformations. It is observed that, the steady-state bending strain distribution in a specimen subjected to a smaller deflection amplitude is almost the same in upward and downward bending but that it has a larger amplitude in the direction of the virgin bending in a specimen subjected to a larger deflection amplitude. It is not clear from the experimental evidence so far obtained, whether this circumstance is solely due to the initial perfectly plastic behavior or to the lateral torsional deformation. Since, however, the plastic region in a specimen subjected to a smaller deflection amplitude has been indeed subjected to tension and compression of an almost equal strain amplitude, it is a reasonable first-order approximation to assume that a steady-state bending strain distribution has an equal amplitude in downward and upward bending. Deviation of the observed distribution from the assumed distribution may be regarded to be of a second-order quantity. This assumption implies that, the steady-state stress distribution in a specimen at the prescribed maximum or minimum deflection configuration is governed by the skeleton stress-strain relations which have been derived in Chapter 8. The stress distribution over a cross-section in a plastic region based upon Eq.(1) of Chapter 8 is as shown in Fig.1(b), if the elastic response is not to exhibit any softening behavior up to $\varepsilon = \varepsilon_y$ in the converging process to the skeleton curve given by Eq.(1), while the stress distribution based upon Eq.(5) of Chapter 8 is as shown in Fig.1(d). Although the sharp peak in Fig.1(b) is hypothetical, the form of Eq,(1) is advan-

tageous in deriving a hysteretic load-deflection relation, On the other hand, Eq.(5) which appears to be more realistic, will be useful only for a skeleton load-deflection relation. The principal advantage of the above assumtion is that an analytical steady-state solution may be derived in an explicit and closed form with the use of the "approximately equivalent sandwich section" defined below.

An idealized sandwich section consists of two flanges of concentrated areas carrying normal stresses only and a shear resistant core which does not carry normal stress. A sandwich section is said to be equivalent to the original wide-flange section if (1) the extreme fibre strains $\pm\varepsilon_a$ and the curvature κ at the section are the same and (2) the corresponding extreme fiber stresses $\pm\sigma_a$ and the bending moments are the same. Due to the nonlinear stress-strain relation fitting considerably well to the experimental result, the equivalent section is dependent upon the nonlinear stress distribution. It is more convenient to define an approximately equivalent sandwich section which may be applied throughout a plastic region without regard to nonlinear stress distributions. The approximately equivalent sandwich section is defined as that section which has the original depth H and the equivalent concentrated flange area only at the particular section where $\sigma_a = \sigma_y$ and $\varepsilon_a = \varepsilon_y + \varepsilon_{py}$. It is called "approximately equivalent" since the aforementioned conditions are satisfied only approximately at sections other than the particular section.

The equivalence conditions can be satisfied precisely throughout an elastic region. The concentrated area of a flange of the equivalent sandwich section in an elastic region is given by

$$A_e H = Z_e \qquad (1)$$

where Z_e denotes the elastic section modulus. The concentrated area of the

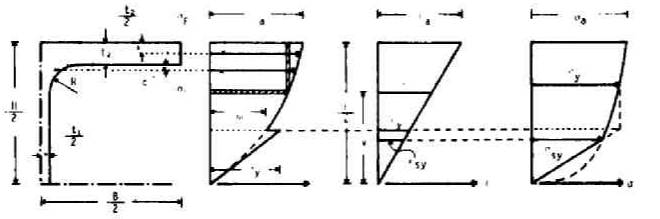

(a) Cross-section (b) Stress Distribution (c) Strain Distribution (d) Stress Distribution

Fig. Idealized Stress Distribution in a Steady-state.

Fig.1

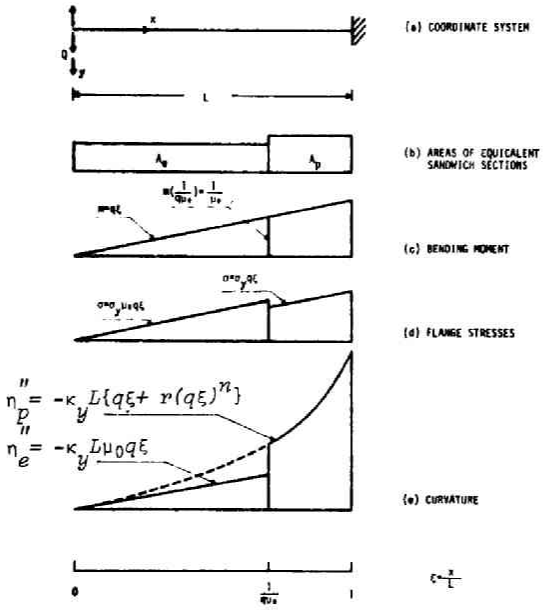

Fig.2

Table 1

	Series A						Series B				
Specimen No.	11	12	13	14	15	16	17	18	19	20	21
M_p/σ_y (cm³)	91.4	92.6	91.5	92.0	90.4	84.8	89.4	88.3	88.6	89.3	88.9
M_p (tcm)	264	258	265	258	268	238	256	249	254	251	251
σ_y (t/cm²)	2.89	2.79	2.90	2.81	2.97	2.80	2.87	2.82	2.87	2.81	2.83
ε_y (x10⁻³)	1.38	1.33	1.38	1.34	1.41	1.33	1.37	1.34	1.37	1.34	1.35
ε_{yp} (x10⁻³)	2.87	2.36	2.90	2.47	3.23	2.38	3.35	3.20	3.35	3.13	3.25
r	2.08	1.77	2.10	1.84	2.29	1.79	2.52	2.38	2.52	2.34	2.41
n	5.5						4.3				
M_y/σ_y (cm³)	88.1	89.2	88.1	88.7	87.1	81.9	86.1	85.1	85.4	85.9	85.6
M_y (tcm)	255	249	256	246	259	229	247	240	245	241	242
M_0/σ_y (cm³)	79.9	80.7	79.7	80.3	78.7	74.5	78.0	77.1	77.2	77.8	77.5
ν_0	1.103	1.105	1.106	1.104	1.107	1.100	1.103	1.103	1.106	1.103	1.105
Q_a (ton)	1.45	1.49	1.58	1.57	1.66	1.54	1.56	1.63	1.65	1.50	1.44
$q_a=QL/M_y$	1.023	1.079	1.108	1.149	1.151	1.211	1.135	1.222	1.210	1.116	1.072
δ_a (mm)	50	60	75	80	90	100	75	90	100	60	50
δ_a	0.0278	0.0333	0.0416	0.0445	0.0500	0.0555	0.0416	0.0500	0.0555	0.0333	0.0278
δ_{ap}	0.0089	0.0148	0.0217	0.0248	0.0289	0.0345	0.0213	0.0286	0.0338	0.0138	0.0087
$\bar{n}$	4.5						3.8				
r_s	0.723	0.746	0.719	0.746	0.701	0.745	0.640	0.650	0.640	0.661	0.647
M_s/σ_y (cm³)	88.5	89.5	88.4	89.1	87.5	82.1	86.0	85.0	85.2	85.9	85.3
M_s (tcm)	256	250	256	249	260	230	247	240	244	241	242

approximately equivalent sandwich section associated with the stress distribution shown in Fig.1(b), is given by

$$A_P = \left(\frac{\sigma_F}{\sigma_y}\right)(B-t_1)\left(1-\frac{t_2}{H}\right)t_2 + \left(\frac{\sigma_R}{\sigma_y}\right)(4-\pi)\left(\frac{1}{2}-\frac{t_2+c}{H}\right)R^2 + \frac{1}{2}f_w t_1 H \qquad (2a)$$

The symbols appearing in this equation are defined in Fig.1,. The average stresses σ_F in a flange and σ_R in a round corner may be evaluated by the standard Taylor expansion of $\varepsilon(\sigma)$ about $\sigma=\sigma_y$ as follows:

$$\frac{\sigma_F}{\sigma_y} = 1 - \frac{(1+r)t_2}{(1+nr)H}, \qquad \frac{\sigma_R}{\sigma_y} = 1 - \frac{2(1+r)(t_2+c)}{(1+nr)H} \qquad (2b,c)$$

where $r = \varepsilon_{py}/\varepsilon_y$, as was defined in Part II.

The third term representing the contribution of the web stresses to the resultant moment may be evaluated by an integration similar to that employed in Ref.[1,2] and f_w is given by

$$f_w = \frac{1}{3(1+r)^2}\left\{2 + \frac{3(1+n)r}{n+2} + \frac{3nr^2}{2n+1}\right\} + \frac{1}{2(1+r)^2}\left(\frac{\sigma_m}{\sigma_y}\right)\left\{\frac{1}{3}\left(\frac{\sigma_m}{\sigma_y}\right) + \frac{2r}{n+2}\left(\frac{\sigma_m}{\sigma_y}\right)^{n+1} + \frac{r^2}{2n+1}\left(\frac{\sigma_m}{\sigma_y}\right)^{2n} - 1\right\} \qquad (2d)$$

where

$$\left(\frac{\sigma_m}{\sigma_y}\right) + r\left(\frac{\sigma_m}{\sigma_y}\right)^n = 1 \qquad (\sigma_m > 0)$$

The resultant moment corresponding to this stress distribution is denoted by M_y, while that of elastic stress distribution with the extreme fibre stress σ_y, by M_o. The ratio M_y/M_o is denoted by μ_o. It is noted that $A_p/A_e = \mu_o$.

The concentrated area of the approximately equivalent sandwich section associated with the stress distribution shown in Fig.1(d) may also be represented by Eq.(2a) if n is replaced by $\bar{n}$ in Eq.(2b and c) and if f_w is estimated by

$$f_w = \frac{1}{3(1+r)^2} + \frac{\bar{n}}{2\bar{n}+1}\left[1 - \frac{r_s^3}{(1+r)^3}\right] \qquad (2e)$$

The resultant moment corresponding to this stress distribution is denoted by M_s and the ratio M_s/M_o, by μ_s.

3. STEADY-STATE SOLUTION

3.1 SKELETON LOAD-DEFLECTION CURVE-1 In accordance with the foregoing assumptions and idealization, a beam has the flange area A_e in an elastic region and A_p in a plastic region, and is subjected to alternating bending as a cantilever shown in Fig.2(c). The coordinate system and symbols to be used are shown in Fig.2. It is convenient to introduce the following dimensionless quantities:

$$\xi = \frac{x}{L}, \quad \eta = \frac{y}{L}, \quad m = \frac{M}{M_y}, \quad q = \frac{QL}{M_y} \qquad (3)$$

The lower flange stresses in the elastic and plastic regions may then be written as

$$\frac{\sigma}{\sigma_y} = \frac{A_p}{A_e}\,\frac{\sigma A_e H}{\sigma_y A_p H} = \mu_o m = \mu_o \frac{Qx}{M_y} = \mu_o q\xi \qquad (4)$$

$$\frac{\sigma}{\sigma_y} = \frac{\sigma A_p H}{\sigma_y A_p H} = m = q\xi \qquad (5)$$

respectively. The curvature-displacement relation may be reduced to

$$\kappa L = L\frac{d^2y}{dx^2} = \frac{d^2\eta}{d\xi^2} = \eta'' \qquad (6)$$

where a prime denotes differentiation with respect to ξ.

After a steady-state has been attained in a few cycles of alternating plastic bending, the state of stress in a flange at a maximum deflection may be considered to be governed by the skeleton stress-strain relation. The variation of the state of stress as the load and deflection are varied, must be considered to be governed by the hysteretic stress-strain relation.

If it may be assumed that no softening occurs in the elastic region and that the skeleton stress-strain relation

$$\frac{\varepsilon}{\varepsilon_y} = \frac{\sigma}{\sigma_y}\left[1+ r\left|\frac{\sigma}{\sigma_y}\right|^{n-1}\right] \qquad (7)$$

which has been derived in Chapter 8, can be applied only to the plastic region in the steady state, then the corresponding skeleton load-deflection relation may be obtained as follows.

The elastic region is defined by

$$0 \le |M| \le M_o \qquad or \qquad 0 \le \xi \le 1/|q|\mu_o \qquad (8)$$

The differential equation governing the deflection η_e in the elastic region may be written, in view of Eq.(4), as

$$-\frac{\eta_e''}{\kappa_y L} = \frac{\varepsilon}{\varepsilon_y} = \frac{\sigma}{\sigma_y} = \mu_o q\xi \quad (where\ \kappa_y = 2\varepsilon_y/H) \qquad (9)$$

Substitution of Eq.(5) into Eq.(7) and use of Eq.(6) provide the differential equation governing the deflection η_p in the plastic region.

$$-\frac{\eta_p''}{\kappa_y L} = \frac{\varepsilon}{\varepsilon_y} = \frac{\sigma}{\sigma_y}\left\{1 + r\left|\frac{\sigma}{\sigma_y}\right|^{n-1}\right\} = q\xi\left\{1 + r|q\xi|^{n-1}\right\} \qquad (10)$$

The general solutions to Eq.(9) and (10) may readily be obtained. Integration constants can be determined by the boundary conditions $\eta_e(0) = 0$ and $\eta_p'(1) = 0$ and the continuity conditions $\eta_e(1/|q|\mu_o) = \eta_p(1/|q|\mu_o)$ and $\eta_e'(1/|q|\mu_o) = \eta_p'(1/|q|\mu_o)$. The solution $\eta_p(\xi)$ may be written as

$$\eta_p = -\kappa_y L\, q\left\{\left(\frac{\xi^3}{6} - \frac{\xi}{2}\right) + \frac{r|q|^{n-1}}{n+1}\left(\frac{\xi^{n+2}}{n+2} - \xi\right) + \frac{1-\mu_o}{3|q|^3\mu_o^3} + \frac{r}{n+2}\frac{1}{|q|^3\mu_o^{n+2}}\right\} \qquad (11)$$

The deflection amplitude $\eta_p(1) = \delta_a$ for a load amplitude q_a is given by

$$\delta_a = \kappa_y L q_a\left\{\frac{1}{3}\left(1 + \frac{\mu_o^{-1}}{|q_a|^3\mu_o^3}\right) + \frac{r|q_a|^{n-1}}{n+2}\left(1 - \frac{1}{|q_a|^{n+2}\mu_o^{n+2}}\right)\right\} \qquad (12)$$

$$(|q_a| \ge 1/\mu_o)$$

If the beam is entirely elastic, then $A = A_e$ throughout and the deflection is given by

$$\delta_{ae} = \frac{1}{3} \kappa_y L q_a \mu_o \qquad (13)$$

The plastic component δ_{ap} of the deflection has been called the plastic deflection and is defined as the difference $\delta_a - \delta_{ae}$. The expression of δ_{ap} may be reduced to

$$\delta_{ap} = \kappa_y L q_a \left\{ -\frac{1}{3}(\mu_o - 1)\left(1 - \frac{1}{|q_a|^3 \mu_o^3}\right) + \frac{r|q_a|^{n-1}}{n+2}\left(1 - \frac{1}{|q_a|^{n+2}\mu_o^{n+2}}\right)\right\} \qquad (14)$$

The curve described by Eq.(12) is the skeleton load-deflection curve. It should be noted that Eq.(12) does not represent the load-deflection curve in the usual sense and only gives the load amplitude for a prescribed deflection amplitude. Eq.(11) represents the deflected shape at the state of load and deflection expressed by a tip of a hysteresis curve.

3.2 HYSTERETIC LOAD-DEFLECTION CURVE If the load-deflection curve of a beam starting from a state of deflection $(\delta_a > 0,\ q_a > 0)$ on the skeleton load-deflection curve passes through its symmetric point $(-\delta_a, -q_a)$ on the skeleton curve when subjected to reversed bending and if the state of deformation at $(-\delta_a, -q_a)$ is the precise reverse of that at (δ_a, q_a), then there exists indeed a closed hysteretic load-deflection curve in the steady-state. The lower flange stress and strain at (δ, q) denoted by $\sigma(\xi)$ and $\varepsilon(\xi)$, respectively are governed by the hysteretic stress-strain relation;

$$\frac{\varepsilon(\xi) - \varepsilon_a(\xi)}{2\varepsilon_y} = \frac{\sigma(\xi) - \sigma_a(\xi)}{2\sigma_y}\left\{1 + r\left|\frac{\sigma_a(\xi)}{\sigma_y}\right|^{n-n'}\left|\frac{\sigma(\xi) - \sigma_a(\xi)}{2\sigma_y}\right|^{n'-1}\right\} \qquad (15)$$

which has been derived in Chapter 8. If the curvature and bending moment distributions at (δ_a, q_a) and at a subsequent state (δ, q) are denoted by $\kappa_a(\xi)$, $\kappa(\xi)$ and $m_a(\xi)$ and $m(\xi)$, respectively, then the curvature-moment relation

may be reduced to

$$\frac{\kappa(\xi) - \kappa_a(\xi)}{2\kappa_y} = \frac{m(\xi) - m_a(\xi)}{2}\left\{1 + r|m_a(\xi)|^{n-n'}\left|\frac{m(\xi) - m_a(\xi)}{2}\right|^{n'-1}\right\} \qquad (16)$$

The differential equation governing the deflection $\eta_p(\xi)$ in the plastic region may be written as

$$\eta_p'' - \eta_a'' = -2\kappa_y L\left(\frac{q - q_a}{2}\right)\left\{\xi + r\, q_a^{n-n'}\left|\frac{q - q_a}{2}\right|^{n'-1}\xi^n\right\} \qquad (17)$$

where η_a denotes the deflection function at $(\delta_a,\ q_a)$. It should be noted that the power of ξ in the nonlinear term is again n. The general solutions to Eq.(17) and for the elastic region may readily be obtained. Use of the boundary and continuity conditions in the general solutions furnishes the deflection function at a subsequent state $(\delta,\ q)$ and the hysteretic load-deflection relation as follows:

$$\eta_p - \eta_a = -2\kappa_y L\left(\frac{q-q_a}{2}\right)\left\{\left(\frac{\xi^3-3\xi}{6} - \frac{\mu_o^{-1}}{3q_a^3\mu_o^3}\right) + rq_a^{n-n'}\left|\frac{q-q_a}{2}\right|^{n'-1}\left(\frac{1}{(n+1)}\left(\frac{\xi^{n+2}}{n+2} - \xi\right) + \frac{1}{(n+2)q_a^{n+2}\mu_o^{n+2}}\right)\right\} \qquad (18)$$

$$\delta - \delta_a = \kappa_y L(q-q_a)\left\{\frac{1}{3}\left(1 + \frac{\mu_o^{-1}}{q_a^3\mu_o^3}\right) + \frac{rq_a^{n-n'}}{n+2}\left|\frac{q-q_a}{2}\right|^{n'-1}\left(1 - \frac{1}{q_a^{n+2}\mu_o^{n+2}}\right)\right\} \qquad (q_a \geq 1/\mu_o) \qquad (19)$$

It may readily be confirmed that the curve defined by Eq.(19) passes through the point $(-\delta_a, -q_a)$ and that $\eta_p(\xi) = -\eta_a(\xi)$ at $(-\delta_a,\ -q_a)$. Similarly the load-deflection curve starting from $(-\delta_a,\ -q_a)$ may be shown to pass through $(\delta_a,\ q_a)$ Eq.(19) gives therefore a half of the steady-state hysteresis loop and the other half may be described by the equation similar to Eq.(19) in which $\delta - \delta_a$

and $q-q_a$ are replaced by $\delta+\delta_a$ and $q+q_a$, respectively. It may therefore be concluded that, once the state of deformation represented by $\pm\,\eta_a(\xi)$ is attained at $(\pm\delta_a, \pm q_a)$ through the converging process described in the preceding section, the subsequent load-deflection curve is a steady-state hysteresis loop consisting of the curve given by Eq.(19) and the other half. This hysteresis loop is the asymptote to which an actual load-deflection curve will approach after a number of cycles. It has been shown in Chapter 7, that a beam apparently attains a steady state quite rapidly in a few cycles.

3.3 PLASTIC ENERGY DISSIPATION The plastic energy dissipated in a cantilever beam during a steady-state hysteretic cycle can be evaluated with the use of Eqs.(12) and (19). If the new coordinates $\bar{q} = q-q_a$ and $\bar{\delta} = \delta-\delta_a$ with the origin at the tip (δ_a, q_a) of a hysteresis loop, then the area d_p enclosed by the hysteresis loop may be represented by

$$d_p = M_y \left(4q_a\delta_a - 2\int_o^{-2q_a} \bar{\delta}\, d\bar{q} \right) \qquad (20)$$

Substitution of Eq.(12) and Eq.(19) into Eq.(20) provides

$$d_p = \kappa_y L\, M_y \left(\frac{4r}{n+2}\right)\left(\frac{n'-1}{n'+1}\right)\left(q_a^{\,n} - \frac{1}{q_a^{\,2}\mu_o^{\,n+2}}\right) q_a \qquad (21)$$

3.4 δ_{ap}~N_c RELATION For a prescribed δ_a, Eq.(12) determines q_a and hence the strain at any point may be calculated by Eq.(5) and Eq.(7) or by Eq.(10). The largest extreme fiber strain for a prescribed δ_a occurs at $\xi = 1$ and the total and plastic strain amplitudes are given by

$$\varepsilon_a = \varepsilon_y(q_a + r q_a^{\,n}) \qquad (22a)$$

$$\varepsilon_{ap} = \varepsilon_{py}\, q_a^{\,n} \qquad (22b)$$

respectively, in tension and compression. If these estimates of the largest strains are accurate and if the ε_{ap}~N_c relation, Eq.(7) of Part II may be applied also to ε_{ap} here, an idealized but approximate δ_{ap}~N_c relation can be

derived therefrom.

3.5 SKELETON LOAD-DEFLECTION CURVE - 2 If the skeleton stress-strain relation given by Eq.(5) of Chapter 8:

$$\frac{\varepsilon}{\varepsilon_y} = (1 + r) \left(\frac{\sigma}{\sigma_y} \right) \left| \frac{\sigma}{\sigma_y} \right|^{\bar{n}-1}$$

is applied to the present problem, the corresponding stress distribution at a section in a plastic region is as shown in Fig.1(d). Through a manipulation similar to that of *Section 3.1*, the skeleton load-deflection relation may be obtained and reduced to

$$\delta_a = \kappa_y L \, q_a \left\{ \left(\frac{1+r}{\bar{n}+2} \right) q_a^{\bar{n}-1} + \left(\frac{1}{3\mu_s^2} - \left(\frac{1+r}{\bar{n}+2} \right) \frac{1}{\mu_s^{\bar{n}+2}} \right) \Big/ q_a^{3} \right\} \qquad (23)$$

where $q_a = Q_a L / M_s > 0$. The largest absolute extreme fibre strain must now be estimated by Eq.(5) of Chapter 8 rewritten above.

$$\varepsilon_a = \varepsilon_y (1 + r) q_a^{\bar{n}} \quad , \quad \varepsilon_{ap} = \varepsilon_y (1 + r) q_a^{\bar{n}} - \varepsilon_y q_a \qquad (24)$$

4. NUMERICAL RESULT AND DISCUSSION

Table 1 summarises the cross-sectional properties, material properties and some nondimensionalized data from the test result of all the H-specimens. The elastic and plastic section modulae have been computed from the cross-sectional dimensions which were measured by vernier calipers and micrometers. The yield stress may vary from specimen to specimen even within the same series. The tension-compression tests were conducted only on two series of plate specimens cut out of two different H-specimens. Since the virgin load-deflection curve of every H-specimen exhibited a perfectly-plastic behavior, however, the yield stresses were computed from the fully-plastic moments which were considered to have been attained. The yield stress of B-17

so computed is 2.87 ton/cm^2, while the average lower yield stress obtained from the tension-compression tests on B-17 plate specimens was 2.94 ton/cm^2. Since the material skeleton curves have been obtained only on one H-specimen in a Series in Chapter 8, it is assumed here that all the H-specimens in a Series have the same material skeleton curve. From Fig.5 of Chapter 8, ε_{py} may then be read for each yield stress and $r = \varepsilon_{py}/\varepsilon_y$ may be computed. The values of M_y/σ_y and M_s/σ_y were computed with the use of Eqs.(2) and measured cross-sectional dimensions. The averages of a pair of measured load amplitudes and plastic deflection amplitudes, respectively are also included in Table 1 as Q_a and Δ_{ap} together with their dimensionless values.

The theoretical skeleton load-deflection curves for each H-specimen may be drawn with the use of Eqs.(14) and (23). Fig.3(a) and (b) show the log-log plots of the theoretical $q_a \sim \delta_{ap}$ relations and the corresponding experimental points for Series A and B, respectively. Since M_s is very close to M_y for all the H-specimens as shown in Table 1 , an experimental load amplitude normalized with respect to M_s/L has been regarded, in the scale of Fig.3, to be the same as the amplitude normalized with respect to M_y/L. It is apparent that both of the theoretical curves predicted by Eq.(14) and (23) which are different from specimen to specimen fit the experimental points very well mostly within a few percent deviations and that the predictions due to Eq.(23) are slightly closer to experimental points.

Fig.4 shows three theoretical hysteretic load-deflection curves given by Eq.(19) and the corresponding experimental curves to be compared with. Fig.5(a) and (b) show some theoretical $[q-q_a]$-$[\delta-\delta_a]_p$ curves in log-log scale to compare with nondimensionalized experimental points. Apparently, the theoretical curves predict the experimental result considerably well except

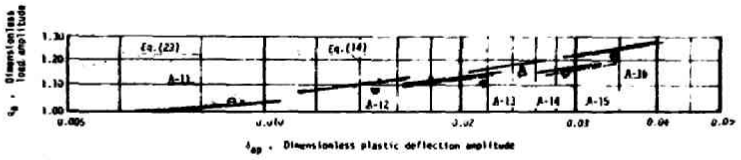

Fig.3a

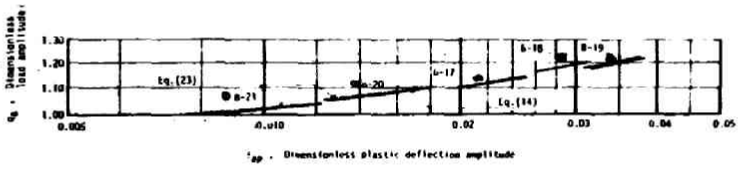

Fig.3b

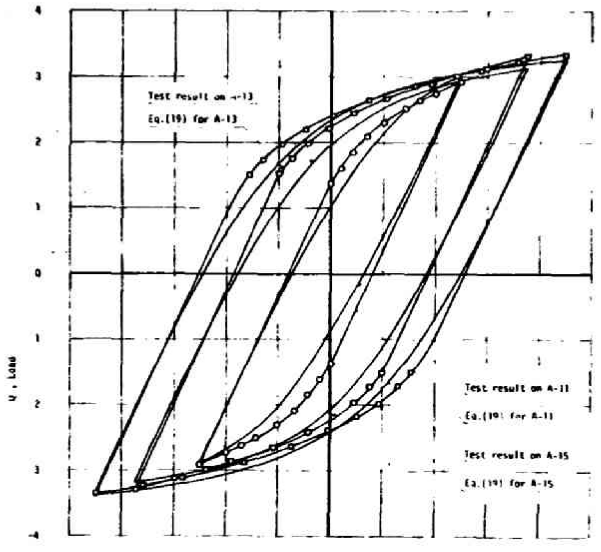

Fig.4

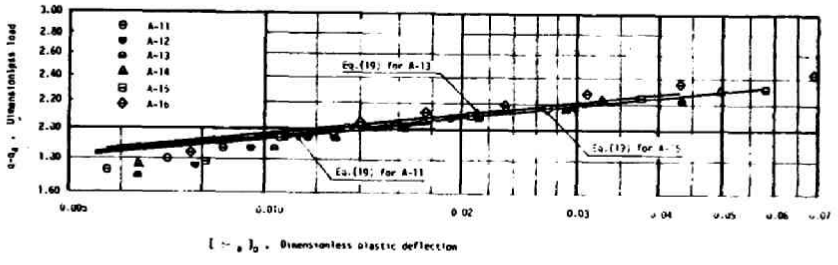

Fig.5a

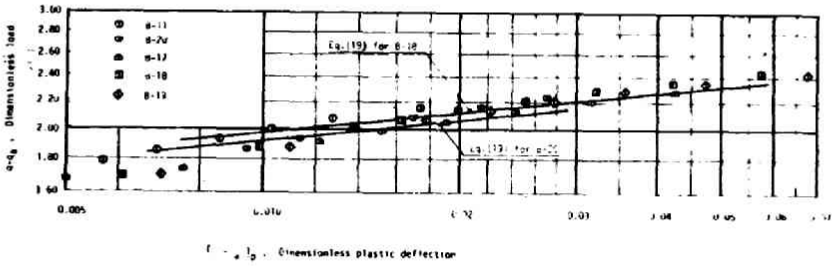

Fig.5b

near the shoulders which are sharper than those of experimental curves due to the sandwich approximation.

The plastic energy dissipated in a hysteretic cycle has been computed by means of Eq.(21) in the dimensionless form and plotted in Fig.6. Since the theoretical hysteresis curves have sharper shoulders than the experimental curves as has been pointed out above, Eq.(21) overestimates the plastic energy. It is observed that the theoretical predictions are considerably close to the straight lines fitting the experimental points and that the deviations are mostly about *10* % of the experimental values. Although no simple relation between d_p/M_y and δ_{ap} can be derived from Eq.(14) and Eq.(21), it has been observed in the process of computation that the theoretical result is fairly close to the evaluation by

$$\frac{d_p}{M_y} = 4\left(\frac{n'-1}{n'+1}\right)\delta_{ap}q_a \qquad (25)$$

Strains were measured at the sections located at 6cm from the respective midspans. The theoretical estimates of strains must therefore be made for $\xi=0.967$. The solid and dot-dash lines in Fig.7 are the theoretical estimates due to Eq.(10) and Eq.(24), respectively. Since the experimental points for specimens *B-18* and *B-19* show considerable scatter, it is difficult to estimate the essential deviation of the theoretical values from the experimental values. It may, however, be observed that the deviations from the average values of the experimental points are roughly within *20* % of the average values.

If the largest extreme fibre strain may be assumed to obey the plastic fatigue toughness relation, Eq.(7) in Chapter 8, then the theoretical δ_{ap}~N_c relations may be obtained for all the H-specimens. The solid and dot-dash lines in Fig.8 show the δ_{ap}~N_c curves computed from Eqs.(14) and (22) and from Eqs.(23) and (24), respectively. Apparently the difference

between the two estimates is only slight. These idealized δ_{ap}~N_c relations are based upon, among others, the assumptions that no local or lateral torsional deformation which would increase local strains occurs and that the effect of stress and strain gradients is of a second-order quantity. When the idealized δ_{ap}~N_c curves are compared with the experimental δ_{ap}~N_{HF} relations, it must be cautioned that the definition of N_{HF} is different from that of N_c. It has already been pointed out in Chapter 7 that a number of hair cracks had been observed long before a deep crack penetrated through a flange of a H-specimen. The detection of hair cracks was made only with naked eyes and was not of a uniform accuracy. In spite of these reservations , the idealized δ_{ap}~N_c curves in Fig.8 have revealed some features of the fatigue ductility of wide-flange members and explained partly the tendency that a pair of H-specimens with different skeleton stress-strain relations exhibit different fatigue ductility relations even when subjected to the same deflection amplitude. Because of the difference of definitions of N_c and N_{HF} , it may be of interest to draw δ_{ap}~ N_c curves for the longitudinal strains at the inner sides of flanges. If these strains may be estimated from the linear distribution over a cross-section, the curves may be obtained by a simple translation of the previous δ_{ap}~N_c curves as shown by the dashed lines in Fig.8.

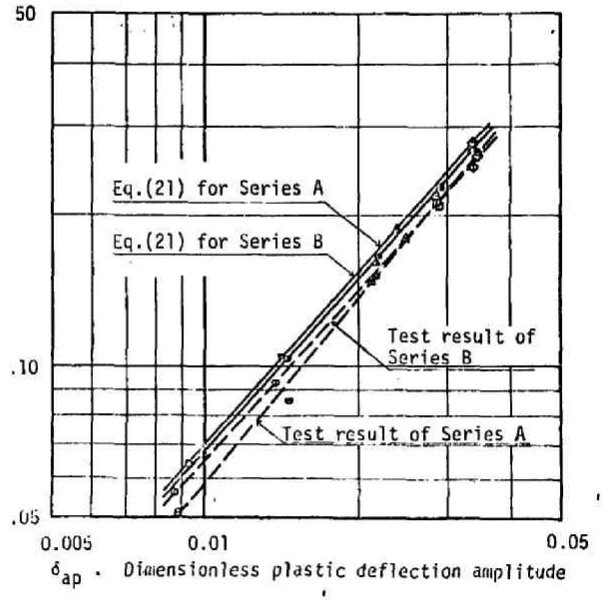

Fig.6

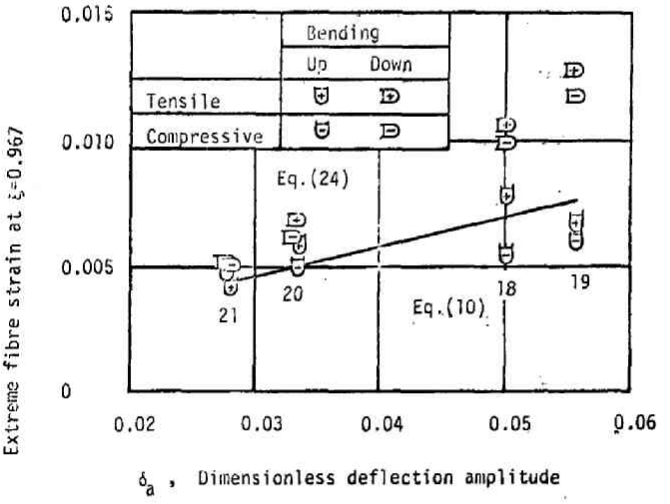

Fig.7

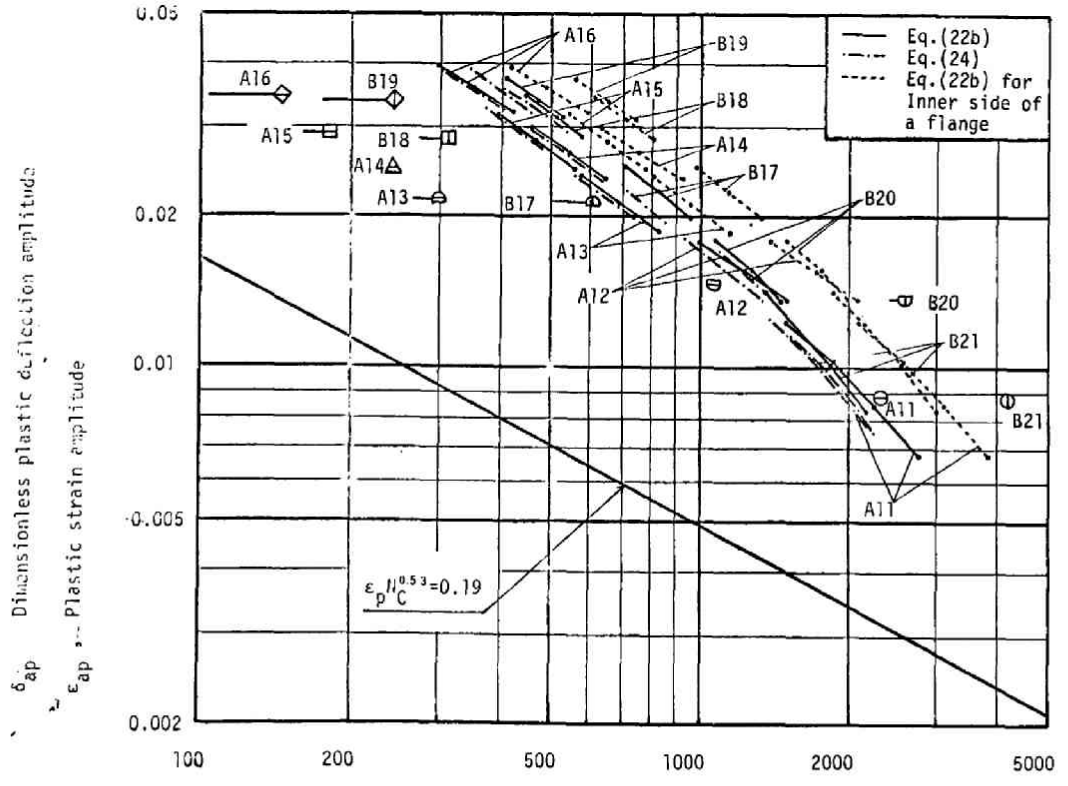

N_{HF} , Cycles to failure of a flange of H specimens

N_C , Cycles to a visible crack in plate specimens

Fig. 8

5. CONCLUSION

The following conclusions may be drawn from the result:

(1) The steady-state theory proposed here as a first-order approximation is able to predict with a considerable accuracy the steady-state load-deflection behaviors of rolled wide-flange members subjected to alternating forced displacements. For specimens subjected to larger deflection amplitudes, the theory is able to predict the initial steady-state behaviors more accurately than the later deteriorated behaviors due to the development of local and lateral torsional deformations. The theoretical skeleton curves based upon the two different skeleton stress-strain relations fit the experimental points very well mostly within a few percent deviations. The theoretical hysteresis curves also predict the experimental curves considerably well except near the sharper shoulders.

(2) The present theory is able to estimate the plastic energy dissipated during a steady-state hysteretic cycle also with a considerable accuracy. The order of magnitude of the overestimation due to the sharper shoulders mentioned above is about *10* % of respective experimental values.

(3) Because of the scatter in measured strain values, it was difficult to assess the deviations of the theoretical predictions from the experimental values. It may, however, be stated that the deviations are about *20*% from the respective averages of the measured strains.

(4) The idealized δ_{ap}~N_c relations derived from the present theory can not be directly compared with the experimental δ_{ap}~N_{HF} relations because of the difference of definitions of N_c and N_{HF} and because of the variations of strain amplitudes due to local buckling and lateral torsional deformations which were developed in specimens subjected to larger deflection amplitudes.

Nevertheless the idealized $\delta_{ap.}$~N_c curves appear to have accounted partly for the fact that a pair of H-specimens of different steels with different skeleton stress-strain relations exhibit different fatigue ductility even when subjected to the same forced deflection amplitude.

REFERENCES

[1] R. D. Chipman, "Dimensionless Inelastic Bending Relationships", Experimental Mech., Vol.20, Feb.1963, pp41-46

[2] M. J. Kaldjian, "Moment-curvature of Beams as Ramberg-Osgood Functions", J. Structural Div., Proc. ASCE, Vol.93,,ST5, Oct.1967, pp53-65

[3] See for instance, S. Igarashi and C. Matsui, "Elastic-plastic Behaviors of Steel Members Subjected to Repeated Combined Stresses",(Part I, II) Summaries of Technical Papers of the 1969 Annual Meeting of A.I.J. pp1057-1060

[4] F. Baron and M. S. Venkatesan, "Inelastic Response for Arbitrary Histories of Loads", J. Structural Div., Proc. ASCE, Vol.95, EM3, June 1969, pp763-786

CHAPTER 10

PLASTIC ANALYSIS OF SHELLS OF REVOLUTION UNDER AXISYMMETRIC LOADS*

1. INTRODUCTION

In this chapter and the next chapter, approximate analytical methods of finding plastic strengths of shells of revolution and general shallow shells will be proposed, respectively. Numerical methods of plastic analysis[N1] and finite element methods of elastic-plastic analysis[N2] have been extensively developed during the last five years and are useful for solving complicated practical problems. On the other hand, an analytical solution to a problem of limit analysis of a shell, when obtained explicitly, represents itself a law governing the nature of plastic strength of the shell, serves for a ready estimate of the plastic strength without appealing to a computer program and is useful for an understanding of the essential features of the plastic strength with respect to various parameters contained in the solution. An analytical solution with a sufficient accuracy may be utilized as a standard with respect to which the accuracy of a numerical solution can be tested. An approximate analytical solution serves also for these purposes, even if approximately. In this chapter, an analytical method of limit analysis based upon piecewise quadratic yield conditions is developed for axisymmetric problems of shells of revolution.

---

* This chapter is mostly based upon the author's paper,"Plastic Analysis of Shells of Revolution under Axisymmetric Loads," Ingenieur-Archiv, 34. Band, 4. Heft, 1965, S. 238-247. The practical usefulness and the good accuracy of the proposed solutions have been demonstrated in considerable detail for conical shells by J. C. Gerdeen, "Shell Plasticity-Piecewise Smooth Trajectories on the NAKAMURA Yield Surface," Dissertation submitted to Stanford University, Oct. 1965. A summary of the dissertation was presented by Gerdeen as a sectional lecture, "Axisymmetric Plastic Collapse of Shells of Revolution according to the Nakamura yield criterion," at the 12th Int. Congress of Applied Mechanics held at Stanford Univ., Aug. 26-31, 1968, Proc. (Ed. Hetényi and Vincenti) pp. 209-220. Springer-Verlag, 1969.

This chapter has been included for the following two reasons: (1) To demonstrate the basic idea of deriving a good approximate yield condition such that velocity equations are uncoupled from the equilibrium equations. This idea has led to the result of Ch.11. (2) To prepare for Ch.12 where it is shown that the advantage of the uncoupled velocity equations in Ch.10 is still available for finite-deflection problems and that general solutions can be obtained analytically.

The yield condition for an element of a shell of revolution subjected to axisymmetric loads has been derived by Onat and Prager [1] based upon the Tresca yield criterion. Since this condition is represented piecewise by different parametric formulas, its direct application to practical boundary value problems cannot in general furnish complete solutions successfully, not only because of the mathematical difficulty due to the non-linearity, but also because of the difficulty that one does not know a priori which part of the piecewise regular yield condition is to be used for a specific problem. For these reasons only in a special case of conical shells, the exact solutuon has been obtained by Onat [2] and by Lance and Onat [3]. Some techniques of approximation have been presented by Drucker and Shield [4] and by Hodge [5], [6], [7] to obtain good lower and upper bounds on the collapse loads of spherical, torispherical and conical shells.

It appears, however, that there are two somewhat different trends in the manner of approximations. One is to obtain merely lower and upper bounds for a shell, problem by problem, assuming some appropriate stress and velocity fields in accordance with the limit analysis theorems. The other is an attempt to obtain a complete solution to a particular boundary value problem based on an extremely simplified or linearized yield condition [6], [7]. The former necessarily requires some trial and error processes to be carried out intelligently in order to approach correct collapse loads with respect to the yield conditions chosen for the problems. The piecewise linear approximation has the advantage of mathematical simplicity. However, since the linearized yield surface consists of twelve hyperplanes, a reasonable hypothesis as to the choice of hyperplanes may be difficult and the difference between the upper and lower bounds obtained from this approximation is not sufficiently small.

In this chapter a general theory based upon a better approximate yield condition, which can furnish complete solution for any shell of revolution, is proposed. It will be shown that three pairs of parabolic hypercylindrical yield hypersurfaces constitute a very good approximate yield condition to the original yield condition derived from the Tresca criterion, partly coinciding with it and partly circumscribing it in a four-dimensional generalized-stress space. The advantage of this approximation lies, besides the good accuracy illustrated later, in the fact that it does not result in mathematical difficulties and that a set of general solutions for general shells of revolution will be obtained for all the constituent yield hypersurfaces almost explicitly in the sense that they contain quadratures only. As soon as an appropriate choice among the four general solutions has been made together with assumptions on the boundaries of the chosen solutions, all the integration constants and the collapse load factor can be determined from the boundary conditions. By checking the remaining yield inequalities numerically, one can then determine whether the solution is really complete or not. Since the approximate hypersurface circumscribes the exact Tresca hypersurface, the load factor thus obtained is an upper bound to the exact one with respect to the Tresca criterion. It is shown that the corresponding lower bound is then immediately obtained by multiplying by 0.851. The theory is illustrated by obtaining the solution for a shallow truncated conical shell subjected to a line load.

2. EQUATIONS OF EQUILIBRIUM AND KINEMATIC RELATIONS

The stress resultants, radii of curvature and coordinates are defined in Fig.1. The well-known equations of equilibrium and kinematic relations for a general shell of revolution under axisymmetric loads are repeated here for easy reference [8] in terms of the dimensionless quantities defined by

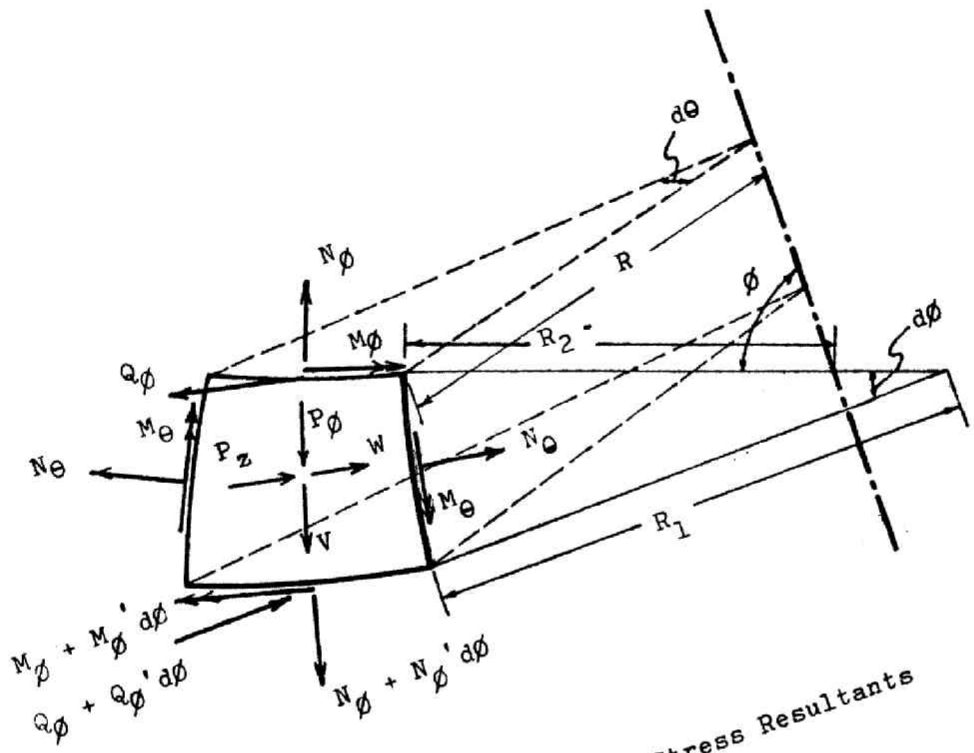

Fig.1 Shell Element and Stress Resultants

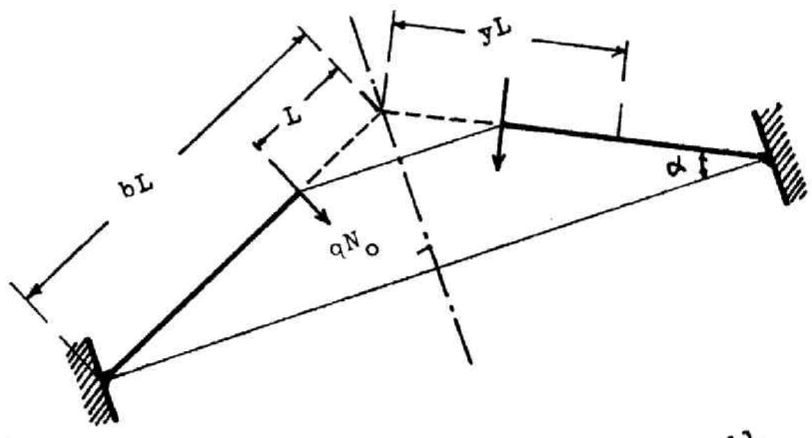

Fig.3 Clamped Truncated Conical Shell

$$n_\phi = \frac{N_\phi}{N_0}, \quad n_\theta = \frac{N_\theta}{N_0}, \quad m_\phi = \frac{M_\phi}{M_0}, \quad m_\theta = \frac{M_\theta}{M_0}, \quad k = \frac{M_0}{N_0 L} = \frac{H}{4L},$$
$$q_\phi = \frac{Q_\phi}{N_0}, \quad p_\phi = \frac{P_\phi L}{N_0}, \quad p_z = \frac{P_z L}{N_0}, \quad r = \frac{R}{L}, \quad r_1 = \frac{R_1}{L}, \quad r_2 = \frac{R_2}{L} \tag{1}$$

where H without a subscript and L denote the thickness and a typical length of the shell, respectively. M_0 and N_0 are the yield bending moment and yield normal force per unit length given by

$$M_0 = \frac{1}{4}\sigma_y H^2 , \qquad N_0 = \sigma_y H$$

where σ_y denotes the yield stress in simple tension of the perfectly plastic material. There are three equations of equilibrium, which may be written as

$$(rm_\phi)' - r_1 n_\theta \cos\phi \quad rq_\phi + rr_1 p_\phi = 0$$
$$r_1 n_\theta \sin\phi + rn_\phi + (rq_\phi)' + rr_1 p_z = 0 \tag{2a-c}$$
$$k[(rm_\phi)' - r_1 m_\theta \cos\phi] \quad rr_1 q_\phi = 0$$

the primes indicating derivatives with respect to ϕ. From the standpoint of the general theory of limit analysis, the stress resultants N_ϕ, N_θ, M_ϕ and M_θ are the generalized stresses. The corresponding generalized plastic strain-rates are the principal rates of extension and of curvature of the middle surface denoted by

$$\varepsilon_\phi, \quad \varepsilon_\theta, \quad K_\phi, \quad K_\theta$$

respectively. Reduced rates of curvature are defined by

$$\kappa_\phi = \frac{M_0}{N_0} K_\phi, \quad \kappa_\theta = \frac{M_0}{N_0} K_\theta$$

Then the rate of dissipation of mechanical energy may be written as

$$D_i = N_0(n_\phi \varepsilon_\phi + n_\theta \varepsilon_\theta + m_\phi \kappa_\phi + m_\theta \kappa_\theta) \tag{3}$$

Reduced velocities are

$$v = V/L, \quad w = W/L$$

where V and W are the velocity components shown in Fig.1. The kinematic relations may be written as follows:

$$\varepsilon_\phi = \frac{v' - w}{r_1}, \quad \varepsilon_\theta = \frac{v \cot\phi - w}{r_2}$$

$$\kappa_\phi = \frac{k}{r_1}\left(\frac{v + w'}{r_1}\right)', \quad \kappa_\theta = -\frac{k \cot\phi}{r_2}\frac{v + w'}{r_1} \tag{4a-d}$$

3. APPROXIMATE YIELD CONDITION

The yield condition and the associated flow law for the present problem derived from the Tresca yield criterion by Onat and Prager [1] are summarized here for the ensuing discussion. The three parameters

$$\xi = -\frac{\varepsilon_\phi}{4\kappa_\phi}, \quad \eta = \frac{\varepsilon_\phi + \varepsilon_\theta}{4(\kappa_\phi + \kappa_\theta)}, \quad \zeta = \frac{\varepsilon_\theta}{4\kappa_\theta}$$

describe the location of the zeros of the principal strain-rates on a normal to the shell. The yield hypersurface H is defined piecewise by six sets of parametric representations and the six quadratic expressions shown in Tables 1 and 2. Each constituent hypersurface is denoted by G or H with appropriate subscripts as shown in the first column of Tables 1 and 2 and is to be subjected to appropriate restrictions stated in reference [1].

In order to establish a good approximate yield condition, it is

Table 1 Non-cylindrical parts of the Tresca hypersurface

Hyper-surface	Inter-mediate Parameter	n_ϕ	n_θ	m_ϕ	m_θ
G_ϕ^+	ξ	$-(\xi + \eta)$	$-(\eta - \zeta)$	$1 - 2(\xi^2 + \eta^2)$	$2(\zeta^2 \quad \eta^2)$
G_ϕ^-	ξ	$(\xi + \eta)$	$(\eta \quad \zeta)$	$-1 + 2(\xi^2 + \eta^2)$	$- 2(\zeta^2 \quad \eta^2)$
$G_{\phi\theta}^+$	η	$-(\xi + \eta)$	$-(\eta + \zeta)$	$1 \quad 2(\xi^2 + \eta^2)$	$1 - 2(\eta^2 + \zeta^2)$
$G_{\phi\theta}^-$	η	$(\xi + \eta)$	$(\eta + \zeta)$	$-1 + 2(\xi^2 + \eta^2)$	$-1 + 2(\eta^2 + \zeta^2)$
G_θ^+	ζ	$-(\eta - \xi)$	$-(\eta + \zeta)$	$2(\xi^2 \quad \eta^2)$	$1 - 2(\eta^2 + \zeta^2)$
G_θ^-	ζ	$(\eta - \xi)$	$(\eta + \zeta)$	$2(\xi^2 \quad \eta^2)$	$-1 + 2(\eta^2 + \zeta^2)$

Table 2 Parabolic hypercylinders

Hyper-surface	Yield condition		ε_ϕ : ε_θ : κ_ϕ: κ_θ	
H_ϕ^+	$m_\phi + n_\phi^2 = 1$	(5a)	$2n_\phi$: 0 : 1: 0	(5b)
H_ϕ^-	$m_\phi + n_\phi^2 = 1$	(6a)	$2n_\phi$: 0 : -1: 0	(6b)
$H_{\phi\theta}^+$	$m_\phi \quad m_\theta + (n_\phi - n_\theta)^2 = 1$	(7a)	$2(n_\phi - n_\theta)$: $-2(n_\phi - n_\theta)$: 1: -1	(7b)
$H_{\phi\theta}^-$	$- m_\phi + m_\theta + (n_\phi - n_\theta)^2 = 1$	(8a)	$2(n_\phi - n_\theta)$: $-2(n_\phi - n_\theta)$: -1: 1	(8b)
H_θ^+	$m_\theta + n_\theta^2 = 1$	(9a)	0 : $2n_\theta$: 0: 1	(9b)
H_θ^-	$- m_\theta + n_\theta^2 = 1$	(10a)	0 : $2n_\theta$: 0: -1	(10b)

necessary first to investigate and to visualize the hypersurface H representing the exact condition. For the purpose of visualization, it has been represented in Fig.2 as a one-parameter family of two-dimensional surfaces, where the subscripts 1 and 2 may stand either for θ and ϕ or for ϕ and θ, respectively [9]

H consists of three pairs of parabolic hypercylindrical hypersurfaces and three pairs of non-cylindrical but piecewise smooth hypersurfaces. One sees in Fig.2 that the former occupy a substantial part of the total and are patched by the latter fairly smoothly but with some singularities in the sense that normals are not defined uniquely at the intersections of G- and H-hypersurfaces. The pictures suggest to consider an approximation by means of the three pairs of parabolic hypercylinders. It is quite natural and reasonable to extend these hypercylindrical hypersurfaces to circumscribe the remaining non-cylindrical parts. The totality of the proposed approximate hypersurface will be denoted by H^*. It may be expected that H^* is very close to H and yet a simple approximation from outside and that the original characteristic features will be well retained. The yield conditions and associated flow laws of H^* are given by Table 2. Flow laws for any inter-sections of two, three or four hypersurfaces may be derived by the same technique as used for the Tresca criterion [9], [10], [11].

The question arises as to how close H^* is to H. Since H^* circumscribes H completely, a solution based upon H^* yields an upper bound on the exact collapse load based upon H. If H^* is shrunk by a factor ω such that the reduced hypersurface ωH^* inscribes H, then a solution based upon ωH^* furnishes a lower bound on the exact collapse load, since such a solution gives a statically admissible stress field for H. Denote by p_c and p_c^* the collapse load factors based upon H and H^*, then

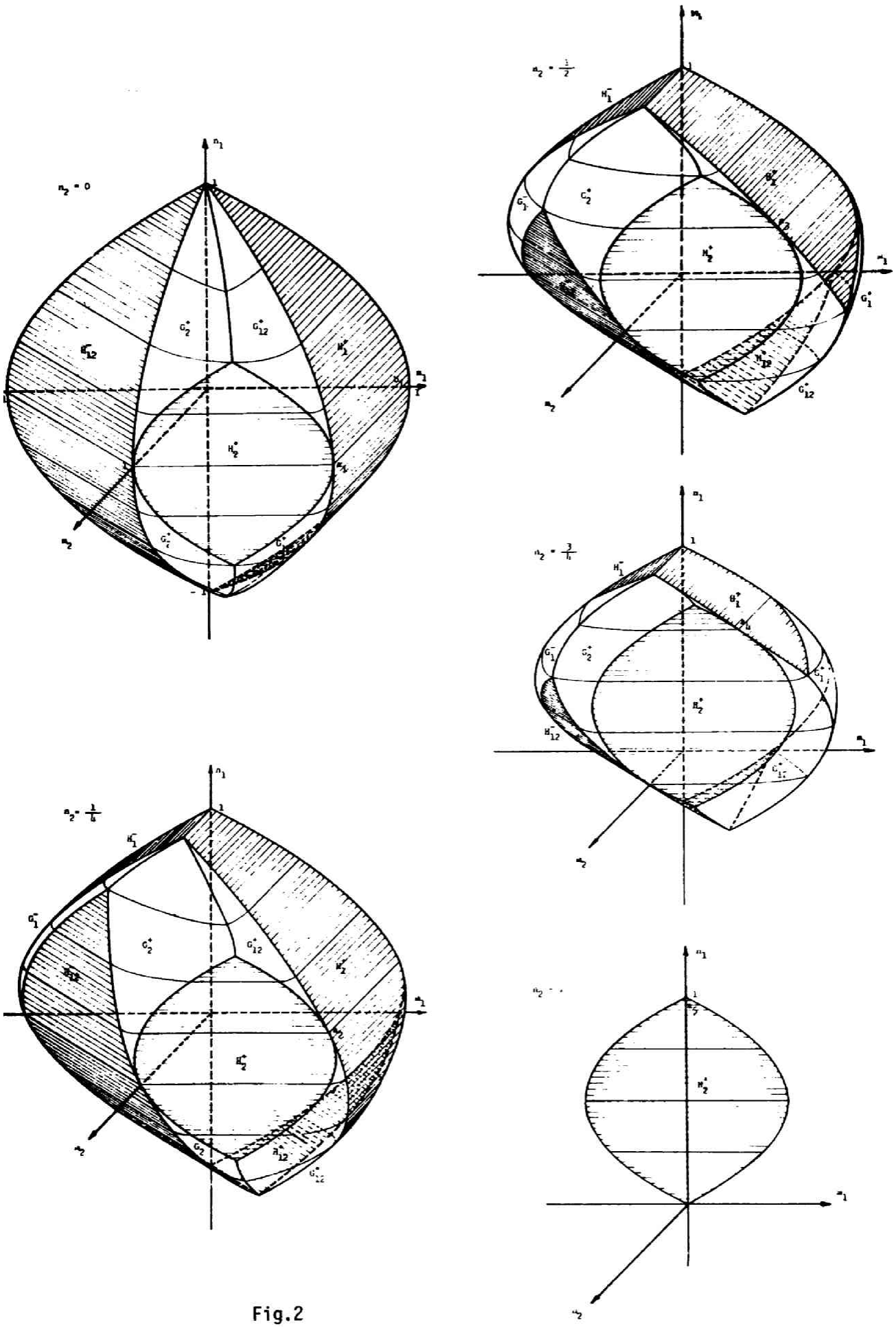

Fig.2

$$\omega p_c^* \leqq p_c \leqq p_c^* \qquad (0 \leqq \omega \leqq 1)$$

This implies that, the more closely the value of ω approaches unity, the closer the lower bound is to the upper bound. Hence the largest admissible value of ω may be taken as a measure of the accuracy of the proposed approximation. In order to determine the largest value of ω, it suffices, by virtue of the convexity of H and H^*, to examine if all the corner points of ωH^* are on or inside H. A corner point is an intersection of four hypersurfaces. The number of possible choices of hypersurfaces among six is $\binom{6}{4} = 15$. However, consideration of symmetry of H and H^* reduces those fifteen cases to six es essential ones. Moreover there are still two yield inequalities to be satisfied in each case. Thus it suffices to examine if the following four typical corner points of ωH^* are imbedded in H.

		(n_1, n_2, m_1, m_2)
1.	$H_1^+ \cap H_1^- \cap H_2^+ \cap H_2^-$	$(1, 1, 0, 0)$
2.	$H_1^+ \cap H_1^- \cap H_{12}^+ \cap H_{12}^-$	$(1, 0, 0, 0)$
3.	$H_1^+ \cap H_1^- \cap H_2^+ \cap H_{12}^-$	$(1, \frac{1}{2}, 0, \frac{3}{4})$
4.	$H_{12}^+ \cap H_{12}^- \cap H_1^+ \cap H_2^+$	$(-\frac{1}{2}, \frac{1}{2}, \frac{3}{4}, \frac{3}{4})$

It turns out that the largest admissible value of ω is 0.851, whence

$$0.851\, P_c^* \leqq P_c \leqq p_c^* \qquad (11)$$

This is a considerable improvement compared to the linear approximation proposed by Hodge [7] in which

$$0.618\, p_c^* \leqq p_c \leqq p_c^*$$

4. GENERAL SOLUTIONS

The system of differential equations for any one of the six parabolic hypersurfaces consists of eq. (2a-c), eq. (4a-d) and the yield condition and associated flow law from one line of Table 2. Since a flow law provides three ratios between the strain-rates, there are 11 equations for 11 unknowns.

(1) General solution for H_ϕ^+ and H_ϕ^-

The flow laws (5b) and (6b) require

$$\varepsilon_\theta = 0 , \qquad \kappa_\theta = 0 , \qquad \varepsilon_\phi/\kappa_\phi = \pm 2n_\phi$$

Substitution of the first two equations into the kinematic relations (4a-d) yields the differential equations for the velocity field. The general solution is given by

$$v = A \sin \phi , \qquad w = A \cos \phi$$

It is seen from eqs. (4) that ε_ϕ and κ_ϕ vanish identically. The solution therefore represents merely a rigidbody translation and does not represent any plastic velocity field, except along some discontinuities which will be discussed later.

(2) General solution for $H_{\phi\theta}^+$ and $H_{\phi\theta}^-$

The flow laws (7b) and (8b) provide the following three conditions:

$$\frac{\varepsilon_\phi}{\varepsilon_\theta} = -1 , \qquad \frac{\kappa_\phi}{\kappa_\theta} = -1 , \qquad \frac{\varepsilon_\theta}{\kappa_\theta} = \pm 2(n_\phi \quad n_\theta) \qquad (12a\text{-}c)$$

If the kinematic relations (4c,d) are substituted into (12b), the following

differential equation is obtained:

$$\left(\frac{v + w'}{r_1}\right)' r_2 \sin\phi + \frac{v + w'}{r_1} r_1 \cos\phi = 0 \qquad (13)$$

Since r_1 and r_2 satisfy the condition

$$(r_2 \sin\phi)' = r_1 \cos\phi, \qquad (14)$$

the first integral of (13) is

$$\frac{v + w'}{r_1} = \frac{B_1}{r_2 \sin\phi} \qquad (15)$$

where B_1 denotes an integration constant.* The condition (12a) gives

$$v' - w + \frac{r_1}{r_2} (v \cot\phi \quad w) = 0$$

Substitution of v from (15) and use of (14) yields the differential equation

$$w'' + \left(\frac{r_1}{r_2} \cot\phi\right) w' + \left(1 + \frac{r_1}{r_2}\right) w = \frac{B_1 r_1'}{r_2 \sin\phi} \qquad (16)$$

It can easily be proved by substitution that $w = B_2 \cos\phi$ is a complementary solution of eq. (16). The general solution of eq. (16) may then be obtained by the standard technique of setting $w = U(\phi) \cos\phi$. The result is

---

* Here and in the following, B and C denote integration constants for $H^{+}_{\phi\theta}$ (or $H^{-}_{\phi\theta}$) and for H^{+}_{θ} (or H^{-}_{θ}), respectively. B_1, B_2, B_3, C_1, C_2 and C_3 will be associated with velocity fields, and B_4, B_5, B_6, C_4, $C_5$and C_6 with stress fields.

$$w = \cos\theta \left[B_3 + B_1 \int \frac{r_1 \cos\phi + x(\phi) + \frac{B_2}{B_1}}{r_2 \sin\phi \cos^2\phi} \, d\phi \right] \tag{17}$$

where $x(\phi)$ is defined by

$$x(\phi) = \int r_1 \sin\phi \, d\phi \tag{18}$$

Upon substitution of (17) into (15), v is obtained. Upon substitution of (4b, d) into (12c) and introduction of the known velocity components v and w, one obtains

$$\pm (n_\phi \quad n_\theta) = \frac{1}{2k \cos\phi} \left(x(\phi) + \frac{B_2}{B_1} \right) \tag{19}$$

The upper and lower signs refer to $H^+_{\phi\theta}$ and $H^-_{\phi\theta}$, respectively, in eqs. (19) to (27). The three equations of equilibrium (2a-c), the yield condition (7a) or (8a), and eq. (19) are five equations for the five unknown stresses. Substitution of (19) into (7a) or (8a) furnishes

$$m_\phi - m_\theta = \pm \left[1 \quad \frac{1}{4k^2 \cos^2\phi} \{ x(\phi) + \frac{B_2}{B_1} \}^2 \right] \tag{20}$$

Multiplying (2a) by $\sin\phi$ and (2b) by $\cos\phi$, adding them and then integrating the resulting differential equation yields

$$rm_\phi \sin\phi + rq_\phi \cos\phi = - \int r \, r_1 \{ p_\phi \sin\phi + p_z \cos\phi \} \, d\phi + B_4 \tag{21}$$

After writing eq. (2a) in the form

$$-rm_\phi' - rq_\phi = -r \, r_1 \, p_\phi - (n_\phi \quad n_\phi) \, r_1 \cos\phi \tag{22}$$

and substituting eqs. (19) and (20), one finds the differential equation

$$n_\phi' + n_\phi \tan \phi = F_1(\phi) \tag{23}$$

where

$$F_1(\phi) = -r_1 p_\phi + \frac{r_1}{2kr}\left(x + \frac{B_2}{B_1}\right)$$

$$- \frac{1}{r \cos \phi} \int r\, r_1 (p_\phi \sin \phi + p_z \cos \phi)\, d\phi + \frac{B_4}{r \cos \phi} \tag{24}$$

The general solution of eq. (23) is

$$n_\phi = \cos \phi \left(B_5 + \int \frac{F_1(\phi)}{\cos \phi}\, d\phi \right) \tag{25}$$

From eq. (21) q_ϕ follows as

$$q_\phi = -\sin \phi \left(B_5 + \int \frac{F_1(\phi)}{\cos \phi}\, d\phi \right)$$

$$\frac{1}{r \cos \phi} \int r\, r_1 (p_\phi \sin \phi + p_z \cos \phi)\, d\phi + \frac{B_4}{r \cos \phi} \tag{26}$$

With the help of eq. (14), eq. (2c) may be written in the following form :

$$m_\phi' = \frac{1}{k} r_1 q_\phi \quad (m_\phi \quad m_\theta) \frac{r_1 \cos \phi}{r_2 \sin \phi} \tag{27}$$

The right-hand side of this equation is completely known from eqs. (20) and (26), and a simple quadrature yields m_ϕ

(3) General solutions for H_θ^+ and H_θ^-

The flow laws (9b) and (10b) furnish the following three conditions :

$$\varepsilon_\phi = 0 \,, \qquad \kappa_\phi = 0 \,, \qquad \frac{\varepsilon_\theta}{\kappa_\theta} = \pm 2n_\theta \tag{28a-c}$$

Substituting here the kinematic relations (4a, c) and then integrating the second equation once, one finds

$$w = v'$$

$$v + w' = C_1 r_1$$

The general solution of this system of differential equations is given by

$$v = C_1(r_2 \sin^2 \phi - x(\phi)\cos \phi) + C_2 \sin \phi + C_3 \cos \phi$$

$$w = C_1(x(\phi)\sin \phi + r_2 \sin \phi \cos \phi) + C_2 \cos \phi \quad C_3 \sin \phi \tag{29a,b}$$

Substitution of these expressions and of eqs. (4b, d) into eq. (28c) yields

$$n_\theta = \pm \frac{1}{2k \cos \phi} \left(\frac{C_3}{C_1} \quad x(\phi) \right) \tag{30}$$

The upper and lower signs here and in eqs. (31) (33) refer to H_θ^+ and H_θ^-, respectively. The first equation of equilibrium (2a) may now be written as

$$rq_\phi = (rn_\phi)' \pm \frac{r_1}{2k} \left(\frac{C_3}{C_1} \quad x(\phi) \right) + r\, r_1 p_\phi \tag{31}$$

Since eq. (21) has been derived solely from the equations of equilibrium (2), it is independent of the yield hypersurfaces and is valid also for H_θ^+ and H_θ^-. From eqs. (21) and (31), a first-order differential equation for (rn_ϕ) can be derived, which has the general solution

$$rn_\phi = \cos\phi \left[C_5 + \int \left\{ \frac{\mp\, r_1}{2k \cos\phi} \left(\frac{C_3}{C_1} - x(\phi) \right) - \frac{r\, r_1 p_\phi}{\cos\phi} + \frac{C_4}{\cos^2\phi} \right\} d\phi \right.$$

$$\left. \int \frac{d\phi}{\cos^2\phi} \int r\, r_1 \, (p_\phi \sin\phi + p_z \cos\phi)\, d\phi \right] \qquad (32)$$

Now rq_ϕ follows from eq. (21). The bending moment m_θ is obtained by substituting eq. (30) into the yield conditions (9a) and (10a)

$$m_\theta = \mp \left[1 - \frac{1}{4k^2 \cos^{-2}\phi} \left(\frac{C_3}{C_1} - x(\phi) \right)^2 \right] \qquad (33)$$

Since rq_ϕ and m_θ are known, rm_ϕ may be obtained by a simple quadrature of the third equation of equilibrium (2c).

It should be noted that the simple, double and triple quadratures appearing in these general solutions may be carried out explicitly for a class of shells for which

$$r = a \sin^m \phi \cos^n \phi$$

where $a > 0$ and m and n are not to be negative odd integers (including $n = +1$). Also the cases of a spherical shell (m, n = 1, 0) and of a paraboloid (m, n = -2, 0) can easily be handled. More generally, the general solutions may be evaluated explicity in terms of elementary functions for the following classes of shells

$$\text{(A)} \quad r = a\, e^{\alpha\phi} \sin^m \phi \cos^n \phi$$

$$\text{(B)} \quad r = b\phi^j \sin^m \phi \cos^n \phi$$

with appropriate restrictions on the integers j, m and n.

5 DISCONTINUITIES

After the general solutions have been obtained, all that is necessary to solve a specific problem is to determine the free constants from a set of boundary and continuity conditions. However, besides the diffculty of unknown boundaries of a plastic region, it has still to be found out which of the four hypersurfaces should be used in any given case, and this question brings forth the principal difficulty which is common to all piecewise regular yield conditions. A set of boundary conditions and consideration of limiting cases of the problem leads very often to an appropriate choice of the general solutions. In contrast to the elastic theory of shells, however, some of the boundary and continuity conditions admit several possibilities depending upon whether or not discontinuities in stresses or velocities appear across the point in question. It is necessary, therefore, to investigate the nature of possible discontinuities in stress and velocity fields associated with the present approximate yield hypersurface. Attention will be confined here to the formation of a "hinge circle", which will appear later in the example.

Consideration of equilibrium of a shell element containing a discontinuity leads to the conclusion that the stresses n_ϕ , m_ϕ and q_ϕ must be continuous but that m_θ and n_θ may be discontinuous.

A hinge circle is defined as a circle on the shell along which v or w' is discontinuous. Hence v' or w'' must be numerically very large compared to all lower derivatives. The kinematic conditions (4) show that then ε_ϕ, $\kappa_\phi \gg \varepsilon_\theta$, κ_θ, and from Table 2 it may be seen that this is only possible on H_ϕ^+ and H_ϕ^-. Since, however, these parts of the yield surface represent rigid-body displacements without true plastic flow, the stress point corresponding to a hinge circle must be sought on the <u>boundaries</u> of H_ϕ^+ or H_ϕ^-. A more detailed discussion has been given in [9]. The boundary of H_ϕ^+ (or H_ϕ^-)

consists of its intersections with the other hypersurfaces and hence there are various kinds of hinge circles. In order to discuss the behavior of a solution in stress space, the concept of a "stress trajectory" is useful. From the solution of a problem a generalized stress set $(n_\phi, n_\theta, m_\phi, m_\theta)$ may be formed for every point of the shell. The locus of these points in stress space is called the stress trajectory of the problem. Let a hinge circle be at $\phi = \phi_0$. When a stress trajectory lies partly in a hypersurface H_a (for $\phi < \phi_0$) and partly in H_b (for $\phi > \phi_0$) and may have some discontinuity at $\phi = \phi_0$, this discontinuity is called a discontinuity of type $H_a \to H_b$.

Consider now a discontinuity of type $H_\phi^+ \to H_\theta^+$. The flow laws for H_ϕ^+ and H_θ^+ hold for $\phi < \phi_0$ and $\phi > \phi_0$, respectively. Let Δv and $\Delta w'$ be the finite jumps in v and w' across $\phi = \phi_0$, respectively; they may easily be calculated from the velocity field of H_θ^+. Then the most singular parts of ε_ϕ and of κ_ϕ may be written as

$$\varepsilon_\phi = \frac{\Delta v}{r_1}\,\delta(\phi - \phi_0)$$

$$\kappa_\phi = -\frac{k}{r_1}\,\Delta\left(\frac{v + w'}{r_1}\right)\delta(\phi - \phi_0)$$

where $\delta(\phi - \phi_0)$ denotes a Dirac delta function. The flow law (5b) gives

$$n_\phi = \frac{\varepsilon_\phi}{2k_\phi} = -\Delta v/2k\Delta\left(\frac{v + w'}{r_1}\right) \tag{34}$$

The bending moment m_ϕ must satisfy the yield condition (5a)

$$m_\phi = 1 - n_\phi^2 = 1 - \left(\frac{\varepsilon_\phi}{2k_\phi}\right)^2 \tag{35}$$

because of its continuity. For any other type of hinge circles, Δv and $\Delta w'$ may also be calculated from the velocity fields and conditions similar to

eqs. (34) and (35) may be obtained explicitly.

6. CONICAL SHELL

The present theory is also applicable to shell problems in other coordinates as, for instance, a cone (Fig.3). Instead of ϕ, the coordinate $y = Y/L$ is used, but for easy reference ϕ will be retained as a subscript. The equilibrium conditions for the cone are the following:

$$\begin{aligned} (y\, n_\phi)' \quad n_\theta + y\, p_\phi &= 0 \\ (y\, q_\phi)' + n_\theta \tan\alpha + y\, p_z &= 0 \\ k(y\, m_\phi)' - k\, m_\theta - y\, q_\phi &= 0 \end{aligned} \tag{36a-c}$$

where the dots denote d fferentiation with respect to y. The kinematic relations are

$$\begin{aligned} \varepsilon_\phi &= v' , \qquad \varepsilon_\theta = \frac{1}{y}(v \quad w\tan\alpha) \\ \kappa_\phi &= -k\, w'' , \qquad \kappa_\theta = \frac{k\, w'}{y} \end{aligned} \tag{37}$$

The procedure of obtaining the general solutions is the same as before. Those for $H^{+}_{\phi\theta}$ and $H^{-}_{\phi\theta}$ are derived here for later use in an example. As in the general case, the flow laws (7b) and (8b) yield the relations (12). From (12b) and (37) one finds

$$\frac{w''}{w'} = \quad \frac{1}{y}$$

whence

$$w = B_1 \ln y + B_2 \tag{38}$$

Eq.(12a) provides a first-order differential equation for v, whose general solution is

$$v = B_1 \tan\alpha \ln y \quad (B_1 - B_2)\tan\alpha + B_3 y^{-1} \tag{39}$$

The third ratio (12c) furnishes then

$$n_\phi \quad n_\theta = \mp \frac{1}{2k} \left(\frac{B_3}{B_1} \quad y \tan \alpha \right) \tag{40}$$

where $|n_\phi \quad n_\theta| < 1$. The upper and lower signs refer to $H^{+}_{\phi\theta}$ and $H^{-}_{\phi\theta}$, respectively. Upon substituting (40) into the yield conditions (7a) and (8a), one finds

$$m_\phi - m_\theta = \mp \left[1 - \frac{1}{4k^2} \left(\frac{B_3}{B_1} \quad y \tan \alpha \right)^2 \right] \tag{41}$$

and from eqs.(36a) and (40) by simple quadrature

$$n_\phi = \mp \frac{1}{2k} \left(\frac{B_3}{B_1} \ln y \quad y \tan \alpha \right) \quad \int p_\phi dy + B_4 \tag{42}$$

If (42) is substituted into (40), one obtains

$$n_\theta = \mp \frac{1}{2k} \left[\frac{B_3}{B_1} (1 + \ln y) \quad 2y \tan \alpha \right] \quad \int p_\phi \, dy + B_4 \tag{43}$$

Equation (36b) may then be integrated to yield q_ϕ. Since q_ϕ and $(m_\phi \quad m_\theta)$ are now known, eq.(36c) may also be integrated to find m_ϕ.

7. CLAMPED TRUNCATED CONICAL SHELL SUBJECTED TO A LINE LOAD ALONG ITS SHORTER EDGE

Let $y = 1$ and $y = b$ be the inner and outer boundaries, respectively (Fig.3). A line load with the dimensionless intensity q is applied at the inner boundary, normal to the shell. The solution is facilitated when the shell is shallow, because then the stress trajectory may be expected to be in the vicinity of that for a circular plate with similar boundary conditions. Since the velocity field of the plate is represented by a surface of revolution with negative Gaussian curvature, its stress trajectory lies on the side $m_\theta \quad m_\phi = 1$ of a Tresca hexagon for m_ϕ and m_θ. Its four-dimensional counterpart is the hyper-surface $H^{-}_{\phi\theta}$. Furthermore, in analogy to the known velocity field of a clamped plate without a hole, one may expect a hinge circle to develop along the outer boundary. For the Tresca hexagon, $m_\phi = -1$ is the boundary

conditon when such a hinge circle is to appear. The four-dimensional counterpart of this is to assume that the stress trajectory being in $H^-_{\phi\theta}$ reaches H^-_{ϕ} for $y = b$.

At the edge $y = b$ there must be $w = 0$. This determines B_2 in eq.(38) and yields

$$w = B_1 \ln \frac{y}{b}, \quad v = -B_1 \tan \alpha (1 - \ln \frac{y}{b}) + \frac{B_3}{y} \qquad (44a,b)$$

The boundary values of v and $w^{\cdot}$ calculated from these formulas do not vanish, as they should, and represent the jumps of these functions across the hinge circle:

$$\Delta w^{\cdot} = -\frac{B_1}{b}, \qquad \Delta v = B_1 \left(\tan \alpha - \frac{B_3}{B_1} \frac{1}{b} \right)$$

The flow law (6b), when applied to the hinge circle $y = b$, yields

$$n_\phi = -\frac{\varepsilon_\phi}{2\kappa_\phi} = \frac{\Delta v}{2k\Delta w^{\cdot}} = \frac{-1}{2k} \left(b \tan \alpha \quad \frac{B_3}{B_1} \right) \qquad (45)$$

In eq.(45) it is assumed that $|\varepsilon_\phi / 2\kappa_\phi| < 1$. The yield condition (6a) must also be satisfied:

$$m_\phi = -1 + n_\phi^2 = -1 + \frac{1}{4k^2} \left(b \tan \alpha - \frac{B_3}{B_1} \right)^2 \qquad (46)$$

The boundary conditions may now be summarized as follows:

at $y = 1$: $n_\phi = 0$, $m_\phi = 0$, $q_\phi = -q$

at $y = b$: $w = 0$, eq.(45), eq.(46)

These six conditions determine the collapse load q_c and five out of six integration constants, leaving an indeterminate multiplier in the resulting velocity field. The result is as follows:

$$q_c = \frac{k(1 + \ln b))}{\ln b} + \frac{\tan^2 \alpha}{8k \ln b} \left(3b^2 \quad 1 - \frac{2(2b - 1)^2}{1 + \ln b} \right) \qquad (47)$$

$$n_\phi \quad n_\theta = \frac{-\tan \alpha}{2k} \left(y \quad \frac{2b \quad 1}{1 + \ln b} \right)$$

$$n_\phi = \frac{\tan \alpha}{2k} \left(y \quad 1 \quad \frac{2b \quad 1}{1 + \ln b} \ln y \right)$$

$$n_\theta = \frac{-\tan\alpha}{2k}(2b \quad 1)\left\{\frac{1 + \ln y}{1 + \ln b} \quad \frac{2y \quad 1}{2b - 1}\right\} \qquad (48a\text{-}f)$$

$$q_\phi = \frac{-\tan^2\alpha}{2k}(y \quad 1 \quad \frac{2b \quad 1}{1 + \ln b}\ln y) - \frac{q_c}{y}$$

$$m_\phi = \left[1 \quad \frac{q_c}{k}\right]\ln y \quad \frac{\tan^2\alpha}{8k^2}\left[\{\frac{2(2b \quad 1)^2}{(1 + \ln b)^2} \quad \frac{4(2b \quad 1)}{1 + \ln b}y\}\ln y\right.$$

$$\left. + 3y^2 \quad 4y + 1\right]$$

$$m_\theta = 1 + m_\phi \quad (n_\phi - n_\theta)^2$$

It should be noted that the result may easily be checked by applying the principle of virtual work on the stress and velocity fields obtained above. In order that eqs.(47) and (48) really constitute a complete solution, the remaining yield inequalities must not be violated and no finite portion of the stress trajectory should be on the boundary of $H_{\phi\theta}$. This means that the solution (47), (48) is valid only for certain values of tan α. This restriction is drawn as $(\tan\alpha)_{max}$ in Fig.4 where a family of $q_c(b, \tan\alpha)$-curves are shown. A q_c-curve obtained from eq.(47) for a constant value of tan α achieves a minimum at a finite value of b except when tan α = 0, the case of an annular plate. This implies that only portions of the curves may represent actual collapse loads. The assertion that q_c cannot increase as b is increased may be proved by a direct application of the limit analysis theorems [12], [13]. Thus only that part of a q_c-curve which is decreasing with respect to b on the left of the minimum for a particular value of tan α as shown in Fig.4., can represent actual collapse loads, provided that the minimum is below the $(\tan\alpha)_{max}$-curves. If the latter is below the former, then the restriction due to the latter applies first. The stress distributions have been obtained for (b, tan α) = (1.25, 0.01), (3.00, 0.01), (5.00, 0.01) and (1.25, 0.20) and the corresponding stress trajectories are shown in Fig.5. The result assures

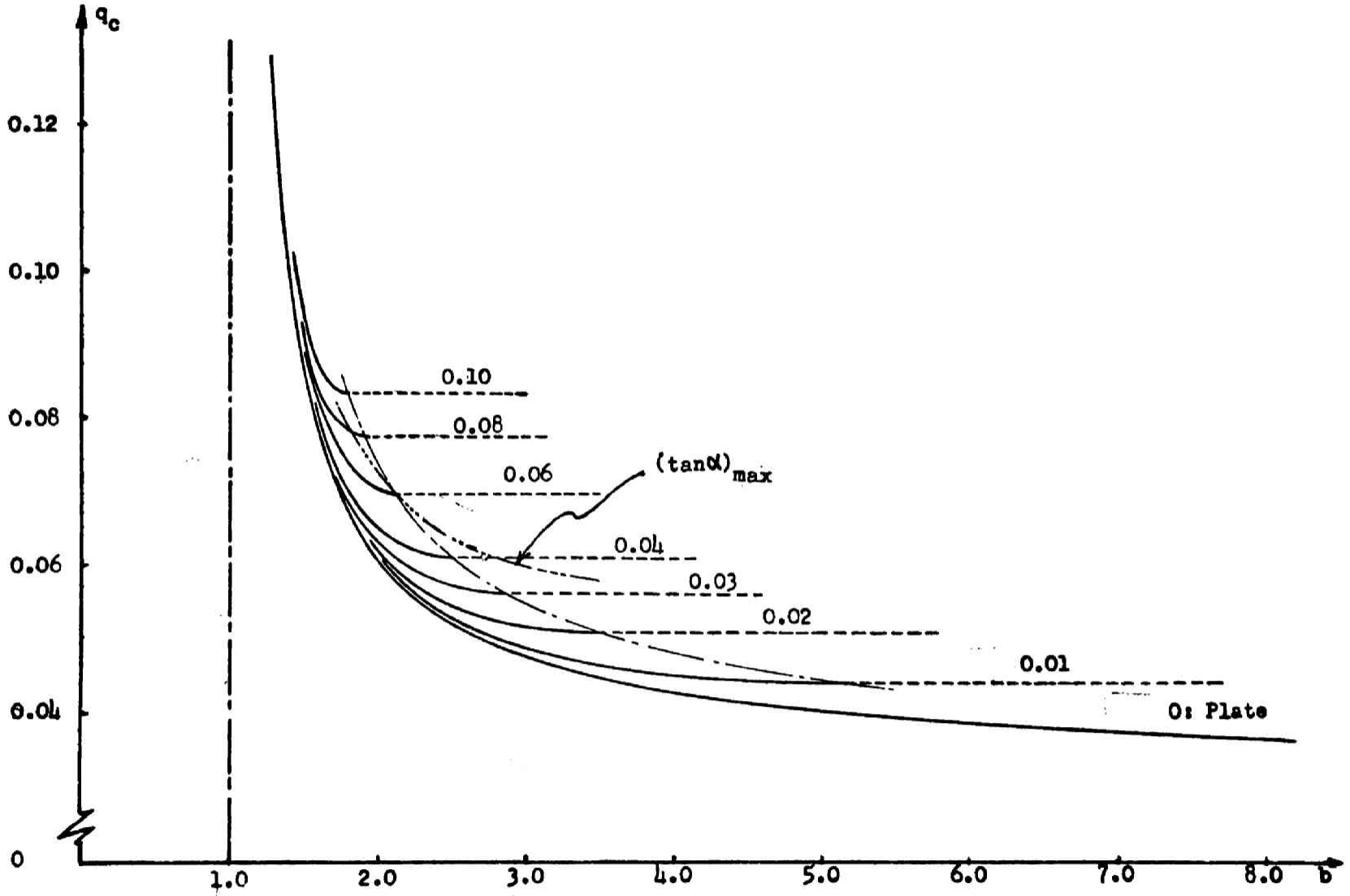

Fig.4 The Collapse Load q_c with Respect to the Parameter $\tan\alpha$

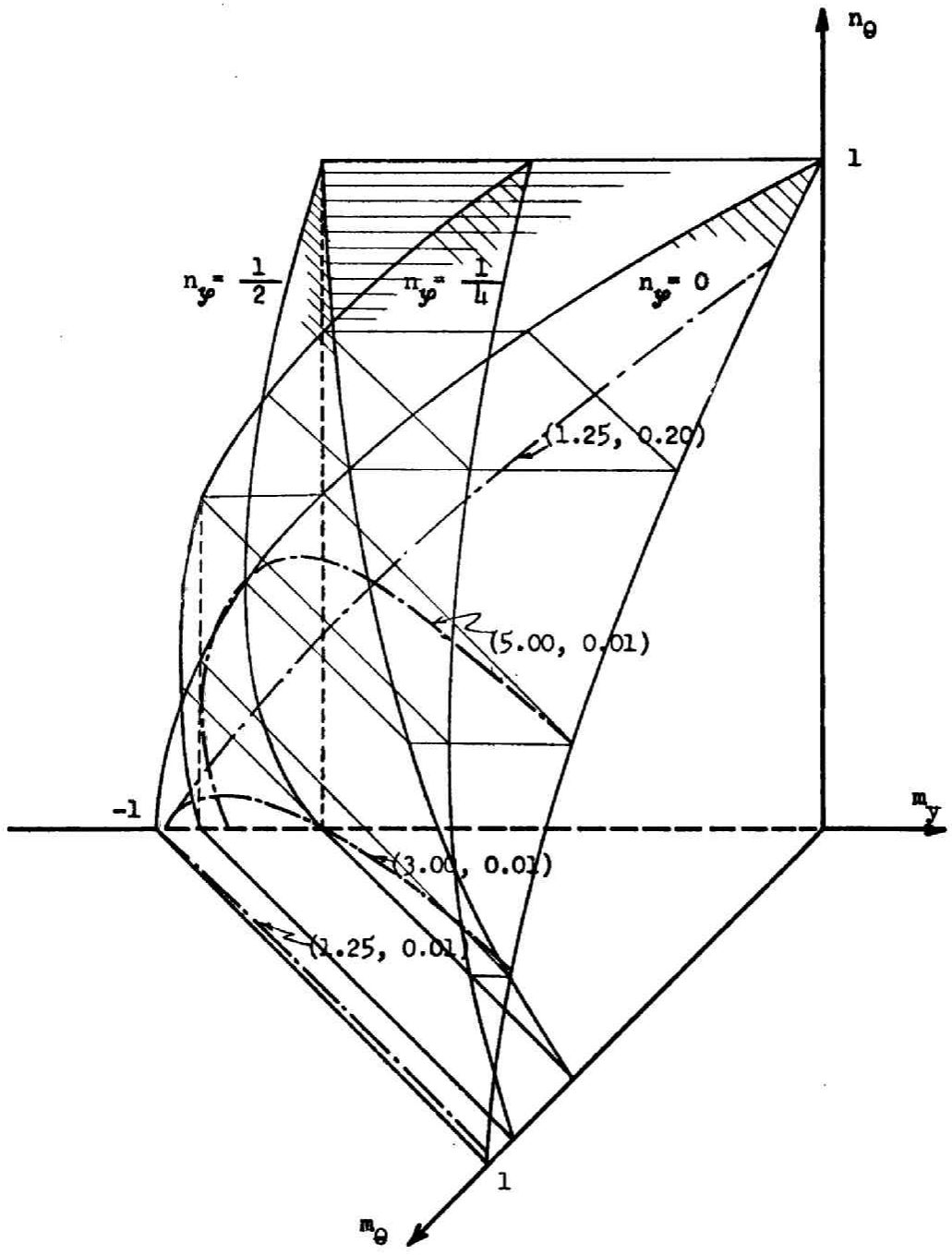

Fig.5 Stress Trajectories in $(n_\theta, m_{y\varphi}, m_\theta)$-space with $n_{y\varphi}$ as a Parameter.

that the remaining yield inequalities are nowhere violated.

8. EXTENSIONS

The proposed method is applicable directly to shells of variable thickness. The yield conditions (5a ~ 10a) depend then upon ϕ. Let $\bar{M}_0$ and $\bar{N}_0$ denote the standard yield moment and yield axial force, respectively, at some value of ϕ, say ϕ_0. Let $t(\phi)$ denote the ratio of the shell thickness at ϕ to that at ϕ_0. The yield conditions nondimensionalized in terms of $\bar{M}_0$ and $\bar{N}_0$ may be written as

$$\left.\begin{aligned} m_\phi - n_\phi^2 &= [t(\phi)]^2 \\ m_\phi - m_\theta - (n_\phi \quad n_\theta)^2 &= [t(\phi)]^2 \\ m_\theta - n_\theta^2 &= [t(\phi)]^2 \end{aligned}\right\} \quad (49a\text{-}c)$$

The yield hypersurface at ϕ is therefore considered to be inflated or shrunk by the factor $[t(\phi)]^2$ with precisely the same shape as that at ϕ_0. The associate flow laws remain the same as Eqs.(5a ~ 10b). The first terms in the square brackets of Eqs.(20) and (33) must only be replaced by $[t(\phi)]^2$.

If a shell is composed of a perfectly-plastic material which obeys a modified Tresca criterion with different yield stresses in tension and compression, the yield conditions Eqs.(5a ~ 10a) for a shell element must be modified respectively as follows:

$$\left.\begin{aligned} &(5a)\\ &(6a) \end{aligned}\right\} \rightarrow \quad \pm m_\phi = \frac{1+\lambda}{2} \quad \frac{1}{2(1+\lambda)} \left[n_\phi + \frac{1 \quad \lambda}{2}\right]^2$$

$$\left.\begin{aligned} &(7a)\\ &(8a) \end{aligned}\right\} \rightarrow \quad \begin{aligned} \pm (m_\phi \quad \lambda m_\theta) &= \frac{1+\lambda}{2} \quad \frac{1}{2(1+\lambda)} \left[n_\phi \quad \lambda n_\theta + \frac{1 \quad \lambda}{2}\right]^2 \\ \pm (m_\theta \quad \lambda m_\phi) &= \frac{1+\lambda}{2} - \frac{1}{2(1+\lambda)} \left[n_\theta \quad \lambda n_\phi + \frac{1-\lambda}{2}\right]^2 \end{aligned} \quad (50a\text{-}c)$$

$$\left.\begin{matrix}(9a)\\(10a)\end{matrix}\right\} \rightarrow \quad \pm m_\theta = \frac{1+\lambda}{2} \quad \frac{1}{2(1+\lambda)} \left[n_\theta + \frac{1-\lambda}{2}\right]^2 \qquad (50d)$$

where λ denotes the ratio of the tensile yield strength to the compressive yield strength of the material. Eqs.(50a ~ d) have been derived by the present author [14, 15]. It should be noted that the approximate yield hypersurface consists of 4 pairs of parabolic hypersurfaces. The associated flow law contains λ. Since the piecewisely parabolic nature is retained in Eqs.(50), the equations for velocity fields are again uncoupled, and therfore the general solutions can be obtained by a procedure analogous to that shown in Section 4.

9. CONCLUDING REMARKS

Since the original Tresca yield hexagon is a piecewise continuous curve, the resulting yield hypersurface for a shell element necessarily has piecewise regularity and so does the present approximate hypersurface. It seems impossible to decrease the number of constituent hypersurfaces to less than six. The present approximation seems, therefore, to be the most natural and reasonable one in view of the Tresca hexagon. It has mathematical simplicity and gives a set of close bounds on the collapse load as indicated by eq.(11). The general solution can be obtained almost explicitly for all the constituent hypersurfaces and an appropriate choice out of the four general solutions must only be made for a specific problem together with the assumptions on the boundaries of the chosen solutions. If a stress trajectory is to lie in an intersection of two, three or four hypersurfaces, it may be possible to solve those two, three or four yield conditions and the three equations of equilibrium for five unknown stresses without regard to the corresponding flow laws. The stress solution and the flow law then determine the associated velocity field. It may be expected, however, that only under special circumstances a stress trajectory lies in an intersection of three or four

hypersurfaces since the number of conditions exceeds the number of unknowns. The simple example of a shallow conical shell illustrates the procedure to obtain a complete solution and shows that, if a stress trajectory lies in only one hypersurface, a set of integration constants can easily be determined.

REFERENCES

N 1. See for instance, R.H.Lance and C.H. Lee, "The Yield Point Load of a Conical Shell," Int.J.Mech.Sci., Vol.11, (1969), pp120-143.

N 2. See for instance, Marcal, P.V. "Finite Element Analysis of Combined Problems of Nonlinear Material and Geometric Behavior," Computational Methods in Applied Mechanics, pp133-149.

1. Onat, E.T., and W.Prager, "Limit Analysis of Shells of Revolution," Roy. Netherlands Acad. Sci., ser. B, 57, (1954), pp534-548

2. Onat, E.T., "Plastic Analysis of Shallow Conical Shells," J.Eng.Mech.Div., Proc.ASCE, 86 (1960), No.EM 6, pp2675-1-12

3. Lance, R.H., and E.T.Onat, "Analysis of Plastic Shallow Conical Shells," J.Appl.Mech., 30 (1963), pp.199-209

4. Drucher, D.C., and R.T.Shield, "Limit Analysis of Symmetrically Loaded Thin Shells of Revolution," J.Appl.Mech., 26, (1959), pp61-68

5. Hodge, Jr., P.G., "The Collapse Load of a Spherical Cap," Proc.Fourth Midwest Conf. on Solid Mechanics, Austin, 1959, pp108-126

6. Hodge, Jr., P.G., "Plastic Analysis of Rotationally Symmetric Shells," DOMIIT Report No.1-6, 1959, Illinois Institute of Technology

7. Hodge, Jr., P.G., "Yield Conditions for Rotationally Symmetric Shells Under Axisymmetric Loading," J.Appl.Mech., 27,(1960), pp323-331

8. Flügge, W., "Stresses in Shells," Springer-Verlag, Berlin, 1960

9. Nakamura,Tsuneyoshi, "Plastic Analysis of Shells of Revolution under Axisymmetri Loads," Ph.D. Thesis, Stanford University, Stanford California, 1961.

10. Prager, W., "On the Use of Singular Yield Conditions and Associated Flow Rules," J.Appl.Mech., 20, (1953), pp317-320

11. Koiter, W.T., "General Theorems for Elastic Plastic Solids," Progress in Solid Mechanics, Vol.1, Ed. by I.N.Sneddon and R.Hill, North-Holland Publishing Company, Amsterdam, 1960, pp165-221

12. Drucker, D.C., W.Prager, and H.J.Greenberg, "Extended Limit Design Theorems for Continuous Media," Q.Appl.Math., 9, (1952), pp381-389

13. Ross, Jr., E.W., "On the Effect of Boundary and Loading Conditions in the Limit Analysis of Plastic Structures," J.Appl.Mech., 24,(1957), pp314-315

14. Tsuneyoshi Nakamura, "Studies on Limit Analysis of Structures," Thesis for M.Eng. submitted to Kyoto University, Mar.1958, pp99-101

15. Y.Yokoo, O.Matsuoka and Tsuneyoshi Nakamura, "On General Yield Conditions for Shells," Trans.A.I.J. No.60, Oct. 1958, pp421-424

CHAPTER 11

LIMIT ANALYSIS OF NON-SYMMETRIC SANDWICH SHELLS

1. INTRODUCTION

It appears that previous analytical investigations on the limit analysis of shells have been restricted to axisymmetric problems except a few papers on long cylindrical shell roofs [1], [2]. In axisymmetric problems, the directions of principal direct forces and moments are known *a priori* and the Tresca yield condition derived by Onat and Prager [3] may be applied. It has been shown in the preceding chapter that the stress and velocity equations may be uncoupled in piecewise quadratic approximation and that workable solutions may be obtained piecewisely, resulting in better bounds on load factors.

In a general non-symmetric problem, the directions of principal direct forces do not, in general, coincide with those of principal moments and both are not known *a priori*. Therefore there is no advantage in using the Tresca yield condition. The Mises yield condition for a uniform shell, however, becomes highly complicated and can hardly be employed for practical problems. Since six generalized stresses must be considered for a non-symmetric problem, the yield condition may be conceived geometrically as a hypersurface in a six-dimensional generalized stress space. A linear approximate yield condition may be considered just as in axisymmetric problems, but it would result in a number of faces or hyperplanes. Since a polyhedron in a six-dimensional space can hardly be visualized, a correct choice of hyperplanes may be very difficult for a specific boundary value problem. Therefore a practically workable yield condition must be, at worst, such that it does not result in non-linear coupling between the stress and velocity equations and that it consists of only a few pieces. In the present paper, the yield condition for a non-symmetric sandwich

---

This chapter is based upon the author's paper, "Limit Analysis of Non-symmetric Sandwich Shells," presented at the I.A.S.S. Symposium on Non-classical Shell Problems, Sept.2-5, 1963, NON-CLASSICAL SHELL PROBLEMS (W.Olszak and A.Sawszuk, Editors) pp768-784, Warszawa, 1964. The content of the paper was introduced to Italian engineers by M.Capurso in an amplified form, "Sulla determinazione del carico di collasso nelle superfici a doppia curvertura," Nota I, II, Construzioni metalliche n.5 and n.6-1965. The proposed method was recently introduced to Russian engineers by M.Sh.Mikeladze, "An Introduction to the Technical Theory of Perfectly-plastic Thin Shells," (In Russian) Ch.4., Tbilisi, Georgian SSR, USSR, 1969

shell is derived as a generalization of the one for axisymmetric problems proposed by Hodge [7] to use as an approximate yield condition of a uniform shell.* It is shown that the proposed condition does satisfy both of these requirements. This is not sufficient, however. The second difficulty lies in the fact that the shape of the boundary of a plastic region is not known *a priori* for a specific problem. It is then necessary to utilize the upper and lower bound theorems of limit anslysis assuming some suitable boundary of a plastic region. It is illustrated by an example that consideration of strong discontinuities in a velocity field enables one to obtain readily upper bounds on a collapse load factor.

2. YIELD CONDITION AND FLOW LAW FOR A SANDWICH SHELL

A typical sandwich shell element is shown in Fig.1 where 1 and 2 denote two orthogonal curvilinear coordinates on the middle surface of a shell. Besides the customary assumptions made in the limit analysis of structures and in the linear kinematic relations of thin shells in the category of Love's first approximation, the following assumptions are made for the sandwich construction. (A) The two facings or cover sheets with constant distance $2H$ everywhere are regarded as isotropic solid membranes of small equal thickness J and composed of a perfectly-plastic material satisfying the Mises yield condition. The shear stresses in the facings normal to their planes may be naglected and the stresses $(\overline{\sigma}_1, \overline{\sigma}_2, \overline{\tau})$ in the upper facing and $(\underline{\sigma}_1, \underline{\sigma}_2, \underline{\tau})$ in the lower facing parallel to their planes (Fig.1) may be assumed to be distributed uniformly over the thickness of the facings. (B) The load carrying capacity of the core in the plane of the sandwich is negligible. The core carries only the shear stresses normal to the middle surface and does not yield or fail due to the shear stresses.

The state of stress in a shell is approximately plane and may be described by the resulting moments, direct forces and shears. However, because of the basic assumption that straight lines normal to the undeformed middle surface remain straight and normal to the deformed middle surface, the transverse shear strains are neglected. The transverse shear forces appearing in the equa-

---

* It was learned at the Symposium that A.Sawszuk and J.Rychlewski had obtained the same yield condition and associated flow law in 1960 in Poland and investigated only the geometry of yield hypersurface. The derivation of Eqs. (6), (7) and (8) in this chapter was therefore a second but independent presentation. However, the main contribution of the author's paper lies in the discovery that the velocity equations for a constituent yield hypersurface are uncoupled from the equilibrium equations and may be reduced to a single partial differential equation in terms of the normal displacement for shallow shells and in the proposed method of obtaining upper and lower bounds on the limit loads by means of discontinuous collapse mechanisms.

tions of equilibrium have the nature of reaction and are not generalized stresses. For general non-symmetric problems, it is necessary to consider the six generalized stresses defined by

$$N_1 = (\underline{\sigma}_1 + \overline{\sigma}_1)J, \quad N_2 = (\underline{\sigma}_2 + \overline{\sigma}_2)J, \quad N_{12} = (\underline{\tau} + \overline{\tau})J$$
$$M_1 = (\underline{\sigma}_1 - \overline{\sigma}_1)HJ, \quad M_2 = (\underline{\sigma}_2 - \overline{\sigma}_2)HJ, \quad M_{12} = (\underline{\tau} - \overline{\tau})HJ \tag{1}$$

where N_1 and N_2 are the direct forces, N_{12} the shear force parallel to the planes of the facings, M_1 and M_2 the bending moments, and M_{12} the twisting moment. The corresponding generalized strain-rates are the extension rates ε_1 and ε_2, the rate of shear ε_{12}, the curvature rates K_1 and K_2, and rate of twist K_{12} of the middle surface. The facings experience the extension rates $\varepsilon_1 \pm HK_1$ and $\varepsilon_2 \pm HK_2$ and the rate of shear $\varepsilon_{12} \pm HK_{12}$. It is convenient to use the dimensionless quantities

$$n_\alpha = \frac{N_\alpha}{N_0}, \quad m_\alpha = \frac{M_\alpha}{M_0}, \quad \kappa_\alpha = \frac{M_0}{N_0} K_\alpha \tag{2}$$

where $N_0 = 2J\sigma_0$ and $M_0 = 2HJ\sigma_0$, σ_0 being the yield stress in simple tension, and where the subscript α may stand for either 1, 2, or 12. The rate of dissipation of mechanical energy per unite area of the middle surface has the form

$$D_i = N_0(n_1\varepsilon_1 + n_{12}\varepsilon_{12} + n_2\varepsilon_2 + m_1\kappa_1 + m_{12}\kappa_{12} + m_2\kappa_2) \tag{3}$$

At a generic point of the shell, the stresses in the facings must satisfy the Mises yield condition

$$\overline{\sigma}_1^2 - \overline{\sigma}_1\overline{\sigma}_2 + \overline{\sigma}_2^2 + 3\overline{\tau}^2 = \sigma_0^2 \tag{4}$$

$$\underline{\sigma}_1^2 \quad \underline{\sigma}_1\underline{\sigma}_2 + \underline{\sigma}_2^2 + 3\underline{\tau}^2 = \sigma_0^2 \tag{5}$$

Elimination of $\overline{\sigma}_1$, $\overline{\sigma}_2$, $\overline{\tau}$, $\underline{\sigma}_1$, $\underline{\sigma}_2$, and $\underline{\tau}$ from eqs.(1) and (4) or (5) furnishes the yield condition of the shell element in terms of the six generalized stresses as follows.

$$F_1 = (n_1 + m_1)^2 - (n_1 + m_1)(n_2 + m_2) + (n_2 + m_2)^2 + 3(n_{12} + m_{12})^2 = 1 \tag{6}$$

$$F_2 = (n_1 - m_1)^2 - (n_1 - m_1)(n_2 - m_2) + (n_2 - m_2)^2 + 3(n_{12} - m_{12})^2 = 1. \tag{7}$$

In a generalized stress space of Cartesian coordinate system (n_1, n_{12}, n_2, m_2, m_{12}, m_2), the proposed yield condition represents a hypersurface consisting of two quadratic hypersurfaces. It is noted that, in a new coordinate system (n_1+m_1, $n_{12} + m_{12}$, $n_2 + m_2$, $n_1 - m_1$, $n_{12} - m_{12}$, $n_2 \quad m_2$), the yield condition exhibits explicitly the character of the Mises yield condition. If a stress point (n_1, n_{12}, n_2, m_1, m_{12}, m_2) in the generalized stress space satisfies $F_1 = 1$ and $F_2 < 1$, the lower facing is at yield point state, whereas if it satisfies $F_2 = 1$ and $F_1 < 1$, the upper facing is at yield point state. In any case the shell element is at yield point state since none of the facings has bending resistance itself. If $F_1 = F_2 = 1$, both of the facings are at yield point state.

The plastic potential flow law states that the strain-rate vector (ε_1, ε_{12}, ε_2, κ_1, κ_{12}, κ_2) is directed along the outward normal to the yield surface. Since the present yield surface is defined by the two functions $F_1 = 1$ and $F_2 = 1$, the normal is not defined uniquely at the intersection of the two constituent hypersurfaces and two parameters will be necessary to follow Koiter's definition [8]. The associated flow law may be given by

$$\varepsilon_1 = \mu\{2(n_1 + m_1) \quad (n_2 + m_2)\} + \nu\{2(n_1 - m_1) - (n_1 - m_1)\}$$

$$\varepsilon_{12} = 6\mu(n_{12} + m_{12}) + 6\nu(n_{12} - m_{12})$$

$$\varepsilon_2 = \mu\{2(n_2 + m_2) \quad (n_1 + m_1)\} + \nu\{2(n_2 \quad m_2) - (n_1 - m_1)\}$$

$$\kappa_1 = \mu\{2(n_1 + m_1) \quad (n_2 + m_2)\} \quad \nu\{2(n_1 - m_1) - (n_2 - m_2)\}$$

$$\kappa_{12} = 6\mu(n_{12} + m_{12}) - 6\nu(n_{12} - m_{12})$$

$$\kappa_2 = \mu\{2(n_2 + m_2) \quad (n_1 + m_1)\} - \nu\{2(n_2 - m_2) - (n_1 - m_1)\} \qquad (8a\text{-}f)$$

where (i) if $F_1 = 1$ and $F_2 < 1$, then $\mu > 0$ and $\nu = 0$
(ii) if $F_1 < 1$ and $F_2 = 1$, then $\mu = 0$ and $\nu > 0$
(iii) if $F_1 = 1$ and $F_2 = 1$, then $\mu > 0$ and $\nu > 0$.

3. APPROACH TO NON-SYMMETRIC PROBLEMS

It seems convenient to introduce here the concept of a "solution surface" in the generalized stress space. In an axisymmetric problem, a stress solution may be regarded as a parametric representation of a space curve lying in a yield hypersurface in terms of an independent variable. In a general non-symmetric

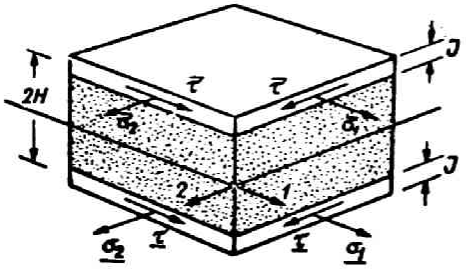

Fig.1 Sandwich shell element

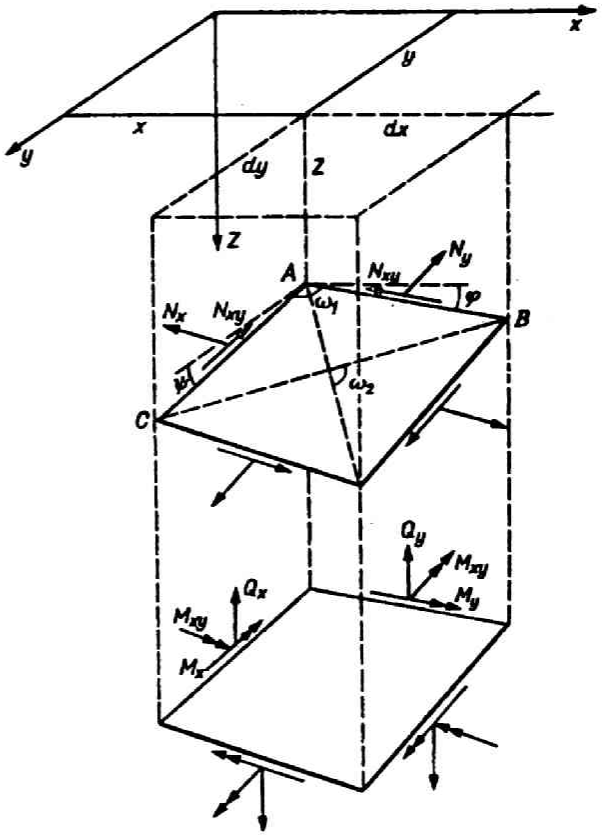

Fig.2 Shallow shell element and stress resultants

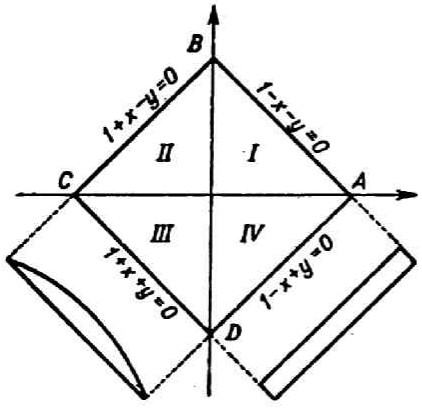

Fig.3 Parabolic cylinder.

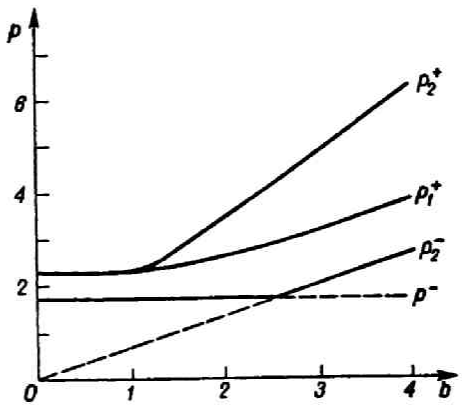

Fig.4 Upper and lower bounds on the load factor.

problem, a stress solution for a finite portion of a plastic region contains two parameters or independent variables. Geometrically the solution may be represented by a surface lying in a yield hypersurface in the six-dimensional stress space. This surface will henceforth be called a "solution surface". Then the general approach to a non-symmetric problem may be stated with this terminology as follows.

Although the present yield condition is piecewise quadratic, it may be shown that the resulting stress and velocity equations are uncoupled for each constituent yield condition. It is noted that if a portion of a solution surface lies entirely either on $F_1 = 1$ or on $F_2 = 1$, then $\nu = 0$ or $\mu = 0$, respectively. Then there are three simple ratios between the generalized strain-rates given in the flow law (8)

$$\frac{\varepsilon_1}{\kappa_1} = \pm 1, \quad \frac{\varepsilon_{12}}{\kappa_{12}} = \pm 1, \quad \frac{\varepsilon_2}{\kappa_2} = \pm 1 \tag{9}$$

where all the plus signs are for the case $F_1 = 1$ and the minus signs for $F_2 = 1$. Hence the velocity fields corresponding to the cases (i) and (ii) are of a fairly restricted nature, whereas in the third case, the corresponding stress fields are of comparatively restricted nature satisfying both of (6) and (7) In any orthogonal curvilinear coordinate system on the middle surface of the shell, all the strain-rates may be expressed linearly in terms of three velocity components and their spatial derivatives just as in the linear theory of thin elastic shells [9]. Hence the three simple ratios (9) provide a system of three linear partial differential equations for the three velocity components. Once the general solution of this system is obtained, the remaining two ratios between the generalized strain-rates may be regarded as two equations for stresses . The yield condition appears then to bring the non-linearity into the system of stress equations. The non-linearity is not essential, however. The quantities μ and ν which may be expressed as (11) and (12) later, in terms of the known generalized strain-rates are now known functions of the coordinates. Hence three equations of (8), e.g. (8d, e and f) become linear equations for the generalized stresses. These three equations of equilibrium form a system of linear algebraic and partial differential equations for the six generalized stresses. However, if a finite portion of the solution surface lies in the intersection of the two constituent hypersurfaces, the velocity and stress equations are coupled and can not, in general, be solved easily. This is one of the difficulties. Even

if the uncoupled velocity equations are relatively simple as will be shown for shallow shells later, one encounters the second difficulty that the shape of the boundary of a plastic region is not known *a priori* and does not coincide, in general, with the boundary of the shell. A way of solving these difficulties is to make use of the upper and lower bound theorems of limit analysis. In the former case it is even difficult to find a kinematically admissible velocity field. A way to overcome such a difficulty is to consider a discontinuous velocity field consisting of several rigid body motions [10]. In the latter case a velocity field satisfying the uncoupled velocity equations and the velocity boundary conditions can be found for an assumed plastic region. The total rate of internal dissipation of energy can then be computed. Substitution of eqs.(8) into (3) furnishes

$$D_i = 2N_0(\mu + \nu). \tag{10}$$

It may be readily verified that μ and ν are expressed in terms of the generalized strain-rates as follows:

$$2\mu = \frac{1}{\sqrt{3}}\left[(\varepsilon_1+\kappa_1)^2+(\varepsilon_1+\kappa_1)(\varepsilon_2+\kappa_2)+(\varepsilon_2+\kappa_2)^2+\left(\frac{\varepsilon_{12}+\kappa_{12}}{2}\right)^2\right]^{\frac{1}{2}}$$

$$2\nu = \frac{1}{\sqrt{3}}\left[(\varepsilon_1-\kappa_1)^2+(\varepsilon_1-\kappa_1)(\varepsilon_2-\kappa_2)+(\varepsilon_2-\kappa_2)^2+\left(\frac{\varepsilon_{12}-\kappa_{12}}{2}\right)^2\right]^{\frac{1}{2}} \tag{11}$$

where μ and ν are both positive for the intersection $F_1 = F_2 = 1$. But the expression may be considerably simplified for a constituent hypersurface $F_1 = 1$ or $F_2 = 1$ because of the simple ratios (9).

$$D_i = \frac{2N_0}{\sqrt{3}}\left[\varepsilon_1^2+\varepsilon_1\varepsilon_2+\varepsilon_2^2+\left(\frac{\varepsilon_{12}}{2}\right)^2\right]^{\frac{1}{2}} = \frac{2N_0}{\sqrt{3}}\left[\kappa_1^2+\kappa_1\kappa_2+\kappa_2^2+\left(\frac{\kappa_{12}}{2}\right)^2\right]^{\frac{1}{2}}. \tag{12}$$

The generalized strain-rates are known from the assumed velocity solution and hence we may integrate the known expression of D_i over the whole plastic region. The kinematically admissible multiplier associated with the assumed velocity field may then be obtained by equating the total rate of internal dissipation to the total rate of dissipation of external energy. In many cases the integrand given by eqs.(11) may be mathematically complicated. Then the difficulty of integration may be avoided by considering again a discontinuous velocity field mentioned above.

4. A CONSISTENT SET OF THE STRAIN-RATE VELOCITY RELATIONS AND EQUATIONS OF EQUILIBRIUM FOR A SHALLOW SHELL

The fundamental equations of conventional bending theories of thin elastic shells in the category of Love's first approximation contain an inconsistency in the sense that the strains do not all vanish for small rigid body rotations of a shell except for axisymmetric problems [11]. The following set of strain-rate velocity relations and equilibrium equations may be applied therefore only for those plastic regions where such effects are negligible. If a velocity field is to contain several rigid portions separated by plastic regions or by discontinuities, then their rigid body rotations must be treated separately from the present strain-rate velocity relations as will be illustrated in the later example.

Figure 2 shows an element of a shallow shell described by the distance $Z = Z(X,Y)$ of its middle surface from the (X,Y)plane. The dimensionless coordinates are defined by

$$x = \frac{X}{L}, \quad y = \frac{Y}{L}, \quad z = \frac{Z}{L},$$

where L is a typical shell length. It is noted that the present rectangular coordinate system does not form an orthogonal net when projected onto the middle surface of the shell. Hence the shell element is skew as shown in Fig.2. However, since it is assumed in the shallow shell theory [12] that

$$z_x^2 << 1, \quad z_x z_y << 1, \quad z_y^2 << 1 \tag{13}$$

where the subscripts x and y denote differentiation with respect to x and y, respectively, the angle between the two sides $\overline{AB}$ and $\overline{AC}$ on the middle surface may be approximated as

$$\sin \omega_1 = \sqrt{(1 \quad \sin \phi \sin \psi)} \cong \sqrt{(1 \quad z_x z_y)} \cong 1$$

and the angle between the two diagonals on the middle surface as

$$\sin \omega_2 = \frac{2\sqrt{(1 - \tan^2\phi - \tan^2\psi)}}{\sqrt{[2 + (\tan \phi + \tan \psi)^2]}\sqrt{[2 + (\tan \psi - \tan \phi)^2]}} \cong 1.$$

Hence even if the yield condition for such a skew element may be actually subjected to certain deformation and modification from eqs.(6) and (7) as a function of x and y, its influence is negligible for a shallow shell. The use of the proposed yield condition and associated flow law for the shallow shell element is therefore consistent with the shallow shell approximation. The subscripts 1, 2, and 12 in the preceding expressions (1) through (12) should now be replaced by x, y, and xy, respectively for use in the following. The six generalized stresses are n_x, n_{xy}, n_y, m_x, m_{xy}, and m_y and the corresponding generalized strain-rates are ε_x, ε_{xy}, ε_y, κ_x, κ_{xy}, and κ_y. Let U and V denote the tangential velocity components in (X,Z)— and (Y,Z)— planes, respectively, and W the velocity component normal to the middle surface. The following reduced velocity components are used in the following:

$$u = \frac{U}{L}, \quad v = \frac{V}{L}, \quad w = \frac{W}{L}.$$

The consistent set [13] of the strain-rate velocity relations and equilibrium equations for the shallow shell under the assumption of (13) and of infinitesimal deformation are given by

$$\varepsilon_x = \frac{\partial u}{\partial x} - z_{xx}w, \quad \varepsilon_{xy} = \frac{\partial u}{\partial y} + \frac{\partial v}{\partial x} - 2z_{xy}w, \quad \varepsilon_y = \frac{\partial v}{\partial y} - z_{yy}w$$

$$\kappa_x = -k\frac{\partial^2 w}{\partial x^2}, \quad \kappa_{xy} = -2k\frac{\partial^2 w}{\partial x \partial y}, \quad \kappa_y = -k\frac{\partial^2 w}{\partial y^2} \tag{14}$$

$$\frac{\partial n_x}{\partial x} + \frac{\partial n_{xy}}{\partial y} + 6kp_x = 0, \quad \frac{\partial n_{xy}}{\partial x} + \frac{\partial n_y}{\partial y} + 6kp_y = 0$$

$$\frac{\partial^2 m_x}{\partial x^2} + 2\frac{\partial^2 m_{xy}}{\partial x \partial y} + \frac{\partial^2 m_y}{\partial y^2} + \frac{1}{k}(z_{xx}n_x + 2z_{xy}n_{xy} + z_{yy}n_y) + 6p_z = 0 \tag{15}$$

where

$$k = \frac{M_0}{N_0 L}, \quad p_x = \frac{P_x L^2}{6M_0}, \quad p_y = \frac{P_y L^2}{6M_0}, \quad p_z = \frac{P_z L^2}{6M_0}$$

5. DIFFERENTIAL EQUATIONS FOR VELOCITY FIELDS AND STRONG DISCONTINUITIES

If a solution surface for a finite plastic region lies entirely on $F_1 = 1$ or $F_2 = 1$, then the three simple ratios (9) hold for that region and may be reduced, for the present shallow shell, to the following system of differential equations

$$\frac{\partial u}{\partial x} - z_{xx}w \pm k\frac{\partial^2 w}{\partial x^2} = 0$$

$$\frac{\partial v}{\partial y} - z_{yy}w \pm k\frac{\partial^2 w}{\partial y^2} = 0$$

$$\frac{\partial u}{\partial y} + \frac{\partial v}{\partial x} \quad 2z_{xy}w \pm 2k\frac{\partial^2 w}{\partial x \partial y} = 0 \qquad (16)$$

where the plus sign corresponds to the case $F_1 = 1$, whereas the minus sign to $F_2 = 1$. The velocity components u and v may readily be eliminated from eqs.(16) and the resulting single differential equation for w becomes

$$\frac{\partial^2}{\partial x^2}(z_{yy}w) \quad 2\frac{\partial^2}{\partial x \partial y}(z_{xy}w) + \frac{\partial^2}{\partial y^2}(z_{xx}w) = 0. \qquad (17)$$

Depending upon the form of $z = z(x,y)$, eq.(17) may be elliptic, parabolic, or hyperbolic. If z is quadratic in x and y, eq.(17) contains constant coefficients only and may readily be reduced to the standard forms. General solutions can be obtained for various coordinate systems but the second difficulty arises as has been mantioned in Sec.3 and it is necessary to utilize the upper bound theorem of limit analysis, assuming a suitable boundary shape for which the general solution is readily obtained. If the upper bound theorem must be used anyway, a simpler application may be desirable. It is shown in the later example that consideration of a discontinuous velocity field simplifies the computation of the rate of dissipation of internal energy for a polygonal shell and hence enables one to obtain readily an upper bound on the collapse load factor. It may be expected that a better bound is obtained from an assumed velocity field consisting of rigid regions and finite plastic regions governed by eqs.(16) and (17), but this problem will be left for further study.

It is convenient to consider a local coordinate system (ξ,η) at a generic point P on a stationary strong discontinuity D [14], P being the origin of this system and the ξ axis normal to D at P on the middle surface. The continuity of w itself must be postulated since the effects of the transverse shears have been neglected . Then just as in the plate discontinuity [14], $\partial w/\partial \xi$ may be discontinuous across D. If $\bar{u}$ and $\bar{v}$ denote the velocity components in ξ and η directions, $\bar{u}$ and $\bar{v}$ themselves may also be discontinuous across D. Let the amount of jumps in $\bar{u}$, $\bar{v}$ and $\partial w/\partial \xi$ be denoted by Δu, Δv and $\Delta(\partial w/\partial \xi)$, respectively.

Then the plastic flow of a particle on D may be described by

$$\varepsilon_\xi : \varepsilon_{\xi\eta} : \varepsilon_\eta : \kappa_\xi : \kappa_{\xi\eta} : \kappa_\eta = \Delta u : \Delta v : 0 : -\kappa\Delta\left(\frac{\partial w}{\partial \xi}\right) : 0 : 0.$$

Then from eqs.(10) and (11), the rate of internal dissipation per unit length of D may be found as follows:

$$D_i = \frac{N_0 L}{\sqrt{3}} \left\{ \left[\left\{ \Delta u - k\Delta\left(\frac{\partial w}{\partial \xi}\right) \right\}^2 + \left(\frac{\Delta v}{2}\right)^2 \right]^{\frac{1}{2}} + \left[\left\{ \Delta u + k\Delta\left(\frac{\partial w}{\partial \xi}\right) \right\}^2 - \left(\frac{\Delta v}{2}\right)^2 \right]^{\frac{1}{2}} \right\}. \quad (18)$$

Since Δu, Δv and $\Delta(\partial w/\partial \xi)$ vary with respect to η along D in general, the stress points corresponding to the strong discontinuity lie almost always in the intersection of the two hypersurfaces.

6. HYPERBOLIC PARABOLOID WITH AN ELLIPTIC BOUNDARY UNDER UNIFORM PRESSURE P

The middle surface of the hyperbolic paraboloid is defined by

$$z = \frac{x^2}{2a} - \frac{y^2}{2b}, \quad x^2 + \frac{a}{b} y^2 \leq 1, \quad a^2, b^2 >> 1.$$

The shell is subjected to uniform pressure $P_z = P$. The dimensionless pressure is defined by $p = PL^2/6M_0$. It is assumed for the sake of simplicity that the shell is roller-supported normal to the shell surface along the elliptic boundary. The velocity boundary condition is therefore $w = 0$ at $x^2 + ay^2/b = 1$ only. It is assumed that the solution surface for the shell lies entirely in $F_1 = 1$. Equation (17) becomes

$$\frac{1}{a} \frac{\partial^2 w}{\partial y^2} - \frac{1}{b} \frac{\partial^2 w}{\partial x^2} = 0.$$

The differential equation and the boundary condition may be satisfied by

$$w = \delta\{1 - x^2 - \frac{a}{b} y^2\}.$$

The corresponding solutions for u and v may readily be obtained from eqs.(16) Substitution of

$$w_{xx} = -2\delta, \qquad w_{xy} = 0, \qquad w_{yy} = -\frac{2a}{b}\delta$$

into eq.(12) provides

$$D_i = \frac{4kN_0\delta}{\sqrt{3}}\sqrt{\left(1 + \frac{a}{b} + \frac{a^2}{b^2}\right)} \quad \text{(constant everywhere)}.$$

An upper bound on the collapse load can be found by equating the total rate of internal dissipation to the rate of external energy dissipation,

$$p^+ = \frac{4}{3\sqrt{3}}\sqrt{\left(1 + \frac{a}{b} + \frac{a^2}{b^2}\right)}$$

A lower bound may be obtained by considering a statically admissible stress field for an elliptic plate. If it is assumed that

$$n_x = n_{xy} = n_y = 0,\ m_x = m_y = \frac{3pb}{a+b}\{1 \quad x^2 \quad \frac{a}{b}y^2\},\quad m_{xy} = 0, \tag{19}$$

the equations of equilibrium and the stress boundary conditions are satisfied. Substitution of eqs.(19) into the yield conditions (6) and (7) leads to

$$\frac{3pb}{a+b}\{1 - x^2 - \frac{a}{b}y^2\} \lesssim 1.$$

The maximum value of the left-hand side occurs at the origin. Hence a lower bound is given by

$$p^- = \frac{1}{3}\left(1 + \frac{a}{b}\right).$$

7 PARABOLIC CYLINDER WITH A SQUARE BOUNDARY UNDER UNIFORM PRESSURE

Let $2L$ be the length of a diagonal of the boundary square.

The middle surface of the parabolic cylinder is described by

$$z = \frac{c}{2}(x \quad y)^2, \qquad 1 \quad x - y \geq 0, \qquad 1 + x \quad y \geq 0,$$
$$1 + x + y \geq 0, \qquad 1 \quad x + y \geq 0.$$

This choice of the rectangular coordinate system will be convenient in the later discussion of the strong discontinuity in the velocity field. Since it has been assumed that $z_x^2 \ll 1$, $z_x z_y \ll 1$, and $z_y^2 \ll 1$, the rise of the shell is within the limit $c^2 \ll 1$. The shell is assumed to be simply supported along the four edges $\widehat{AB}(1 \quad x - y = 0)$, $\overline{BC}(1 \quad x - y = 0)$, $\widehat{CD}(1 + x + y = 0)$, and

$\overline{DA}(1 - x + y = 0)$, and is subjected to uniform pressure P. (See Fig.3). The dimensionless pressure is defined by $p = PL^2/6M_0$. For a square plate, a good upper bound has been obtained by considering a velocity field in which the plate deforms into a square pyramid [10]. It is quite natural therefore to consider a similar field for w but with appropriate associated fields of u and v. It is assumed that the four curved triangular portions ΔOAB, ΔOBC, ΔOCD, and ΔODA perform rigid body rotations $\sqrt{2}\theta$ about axes parallel to the straight lines $\overline{AB}$, $\overline{BC}$, $\overline{CD}$, and $\overline{DA}$, respectively and rigid body translations $\sqrt{2}\delta$ outwardly normal to $\overline{AB}$, $\overline{BC}$, $\overline{CD}$, and $\overline{DA}$, respectively and that the same strong discontinuity appears along $\widehat{OA}$, $\widehat{OB}$, $\widehat{OC}$, and $\widehat{OD}$. Then the velocity field satisfying $w = 0$ and $|u| = |v|$ along the four edges may be written as

Region I, $\Delta OAB : w = \theta(1 - x - y),\ u = v = \delta - \frac{1}{2}c\theta\{1 - (x - y)^2\}$

II, $\Delta OBC : w = \theta(1 + x - y),\ u = -v = -\delta + \frac{1}{2}c\theta\{1 - (x - y)^2\}$

III, $\Delta OCD : w = \theta(1 + x + y),\ u = v = -\delta + \frac{1}{2}c\theta\{1 - (x - y)^2\}$

IV, $\Delta ODA : w = \theta(1 - x + y),\ u = -v = \delta - \frac{1}{2}c\theta\{1 - (x - y)^2\}.$ (20)

Because of the shallowness $c^2 \ll 1$, the projection of the (x, y) coordinate system upon the middle surface may be taken as the local coordinate system for the discontinuity within the present approximation. The amounts of jumps in u, v and $\partial w/\partial x$ across the discontinuity $\widehat{OB}$ are

$$\Delta u = 2\delta - c\theta(1 - y^2), \quad \Delta v = 0, \quad \Delta\left(\frac{\partial w}{\partial x}\right) = -2\theta.$$

Since $\Delta v = 0$, the plastic flow of a particle on $\widehat{OB}$ may be described by

$$\varepsilon_x : \varepsilon_{xy} : \varepsilon_y : \kappa_x : \kappa_{xy} : \kappa_y = 2\delta \quad c\theta(1 - y^2) : 0 ; 0 : 2k\theta : 0 : 0.$$

The rate of internal dissipation of energy per unit length of OB may be evaluated by eq.(18) and is reduced to

$$D_{\widehat{OB}} = \frac{N_0 L}{\sqrt{3}}\{|2\delta - c\theta(1 - y^2) + 2k\theta| + |2\delta - c\theta(1 \quad y^2) - 2k\theta|\} \qquad (21)$$

For the sake of simplicity, the following two cases will be considered.

Case 1. If $\Delta u = 0$ at $y = 0$, i.e. $2\delta = c\theta$, then the total dissipation rate in $\widehat{OB}$ may be evaluated in two parts. If $2k \geq cy^2$ everywhere for $0 \leq y \leq 1$,

i.e. $1 \geq c/2k$, then eq.(21) is reduced to

$$\overline{D}_{\widehat{OB}} = \frac{4}{\sqrt{3}} kN_0L^2\theta = \frac{4}{\sqrt{3}} M_0L\theta.$$

If $c/2k \geq 1$, then there exists a value of y in $0 \leq y \leq 1$ such that $cy^2 = 2k$. Let $c/2k = b$. Physically b represents the ratio of the rise to the thickness of the shell.

$$\overline{D}_{\widehat{OB}} = \frac{4}{\sqrt{3}} kN_0L^2\theta\{\int_0^{\frac{1}{\sqrt{b}}} dy + b\int_{\frac{1}{\sqrt{b}}}^{1} y^2dy\} = \frac{4}{3\sqrt{3}} M_0L\theta \left(b + \frac{2}{\sqrt{b}}\right)$$

The total rate of internal dissipation through the four strong discontinuities is $4(\overline{D}_{\widehat{OB}})$ The external energy rate is given by

$$\overline{D}_e = \int_A PW dA = 4M_0L\theta p.$$

Therefore an upper bound on p is given by

$$p_1^+ = \frac{4}{\sqrt{3}} \text{ for } b \leq 1, \; p_1^+ = \frac{4}{3\sqrt{3}} \left(b + \frac{2}{\sqrt{b}}\right) \text{ for } b \geq 1.$$

The value of p_1^+ is plotted in Fig.4 with respect to b. When $c = 0$ and hence $b = 0$, the value of p_1^+ is reduced to the upper bound for a square plate [10]. Evidently the known lower bound for a square plate gives a lower bound for the present shell. Hence

$$p_1^- = \frac{2}{q}(6 + \sqrt{3}).$$

Case 2. If the outward sliding of the four curved triangular portions is restrained and hence $\delta = 0$, then $\Delta u = 0$ at $y = 1$. If $2k \geq a(1 - y^2)$ for $0 \leq y \leq 1$, i.e. $1 \geq b$, then the same upper bound as for the case 1 is obtained. If $b \geq 1$, there exists a value of y in $0 \leq y \leq 1$ such that $1 - y^2 = 1/b$, i.e. $y = \sqrt{(1 - 1/b)}$ Then it may readily be found that

$$D_{\widehat{OB}} = \frac{4}{\sqrt{3}} N_0 k L^2 \theta \{ \int_0^{\sqrt{1 - \frac{1}{b}}} b(1 - y^2) dy - \int_{\sqrt{1 - \frac{1}{b}}}^{1} dy \}$$

$$= \frac{4}{\sqrt{3}} \{1 + \frac{2(b - 1)}{3} \sqrt{\left(\frac{b - 1}{b}\right)}\} M_0 L \theta .$$

Therefore an upper bound on p for this case is given by

$$p_2^+ = \frac{4}{\sqrt{3}} \{1 + \frac{2(b \quad 1)}{3} \sqrt{\left(\frac{b - 1}{b}\right)}\} \text{ for } b \geq 1.$$

It is noted that a lower bound on p may be obtained from the membrane solution for this case. The maximum lower bound based upon the membrane solution is obtained when

$$n_x = n_y = -\frac{1}{2}, \quad n_{xy} = \frac{1}{2}, \quad m_x = m_{xy} = m_y = 0.$$

This solution satisfies the yield conditions $F_1 = 1$ and $F_2 = 1$ and furnishes

$$p_2^- = \frac{2c}{6k} = \frac{2}{3} b.$$

The lower bound for the square plate is still a lower bound for this case, again. The values of p_2^+ and p_2^- are plotted in Fig.4 to compare with p_1^+

CONCLUDING REMARKS

The exact yield condition for a uniform shell element composed of a perfectly plastic material obeying the Tresca or Mises yield condition is quite complicated and its application to practical non-symmetric problems is very difficult. Therefore the first step of studying non-symmetric problems is to find a practically workable yield condition. The sandwich approximation proposed in the present paper may be of practical use in the following sense. First, it consists only of two hypersurfaces. Secondly, the velocity and stress equations are uncoupled for the constituent hypersurfaces and kinematically admissible velocity fields may be found comparatively easily for practical problems. The yield condition has been applied to shallow shells and a single partial differential equation for the normal velocity component has been obtained. The differential equation becomes simple for quadratic surfaces. As an example, a

kinematically admissible velocity field has been proposed for a hyperbolic paraboloid with an elliptic boundary. Thirdly, consideration of strong discontinuities in a velocity field based upon the present yield condition simplifies the computation of upper bounds on a collapse load factor, especially for a shell with a polygonal boundary. This has been illustrated for a parabolic cylinder.

REFERENCES

1. M.N.Fialkow, Limit analysis of simply supported circular shell roof, *Proc. ASCE, Eng. Mech. Div.*, Paper 1706, 1958.
2. A.Sawczuk, On experimental foundations of the limit analysis theory of reinforeced concrete shells, *Proc. of Symp. Shell Research, IASS*, pp.217-231.
3. E.T.Onat and W.Prager, Limit analysis of shells of revolution, *Koninkl. Nederl. Akademie van Wetenschappen*, B.57, No.5, 1954, pp.534-548.
4. See, for instance, E.T.Onat, Plastic analysis of shallow conical shells, *Proc. ASCE, Eng. Mech. Div.*, Dec. 1960, pp.1-12.
5. See, for instance, P.G.Hodge, Jr., Yield conditions for rotationally symmetric shells under axisymmetric loading, *J Appl. Mech.*, 27, 1960, pp.323-330.
6. T.Nakamura, *Plastic analysis of Shells of Revolution under Axisymmetric loads*, Dissertation, Stanford University, 1961
7. P.G.Hodge, Jr., The Mises yield condition for rotationally symmetric shells, *Quart. Appl. Math.*, 18, No.4, 1961, pp.305-311.
8. W.T.Koiter, Stress-strain relations, uniqueness and variational theorems for elastic-plastic materials with a singular yield surface, *Quart. Appl. Math.*, 11, 1953, pp.350-354.
9. See, for instance, W.Flügge, *Stresses in Shells*, Springer-Verlag, 1960.
10. See, for instance, P.G.Hodge, Jr., *Plastic Analysis of Structures*, McGraw-Hill, 1959.
11. J.L.Sanders, Jr., *An Improved First Approximation Theory for Thin Shells*, NASA. Tech. Rep. R-24, 1959.
12. D.A.Conrad, *Singular Solutions in the Theory of Shallow Shells*, Dissertation, Stanford University, 1957.
    Kh. M.Mushtari, K.Z.Galimov, *Non-linear Theory of Thin Elastic Shells*, The Israel Program for Scientific Translations, 1961.
13. P.G.Hodge, Jr. and C.Lakshmikantham, *Limit Analysis of Shallow Shells of Revolution*, DOMIIT, Rep.1-16, Illinois Inst. Tech., 1962.
14. W.Prager, Discontinuous fields of plastic stress and flow, *Proc. Second Natl. Congr. Appl. Mech.*, Ann Arbor, Mich., 1954, pp.21-32.

APPENDIX

The proposed method has been applied to shallow parabolic cylindrical shells with various rectangular plans by Y.Yokoo, T.Matsui and the present author.* The following results extracted from their paper will demonstrate the use fulness of the method and therefore will be included here as an appendix.

Upper bounds on the collapse loads

A natural attempt in finding a kinematically admissible velocity field is to consider for w a roof-shaped collapse mode similar to the one for a rectangular plate, together with appropriate associated fields of u and v. This type of collapse will be called a total collapse mode. The corresponding upper bound on the collapse load increases rapidly as the rise of the shell is increased as will be shown later. Therefore in order to obtain better bounds, it is necessary to take into account the characteristics of edge disturbances in the bending theory of shells. The partial collapse mode shown in Fig. 3 is one of such possible modes.

(a) Total collapse mode A ($\cot\alpha \leq \lambda$)

It is assumed that the strong discontinuities appear as indicated by the wavy lines in Fig. 1. The trapezoidal portions I and I′ perform rigid dody rotations $\theta\cot\alpha$ about the axes $\overline{AB}$ and $\overline{CD}$, respectively. The triangular portions II and II′ perform rigid body rotations θ about $\overline{BC}$ and $\overline{AD}$, respectively. Rigid body translations have been assumed to be prevented by strong corner reinforcements. Then the velocity field may be described by

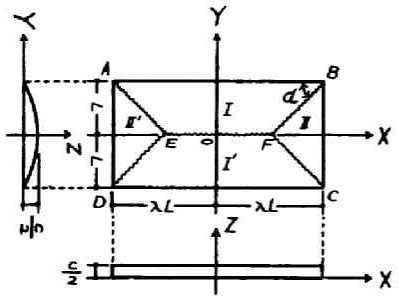

Fig. 1 Total collapse mode A.

Portion I : $u=0,\ v=c\theta\cot\alpha(1-y^2)/2,$
$w=\theta\cot\alpha(1-y)$

II : $u=c\theta(1-y^2)/2,\ v=0,$
$w=\theta(\lambda-x)$

The corresponding jump quantities may be obtained as

Along $\widehat{BF}$: $\Delta\hat{u}=-c\theta\,\mathrm{cosec}\,\alpha(1-y^2)/2,$
$\Delta\hat{v}=0,\ \Delta\left(\frac{\partial w}{\partial\xi}\right)=\theta\,\mathrm{cosec}\,\alpha$

Along $\widehat{EF}$: $\Delta\hat{u}=-c\theta\cot\alpha,$
$\Delta\hat{v}=0,\ \Delta\left(\frac{\partial w}{\partial\xi}\right)=2\theta\cot\alpha$

The rates of internal dissipation of energy per unit length of BF and EF can be evaluated by Eq. (9) and are reduced to

$$D_{\widehat{BF}}=\frac{N_0L\,\mathrm{cosec}\,\alpha}{\sqrt{3}}\left\{\left|\frac{c\theta}{2}(1-y^2)-k\theta\right|-\left|\frac{c\theta}{2}(1-y^2)-k\theta\right|\right\}$$

$$D_{\widehat{EF}}=\frac{2N_0L\cot\alpha}{\sqrt{3}}\left\{\left|\frac{c\theta}{2}-k\theta\right|+\left|\frac{c\theta}{2}+k\theta\right|\right\}$$

The integration of the energy dissipation along the strong discontinuities depend upon the parameter $b=c/2k$ which is physically the ratio of the rise to the thickness of the shell.

(i) $b\leq 1$. $D_{\widehat{BF}}=2\,\mathrm{cosec}^2\alpha\,M_0L\theta/\sqrt{3}$, $\quad D_{\overline{EF}}=8\cot\alpha(\lambda-\cot\alpha)M_0L\theta/\sqrt{3}$

(ii) $b\geq 1$: $D_{\widehat{BF}}=\frac{2\,\mathrm{cosec}^2\alpha}{3\sqrt{3}}\left\{3+2(b-1)\sqrt{\frac{b-1}{b}}\right\}M_0L\theta$

$D_{\overline{EF}}=8b\cot\alpha(\lambda-\cot\alpha)M_0L\theta/\sqrt{3}$

The external energy rate is given by

$$D_e=\int_A PW\,dA=4\cot\alpha(3\lambda-\cot\alpha)pM_0L\theta$$

where the dimensionless pressure p is given by $p=PL^2/6M_0$. Therefore upper bounds on the col-

---

* Yoshitsura Yokoo, Tsuneyoshi Nakamura and Tetsuya Matsui, "Limit Analysis of Shallow Parabolic Cylindrical Shells," Trans. A.I.J. No.106, Dec.1964,pp10-19.

lapse load p_c are given by

(i) $b\leq 1$: $$p^+=\frac{2}{\sqrt{3}}\frac{1+\lambda\cot\alpha}{\cot\alpha(3\lambda-\cot\alpha)} \quad \cdots\cdots (10\,a)$$

(ii) $b\geq 1$: $$p^+=\frac{2}{3\sqrt{3}}\frac{\{3+2(b-1)\sqrt{(b-1)/b}\}\operatorname{cosec}^2\alpha+3b\cot\alpha(\lambda-\cot\alpha)}{\cot\alpha(3\lambda-\cot\alpha)} \quad \cdots\cdots (10\,b)$$

The expression (10 a) coincides with the upper bound on the collapse load for the corresponding rectangular plate.

(b) Total collapse mode **B** ($\cot\alpha\geq\lambda$)

A similar computation may be carried out for this case. It may readily be shown that the expression of the energy dissipation for the case $b\leq 1$ is similar to the previous case for $b\leq 1$. The discontinuity $\widehat{EF}$ is parabolic for this case and the corresponding $\Delta\hat{a}$ is no longer constant. Let $\zeta=\lambda\tan\alpha$ and $\zeta'=1-\zeta$. Then the rate of internal dissipation depends upon ζ' and $\sqrt{(b-1)/b}$ as follows for $b\geq 1$.

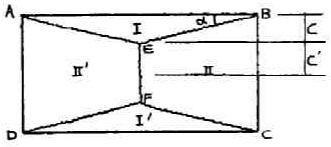

Fig. 2 Total collapse mode. **B**

(i) $\zeta'\geq\sqrt{\frac{b-1}{b}}$: $$p^+=\frac{2}{3\sqrt{3}}\frac{\{3+2(b-1)\sqrt{(b-1)/b}\}+3\lambda^2/\zeta}{\lambda^2(3-\zeta)} \quad \cdots\cdots (11\,a)$$

(ii) $\zeta'\leq\sqrt{\frac{b-1}{b}}$: $$p^+=\frac{2}{3\sqrt{3}}\frac{\{3+2(b-1)\sqrt{(b-1)/b}\}(\zeta^2+\lambda^2)-b\lambda^2\zeta'(3-\zeta')}{\lambda^2(3-\zeta)\zeta^2} \quad \cdots\cdots (11\,b)$$

The parameter α is determined so as to minimize p^+. It has been observed that, for some particular values of λ, Eq. (10 b) furnishes smaller upper bounds than Eqs. (11) for shells with smaller rise and that Eq. (11 b) provides smaller upper bounds than Eq. (10 b) for shells with higher rise.

(c) Partial collapse mode **C**

In view of the edge disturbances in the bending theory, the partial collapse mode shown in Fig. 3 may be expected to appear for shells with higher rise. Plastic flow is assumed to occur locally only in a narrow band of width $2a$ near a generator edge. The trapezoidal parts I and I′ perform rigid body rotations θ about the axes $\overline{AB}$ and $\overline{CD}$, respectively and the triangular parts II and II′, rotate θ about the axes $\overline{BC}$ and $\overline{AD}$, respectively. This mode is similar to mode A with $\alpha=45°$. This choice of α is merely for the sake of simplicity. Some other value of α may furnish somewhat better upper bound. The corresponding energy dissipation can be calculated in a similar fashion to the case (a) except along the strong discontinuity $\overline{CD}$. The results are as follows :

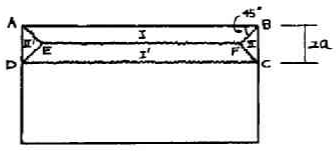

Fig. 3 Partial collapse mode **C.**

(i) $a\leq 1/\sqrt{b}$: $$p^+=\frac{3\lambda+2a}{\sqrt{3}a^2(3\lambda-a)} \quad \cdots\cdots (12\,a)$$

(ii) $a\geq 1/\sqrt{b}$: $$p^+=\frac{\lambda+4a+2a^2b(\lambda-a)+(8/3)(a^2b-1)\sqrt{a^2-1/b}}{\sqrt{3}a^2(3\lambda-a)} \quad \cdots\cdots (12\,b)$$

Lower bounds

The equations of equilibrium for the shallow parabolic cylindrical shell may be written in the following form.

$$\frac{\partial n_x}{\partial x}+\frac{\partial n_{xy}}{\partial y}=0, \qquad \frac{\partial n_{xy}}{\partial x}+\frac{\partial n_y}{\partial y}=0$$

$$\frac{\partial^2 m_x}{\partial x^2}+2\frac{\partial^2 m_{xy}}{\partial x\partial y}+\frac{\partial^2 m_y}{\partial y^2}+\left(\frac{c}{k}\right)n_y+6p=0 \quad \cdots\cdots (13)$$

In view of the membrane solution and the lower bound solution for the corresponding plate [6], it seems appropriate to consider a stress field given in the following form.

$$n_x=n_{xy}=0, \qquad n_y=-n$$

$$m_x=C_1(\lambda^2-x^2), \qquad m_y=C_2(1-y^2), \qquad m_{xy}=-(3p-bn-C_1-C_2)xy$$

$$1\geq C_1,\ C_2,\ n\geq 0 \quad \cdots\cdots (14)$$

It may readily be verified that this set of stresses satisfy Eqs. (13) and the boundary conditions. The coefficients C_1 and C_2 and the direct stress n are determined so as to furnish the largest among all the values of p under which the stress field does not violate the yield conditions (3). By substituting the stresses into the yield functions, the following inequalities are obtained for C_1, C_2 and n.

$$C_1(\lambda^2-x^2)^2-C_1(\lambda^2-x^2)\{-n+C_2(1-y^2)\}+\{-n+C_2(1-y^2)\}^2+3(3p-bn-C_1-C_2)^2x^2y^2\leq 1$$

$$C_1(\lambda^2-x^2)^2-C_1(\lambda^2-x^2)\{n+C_2(1-y^2)\}+\{n+C_2(1-y^2)\}^2+3(3p-bn-C_1-C_2)^2x^2y^2\leq 1 \quad (15a,b)$$

Considered as functions of x^2 for any fixed y, the left hand sides of (15a,b) are both parabolas opening upward. Therefore the left hand sides take on the maximum values at $x^2=0$ or $x^2=\lambda^2$. Similarly for any fixed x the maximum values are at $y^2=0$ or $y^2=1$. Therefore it is sufficient to consider the points (0,0), (0, ± 1), ($\pm\lambda$, 0) and ($\pm\lambda$, ± 1). After some manipulation, it can readily be found that a good lower bound under the above assumption is given by

$$p^-=\frac{1}{3}\left\{n(b-1)+1+\frac{\sqrt{1-n^2}}{\sqrt{3}\lambda}+\frac{-n+\sqrt{4-3n^2}}{2\lambda^2}\right\} \qquad (16)$$

when the upper sheet is at yield point state at ($\pm\lambda$, 0) and ($\pm\lambda$, ± 1) and the lower sheet yielding at (0,0) and ($\pm\lambda$, ± 1); i.e. when

$$C_1=\frac{-n+\sqrt{4-3n^2}}{2\lambda^2}, \qquad C_2=1-n$$

The direct stress n is to be so determined as to maximize p^- in the range $0\leq n\leq 1$. It can easily be seen that the case $n=0$ gives a lower bound for the corresponding rectangular plate, whereas the case $n=1$ for the corresponding membrane [4].

Numerical results and discussion

The upper and lower bounds on the collapse loads have been computed for the cases $\lambda=1$ and $\lambda=2$. The results are shown in Table 1 and 2 and plotted in Fig. 4 and 5. Since $b=c/2k$, c is proportional to b for a constant k. For instance, if $2H/L=1/100$ and $k=1/200$, then $b=100c$. If c varies in

Table 1 Collapse loads for the case $\lambda=1$

Mode	A	B						C							
b	1	2	3	4	5	6	7	8	9	10	12	14	16	18	20
P^+ (α or a)	1.155 (45.0°)	1.648 (35.4°)	2.270 (29.7°)	2.874 (25.6°)	3.574 (22.7°)	4.224 (20.3°)	4.873 (18.9°)	5.490 (0.50)	5.997 (0.50)	6.512 (0.50)	7.554 (0.50)	8.591 (0.47)	9.615 (0.45)	10.628 (0.43)	11.632 (0.42)
P^- (n)	0.859 (0)	0.889 (0.4)	1.089 (0.8)	1.333 (1.0)	1.667 (1.0)	2.000 (1.0)	2.333 (1.0)	2.667 (1.0)	3.000 (1.0)	3.333 (1.0)	4.000 (1.0)	4.667 (1.0)	5.333 (1.0)	6.000 (1.0)	6.667 (1.0)
P^+/P^-	1.34	1.85	2.08	2.16	2.14	2.11	2.09	2.06	2.00	1.95	1.89	1.84	1.80	1.77	1.74

Table 2 Collapse loads for the case $\lambda=2$

Mode	A	B													
b	1	2	3	4	5	6	7	8	9	10	12	14	16	18	20
P^+ (α or a)	0.680 (36.9°)	1.062 (27.3°)	1.500 (22.7°)	1.950 (19.7°)	2.402 (17.5°)	2.853 (15.8°)	3.304 (14.5°)	3.764 (13.4°)	4.210 (12.4°)	4.662 (11.4°)	5.558 (10.4°)	6.471 (9.7°)	7.375 (8.8°)	8.279 (8.3°)	9.186 (7.7°)
P^- (n)	0.513 (0)	0.690 (0.9)	1.000 (1.0)	1.333 (1.0)	1.667 (1.0)	2.000 (1.0)	2.333 (1.0)	2.667 (1.0)	3.000 (1.0)	3.333 (1.0)	4.000 (1.0)	4.667 (1.0)	5.333 (1.0)	6.000 (1.0)	6.667 (1.0)
P^+/P^-	1.33	1.54	1.50	1.46	1.44	1.43	1.42	1.41	1.40	1.40	1.39	1.39	1.38	1.38	1.38

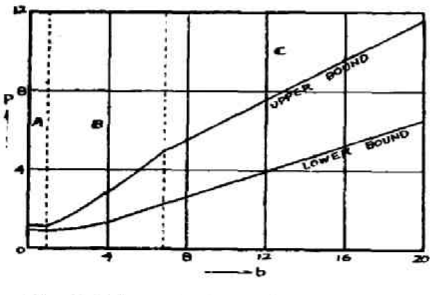

Fig. 4 Collapse loads for the case $\lambda=1$.

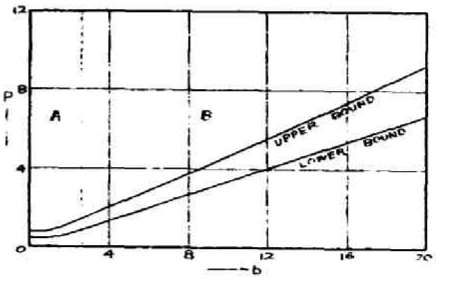

Fig. 5 Collapse loads for the case $\lambda=2$.

the range $0 \leq c \leq 0.2$, then $0 \leq b \leq 20$.

It is observed that for shells with $b \geq 1$, the total collapse mode **A** furnishes better upper bounds for both of the cases $\lambda=1$ and $\lambda=2$. This appears to indicate that the collapse mode of extremely shallow shells will not be very much different from the mode for the corresponding plates.

In the case $\lambda=1$, the total collapse mode **B** results in better upper bounds for shells with intermediate values of b and the corresponding angle α tends to decrease. However, for larger values of b the partial collapse mode **C** provides better upper bounds than any other modes. The width of the corresponding plastic region tends to decrease as b is increased.

In the case $\lambda=2$, the total collapse mode **A** results in better bounds even for $b=2$. But for larger values of b, the total collapse mode **B** provides better bounds than the partial collapse mode **C** in the range of b considered. The corresponding value of α decreases as b is increased and the discontinuities originating from the corners tend to approach the generator edges.

CHAPTER 12

APPLICATIONS OF THE PROPOSED YIELD CONDITIONS TO FINITE-DEFLECTION ANALYSIS OF RIGID-PLASTIC SHELLS

1. INTRODUCTION

While the so-called $P\Delta$-effect upon the load-carrying behaviors of framed structures has been investigated in considerable detail during the last five years as has been described in chapter 3, the effect of geometrical nonlinearities on the carrying capacities of rigid-plastic shells has not been investigated analytically except several papers [1]. A number of useful finite element procedures have been proposed for materially and geometrically nonlinear problems during the last few years [2] Analytical investigations for the combined nonlinear problems of shells appear to have been restricted only to circular cylindrical and spherical shells[1,3]. Duszek [1] has shown that, since nonlinear displacement equations for H_θ^- are uncoupled from the equilibrium equations for shallow spherical shells and since $\dot{\kappa}_\varphi$ leads to a linear equation in terms of w only, an elementary solution can be obtained.

It is shown in this chapter that the advantage of uncoupled equations for velocity fields derived in chapters 10 and 11 is still retained for geometrically nonlinear problems of rigid-plastic shells. Although magnitudes of plastic strains may amount to the order of 10^2, it is assumed that a small strain theory for shells such as Sanders' theory [4] is still applicable and that rotations are moderately small [4] The same notation as in chapters 10 and 11 are used here for shells of revolution and nonsymmetric shells, respectively. The general solutions are derived also for conical shells. Finally, it is shown that a single nonlinear differential equation can be derived also for nonsymmetric shallow sandwich shells in a similar manner to that in chapter 11.

2. KINEMATIC RELATIONS AND EQUATIONS OF EQUILIBRIUM FOR SHELLS OF REVOLUTION

The kinematic relations proposed by Sanders [4] in tensor notation may be reduced for shells of revolution to

$$\left.\begin{aligned} \varepsilon_\theta &= \frac{v\cot\varphi - w}{r_2} & \varepsilon_\varphi &= \frac{v' - w}{r_1} + \frac{1}{2}\rho^2 \\ \kappa_\theta &= -\frac{k\cot\varphi}{r_2}\rho & \kappa_\varphi &= -\frac{k}{r_1}\rho' \end{aligned}\right\} \quad (1a\sim e)$$

$$\rho = \frac{v + w'}{r_1} \qquad \Big)$$

In order to derive the consistent set of equations of equilibrium, the principle of virtual work is utilized.

$$-\int_0^{2\pi}\int^{\varphi}\{n_\theta \frac{\delta v \cot\varphi - \delta w}{r_2} + n_\varphi \left(\frac{\delta v' - \delta w}{r_1} + \rho\frac{\delta v + \delta w'}{r_1}\right)$$

$$+ m_\theta \left(-\frac{k\cot\varphi}{r_2}\right)\delta\rho + m_\varphi \left(-\frac{k}{r_1}\right)\delta\rho'$$

$$+ q_\varphi \left(\frac{\delta v + \delta w'}{r_1} - \delta\rho\right)\} r_1 r d\theta d\varphi$$

$$+\int_0^{2\pi}\int^{\varphi}(p_\varphi \delta v + p_z \delta w)\, r_1 r d\theta d\varphi = 0 \qquad (2)$$

After integration by parts, Eq.(2) may be reduced to

$$\int_0^{2\pi}\int^{\varphi}[\{(rn_\varphi)' - (r_1 n_\theta \cos\varphi \quad q_\varphi r - n_\varphi r\rho + p_\varphi r r_1\}\,\delta v$$

$$+ \{(rq_\varphi)' + (r_1 n_\theta \sin\varphi) + rn_\varphi + (n_\varphi r\rho)' + p_z r r_1\}\,\delta w$$

$$\{k(m_\varphi r)' - k\, m_\theta r_1 \cos\varphi - q_\varphi r r_1\}\delta\rho]\, d\theta d\varphi$$

$$-\int_0^{2\pi}\{[n_\varphi r\delta v]^{\varphi} + [(q_\varphi + n_\varphi\rho)r\,\delta w]^{\varphi} - [km_\varphi r\delta\rho]^{\varphi}\}d\theta = 0 \qquad (3)$$

The equations of equilibrium are given by

$$\left.\begin{aligned}
&(rn_\varphi)' - (q_\varphi + n_\varphi\rho)\, r - (r_1 n_\theta \cos\varphi) + p_\varphi r r_1 = 0\\
&rn_\varphi + [(q_\varphi + n_\varphi\rho)r]' + (r_1 n_\theta \sin\varphi) + p_z r r_1 = 0\\
&k[(m_\varphi r)' \quad m_\theta r_1 \cos\varphi] - q_\varphi r r_1 = 0
\end{aligned}\right\} \quad (4a\sim c)$$

If Eq.(4a) multiplied by $\sin\varphi$ and Eq.(4b) multiplied by $\cos\varphi$ are added and then integrated, the following equation may be obtained:

$$rn_\varphi \sin\varphi + r(q_\varphi + n_\varphi\rho)\cos\varphi = -\int r r_1 (p_\varphi \sin\varphi + p_z \cos\varphi)d\varphi - B \qquad (5)$$

Eq.(4a) may also be written as

$$rn_\varphi' - (q_\varphi + n_\varphi\rho)\, r = -r r_1 p_\varphi - (n_\varphi \quad n_\theta) r_1 \cos\varphi \qquad (6)$$

Elimination of $(q_\varphi + n_\varphi\rho)r$ from Eqs.(5) and (6) provides

$$n_\varphi' + n_\varphi \tan\varphi = F_N(\varphi) \qquad (7)$$

where

$$F_N(\varphi) = -r_1 p_\varphi - (n_\varphi \quad n_\theta)\frac{r_1 \cos\varphi}{r}$$

$$- \frac{1}{r\cos\varphi}\{\int r r_1 (p_\varphi \sin\varphi + p_z \cos\varphi) d\varphi + B\}$$

The form of Eq.(7) is convenient for a later application.

3. GENERAL SOLUTIONS FOR SHELLS OF REVOLUTION

The reduced velocity-strain rate relations (X-4a~d) are homogeneous with respect to an appropriate time scale and no integration with respect to time was necessary. The kinematic relations (1a~e) in the preceding section for small-strain and moderately small rotations (in the terminology of Sanders' theory [4]) of rigid-plastic shells of revolution will, however, result in the incremental relations which are no longer homogeneous with respect to time. It is therefore necessary to denote by a dot differentiation with respect to a time scale. If ζ denotes the normal displacement of a representative point on the middle surface of a shell, ζ may be chosen as an appropriate time scale. The incremental form of Eqs.(1a~e) may be written as

$$\dot{\varepsilon}_\theta = \frac{\dot{v}\cot\varphi - \dot{w}}{r_2}, \qquad \dot{\varepsilon}_\varphi = \frac{\dot{v}' - \dot{w}}{r_1} + \dot{\rho}\rho$$

$$\dot{\kappa}_\theta = -\frac{k\cot\varphi}{r_2}\dot{\rho}, \qquad \dot{\kappa}_\varphi = -\frac{k}{r_1}\dot{\rho}', \qquad \dot{\rho} = \frac{\dot{v} + \dot{w}'}{r_1} \qquad (8a\sim e)$$

The second term in $\dot{\varepsilon}_\varphi$ is the only nonlinear term.

The approximate yield condition and the associated flow law are directly applicable to the present problem. General solutions can be found in a similar manner to those in chapter 10 with a slight modification as follows:

(i) *General Solution for H_φ^+ and H_φ^-.* The general solution

$$v = A\sin\varphi, \qquad w = A\cos\varphi$$

obtained in chapter 10, Section 4 is also the general solution to the present nonlinear case.

(ii) *General Solution for $H_{\varphi\theta}^+$ and $H_{\varphi\theta}^-$.* Since Eqs.(8c and d) are the same as in the linear case, Eq.(X-12b) furnishes Eq.(X-15) again except B_1 now as a function of ζ, *i.e.*

$$\frac{\dot{v} + \dot{w}'}{r_1} = \frac{\dot{B}_1(\zeta)}{r_2 \sin\varphi}, \qquad \frac{v + w'}{r_1} = \frac{B_1(\zeta)}{r_2 \sin\varphi} \qquad (9a,b)$$

Substitution of Eqs.(8a and b) and Eqs.(9a,b) into Eq.(X-12a) provides

$$\frac{\dot{v}' - \dot{w}}{r_1} + \frac{\dot{v}\cot\varphi - \dot{w}}{r_2} + \frac{B_1\dot{B}_1}{r^2} = 0$$

which may be reduced to

$$\dot{w}'' + \frac{r_1'}{r}\dot{w}' + \left(1 + \frac{r_1}{r_2}\right)\dot{w} = \frac{\dot{B}_1}{r}\left(r_1' + \frac{B_1 r_1}{r}\right) \tag{10}$$

The general solution to Eq.(10) can be found in a similar fashion to Eq.(X-17) and written as

$$\dot{w} = \cos\varphi\left\{\dot{B}_3 + \int \frac{\dot{B}_1(r_1\cos\varphi + x(\varphi)) + \dot{B}_1 B_1 \ell nr + \dot{B}_2}{r_2 \sin\varphi \cos^2\varphi}\, d\phi\right\} \tag{11}$$

Upon substitution of (11) into (9a), $\dot{v}$ may be found. Substitution of Eqs.(9a) and (11) into Eqs.(1a and c) provides

$$\left.\begin{aligned} r_2\dot{\varepsilon}_\theta &= \frac{\dot{B}_1[x(\varphi) + \dot{B}_2/\dot{B}_1 + B_1\ell nr]}{r_2 \sin^2\varphi} \\ r_2\dot{\kappa}_\theta &= -k\frac{\dot{B}_1\cos\varphi}{r_2\sin^2\varphi} \end{aligned}\right\} \tag{12}$$

Substitution of (12) into Eq.(X-12c) furnishes

$$\pm(n_\varphi - n_\theta) = \frac{1}{2k\cos\varphi}\left\{x(\varphi) + \frac{\dot{B}_2}{\dot{B}_1} + B_1\ell nr\right\} \tag{13}$$

Substitution of (13) into $F_N(\varphi)$ on the right side of (7) furnishes

$$\left(\frac{n_\varphi}{\cos\varphi}\right)' = \frac{F_N(\varphi)}{\cos\varphi} = \frac{r_1}{2kr\cos\varphi}\left(x(\varphi) + \frac{\dot{B}_2}{\dot{B}_1} + B_1\ell nr\right)$$

$$\frac{r_1 p_\varphi}{\cos\varphi} \quad \frac{1}{r\cos^2\varphi}\left\{\int r r_1 (p_\varphi \sin\varphi + p_z\cos\varphi)d\varphi + B_4\right\} \tag{14}$$

The general solution may be found by a simple quadrature. From Eq.(5) q_φ can then be obtained. Substitution of Eq.(13) into the yield condition Eqs.(X-7a and 8a) provides

$$m_\varphi \quad m_\theta = \pm\left[1 - \frac{1}{4k^2\cos^2\varphi}\left(x(\varphi) + \frac{\dot{B}_2}{\dot{B}_1} + B_1\ell nr\right)^2\right] \tag{15}$$

Since Eq.(4c) can be rewritten as

$$m_\varphi' = \frac{1}{k} r_1 q_\varphi - (m_\varphi - m_\theta)\frac{r_1\cos\varphi}{r_2\sin\varphi} \tag{16}$$

substitution of Eq.(15) and q_φ from Eqs.(5) and (14), into Eq.(16) furnishes m'_φ.

(iii) *General Solution for H_θ^+ and H_θ^-.* The system of equations (X-28a and~b) may be reduced to

$$\dot{\rho}' = 0 \ , \quad \dot{\rho} = \frac{\dot{v} + \dot{w}'}{r_1} = \dot{C}_1 \ , \quad \rho = C_1 \tag{17}$$

$$\dot{v}' - \dot{w} + C_1 \dot{C}_1 r_1 = 0 \tag{18}$$

The general solution of this system of differential equations is given by

$$\begin{aligned} \dot{v} &= \dot{C}_1[r\sin\varphi - x(\varphi)\cos\varphi + C_1(r\cos\varphi + x(\varphi)\sin\varphi)] + \dot{C}_2\sin\varphi + \dot{C}_3\cos\varphi \\ \dot{w} &= \dot{C}_1[r\cos\varphi + x(\varphi)\sin\varphi + C_1(r\sin\varphi - x(\varphi)\cos\varphi)] + \dot{C}_2\cos\varphi - \dot{C}_3\sin\varphi \end{aligned} \tag{19}$$

Substitution of Eqs.(19) into Eq.(X-28c) furnishes

$$n_\theta = \mp \frac{1}{2k\cos\varphi}\left[\frac{\dot{C}_3}{\dot{C}_1} x(\varphi) + C_1(r_1\cos 2\varphi + x(\varphi)\sin 2\varphi)\right] \tag{20}$$

Substitution of Eq.(20) into $F_N(\varphi)$ on the right side of Eq.(7) provides a first order differential equation for n_φ alone. If the general solution for n_φ is substituted into Eq.(5), q_φ can be obtained. The bending moment m_θ is obtained by substituting Eq.(7) into the yield condition (X-9a,10a). Since rq_φ and m_θ are known, m_φ may be obtained from Eq.(4c).

As an example of the general solutions, a conical shell in the state defined by $H^+_{\varphi\theta}$ or $H^-_{\varphi\theta}$ is considered. The kinematic relations (8a~e) must now be replaced by

$$\left.\begin{aligned} \dot{\varepsilon}_\theta &= \frac{1}{y}(\dot{v} \quad \dot{w}\tan\alpha) \ , & \dot{\varepsilon}_\varphi &= \dot{v}' + w'\dot{w}' \\ \dot{\kappa}_\theta &= -\frac{k\dot{w}'}{y} \ , & \dot{\kappa}_\varphi &= -k\dot{w}'' \end{aligned}\right\} \tag{21}$$

The equations of equilibrium are given by

$$\left.\begin{aligned} &(yn_\varphi)' \quad n_\theta + yP_\varphi = 0 \\ &(yq_\varphi)' + n_\theta\tan\alpha + (n_\varphi y w')' + yP_Z = 0 \\ &k(ym_\varphi)' - km_\theta \quad yq_\varphi = 0 \end{aligned}\right\} \tag{22}$$

The solution to the simple differential equation defined by Eq.(X-12b) for $H^+_{\varphi\theta}$ and $H^-_{\varphi\theta}$ is given by Eq.(X-38) except that B_1 and B_2 must now be regarded explicitly as functions of ζ.

$$\dot{w} = \dot{B}_1(\zeta)\ell ny + \dot{B}_2(\zeta) \ , \quad w = B_1(\zeta)\ell ny + B_2(\zeta) \tag{23}$$

Substitution of Eqs.(23) into the differential equation obtained for Eq.(X-12a) provides

$$(y\dot{v})' = (\dot{B}_1 \ell ny + \dot{B}_2)\ tan\alpha - B\dot{B}_1/y \tag{24}$$

Simple quadrature yields

$$\dot{v} = \dot{B}_1\ tan\alpha\ (\ell ny - 1) + \dot{B}_2\ tan\alpha - B_1\dot{B}_1\ \frac{\ell ny}{y} + \frac{\dot{B}_3}{y} \tag{25}$$

The third ratio (X-12c) furnishes then

$$n_\varphi - n_\theta = \mp\ \frac{1}{2k}\ (\frac{\dot{B}_3}{\dot{B}_1} - y\ tan\alpha - B_1 \ell ny) \tag{26}$$

Substitution of Eq.(26) into Eq.(22a) and integration of the resulting equation provides

$$n_\varphi = -\int P_\phi y dy \pm \frac{1}{2k}\ \{\ \frac{\dot{B}_3}{\dot{B}_1}\ \ell ny - y\ tan\alpha\ \ \frac{1}{2}\ B_1(\ell ny)^2\} + \dot{B}_4 \tag{27}$$

Similarly q_φ, m_φ and m_θ can be found by simple quadratures.

4. UNCOUPLED EQUATIONS FOR DISPLACEMENT FIELDS IN NONSYMMETRIC PROBLEMS

Uncoupled equations for displacement fields can also be obtained for geometrically nonlinear problems of nonsymmetric rigid-plastic sandwich shells. The strain-displacement relations (XI-14) must then be replaced by

$$\left.\begin{aligned}
\dot{\varepsilon}_x &= \frac{\partial\dot{u}}{\partial x} - Z_{xx}\dot{w} + \frac{\partial w}{\partial x}\frac{\partial\dot{w}}{\partial x}\ , & \dot{\kappa}_x &= k\ \frac{\partial^2\dot{w}}{\partial x^2} \\
\dot{\varepsilon}_y &= \frac{\partial\dot{v}}{\partial y} - Z_{yy}\dot{w} + \frac{\partial w}{\partial y}\frac{\partial\dot{w}}{\partial y}\ , & \dot{\kappa}_y &= k\ \frac{\partial^2\dot{w}}{\partial y^2} \\
\dot{\varepsilon}_{xy} &= \frac{\partial\dot{u}}{\partial y} + \frac{\partial\dot{v}}{\partial x} - 2Z_{xy}\dot{w} + \frac{\partial w}{\partial x}\frac{\partial\dot{w}}{\partial y} + \frac{\partial w}{\partial y}\frac{\partial\dot{w}}{\partial x}\ , & \dot{\kappa}_{xy} &= -2k\ \frac{\partial^2\dot{w}}{\partial x\partial y}
\end{aligned}\right\} \tag{28}$$

For shallow sandwich shells, the flow law (XI-9) leads to the following system of differential equations in place of (XI-16).

$$\left.\begin{aligned}
&\frac{\partial\dot{u}}{\partial x}\quad Z_{xx}\dot{w} + \frac{\partial w}{\partial x}\frac{\partial\dot{w}}{\partial x} \pm k\ \frac{\partial^2\dot{w}}{\partial x^2} = 0 \\
&\frac{\partial\dot{v}}{\partial y}\quad Z_{yy}\dot{w} + \frac{\partial w}{\partial y}\frac{\partial\dot{w}}{\partial y} \pm k\ \frac{\partial^2\dot{w}}{\partial y^2} = 0 \\
&\frac{\partial\dot{u}}{\partial y} + \frac{\partial\dot{v}}{\partial x}\quad 2Z_{xy}\dot{w} + \frac{\partial w}{\partial x}\frac{\partial\dot{w}}{\partial y} + \frac{\partial w}{\partial y}\frac{\partial\dot{w}}{\partial x} \pm 2k\ \frac{\partial\ \dot{w}}{\partial x\partial y} = 0
\end{aligned}\right\} \tag{29}$$

The velocity components $\dot{u}$ and $\dot{v}$ may readily be eliminated from Eqs.(29a,b) and the resulting single nonlinear differential equation for $\dot{w}$ becomes

$$\frac{\partial^2}{\partial x^2}(Z_{yy}w) \quad 2\frac{\partial^2}{\partial x \partial y}(Z_{xy}w) + \frac{\partial^2}{\partial y^2}(Z_{xx}w)$$

$$- \frac{\partial^2}{\partial x^2}\left(\frac{\partial w}{\partial y}\frac{\partial \dot{w}}{\partial y}\right) \quad \frac{\partial^2}{\partial y^2}\left(\frac{\partial w}{\partial x}\frac{\partial \dot{w}}{\partial x}\right) + \frac{\partial^2}{\partial x \partial y}\left(\frac{\partial w}{\partial x}\frac{\partial \dot{w}}{\partial y} + \frac{\partial w}{\partial y}\frac{\partial \dot{w}}{\partial x}\right) = 0$$

or

$$\frac{\partial^2}{\partial x^2}(Z_{yy}w) - 2\frac{\partial^2}{\partial x \partial y}(Z_{xy}w) + \frac{\partial^2}{\partial y^2}(Z_{xx}w)$$

$$+ \frac{\partial^2 w}{\partial y^2}\frac{\partial^2 \dot{w}}{\partial x^2} + \frac{\partial^2 w}{\partial x^2}\frac{\partial^2 \dot{w}}{\partial y^2} - 2\frac{\partial^2 w}{\partial x \partial y}\frac{\partial^2 \dot{w}}{\partial x \partial y} = 0 \qquad (30)$$

REFERENCES

[1] See for instance, M. Duszek, Plastic Analysis of Shallow Spherical Shells at Moderately Large Deflections," *Theory of Thin Shells, Proc. IUTAM Symposium Copenhagen 1967 edited by F.L.Niordson, pp374-388.*

[2] See for instance, P. V. Marcal, "Finite Element Analysis of Combined problems of Nonlinear Material and Ge metric Behavior," *Proc. ASME Conference on "Computational Approaches in Applied Mechanics", June 1969,* pp133-149.

[3] Coon, M. D. and S. S. Gill, "The Effect of Change of Geometry on the Rigid-plastic Limit Load of Cylinders," *Int.J.Mech.Sci.* 10, 1968, pp355-368.

[4] Sanders, J. L., "Nonlinear Theories for Thin Shells," *Quart. Appl. Math.*, 21, 1963, pp21-36.

CHAPTER 13

FINITE DIFFERENCE EQUATIONS DERIVED FROM NUMERICAL QUADRATURE FORMULAE

1. INTRODUCTION

In an incremental elastic-plastic large-deflection analysis of thin shell structures, it is essential to develop a step-by-step iterative procedure with which an accurate prediction of displacement increments to a prescribed load increment can be made at each step so as not to accumulate errors after a number of increments. For this purpose, the system of simultaneous nonlinear partial differential equations and the associated boundary conditions must first be simulated by a system of finite difference equations which result from ignoring truncation errors. Even if the simultaneous nonlinear finite difference equations are solved within a sufficiently small error by means of an iterative incremental procedure which will be described in the next chapter, the numerical result may still involve errors of more than a few percent if the finite difference simulation is of a low accuracy. Consequently, the stability limit of a shell structure may not then be predicted correctly. It is important therefore to derive an appropriate set of simulating finite difference field and boundary equations with a satisfactory accuracy which are well-balanced from the point of view of the discretization errors involved in a finite difference *solution* but not merely of the truncation errors.

In this chapter, a well-balanced set of finite difference field and boundary equations will be derived from the virtual work equation by applying a two-dimensional numerical quadrature formula. It will be shown by some examples that finite difference boundary equations of a higher accuracy are practically advantageous in order to obtain a sufficiently accurate result suitable for the nonlinear analysis.

Attention will be confined here to circular cylindrical shells but the procedure developed in this and next chapters will be applicable to other shells. Fig.1(a) and (b) show the coordinate axes for a circular cylindrical shell and the stress resultants acting upon a shell element, respectively. The symbols used in this and next chapters are listed in the following.

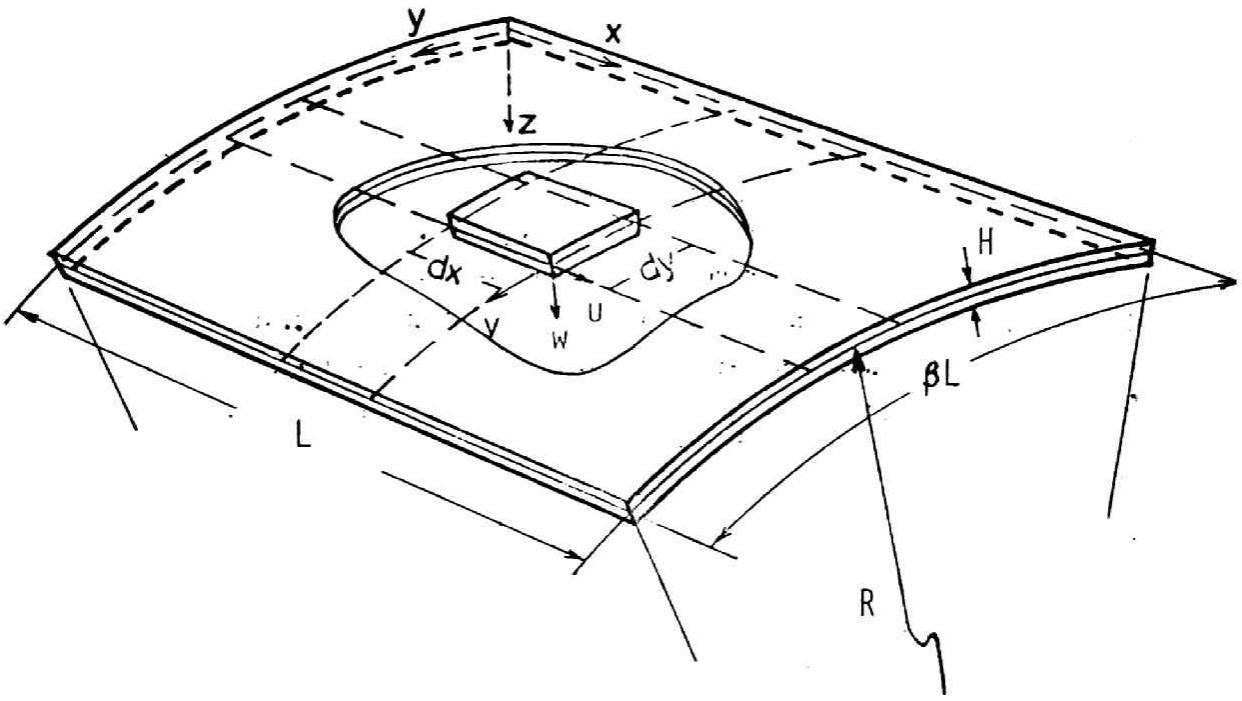

FIG. 1(A) CIRCULAR CYLINDRICAL SHELL

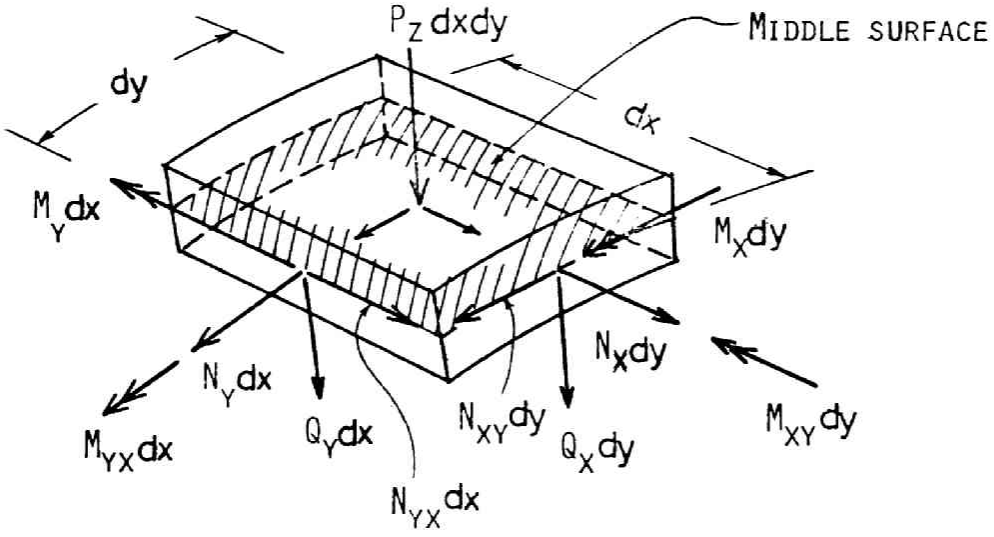

FIG. 1(B) STRESS RESULTANTS AND EXTERNAL FORCE ON A SHELL ELEMENT

SYMBOLS

A	cross-sectional area of a sandwich flange per unit length
$A_\lambda(x, y)$	force resultant in λ-direction at (x, y) acting upon a shell element of unit middle surface area, $\lambda = x, y, z$
$a_\lambda(i, j)$	finite difference expression of $A_\lambda(i, j)$
$[\alpha(i, j)]$	coefficient matrix of numerical double quadrature
B	circumferential length of circular cylindrical shell
$\hat{B}_\lambda(x, y)$	boundary force resultant in λ-direction at boundary x = const., $\bar{B}_\lambda(x, y)$ for boundary y = const.
$\hat{B}_M(x, y)$	boundary moment resultant at boundary x = const.
β	B/L
$\{\hat{\beta}(I, j)\}$	coefficient vector of numerical quadrature along boundary $i = I$
$\hat{b}_\lambda(i, j)$	finite difference expression of $\hat{B}_\lambda(x, y)$
$C(x_c, y_c)$	corner force redultant at corner (x_c, y_c)
$c(i, j)$	finite difference expressions of $C(i, j)$
D	extensional stiffness, $EA/(1 - \nu^2)$
D^e	elastic stiffness matrix
E	modulus of elasticity
ε_x	extensional strain of the middle surface in x-direction
ε_{xy}	shear strain of the middle surface
F_1, F_2	yield functions
G	corner force
g	G/M_0
H	shell thickness
θ	mesh length ratio, $=(\beta/J)/l = B/IJL$
I, J	number of meshes in x and y direction, respectively
(i, j)	node coordinates
K	bending stiffness, $AEH^2/4(1 - \nu^2)$
K_x	change of curvature in x direction
κ_x	$= M_0 K_x / N_0 = K_x H/2$
K_{xy}	change of twist
κ_{xy}	$= M_0 K_{xy} / N_0 = K_{xy} H/2$

L	generator length
l	$1/I$, dimensionless mesh length in x-direction
$\lambda(x, y)$ $\mu(x, y)$	proportionality constant at (x, y) representing rate of plastic flow associated with F_1 and F_2, respectively
M_0	fully plastic moment per unit length, $AH\sigma_0/2$
M_x	bending moment per unit length along x = const.
m_x	$= M_x/M_0$
M_{xy}	twisting moment per unit length along x = const.
m_{xy}	$= M_{xy}/M_0$
N_0	fully plastic uniaxial membrane force, $2H\sigma_0$
N_x	membrane tension in x direction per unit length
n_x	$= N_x/N_0$
N_{xy}	membrane shear along x = const. per unit length
n_{xy}	$= N_{xy}/N_0$
ν	Poisson's ratio
P	external pressure
p	$= PL^2/M_0$
P_L, P_U, P_{LU}	reduction coefficient matrices for plastic stiffness matrices
Q_x	transverse shear force along x = const.
q_x	$= Q_x/N_0$
R	radius of curvature of circular cylindrical shell
ρ	R/L
S_x	reduced transverse shear force
s_x	S_xL/M_0
σ_0	yield stress in simple tension
U, V, W	displacements in X, Y, Z-directions, respectively
u, v, w	$= U/H$, V/H, W/H, respectively
X	coordinate in the generator direction
x	$= X/L$
Y	coordinate in the circumferential direction
y	$= Y/L$
Z	coordinate in the radial direction
z	$= Z/L$

2. VIRTUAL WORK EQUATION

The virtual work equation based upon the classical nonlinear theory [1] of shallow shells may be written for circular cylindrical shells as

$$\left[\int_0^B \{(\hat{N}_x - N_x)\delta U + (\hat{N}_{xy} - N_{xy})\delta V\}dY\right]_{X=0}^{X=L}$$

$$+ \left[\int_0^L \{(\bar{N}_{xy} - N_{xy})\delta U + (\bar{N}_y - N_y)\delta V\}dX\right]_{Y=0}^{Y=B}$$

$$+ \int_0^L\int_0^B \{\left(\frac{\partial N_x}{\partial X} + \frac{\partial N_{xy}}{\partial Y}\right)\delta U + \left(\frac{\partial N_{xy}}{\partial X} + \frac{\partial N_y}{\partial Y}\right)\delta V\}dXdY$$

$$+ \left[\int_0^B (\hat{M}_x - M_x)\delta\left(\frac{\partial W}{\partial X}\right)dY\right]_{X=0}^{X=L} + \left[\int_0^L (\bar{M}_y - M_y)\delta\left(\frac{\partial W}{\partial Y}\right)dX\right]_{Y=0}^{Y=B}$$

$$+ \left[\int_0^B \{\hat{S}_x - \frac{M_x}{\partial X} - 2\frac{\partial M_{xy}}{\partial Y} + (\bar{N}_x - N_x)\frac{\partial W}{\partial X} + (\bar{N}_{xy} - N_{xy})\frac{\partial W}{\partial Y}\}\delta W dY\right]_{X=0}^{X=L}$$

$$+ \left[\int_0^L \{\bar{S}_y - \frac{\partial M_y}{\partial Y} - 2\frac{\partial M_{xy}}{\partial X} + (\bar{N}_{xy} - N_{xy})\frac{\partial W}{\partial X} + (\bar{N}_y - N_y)\frac{\partial W}{\partial Y}\}\delta W dX\right]_{Y=0}^{Y=B}$$

$$- \int_0^L\int_0^B \{\frac{\partial^2 M_x}{\partial X^2} + 2\frac{\partial^2 M_{xy}}{\partial X\partial Y} + \frac{\partial^2 M_y}{\partial Y^2} + \frac{N_y}{R} + P$$

$$- \frac{\partial}{\partial X}(N_x\frac{\partial W}{\partial X} + N_{xy}\frac{\partial W}{\partial Y}) - \frac{\partial}{\partial Y}(N_{xy}\frac{\partial W}{\partial X} + N_y\frac{\partial W}{\partial Y})\}\delta W dXdY$$

$$- \left[(\bar{G} - 2M_{xy})\delta W\right]_{X=0}^{X=L}{}_{Y=0}^{Y=B} = 0 \qquad (1)$$

If the relations between M_0 and N_0:

$$\frac{M_0}{N_0 L} = \frac{H}{2L} = h \quad \text{and} \quad \frac{M_0}{N_0 H} = \frac{1}{2} \qquad (2)$$

are taken into consideration, Eq. (1) may be reduced to the following dimension-

less form for a circular cylindrical sandwich shell:

$$\left[\int_0^B \{(\hat{n}_x - n_x)\delta u + (\hat{n}_{xy} - n_{xy})\delta v\}dy\right]_{x=0}^{x=1}$$

$$+ \left[\int_0^1 \{(\bar{n}_{xy} - n_{xy})\delta u + (\bar{n}_y - n_y)\delta v\}dx\right]_{y=0}^{y=\beta}$$

$$+ \int_0^1\int_0^\beta \{\left(\frac{\partial n_x}{\partial x} + \frac{\partial n_{xy}}{\partial y}\right)\delta u + \left(\frac{\partial n_{xy}}{\partial x} + \frac{\partial n_y}{\partial y}\right)\delta v\}dxdy$$

$$+ h\left[\int_0^\beta (\hat{m}_x - m_x)\delta\left(\frac{\partial w}{\partial x}\right)dy\right]_{x=0}^{x=1} + h\left[\int_0^1 (\bar{m}_y - m_y)\delta\left(\frac{\partial w}{\partial y}\right)dx\right]_{y=0}^{y=\beta}$$

$$+ h\left[\int_0^\beta \{\hat{S}_x - \frac{\partial m_x}{\partial x} - 2\frac{\partial m_{xy}}{\partial y} + 2(\bar{n}_x - n_x)\frac{\partial w}{\partial x} + 2(\bar{n}_{xy} - n_{xy})\frac{\partial w}{\partial y}\}\delta w dy\right]_{x=0}^{x=1}$$

$$+ h\left[\int_0^1 \{\bar{S}_y - \frac{\partial m_y}{\partial y} - 2\frac{\partial m_{xy}}{\partial x} + 2(\bar{n}_{xy} - n_{xy})\frac{\partial w}{\partial x} + 2(\bar{n}_y - n_y)\frac{\partial w}{\partial y}\}\delta w dx\right]_{y=0}^{y=\beta}$$

$$- h\int_0^1\int_0^\beta \{\frac{\partial^2 m_x}{\partial x^2} + 2\frac{\partial^2 m_{xy}}{\partial x\partial y} + \frac{\partial^2 m_y}{\partial y^2} + \frac{n_y}{h\rho} + p$$

$$- 2\frac{\partial}{\partial x}(n_x\frac{\partial w}{\partial x} + n_{xy}\frac{\partial w}{\partial y}) - 2\frac{\partial}{\partial y}(n_{xy}\frac{\partial w}{\partial x} + n_y\frac{\partial w}{\partial y})\}\delta w dxdy$$

$$- h\left[[(\bar{g} - 2m_{xy})\delta w]_{x=0}^{x=1}\right]_{y=0}^{y=\beta} = 0 \qquad (3)$$

Eq.(3) may be written compactly as follows:

$$\int_0^1\int_0^\beta \{\delta u(x, y)\}\{A(x, y)\}dxdy$$

$$+ \left[\int_0^\beta \{\delta u(x, y)\}\{\hat{B}(x, y)\}dy\right]_{x=0}^{x=1} + \left[\int_0^1 \{\delta u(x, y)\}\{\bar{B}(x, y)\}dx\right]_{y=0}^{y=\beta}$$

$$+ \left[[\delta w(x, y) C(x, y)]_{x=0}^{x=1} \right]_{y=0}^{y=\beta} = 0 \tag{4}$$

where

$$\{\delta u(x, y)\}^T = \begin{Bmatrix} \delta u(x, y) \\ \delta v(x, y) \\ \delta w(x, y) \\ \delta w_{,x}(x, y) \\ \delta w_{,y}(x, y) \end{Bmatrix}, \quad \{A(x, y)\} = \begin{Bmatrix} A_x(x, y) \\ A_y(x, y) \\ A_z(x, y) \\ 0 \\ 0 \end{Bmatrix}$$

$$\{\widehat{B}(x, y)\} = \begin{Bmatrix} \widehat{B}_x(x, y) \\ \widehat{B}_y(x, y) \\ \widehat{B}_z(x, y) \\ \widehat{B}_M(x, y) \\ 0 \end{Bmatrix}, \quad \{B(x, y)\} = \begin{Bmatrix} \overline{B}_x(x, y) \\ \overline{B}_y(x, y) \\ \overline{B}_z(x, y) \\ 0 \\ \overline{B}_M(x, y) \end{Bmatrix} \tag{5}$$

$A_\lambda(x, y) = 0$ ($\lambda = x, y, z$) is the equation of force equilibrium in the λ-direction. $\widehat{B}_\lambda(x, y) = 0$ and $\overline{B}_\lambda(x, y) = 0$ represent the force boundary conditions in the λ-direction along a boundary Γ_x described by x = const. and along Γ_y given by y = const., respectively. $\widehat{B}_M(x, y) = 0$ and $\overline{B}_M = 0$ denote the moment boundary conditions along Γ_x and Γ_y, respectively. $C(x, y) = 0$ represents the equilibrium equation for a corner force at a corner defined by the intersection of Γ_x and Γ_y.

3. FINITE DIFFERENCE EQUATIONS DERIVED FROM A NUMERICAL QUADRATURE FORMULA

In the conventional use of the finite difference method, the finite difference operators replaces directly the differential operators in a system of field equations and boundary conditions which have been derived from the requirements that the virtual work must vanish *for any admissible variation of the displacement field.* In the finite difference scheme, however, the degree of freedom of admissible variations is finite and hence the virtual work equation (4) need to be satisfied only with respect to the variations of a set of nodal displacements, which can be given independently. Eq.(4) must then be expressed first in terms of the variations of nodal displacements with the use of a numerical quadrature formula.

There are a number of different numerical quadrature formulae. An error appraisal can be made if it may be assumed that the integrand under consideration has continuous higher derivatives necessary for the estimate. Those virtual

displacement functions are therefore considered here which have continuous higher derivatives up to the degrees desired. The surface and boundary integrals in (4) may be approximated by finite sums of nodal quantities. The coefficients of a finite sum may be different depending upon a numerical quadrature formula to be applied.

For equally-spaced rectangular meshes I x J, there are $3(I + 1)(J + 1)$ unknown nodal displacement components and $2(I + 1) + 2(J + 1)$ unknown nodal slope components. For a set of regularly spaced nodal points in one dimension, a Newton-Cotes numerical quadrature formula involves a smaller error than the corresponding open formula for the same number of meshes provided the end points can be included. It has been demonstrated by Miller [2] that, among various nine-point formulae for a two-dimensional numerical quadrature, the Simpson's rule product provides a considerably accurate result.

Let $\alpha(i, j)$ denote the coefficient of a two-dimensional numerical quadrature formula to be multiplied on the nodal point values of the integrand at node (i, j). Let $\beta^{(x)}(i, j)(i = 0 \text{ and } I)$ and $\beta^{(y)}(i, j)(j = 0 \text{ and } J)$ denote, respectively, the coefficients of a one-dimensional numerical quadrature formula for the boundary integrals along Γ_x and Γ_y. If I and J are even, Simpson's rule can be applied:

$$[\alpha(i, j)] = \frac{1}{9}\begin{bmatrix} 1 & 4 & 2 & 4 & \vdots & & 2 & 4 & 1 \\ 4 & 16 & 8 & 16 & \cdots & & 8 & 16 & 4 \\ 2 & 8 & 4 & 8 & \cdots & & 4 & 8 & 2 \\ \cdots & & & & & & & & \\ \cdots & & & & & & & & \\ \cdots & & & & & & & & \end{bmatrix}$$

$$\{\overline{\beta}(i, j)\} = \{\frac{1}{3} \quad \frac{4}{3} \quad \frac{2}{3} \quad \frac{4}{3} \cdots \cdots \cdots \quad \frac{2}{3} \quad \frac{4}{3} \quad \frac{1}{3}\} \quad \text{for } i = 0 \text{ and } I$$

$$\{\overline{\beta}(i, j)\} = \{\frac{1}{3} \quad \frac{4}{3} \quad \frac{2}{3} \quad \frac{4}{3} \cdots \cdots \cdots \quad \frac{2}{3} \quad \frac{4}{3} \quad \frac{1}{3}\} \quad \text{for } j = 0 \text{ and } J$$

The node intervals or mesh lengths in the x- and y-directions are denoted by l and θl, respectively.

Eq.(4) can be approximated by the following finite sums:

$$\theta l^2 \sum_{j=0}^{J} \sum_{i=0}^{I} \alpha(i, j)\{\delta u(i, j)\}\{A(i, j)\} + \left[[\delta w(i, j)C(i, j)]_{i=0}^{i=I}\right]_{j=0}^{j=J}$$

$$+ \theta l \left[\sum_{j=0}^{J} \beta(i, j)\{\delta u(i, j)\}\{B(i, j)\}\right]_{i=0}^{i=I}$$

$$+ l \left[\sum_{i=0}^{I} \overline{\beta}(i, j)\{\delta u(i, j)\}\{\overline{B}(i, j)\}\right]_{j=0}^{j=J} = 0 \qquad (6)$$

It should be noted that, when a closed formula is applied, the double sum includes virtual work terms dependent upon the virtual displacements of the boundary nodes and similarly the single sums include virtual work terms dependent upon the corner virtual displacements. If these terms are separated and rearranged, Eq.(6) may be written as

$$\theta l^2 \sum_{j=1}^{J-1} \sum_{i=1}^{I-1} \alpha(i, j)\{\delta u(i, j)\}\{A(i, j)\}$$

$$+ \left[\sum_{j=1}^{J-1} \{\delta u(i, j)\}\left(\theta l^2 \alpha(i, j)\{A(i, j)\} + \theta l \widehat{\beta}(i, j)\{\widehat{B}(i, j)\}\right)\right]_{i=0}^{i=I}$$

$$+ \left[\sum_{i=1}^{I-1} \{\delta u(i, j)\}\left(\theta l^2 \alpha(i, j)\{A(i, j)\} + l \overline{\beta}(i, j)\{\overline{B}(i, j)\}\right)\right]_{j=0}^{j=J}$$

$$+ \left[\left[\{\delta u(i, j)\}\left(\theta l^2 \alpha(i, j)\{A(i, j)\} + \theta l \widehat{\beta}(i, j)\{\widehat{B}(i, j)\}\right.\right.\right.$$

$$\left.\left.\left. + l \overline{\beta}(i, j)\{\overline{B}(i, j)\} + \{C(i, j)\}\right)\right]_{i=0}^{i=I}\right]_{j=0}^{j=J} = 0 \qquad (7)$$

The nodal point values of the force and couple resultants in (7) must satisfy the following equations:

(i) Either $\theta l^2\{A(i, j)\} = 0$ or $\{\delta u(i, j)\} = 0$,

($i = 1, \ldots, J-1$ and $j = 1, \ldots, J-1$)

(ii) either $\theta l^2\alpha(i, j)\{A(i, j)\} + l\hat{\beta}(i, j)\{\hat{B}(i, j)\} = 0$ or $\{\delta u(i, j)\} = 0$
$(i = 0, I \text{ and } j = 1, \ldots, J\text{-}1)$

(iii) either $\theta l^2\alpha(i, j)\{A(i, j)\} + \theta l\bar{\beta}(i, j)\{\bar{B}(i, j)\} = 0$ or $\{\delta u(i, j)\} = 0$
$(i = 1, \ldots, I\text{-}1, \text{ and } j = 0, J)$

(iv) either $\theta l^2\alpha(i, j)\{A(i, j)\} + l\hat{\beta}(i, j)\{\hat{B}(i, j)\} + \theta l\bar{\beta}(i, j)\{\bar{B}(i, j)\}$
$+ \{C(i, j)\} = 0, \qquad (i = 0, I \text{ and } j = 0, J)$
or $\{\delta u(i,j)\} = 0.$ (8a-d)

If all the nodal point derivatives in $\{A(i, j)\}$, $\{B(i, j)\}$ and $\{C(i, j)\}$ are replaced by a corresponding finite difference expression, respectively, then a system of finite difference equations with which the system of Eqs.(8) can be approximated, may be obtained. Let $\{a(i, j)\}$ and $\{r_A(i, j)\}$, $\{\bar{b}(i, j)\}$ and $\{r_{\bar{B}}(i, j)\}$, $\{\hat{b}(i, j)\}$ and $\{r_{\hat{B}}(i, j)\}$, and $\{C(i, j)\}$ and $\{r_C(i, j)\}$ denote the finite difference expressions and the associated discretization errors of $\{A(i, j)\}$, $\{\bar{B}(i, j)\}$, $\{\hat{B}(i, j)\}$ and $\{C(i, j)\}$, respectively. The finite difference equations corresponding to Eqs.(8a-d) can be written as follows:

(i) Either
$$\theta l^2\begin{Bmatrix} a_x(i, j) \\ a_y(i, j) \\ a_z(i, j) \end{Bmatrix} = 0 \quad \text{or} \quad \begin{Bmatrix} \delta u \\ \delta v \\ \delta w \end{Bmatrix} = 0 ,$$
$(i = 1, \ldots, I, \text{ and } j = 1, \ldots, J)$

(ii) either
$$l\hat{\beta}(i, j)\begin{Bmatrix} \hat{b}_x(i, j) \\ \hat{b}_y(i, j) \\ \hat{b}_z(i, j) \\ \hat{b}_M(i, j) \end{Bmatrix} + \theta l^2\alpha(i, j)\begin{Bmatrix} a_x(i, j) \\ a_y(i, j) \\ a_z(i, j) \\ 0 \end{Bmatrix} = 0 \quad \text{or} \quad \begin{Bmatrix} \delta u \\ \delta v \\ \delta w \\ \delta w_{,x} \end{Bmatrix} = 0 ,$$
$(i = 0, I, \text{ and } j = 1, \ldots, J\text{-}1)$

(iii) either
$$\theta l\bar{\beta}(i, j)\begin{Bmatrix} \bar{b}_x(i, j) \\ \bar{b}_y(i, j) \\ \bar{b}_z(i, j) \\ \bar{b}_M(i, j) \end{Bmatrix} + \theta l^2\alpha(i, j)\begin{Bmatrix} a_x(i, j) \\ a_y(i, j) \\ a_z(i, j) \\ 0 \end{Bmatrix} = 0 \quad \text{or} \quad \begin{Bmatrix} \delta u \\ \delta v \\ \delta w \\ \delta w_{,y} \end{Bmatrix} = 0 ,$$
$(i = 1, \ldots, I\text{-}1, \text{ and } j = 0, J)$

(iv) either

$$\begin{Bmatrix} 0 \\ 0 \\ C(i,\ j) \\ 0 \\ 0 \end{Bmatrix} + l\hat{\beta}(i,\ j)\begin{Bmatrix} \hat{b}_x(i,\ j) \\ \hat{b}_y(i,\ j) \\ \hat{b}_z(i,\ j) \\ \hat{b}_M(i,\ j) \\ 0 \end{Bmatrix} + \theta l\bar{\beta}(i,\ j)\begin{Bmatrix} \bar{b}_x(i,\ j) \\ \bar{b}_y(i,\ j) \\ \bar{b}_z(i,\ j) \\ 0 \\ \bar{b}_M(i,\ j) \end{Bmatrix} + \theta l^2\alpha(i,\ j)\begin{Bmatrix} a_x(i,\ j) \\ a_y(i,\ j) \\ a_z(i,\ j) \\ 0 \\ 0 \end{Bmatrix} = 0$$

$$(i = 0,\ I,\ \text{and}\ j = 0,\ J)$$

$$\text{or} \quad \begin{Bmatrix} \delta u \\ \delta v \\ \delta w \\ \delta w_{,x} \\ \delta w_{,y} \end{Bmatrix} = 0 . \qquad \text{(9a-d)}$$

The total error r_T consists of the discretization errors of $\{A(i,\ j)\}$, etc. and the error due to the numerical quadrature formula, which will be denoted by $R[\alpha,\ \bar{\beta},\ \hat{\beta}]$. The virtual work done by the unbalanced force resultants at nodes can then be written as

$$\begin{aligned} E_w = \theta l^2 \sum_{j=1}^{J-1} \sum_{i=1}^{I-1} \alpha(i,\ j)\{\delta u(i,\ j)\}\{r_A(i,\ j)\} \\ + \left[\sum_{j=1}^{J-1} \{\delta u(i,\ j)\}\left(\theta l^2\alpha(i,\ j)\{r_A(i,\ j)\} + \theta l\hat{\beta}(i,\ j)\{r_{\hat{B}}(i,\ j)\}\right)\right]_{i\,=\,0}^{i\,=\,I} \\ + \left[\sum_{i=1}^{I-1} \{\delta u(i,\ j)\}\left(\theta l^2\alpha(i,\ j)\{r_A(i,\ j)\} + l\bar{\beta}(i,\ j)\{r_{\bar{B}}(i,\ j)\}\right)\right]_{j\,=\,0}^{j\,=\,J} \\ + \left[\{\delta u(i,\ j)\}\left(\theta l^2\alpha(i,\ j)\{r_A(i,\ j)\} + \theta l\hat{\beta}(i,\ j)\{r_{\hat{B}}(i,\ j)\}\right.\right. \\ \left.\left. + l\bar{\beta}(i,\ j)\{r_{\bar{B}}(i,\ j)\} + \{r_C(i,\ j)\}\right)\right]_{i\,=\,0}^{i\,=\,I}{}_{j\,=\,0}^{j\,=\,J} \\ + R[\alpha,\ \bar{\beta},\ \hat{\beta}] \qquad \text{(10)} \end{aligned}$$

4. HIGHER ORDER FINITE DIFFERENCE EQUATIONS FOR BOUNDARY CONDITIONS

The total discretization error involved in the replacement of Eq.(3) by Eqs.(9) consists of two parts as given by Eq.(10). Since the unbalanced force resultant at an interior point is of $O(l^4)$ if r_A is of $O(l^2)$, the numerical quadrature formula of the Sympson's rule product with an error of $O(l^5)$ is sufficiently accurate. On the other hand, an important problem which arises in applying the finite difference method to practical problems of plates and shells is to formulate an appropriate set of finite difference boundary equations with an accuracy which is "well-balanced" with the accuracy of finite difference field equations. It has been pointed out in [3] that only the Dirichlet problem has been discussed in almost all the literature on the appraisal of the discretization error $W_F - W$ involved in the replacement of an elliptic boundary-value problem for the function W by a finite difference problem for a function W_F. The appraisal of the discretization error due to finite difference boundary equations given in [4] appears to be one of the most detailed treatments.

In order to discuss the essential feature of finite difference boundary equations explicitly, the linear elastic bending problem of a rectangular plate is considered as the simplest example of Eqs.(9). The boundary-value problem is defined by the fourth-order partial differential equation:

$$\frac{\partial^4 w}{\partial x^4} + 2\frac{\partial^4 w}{\partial x^2 \partial y^2} + \frac{\partial^4 w}{\partial y^4} = p(x, y), \tag{11}$$

and the boundary conditions

$$\left.\begin{aligned} &\left(\overline{m}_x + K\left(\frac{\partial^2 w}{\partial x^2} + \nu\frac{\partial^2 w}{\partial y^2}\right)\right)\delta\left(\frac{\partial w}{\partial x}\right) = 0 \\ &\left(\overline{S}_x + K\left\{\frac{\partial^3 w}{\partial x^3} + (2-\nu)\frac{\partial^3 w}{\partial x \partial y^2}\right\}\right)\delta w = 0 \end{aligned}\right\} \quad \text{at } x = \text{const.},$$

$$\left(\overline{g} - 2\frac{\partial^2 w}{\partial x \partial y}\right)\delta w = 0 \qquad \text{at a corner},$$

$$\left.\begin{aligned} &\left(\overline{m}_y + K\left(\frac{\partial^2 w}{\partial y^2} + \nu\frac{\partial^2 w}{\partial x^2}\right)\right)\delta\left(\frac{\partial w}{\partial y}\right) = 0 \\ &\left(\overline{S}_x + K\left\{\frac{\partial^3 w}{\partial x^3} + (2-\nu)\frac{\partial^3 w}{\partial x \partial y^2}\right\}\right)\delta w = 0 \end{aligned}\right\} \quad \text{at } y = \text{const.} \tag{12a-e}$$

It has been customary to apply finite difference expressions of the "same order with respect to the mesh length" to both of the field and boundary equations. When the biharmonic operator is replaced by the finite difference operator of square mesh

$$\diamondsuit_l^2 w_{0,0} = 20w_{0,0} - 8(w_{1,0} + w_{0,1} + w_{-1,0} + w_{0,-1}) + 2(w_{1,1} + w_{-1,1} + w_{1,-1} + w_{-1,-1}) + w_{2,0} + w_{0,2} + w_{-2,0} + w_{0,-2} \quad , \tag{13}$$

the truncation error is given by

$$r_F = \frac{l^2}{6}\left\{\frac{\partial^6}{\partial x^6} + \frac{\partial^6}{\partial x^4 \partial y^2} + \frac{\partial^6}{\partial x^2 \partial y^4} + \frac{\partial^6}{\partial y^6}\right\} w + O(l^3) \equiv \Gamma_F l^2 W_6 \tag{14}$$

Similarly, the truncation errors in the finite difference natural boundary conditions of (12a, b, c) can be bounded by

$$r_M = \Gamma_M l^2 W_4 \quad , \quad r_S = \Gamma_S l^2 W_5 \quad , \quad r_C = \Gamma_C l^2 W_4 \quad ,$$

respectively, where W_4 and W_5 are upper bounds of the fourth and fifth order derivative of w and Γ_M, Γ_S and Γ_C are some numbers independent of w_F and l. It has been shown in [4] that,

$$|| w_F - w || \leq l^2 \{N_F \Gamma_F W_6 + N_M \Gamma_M W_4 + N_S \Gamma_S W_5 + N_C \Gamma_C W_4\} \tag{15}$$

where N_F, N_M, N_S and N_C are numbers which are independent of w_F and l.

So far as all the four terms in the bracket of the right hand side of (15) are roughly of the same order of magnitude, the finite difference expressions of the field and boundary conditions may be considered to be "well-balanced". It should be noted that N_F and (N_M, N_S, N_C) represent essentially sensitivity coefficients of $|| w_F - w ||$ to the field error loads $\Gamma_F W_6 l^2$ and to the boundary error loads $\Gamma_M W_4 l^2$, $\Gamma_S W_S l^2$ and $\Gamma_C W_4 l^2$, respectively. If, for instance,

$$N_F \Gamma_F W_6 << N_M \Gamma_M W_4, \quad N_S \Gamma_S W_5, \quad N_C \Gamma_C W_4 \tag{16}$$

for a region, the influence of the boundary error loads upon the discretization

error is far dominant compared to the influence of the field error loads and it may be more advantageous in practical computation to choose higher accuracy formula for finite difference expressions of boundary equations for a practical range of l.

The crucial point may be demonstrated more clearly by an example for which the influences upon the finite difference solution of the boundary error loads and field error loads can be appraised analytically in a simple form. Consider a rectangular plate simply-supported along $x = 0$ and $x = 1$, clamped along $y = \pm\beta$, and subjected to a distributed load $p(x, y) = p_0 \sin \pi x$. The Levy solution to Eq.(11) may be written as

$$w = \frac{p_0}{\pi^4} \sin \pi x\{1 - C_1 \cosh \pi y - C_2 \pi y \sinh \pi y\} \tag{17}$$

The constants C_1 and C_2 are determined by the boundary conditions along $y = \pm\beta$ as follows:

$$C_1 = \frac{2(\sinh \pi\beta + \pi\beta \cosh \pi\beta)}{2\pi\beta + \sinh 2\pi\beta} \quad , \quad C_2 = -\frac{2 \sinh \pi\beta}{2\pi\beta + \sinh 2\pi\beta}$$

The central deflection is given by

$$w(\tfrac{1}{2}, 0) = p_0(1 - C_1)/\pi^4 \tag{18}$$

When this problem is solved by the system of finite difference equations, $\diamond_{l^2} w_F = p(i, j)$, then the field error loads can be appraised by Eq.(14) and may be reduced to

$$r_F = (1 \quad 4C_2 \cosh \pi\beta)\frac{\pi^2}{6} p_0 l^2 \sin \pi x + O(l^3)$$

An upper bound of the central deflection due to r_F may be estimated as

$$w_{rF}(\tfrac{1}{2}, 0) = \frac{1 - C_1}{\pi^4}(1 - 4C_2 \cosh \pi\beta)\frac{\pi^2}{6} p_0 l^2 + O(l^3) \tag{19}$$

The truncation error of the finite difference boundary equation

$$\frac{\partial w}{\partial y} = \frac{1}{2l}(w_1 - w_{-1})$$

is given by

$$r_B = \frac{l^2}{3}\frac{\partial^3 w}{\partial y^3} + O(l^3)$$

$$= \pm \frac{l^2}{3}\frac{p_0}{\pi}\{(C_1 + 3C_2)\cosh \pi\beta + C_2\pi\beta \sinh \pi\beta\} \sin \pi x + O(l^3)$$

This error may be regarded to represent a forced rotation along $y = \pm\beta$ from the clamped state. The Levy solution to this forced rotation may readily be found and the central deflection due to r_B is bounded by

$$w_{rB}\left(\frac{1}{2}, 0\right) = \frac{2\beta \sinh \pi\beta}{2\pi\beta + \sinh 2\pi\beta}\frac{p_0 l^2}{3\pi}\{(C_1 + 3C_2)\cosh \pi\beta + C_2\pi\beta \sinh \pi\beta\}$$
$$+ O(l^3) \qquad (20)$$

For $\beta = \frac{1}{4}$

$$w_{rF}\left(\frac{1}{2}, 0\right) = 0.00074 p_0 l^2 + O(l^3)$$

$$w_{rB}\left(\frac{1}{2}, 0\right) = 0.042 p_0 l^2 + O(l^3)$$

The ratio $w_{rB}/w_{rF} \cong 57$ indicates how dominant the influence of the boundary error is upon the finite difference solution. The ratio decreases naturally as the length of the clamped sides is decreased. For instance the ratio is about 2.2 for a square plate.

In view of the foregoing discussion, it is apparently advantageous in practical computation to choose a finite difference system such that the discretization error due to the finite difference boundary equations is "well-balanced" with that due to the finite difference field equations. The form of E_W given by Eq.(10) appear to suggest a "well-balanced" set of finite difference equations. If a set of finite difference expressions with truncation errors of $O(l^2)$ are chosen not only for the field equations (9a) but also for the boundary and corner conditions (9b-d), then the virtual works of the error terms at an interior node through virtual displacements $\{\delta u(i, j)\}$ will be of $O(l^4)$, whereas those of the error terms at a boundary node and at a corner are of $O(l^3)$ and $O(l^2)$, respectively. E_W would then be greatly governed by the error terms at boundary nodes and corners. One of possible well-balanced sets of finite difference equations may therefore be defined as that set for which all the error terms not only at interior nodes but also at boundary nodes and at corners in

E_w are of the same order of magnitude, i.e. $O(l^4)$. This implies that the finite difference boundary and corner equations must be such that the truncation errors are of $O(l^3)$ and $O(l^4)$, respectively.

If the rigid boundary conditions

$$\frac{\partial w}{\partial x} \equiv w_{,x} = 0 \quad \text{or} \quad \frac{\partial w}{\partial y} \equiv w_{,y} = 0$$

are to be replaced by a finite difference expression by introducing an imaginary exterior nodal value for w, the truncation error in this case represents an incompatibility of the slope along a boundary. If $w_{,x}$ at a boundary node itself is considered to be an unknown nodal displacement to be set equal to zero exactly, no truncation error will be introduced to the system under consideration. Such a choice, on the other hand, causes a complexity of modifying finite difference field equations in terms of $w_{,x}$ for interior nodes adjacent to a boundary node. If $w_{,x}$, for instance, is to be replaced by a corresponding finite difference expression of $O(l^2)$, the forced rotation due to the truncation error of the finite difference expression would have a far dominant influence on the accuracy of deflections at interior nodes compared to the influence of the field error load. The later example of eliminating the forced rotation illustrates a drastic improvement of the rate of convergence of finite difference solutions.

Eqs.(9b-d) is useful also for discussing possible forms of finite difference boundary and corner equations.

(i) Sor far as no imaginary exterior nodal displacements are introduced into the system, Eqs.(9b-d) in terms of $w_{,x}$ and $w_{,y}$ at boundary nodes and at corners need to be satisfied.

(ii) In place of $w_{,x}$ at a boundary node along x = const., w at an imaginary exterior node adjacent to the boundary node may be "defined" by the finite difference boundary equation, for instance, in the form

$$\frac{\partial w}{\partial x}\Big|_0 = \frac{1}{6l}(-w_2 + 6w_1 - 3w_0 - 2w_{-1}) + O(l^3) \qquad (21)$$

(iii) Each term of Eq.(9b), say, may be required to vanish provided that three further imaginary nodal displacements are defined thereby. If the field equations at a boundary node are replaced by finite difference equations with truncation errors of $O(l^2)$ just as at an interior node, then the truncation errors involved in $\hat{b}_\lambda(i, j) = 0$ need to be of $O(l^3)$ in order to have errors of the same order. The only possible difference of this

procedure from (i) will be that $\hat{b}_\lambda = 0$ can be replaced by non-one-sided finite difference formulae under the sacrifice of introducing additional unknowns.

5. EXAMPLES

It has been well-known [5] that finite difference solutions of a uniformly loaded rectangular plate clamped along the four edges exhibit a considerably poor convergence with respect to mesh length. It is then customary either to increase the number of meshes thus introducing more unknowns, or to apply a higher-accuracy formula [6] to the field equation here by involving a greater number of adjacent nodal pointquantitiesin the finite difference field equations. If a lower-accuracy formula has to be applied anyway at nodes adjacent to a boundary in the latter case, it may be doubtful in view of the foregoing discussion, whether the improvement is really effective in problems involving boundary errors.

When problems involving geometrical and/or material nonlinearity are solved by a successive incremental analysis, the accuracy of a point on a load deflection curve governs the accuracy of subsequent incremental responses, and hence that of a stability limit. In order to illustrate the point in question, the following numerical experiments conducted by A.Kano under the author's suggestion will be helpful.

Fig.2 shows the convergence behaviors of three different classes of finite difference solutions with respect to the mesh length. The numerical result B_2 of $O(l^2)$ has been taken from Tsuboi's book [5] The B_3-curve obtained by A.Kano indicates a drastic improvement gained by applying Eq.(21) for the same system of finite difference equations in [5]. For geometrically and/or materially nonlinear problems, however, the system of finite difference equations **(9a)** is more useful in incorporating the elastic and plastic stiffness matrices. The F_3-curve has been obtained by use of Eqs. **(9a)** for $\rho \to \infty$ and the elastic stiffness matrix. In spite of the lower accuracy of the F_3-curve compared to the B_3-curve, the system of finite difference equations **(9a)** will be used forshells for the convenience of a simpler treatment of stiffness matrices and also for the advantage that the F_3-curve is still considerably better than the B_2-curve.

Fig.3 shows load-central-deflection curves for a clamped circular cylindrical shell obtained by A. Kano by means of the finite difference stiffness matrix method described in the next chapter. The three load-deflection curves for 8, 10 and 12 meshes have been obtained with the use of the finite difference boundary equations of $O(l^2)$ and of $O(l^3)$,respectively. The stability limits

predicted by the finite difference boundary equations of $O(l^2)$ with 8, 10 and 12 meshes are 4.4%, 3.0% and 2.3% less than the corresponding predictions of $O(l^3)$, respectively. Fig.4 shows the convergence behavior with respect to mesh length. Fig.3 and 4 clearly demonstrate the advantage and significance of the use of the higher accuracy formulae for boundary equations.

REFERENCES

[1] See for instance, A. S. Wolmir, "BIEGSAME PLATTEN UND SCHALEN," pp239-252
[2] Miller, J. C. P., "Numerical Quadrature Over a Rectangular Domain in Two or More Dimensions," Part I, J. Math. Computation, Vol. 14, pp13-20, 1960
[3] Forsythe, G. E. and W. R. Wasow, "FINITE-DIFFERENCE METHODS FOR PARTIAL DIFFERENTIAL EQUATIONS,"
[4] Terasawa, K (Ed.), 自然科学者のための数学概論（応用編） Iwanami Shoten, Tokyo, 1960, Ch.4
[5] See for instance, Tsuboi, Y., 平面構造論, Maruzen, Tokyo, 1955, pp117-118 建築弾塑性学（建築学体系 9巻）, Shokokusha, Tokyo, 1955, pp146-150
[6] Collatz, L., "THE NUMERICAL TREATMENT OF DIFFERENTIAL EQUATIONS," 3rd Ed. p382 Springer-Verlag, 1966

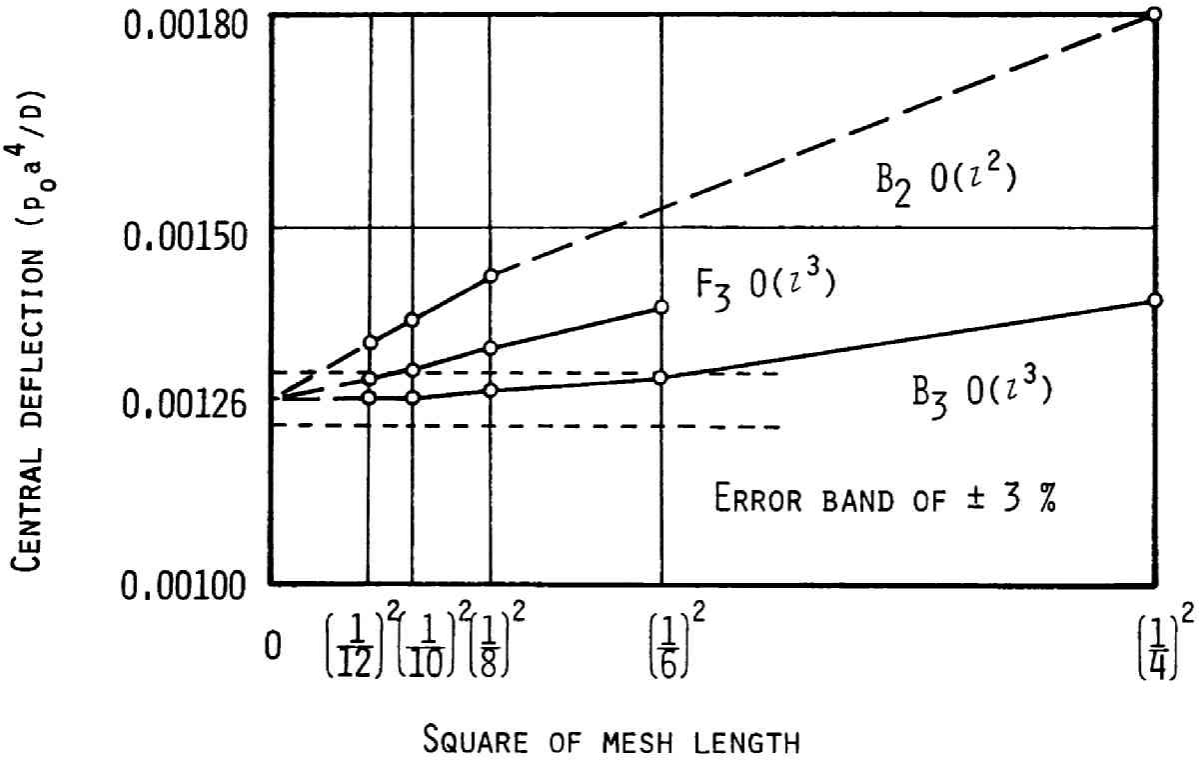

Fig.2 Convergence of finite difference solutions with respect to mesh length (By A. Kano)

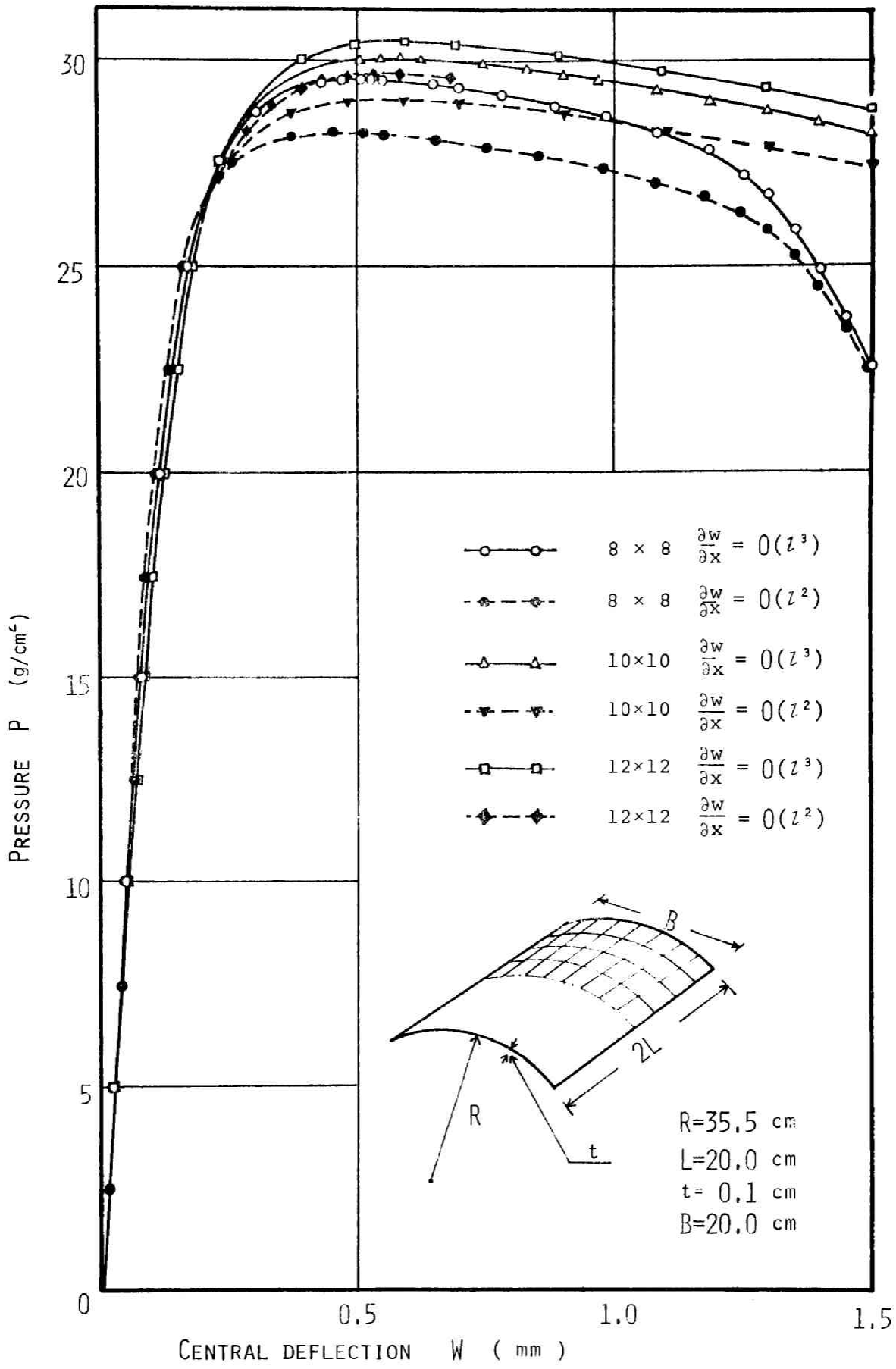

FIG.3 PRESSURE-CENTRAL DEFLECTION CURVES (BY A. KANO)

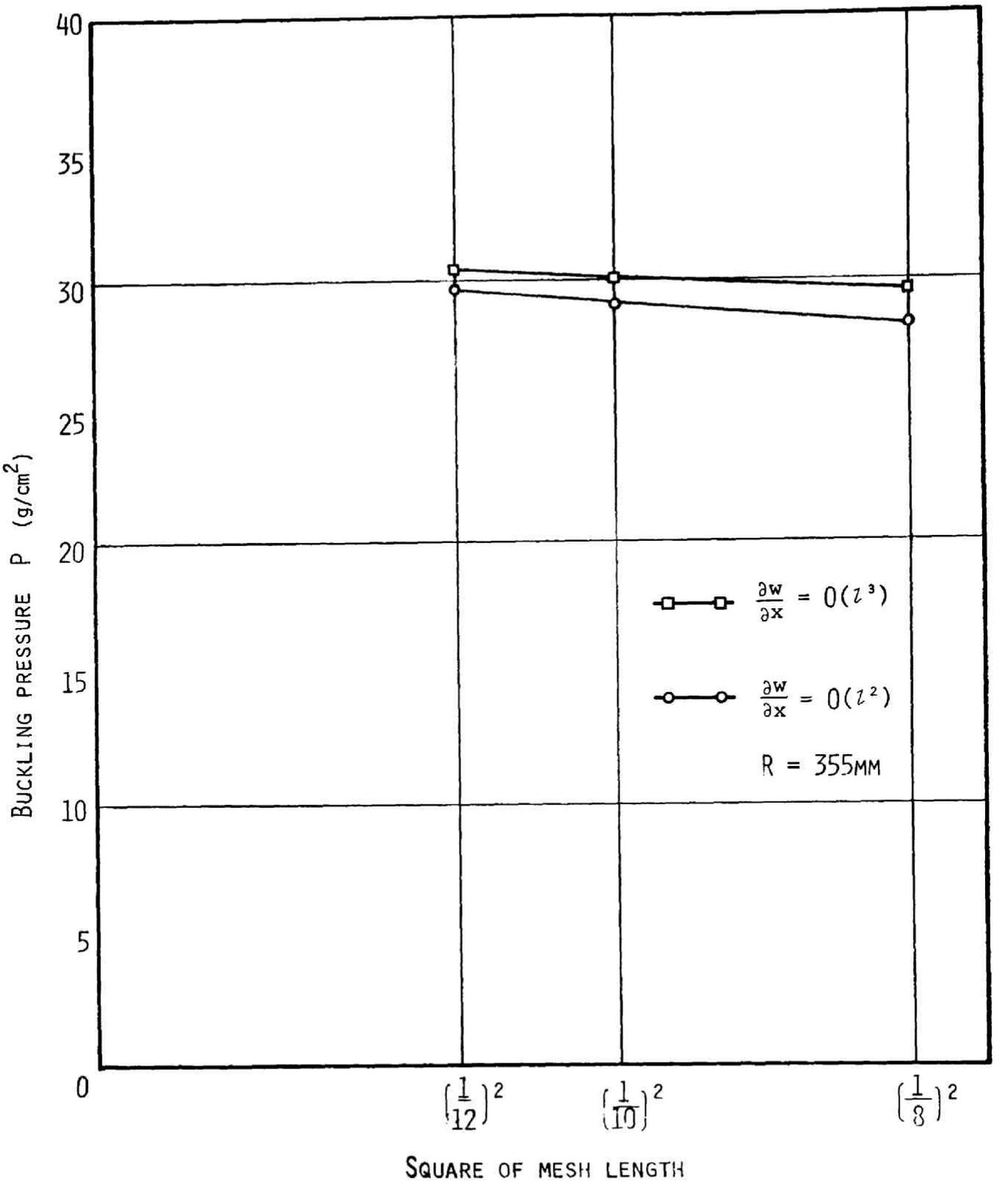

FIG.4 CONVERGENCE OF FINITE DIFFERENCE SOLUTION
(BY A. KANO)

CHAPTER 14
FINITE DIFFERENCE STIFFNESS METHOD FOR ELASTIC-PLASTIC SANDWICH SHELLS

1. INTRODUCTION

Combined geometrically and materially nonlinear problems of plates and shells have been investigated numerically by means of the finite element and finite difference methods during the last few years. The elastic-plastic stiffness matrix concept appears to have been explicitly stated first by Marcal [2] in order to develope a general computational procedure. While Marcal [2] defined the elastic-plastic stiffness matrix as the inverse of the well-known Prandtl-Reuss equation for the von Mises material which can be found numerically, Yamada et al [3] derived an explicit expression for the inverse. The elastic-plastic stiffness matrix for a sandwich plate element has been explicitly derived by Yokoo, Nakamura and Mori [4] Various general formulations have been proposed by Zienkiewicz et al [5] and others [1].

The equations of equilibrium, kinematic relations and elastic-plastic stiffness matrix are all nonlinear involving current values of displacements and generalized stress resultants. In applying any numerical method of an incremental nature as an initial value problem, it is essential that the numerical result at each incremental step has a sufficient accuracy in order not to accumulate propagating errors. For this purpose it is necessary first to have a sufficiently accurate spatial simulation of the original system by means of either finite differnce or finite element methods and secondly to apply, for instance, the Newton mehtod or overrelaxation method to the "exact" incremental equations which retain squares of incremental quantities. The first problem has been the primary motivation for developing the "well-balanced" finite difference system in chapter 13. The second point is essential in correcting successive predictions so as to decrease the errors involved in the incremental procedure within a sufficiently small tolerance limit besides the discretization errors in the spatial simulation.

In this chapter, the elastic-plastic stiffness matrices are first derived for an idealized sandwich shell element in an explicit form. The stiffness matrices may be reduced to the known matrices for plane-stress problems [3] and for plate-bending problems [4] The incremental equations

are summarized in a form in which squares of incremental quantities can be observed explicitly and to which the well-known over-relaxation method [6] can be applied directly. Some of the numerical results due to A. Kano have been shown in Ch.13. Some of the numerical results which have been obtained by Y. Yokoo, T. Mori and the present author will be referred to in the Appendix to this chapter.

2. ELASTIC-PLASTIC STIFFNESS MATRIX FOR A SANDWICH SHELL

The von Mises yield condition for a perfectly plastic shell element has been derived in chapter 11. Similarly, the loading function of the von Mises type for a work-hardening or strain-hardening sandwich shell element may be written as

$$
\begin{aligned}
&F(n_x, n_y, n_{xy}, m_x, m_y, m_{xy}) \\
&=(n_x + m_x)^2 \quad (n_x + m_x)(n_y + m_y) + (n_y + m_y)^2 \\
&\quad + 3(n_{xy} + m_{xy})^2 - f_{eq}{}^2 = 0 \\
&G(n_x, n_y, n_{xy}, m_x, m_y, m_{xy}) \\
&=(n_x \quad m_x)^2 \quad (n_x \quad m_x)(n_y \quad m_y) + (n_y - m_y)^2 \\
&\quad + 3(n_{xy} \quad m_{xy})^2 \quad g_{eq}{}^2 = 0
\end{aligned}
\tag{1a,b}
$$

where f_{eq} and g_{eq} denote the dimensionless equivalent stresses of the lower and upper flanges, respectively. If both flanges are in the plastic region, the associated flow law may be written as

$$
\begin{Bmatrix} d\varepsilon_x^P \\ d\varepsilon_y^P \\ d\varepsilon_{xy}^P \\ d\kappa_x^P \\ d\kappa_y^P \\ d\kappa_{xy}^P \end{Bmatrix} = d\lambda \begin{Bmatrix} 2(n_x + m_x) & (n_y + m_y) \\ 2(n_y + m_y) & (n_x + m_x) \\ 6(n_{xy} + m_{xy}) & \\ 2(n_x + m_x) & (n_y + m_y) \\ 2(n_y + m_y) & -(n_x + m_x) \\ 6(n_{xy} + m_{xy}) & \end{Bmatrix} + d\mu \begin{Bmatrix} 2(n_x - m_x) & -(n_y - m_y) \\ 2(n_y \quad m_y) & -(n_x - m_x) \\ 6(n_{xy} \quad m_{xy}) & \\ -2(n_x - m_x) & +(n_y - m_y) \\ -2(n_y - m_y) & +(n_x - m_x) \\ -6(n_{xy} - m_{xy}) & \end{Bmatrix}
\tag{2}
$$

which may be compactly written as

$$
\begin{Bmatrix} d\varepsilon^P \\ \hline d\kappa^P \end{Bmatrix} = d\lambda \begin{Bmatrix} f \\ \hline f \end{Bmatrix} + d\mu \begin{Bmatrix} g \\ \hline -g \end{Bmatrix}
\tag{3}
$$

where

$$\mathbf{f} \equiv \begin{Bmatrix} f_1 \\ f_2 \\ f_3 \end{Bmatrix} = \begin{Bmatrix} 2(n_x + m_x) & (n_y + m_y) \\ 2(n_y + m_y) & (n_x + m_x) \\ 6(n_{xy} + m_{xy}) & \end{Bmatrix} \qquad \text{and}$$

$$\mathbf{g} \equiv \begin{Bmatrix} g_1 \\ g_2 \\ g_3 \end{Bmatrix} = \begin{Bmatrix} 2(n_x - m_x) & (n_y \quad m_y) \\ 2(n_y - m_y) & (n_x \quad m_x) \\ 6(n_{xy} - m_{xy}) & \end{Bmatrix} \qquad (4a,b)$$

As may be seen from Eqs.(1a,b), the lower and upper flanges are in the state of plane stress. The definition of the equivalent or effective plastic strain increments in three dimensions leads to the following expressions for the lower and upper flanges, respectively:

$$de_f = \sqrt{\frac{2}{3}} \left[(d\varepsilon_x^P + d\kappa_x^P)^2 + (d\varepsilon_y^P + d\kappa_y^P)^2 + (d\varepsilon_x^P + d\kappa_x^P + d\varepsilon_y^P + d\kappa_y^P)^2 + 2\{\tfrac{1}{2}(d\varepsilon_{xy}^P + d\kappa_{xy}^P)\}^2 \right]^{\frac{1}{2}}$$

$$de_g = \sqrt{\frac{2}{3}} \left[(d\varepsilon_x^P \quad d\kappa_x^P)^2 + (d\varepsilon_y^P \quad d\kappa_y^P)^2 + (d\varepsilon_x^P \quad d\kappa_x^P + d\varepsilon_y^P - d\kappa_y^P)^2 + 2\{\tfrac{1}{2}(d\varepsilon_{xy}^P \quad d\kappa_{xy}^P)\}^2 \right]^{\frac{1}{2}} \qquad (5a,b)$$

Substitution of Eq.(2) into (5a,b) provides

$$d\lambda = \frac{de_f}{4f_{eq}} \quad , \qquad d\mu = \frac{de_g}{4g_{eq}} \qquad (6a,b)$$

The plastic work done per unit area of the middle surface is given by

$$\begin{aligned} dw^P &= (n_x + m_x)(d\varepsilon_x^P + d\kappa_x^P) + (n_y + m_y)(d\varepsilon_y^P + d\kappa_y^P) + (n_{xy} + m_{xy})(d\varepsilon_{xy}^P + d\kappa_{xy}^P) \\ &\quad + (n_x - m_x)(d\varepsilon_x^P - d\kappa_x^P) + (n_y \quad m_y)(d\varepsilon_y^P + d\kappa_y^P) + (n_{xy} \quad m_{xy})(d\varepsilon_{xy}^P - d\kappa_{xy}^P) \\ &= 4f_{eq}^2 d\lambda + 4g_{eq}^2 d\mu \\ &= f_{eq}\, de_f + g_{eq}\, de_g \end{aligned} \qquad (7)$$

If the lower flange is in the plastic region and the upper flange remains in the elastic state, $d\mu=0$ and Eqs.(4a),(5a),(6a) should be applied together with $de_g=0$ in Eq.(7), and vice versa.

The total strain increment consists of the elastic and plastic strain increments:

$$\left\{ \begin{array}{c} d\boldsymbol{\varepsilon} \\ \hline d\kappa \end{array} \right\} = \left\{ \begin{array}{c} d\boldsymbol{\varepsilon}^e \\ \hline d\kappa^e \end{array} \right\} + \left\{ \begin{array}{c} d\boldsymbol{\varepsilon}^P \\ \hline d\kappa^P \end{array} \right\} \tag{8}$$

The elastic strain increment is related to the stress increment by the elastic stiffness matrix

$$\left\{ \begin{array}{c} dn_x \\ dn_y \\ dn_{xy} \\ dm_x \\ dm_y \\ dm_{xy} \end{array} \right\} = D^e \left\{ \begin{array}{c} d\varepsilon_x^e \\ d\varepsilon_y^e \\ d\varepsilon_{xy}^e \\ d\kappa_x^e \\ d\kappa_y^e \\ d\kappa_{xy}^e \end{array} \right\} = C \left[\begin{array}{ccc:ccc} 1 & \nu & 0 & & & \\ \nu & 1 & 0 & & \mathbf{0} & \\ 0 & 0 & \frac{1-\nu}{2} & & & \\ \hdashline & & & 1 & \nu & 0 \\ & \mathbf{0} & & \nu & 1 & 0 \\ & & & 0 & 0 & \frac{1-\nu}{2} \end{array} \right] \left\{ \begin{array}{c} d\varepsilon_x^e \\ d\varepsilon_y^e \\ d\varepsilon_{xy}^e \\ d\kappa_x^e \\ d\kappa_y^e \\ d\kappa_{xy}^e \end{array} \right\} \tag{9}$$

where

$$C = \frac{E}{\sigma_o(1 - \nu^2)} \tag{10}$$

For the later convenience, Eq.(9) is written as

$$\left\{ \begin{array}{c} d\mathbf{n} \\ \hline d\mathbf{m} \end{array} \right\} = C \left[\begin{array}{c:c} A & 0 \\ \hline 0 & A \end{array} \right] \left\{ \begin{array}{c} d\boldsymbol{\varepsilon}^e \\ \hline d\kappa^e \end{array} \right\} \tag{11}$$

Substitution of (3) and (8) into (9) furnishes

$$\left\{ \begin{array}{c} d\mathbf{n} \\ \hline d\mathbf{m} \end{array} \right\} = C \left[\begin{array}{c:c} A & 0 \\ \hline 0 & A \end{array} \right] \left\{ \begin{array}{c} d\boldsymbol{\varepsilon} \\ \hline d\kappa \end{array} - \begin{array}{c} \mathbf{f} d\lambda - \mathbf{g} d\mu \\ \hline \mathbf{f} d\lambda + \mathbf{g} d\mu \end{array} \right\} \tag{12}$$

Differentiation of Eqs.(1a,b) yields

$$\left. \begin{array}{l} \{ \mathbf{f}^T \,\vdots\, \mathbf{f}^T \} \left\{ \begin{array}{c} d\mathbf{n} \\ \hline d\mathbf{m} \end{array} \right\} = 2 f_{eq}\, df_{eq} \\ \{ \mathbf{g}^T \,\vdots\, -\mathbf{g}^T \} \left\{ \begin{array}{c} d\mathbf{n} \\ \hline d\mathbf{m} \end{array} \right\} = 2 g_{eq}\, dg_{eq} \end{array} \right\} \tag{13a,b}$$

Substitution of (12) into (13a,b) provides

$$\{ \mathbf{f}^T A \,\vdots\, \mathbf{f}^T A \} \left\{ \begin{array}{c} d\boldsymbol{\varepsilon} \\ \hline d\kappa \end{array} \right\} - 2\mathbf{f}^T A \mathbf{f} d\lambda = 2\left(\frac{H'_f}{C}\right) f_{eq}\, de_f$$

$$\{\ g^T A\ \vdots\ -g^T A\ \}\left\{\begin{array}{c} d\varepsilon \\ \hline d\kappa \end{array}\right\} - 2g^T A g d\mu = 2\left(\frac{H'_g}{C}\right) g_{eq}\, de_g \qquad \Big\} \quad (14a,b)$$

where

$$H'_f = \frac{df_{eq}}{de_f} \qquad \text{and} \qquad H'_g = \frac{dg_{eq}}{de_g} \qquad (15a,b)$$

represent the slopes of the equivalent stress-plastic strain curves. The right hand sides of Eqs.(14a,b) may be expressed in terms of $d\lambda$ and $d\mu$, respectively by the use of Eqs.(6a,b). The following expressions may then be obtained for $d\lambda$ and $d\mu$.

$$d\lambda = \psi_f\{\ f^T A\ \vdots\ f^T A\ \}\left\{\begin{array}{c} d\varepsilon \\ \hline d\kappa \end{array}\right\}, d\mu = \psi_g\{\ g^T A\ \vdots\ -g^T A\ \}\left\{\begin{array}{c} d\varepsilon \\ \hline d\kappa \end{array}\right\} \quad (16)$$

where the scalars ψ_f and ψ_g are defined, respectively, by

$$\psi_f = \frac{1}{2[f^T A f + 4f_{eq}{}^2 H'_f/C]} \quad , \quad \psi_g = \frac{1}{2[g^T A g + 4g_{eq}{}^2 H'_g/C]} \qquad (17)$$

The desired elastic-plastic stiffness matrix may be obtained by substituting (16) into (12).

$$D_{LU} = D^e P_{LU}$$

where

$$P_{LU} = \left[\begin{array}{c|c} I - \psi_f f f^T A - \psi_g g g^T A & -\psi_f f f^T A + \psi_g g g^T A \\ \hline -\psi_f f f^T A + \psi_g g g^T A & I - \psi_f f f^T A - \psi_g g g^T A \end{array}\right] \qquad (18a)$$

I denotes 3×3 identity matrix. P_{LU} represents the reduction of stiffness in the plastic range and therefore will be called a reduction coefficient matrix. If the lower flange only or the upper flange only is in the plastic range, the reduction coefficient matrices of the elastic-plastic stiffness matrices are given respectively by

$$P_L = \left[\begin{array}{c|c} I - \psi_f f f^T A & -\psi_f f f^T A \\ \hline \psi_f f f^T A & I - \psi_f f f^T A \end{array}\right] \qquad (18b)$$

$$P_U = \left[\begin{array}{c|c} I - \psi_g g g^T A & \psi_g g g^T A \\ \hline \psi_g g g^T A & I - \psi_g g g^T A \end{array}\right] \qquad (18c)$$

For a sandwich plate in the state of plane stress, D_{LU} is reduced to the known matrix given explicitly by Yamada et al [3]. It should,

however, be noted that $m_x=m_y=m_{xy}=0$ implies only f=g and hence that the non-diagonal submatrices of P_{LU} may not necessarily vanish unless $\psi_f=\psi_g$ or $f_{eq}=g_{eq}$ and $H'_f=H'_g$. Similarly, for a sandwich plate under bending only, $n_x=n_y=n_{xy}=0$ and hence g=-f Again the non-diagonal submatrices of P_{LU} may not vanish unless $f_{eq}=g_{eq}$ and $H'_f=H'_g$ and therefore $d\varepsilon$ may not be identically zero.

3. SUCCESSIVE OVERRELAXATION

Various methods of nonlinear numerical analysis have been applied to shell structures. The purpose of the present section is to demonstrate the procedure of applying the well-known over relaxation method [6] to the nonlinear shell analysis and of incorporating the elastic-plastic stiffness matrices (18a,b,c) and the well-balanced finite difference boundary equations proposed in chapter 13. The nonlinear system consists of the finite difference equations of equilibrium at interior and boundary points, the finite difference kinematic relations and the elastic-plastic stiffness matrices.

Let L_x, L_y, L_{xx}, L_{xy} and L_{yy} denote symbolically finite difference operators corresponding respectively to

$$\frac{\partial}{\partial x}\ ,\quad \frac{\partial}{\partial y}\ ,\quad \frac{\partial^2}{\partial x^2}\ ,\quad \frac{\partial^2}{\partial x \partial y} \text{ and } \frac{\partial^2}{\partial y^2}\ .$$

The value of a field quantity F at the end of the k-th incremental step is denoted by $F_{,k}$. Let $\Delta_\kappa F$ denote the increment of F in the k-th incremental step from $F_{,k-1}$, *i.e*

$$F_{,k} = F_{,k-1} + \Delta_\kappa F$$

The incremental equations of equilibrium for a circular cylindrical sandwich shell may readily be derived from Eq.(XIII-3) and written in the following matrix form

$$\begin{bmatrix} L_x & 0 & L_y & 0 & 0 & 0 \\ 0 & L_y & L_x & 0 & 0 & 0 \\ 2L_{xx}(w_{,k-1}+\Delta_\kappa w) & 2L_{yy}(w_{,k-1}+\Delta_\kappa w)+\frac{1}{h\rho} & 4L_{xy}(w_{,k-1}+\Delta_\kappa w) & hL_{xx} & hL_{yy} & 2hL_{xy} \end{bmatrix} \left\{ \begin{matrix} \Delta_\kappa n \\ \hline \Delta_\kappa m \end{matrix} \right\}$$

$$= \begin{Bmatrix} 0 \\ 0 \\ 2n_{x,k-1}L_{xx}\Delta_\kappa w + 2n_{y,k-1}L_{yy}\Delta_\kappa w + 4n_{xy,k-1}L_{xy}\Delta_\kappa w \end{Bmatrix}$$

The finite difference boundary equations must also be included. The constitutive equations may be summarized as

$$\left\{ \begin{array}{c} \Delta_K n \\ \hline \Delta_K m \end{array} \right\} = \bar{D} \left\{ \begin{array}{c} \Delta_K \varepsilon \\ \hline \Delta_K \kappa \end{array} \right\} \tag{20}$$

where $\bar{D}=D^e$, D_{LU}, D_L or D_U. The incremental kinematic relations can also be written in the following matrix form

$$\left\{ \begin{array}{c} \Delta_K \varepsilon \\ \hline \Delta_K \kappa \end{array} \right\} = T \left\{ \begin{array}{c} \Delta_K u \\ \Delta_K v \\ \Delta_K w \end{array} \right\} \tag{21}$$

where

$$T = \left[\begin{array}{ccc} hL_x & 0 & h^2\{(L_x w_{,k-1})L_x + \frac{h^2}{2}(L_x \Delta_K w)L_x\} \\ 0 & hL_y & h^2\{(L_y w_{,k-1})L_y + \frac{h^2}{2}(L_y \Delta_K w)L_y - \frac{1}{h\rho}\} \\ \frac{h}{2}L_y & \frac{h}{2}L_x & \frac{h^2}{2}\{(L_x w_{,k-1})L_y + (L_y w_{,k-1})L_x + \frac{1}{2}(L_x \Delta_K w)L_y + \frac{1}{2}(L_y \Delta_K w)L_x \\ 0 & 0 & -\frac{h^2}{2}L_{xx} \\ 0 & 0 & -\frac{h^2}{2}L_{yy} \\ 0 & 0 & -\frac{h^2}{2}L_{xy} \end{array} \right] \tag{22}$$

The nonlinear system defined symbolically by Eqs.(19,22) must further be written in terms of nodal quantities in actual computational operation.

Since the coefficient matrices in Eqs.(19) and (22) involve the current incremental values $\Delta_K w$, an iterative procedure is necessary within the k-th incremental step. For this purpose $\Delta_K w$ in the coefficent matreces are replaced by $\Delta_{K,r-1} w$ when $\Delta_{K,r} w$ are computed with the starting value $\Delta_{K,0} w=0$. When $|\Delta_{K,r} w - \Delta_{K,r-1} w| \;/\; |w_{k-1}| < \delta$, a small positive number, $\Delta_{k,r} w$ is regarded as $\Delta_K w$ and the k-th incremental step is regarded to be finished. The numerical result shown in Fig.3 and 4 in Chapter 13 has been obtained by the procedure described above.

REFERENCES

[1] Marcal,P.V., "Finite Element Analysis of Combined Problems of Nonlinear Material and Geometric Behavior" *Proc. ASME Conference on "Computational Approaches in Applied Mechanics,"* June 1969, pp133-

[2] Marcal,P V., "A Stiffness Method for Elastic-plastic Problems" *Int. J. Mech. Sci., Vol.7* (1965), pp229-238

[3] Yamada.Y., N.Yoshimura and T.Sakurai, "Plastic Stress-strain Matrix and its Application for the Solution of Elastic-plastic Problems by the Finite Element Method," *Int. J. Mech. Sci., Vol.10* (1968) pp343-354

[4] Yokoo,Y., T. akamura and T.Mori, "Numerical Analysis of Elastic-plastic Deformation of Simply-supported Rectangular Plates," *Trans. A.I.J., No.152,* Oct. 1968

[5] Zienkiewicz, O.C., S.Valliappan and I.P.King, "Elasto-plastic Solutions of Engineering Problems 'Initial Stress', Finite Element Approach," *Int. J. Numerical Meth. Engng., Vol.1* (1969) pp75-100

[6] See for instance, W.F.Ames, "NONLINEAR PARTIAL DIFFERENTIAL EQUATIONS IN ENGINEERING," Academic Press, 1965 New York, pp284-287,344,378

APPENDIX

A numerical analysis of elastic-perfectly plastic rectangular plates simply supported along the four straight boundaries have been conducted by T. Mori [4] under the author's suggestion, based upon the infinitesimal deformation theory. Fig. 1 shows the convergence behavior of the load-deflection curves with respect to mesh length. Fig.2 shows a comparison of plastic mesh points in the three different finite difference solutions prevailed under the two same load levels. The concept of the "solution surface" has been introduced in Ch.11, p224. Fig. 3 shows the variations of the solution surface for different uniform load levels.

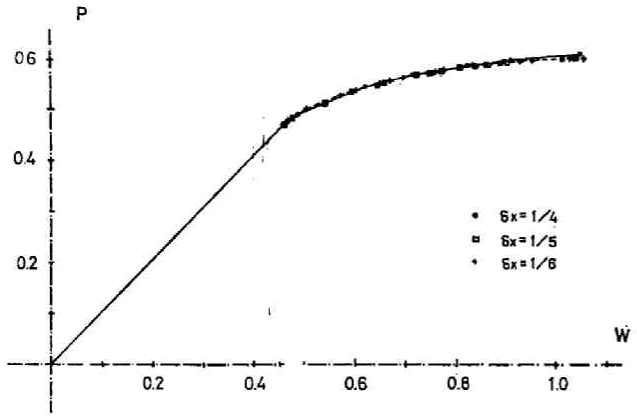

Fig.1 Load-central deflection curves.

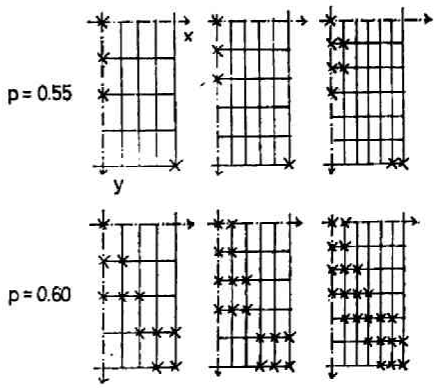

Fig.2 Plastic mesh points at different load levels.

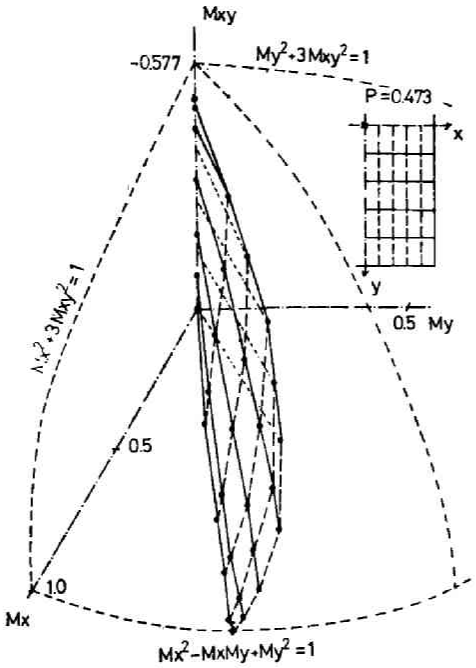

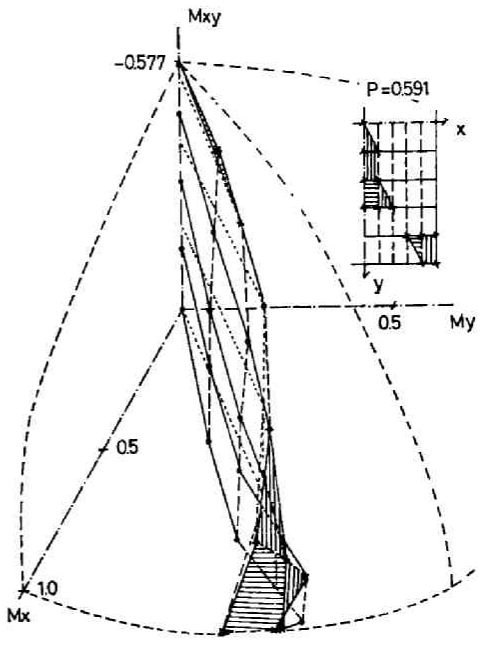

Fig.3 Variation of the solution surface

構造物の弾塑性解析法（要約）

中村恒善

本論文は、4部14章から成り、梁、柱、骨構造系、平面板曲面板構造に対して それぞれ有用な弾塑性解析法、塑性設計法、および塑性解析法を提示している。第1章を除く各章の内容は、第 頁中1表に示したように、構造物の種類、材料の性質の理想化の仕方、たわみが微小か有限かによって 4種類に分類され、各部を構成している。第2，3，4，5，7，8，9，10，11章は、それぞれ既に発表した原著論文に基き、第6章はその梗概のみ発表されたものである。また 第12，13および14章もそれぞれ、かなりの、または若干の新しい結果を含んでいる。

本研究において提案されている種々の弾塑性解析法、塑性設計法、塑性解析法は次の二種類の近似解析手法の いづれも またはいづれかに基いている。即ち、(1) 梁 柱の断面のみならず、平面板曲面板構造の断面も 理想化サンドウィッチ断面に「モデル化」する方法と，(2)降伏条件を、断片的にexplicitに解析表現された近似降伏条件によって置きかえる方法とである。

第1章は序説であって、まず荷重変位挙動の解析を引用して 広義の塑性強度の所謂静的塑性設計上の意義を説明し、次にそれが、一つの構造物の系全体としての靭性（Overall Structural Toughness）において占める役割を明示し、種々の二次効果を含む、より精確な弾塑性解析法、塑性設計法、塑性解析法の必要性と重要性とを指摘している。一つの構造物の、系全体としての延性(ductility)は、それがその系内で大きな塑性変形を経験しつつも破断することなく、系として大変位を経験し得る能力と定義されるのに対して、 その系全体としての靭性（toughness）は それが崩壊または終局状態に達する迄に、その塑性域において大量のエネルギーを吸収し得る能力を表わす言葉と定義される。後者は、その構造物の変位の進行過程における荷重支持能力（広義の塑性強度）によって大きく支配される。故に一つの系の全体的構造靭性の特質を解明するためには、大たわみ域における幾何学的非線型効果を含む弾塑性解析が必要である事を指摘している。次に、塑性強度に影響する諸因子を考慮した弾塑性解析法、塑性設計法、塑性解析法の諸分野の概要を述べ 最後に本研究の範囲と、内容の概要とを述べている。

第1部は第2～5章から成り、完全塑性に理想化された曲げモーメント－曲率関係式で支配される棒材から成る複雑な構造系の荷重支持挙動の解明と、塑性設計法の提示がなされている。

第2章においては、Foulkesの線型最小重量設計理論を高層架構に適用し　その一般解が、適当な制限範囲内の実用的な高層架構に対して、簡潔且explicitな解析表現で与えられる事を示した。この際、「構モーメント」と称する新しい概念の導入が、線型計画法のシンプレックス法による解析的解の誘導を容易ならしめた。得られた解において注目される事は　最も一般的解(10)式によれば　最小スパン長以外の梁はそれぞれの梁間の鉛直荷重を主として支持するように、また最小スパン長の梁とこれらに連結する柱は、層せん断力の殆部をすべて支持するように設計される事が要求される点にある。

第3章においては、第2章の結果を修正して、実用的な初期設計を求める手続を提案している。一つの高層架構に対する第2章の方法による解では各部材の全塑性モーメントのみが割当てられている。これをまず、微小変形理論の範囲内で軸方向力と曲げモーメントの相関降伏条件を満足するように部材断面を決定し　更に弾塑性大たわみに際して生ずる附加モーメントに対して　断面増強を行なう。このように修正設計された架構が、確かに所定の静的置換荷重を支持し得る事、および系全体としての構造靱性を保有することを確かめ　そして確かめた結果修正の必要ある時は修正手続を行なうために、弾－塑性ヒンジ剛性マトリックスも有用である事を述べている。この逐次修正過程を　一つの数的問題として視覚化し、1及び2荷重係数の場合についてその取扱方法を述べている。その計算例は第3章附録に示されている。

第4章においては、矩形ラーメンの別のクラスとして　所謂フィーレンデールラーメンに対して　Foulkes理論に基く最小重量設計方法を展開し　その種々の解を解析的に求めている。外的単純支持の場合には　最小化過程では静定問題に帰せられるのに対して、外的に両端固定の場合には、固定端鉛直反力に関する最小化が必要であってこの際、新たに定義された「形状関数」が重要な役割を果す事が示された。また　系全体を固定梁と見なした時の固定端モーメントに相当する反力に対しては、部材軸力を考慮した上で最小重量設計を論じなければならない事を示した。

第5章においては、非線型計画のGradient Projection Methodをトラス、ラーメンの弾塑性解析に適用する方法が提示され　等価定理のより完全な証明が行なわれている。r次の不静定構造物がS個の荷重係数で指定される荷重群の作用をうける際の、いかなる応力状態も　S個の荷重群の各々に対する弾性理論解と　自己釣合状態を表わす無荷重時のr個の独立な解の一次結合の形で表現され得る。これらの(r+S)個のパラメータをPragerの意味で正規直交化した(r+S)個の基準状態に対する倍数の形に変換すれば　任意の応力状態は　Pragerの応力空間内において　降伏条件を表わす超多面体の内部の1点として視覚化され得る。S個の荷重係数の変化に対応する応答の追跡は、Greenbergの定理により　各瞬間に2次の微分形式を最小ならしめる問題に帰せ

られる。Gradient Projection Methodの特徴は、最大値に到達するために、凸領域の内部を目的関数の勾配最大の方向に横切って進む過程にあるので　上の問題を解くのに適している事が　等価定理の証明の形で示されている。トラス、ラーメンの応答追跡、Shakedown問題の解法　安全荷重域の求め方が　計算例によって詳細に説明されている。

第II部においては　歪硬化の影響を考慮して材料性質の理想化が行なわれた場合の、繰返荷重に対する弾塑性解析法が、梁　柱について提案されている。現象の本質を説明し得る剛塑解が解析的に得られるように　断面のサンドウィッチモデル化が試みられている。

第6章では、最も単純な歪硬化法則として線型履歴歪硬化関係式を用いた場合の柱　梁のための弾塑性解析法を提示している。サンドウィッチ理想化の長所として　軸力と曲げモーメントの相関降伏条件が応力平面上で正方形に視覚化されると同時に、各部フランジの応力状態も同一応力平面上で視覚化され得る事を示し　従って　柱全体の応力状態の変遷が応力平面上で応力経路と呼ばれる曲線の変動として視覚られる事を示している。次に　曲げモーメント曲率関係式が軸力を含む断片的にexplicitな表現で与えられる事を示し　これを片持柱の大たわみ解析に用いている。変動または一定鉛直力と繰返水平力の作用をうける片持柱について　各弾塑性変形段階毎に剛塑完全解が求められる事を示し　また計算結果を例示している。

第7，8，9章においては、実験的研究の結果に基いて　より現実的な歪硬化法則を誘導し　それを用いた梁の定常繰返塑性曲げ問題の近似解法を提示している。まず第7章では　他の研究者との協同研究により得られた梁の繰返塑性曲げ試験結果をまとめている。主な3特徴としては、(1)定変位振巾両振曲げ試験においては　荷重変位曲線と、対応する歪分布が数サイクルのうちに定常応答に収束し　フランジは第1近似としては　ほぼ等しい定歪振巾の引張圧縮をうけるものと見なされること、(2)異なる製造単位からの同様のSS41型鋼梁が明らかに異なる曲げ塑性疲労特性を示した事(3)初期定常状態の1サイクル間に消費されたエネルギーは　両対数紙上で塑性変位振巾と線型関係にあること等が挙げられる。

第8章には、第7章の実験に用いたH型鋼材のフランジについて　定歪振巾引張圧縮両振塑性疲労試験を行なった結果をまとめ　その際得られた履歴応力歪関係図によく合う履歴応力歪関係式並びに　それとは明瞭に区別さるべき骨格応力歪関係式をRamberg-Osgood式を修正した形で導いている。

第9章においては、第6章とは別に非線型歪硬化法則に適した等価サンドウィッチ断面を定義し　これに基く定常状態理論を提案している。第1近似としてのその理論が、

交番強制変位を課せられるH型鋼梁が定常状態荷重変位挙動をかなりの精度で予測し得る事を、数値計算結果と第7章の実験結果との比較により例証している。更に、この理論が一定常履歴サイクル当りの消費塑性エネルギーもかなりの精度で評価し得る事も示している。

第III部においては、剛塑性曲面板構造の微小変形理論に基く極限解析法と、有限たわみ理論に基く塑性解析法とが提示されている。

第10章では、中実断面を有する回転殻が軸対称荷重を受ける場合の極限解析法がまとめられている。トレスカの降伏条件に対応するような6個の放物型超曲面から成る近似降伏超曲面を提示し、それが上界1に対して下界0.851迄精度を向上させ得ることと、その各構成超曲面について一般解が容易に得られるという利点を有する事が示されている。種々の子午線形状を有する曲面板についてその一般解が初等関数のみで表現され得る事を示している。例として、自由内周縁に沿って線荷重の作用をうける外周縁固定の円錐殻を取扱い、その数値計算結果を図示している。

第11章では、従来二層トラスエレメントに用い得る解法の開発と一般非軸対称殻に対する近似解法のために、サンドウィッチ断面を有する一般の非軸対称殻の極限解析法を展開している。まず表板がミゼスの降伏条件に従う完全塑性材料で構成されているとして、6個の断面力で表現される微要素降伏条件式が導かれている。この降伏条件は幾何学的には2次の超曲面を表わすが、いずれの部分に対しても速度に関する方程式と釣合式の間の連成が避けられる事が示された。この降伏条件と対応する流動法則が、偏平殻に適用されるとき結局法線変位に関する単一の偏微分方程式が導かれる。その解の一例として、楕円境界を有する偏平ハイパボリックパラボロイド曲面板が等分布荷重を受ける場合の崩壊荷重係数の上界を求めた。更に崩壊荷重係数の上界計算が不連続速度場の考慮によって単純化される事も示されている。その例として扇形の偏平放物筒殻が等分布荷重をうける場合の崩壊荷重係数の上、下界を求める手続を示し、数値計算例により、その上界下界がライズに関してどのように変化するかを示している。第11章の引用は、偏平放物筒殻の崩壊荷重の上、下界が、形状パラメータに関して如何に変化するかを数値計算した松井の結果を引用している。

第12章においては、第10章、第11章の理論の利点が、たわみ解析においてもほぼ適用される事を指摘している。軸対称殻では、第10章の一般解を求める手続を拡張して、大たわみ域でも一般解の閉型解析表現が得られる事を示している。更に一般非軸対称サンドウィッチ殻についても、第11章におけると同じく、単一の法線変位に関する偏微分方程式が誘導され得る事を示している。

第IV部においては　一般非軸対称殻の数値弾塑性解析法のうち差分法の適用に際して実用上有効な方法を開発し　その際必要な　弾塑性剛性マトリックスが、サンドウィッチ殻ではexplicitな表現で与えられる事を示している。

第13章では、まず　よく知られた仮想仕事式に　閉じた型のNewton-Cotesの数値積分公式を適用すれば　内部格子点のみならず　境界格子点についても、妥当な差分表現が誘導できる事を示している。従来の自由境界点に対する差分公式の適用方法の再解釈と　少ない格子点数で差分解の精度を向上させる方法とを提示している。その例証として著者の示唆の下に叶の行なった数値実験結果によれば、境界方程式の差分精度の向上によって　坪井の著書に引用されている周辺固定正方形板の差分計算結果に比較してはるかに良好な結果が得られる事を示している。また同じく　叶による　周辺固定円筒曲面板の非線型解析結果を援用して　曲げ変形の卓越してくる非線型変形域では　このような境界方程式の差分精度の影響が著るしく従って座屈荷重の精度も影響をうける事を指摘している。

第14章では　まず、サンドウィッチ殻に対する弾塑性マトリックスのexplicitな表現を導き、それが面内変形に対しては山田らの平面応力問題の弾塑性剛性マトリックスに帰せられる事　面内力のない曲げ問題では　[illegible]に帰せられる事を指摘している。最後によく知られたCut-relaxationほのこの弾塑性解析問題への適用方法をまとめている。第13章の叶の数値計算はこの方法による結果である。また第14章附録には　曲げのみをうける長方形平板の弾塑性解析を著者の指示に基いて行なった森の数値計算結果の一部が示されている。

PUBLICATIONS BY THE AUTHOR

PAPERS

TITLES	*JOURNALS*	*VOL.NO.*	*YEAR,MO.*
1. On General Yield Conditions for Shells	Trans. A. I. J.	No.60	1958.10.
2. Limit Analysis of a Spherical Shell Subjected to a Concentrated Load	Trans. A. I. J.	No.60	1958.10.
3. Limit Analysis of Grids	Trans. A. I. J.	No.61	1959. 2.
4. The Load Carrying Capacity Characteristics of Arches under Uniform Lateral Transverse Loadings	Trans. A. I. J.	No.62	1959. 6.
5. Plastic Analysis of Shells of Revolution under Axisymmetric Loads	University Microfilms,(Dissertation)		1962. 1
	Ingenieur-Archiv	34.Band, 4.Heft.	1965. 8.
6. Limit Analysis of Nonsymmetric Sandwich Shells	NON-CLASSICAL SHELL PROBLEMS Proc.1963 I.A.S.S.Symposium		1964.
7. Elastic-plastic Analysis of Trusses by the Gradient Projection Method	Stanford Univ.Tech. Rep. Computer Sci. Div	CS-11	1964. 7
8. Limit Analysis of Shallow Parabolic Cylindrical Shells	Trans. A. I. J.	No.106	1964.12.
9. The Minimum Weight Design of a Class of Tall Multi-story Frames Subjected to Large Lateral Forces, I, II.	Trans. A. I. J.	No.118	1965.12.
	Trans. A. I. J.	NO.119	1966. 1.
	(Proc.15th Japan Natn.Cogr.Appl.Mech)		1966.12.
10. An Approach to the Last Hinge Point Design of Tall Multi-story Frames	Proc.Symp.External Forces & Str.Design.High-rise & Long-Span Structures.		1965. 9.
11. Experimental Investigation of Stability Clamped Partial Circular Cylindrical Shells Subjected to External Pressure	RECENT RESEARCHES OF STRUCTURAL MECHANICS (Tsuboi Anniversary Vol.)		1968.
12. Numerical Analysis of Elastic-plastic Deformation of Simply Supported Rectangular Plates	Trans. A. I. J	No.152	1968.10.
13. To the Final State of Rectangular Frames	Proc.4th W.Conf. Earthq.Eng.Chile.		1969. 1
14. Overall Force-displacement Characteristics of Multi-story Frames	Proc.Symp.Ultimate Strength of Structures & Str.Elem.		1969.12
15. The Minimum Weight Design of Vierendeel Frames	Int. J. Solids & Structures	Vol.6 No.3	1970.3.
16. Load-deflection Behaviors & Plastic	Trans. A. I. J.	No.175	1970. 9
17. Fatigue of Wide-Flange Beams subjected	Trans. A. I. J	No.176	1970.10
18. to Alternating Plastic Bending,I,II,III.	Trans. A. I. J.	No.177	1970.11
19. A New Method of Experimental Buckling of Circular Cylindrical Roof Shell Models with Free Edges Subjected to External Pressure	Int. J. Nonlinear Mechanics	(To be published)	

SURVEY PAPER

1. Elastic-plastic Analysis of Framed Structures -A Survey on the Recent Progress in Japan-	Japan-U.S.Seminar on Matrix Methods of Structural Anal.Design	1969.8.

ABSTRACTS

A denotes "Annual Meeting" and K,"Kinki Branch Meeting".

TITLE	*MEETING*	*YEAR,MO.*
1. Elastic-plastic Analysis of Frames by the Gradient Projection Method of Nonlinear Programming	A	1962. 9.
2. Simplified Minimum Weight Design of Multi-story Frames Subjected to Lateral Forces	K	1963. 2
3. On the Minimum Weight Design of Tall Multi-story Frames Subjected to Lateral Forces	K	1964. 2.
4. On the Ultimate State of a Steel Frame	A	1964.10.
5. On the Solutions of the Minimum Weight Design of Tall Multi-story Frames	A 15th Congr. Appl.Mech.	1965. 9. 1965. 9.
6. Elastic-plastic Behavior of a Linear Strain-hardening Sandwich Column Subjected to Repeated Lateral Loads, I	K A	1966. 5. 1966.10.
7. A Buckling Experiment on Clamped Circular Cylindrical PVC Shell Models Subjected to External Pressure, I	A	1966.10.
8. Elastic-plastic Behavior of Linear Strain-hardening Portal Frames Subjected to Repeated Lateral Loads	K	1967. 4.
9. Elastic-plastic Behavior of Linear Strain-hardening Sandwich Column Subjected to Repeated Lateral Loads,II	K	1967. 4.
10. The Minimum Weight Design of Simply Supported Vierendeel Frames	K.	1967. 4.
11. Buckling Experiments on Clamped Circular Cylindrical PVC Shell Models Subjected to External Pressure, II	K.	1967. 4.
12. Plastic Fatigue of H Steel Members Subjected to Alternating Bending, I, II, III.	A	1967.10.
13. Alternating Plastic Bending Tests of H Steel Columns under Constant Axial Forces	K A	1968. 5. 1968.10
14. Elastic-plastic Analysis of Simply Supported Rectangular Plates	K A	1968. 5. 1968.10.
15. Plastic Fatigue of H Aluminum Members Subjected to Alternating Bending	A	1968.10.
16. A Field Experiment on a Pre-tensioned Plane Cable Frame	A	1968.10.
17. Nonlinear Analysis of a Cable Frame Consisting of a Main Hanger with Bending Stiffness and Latticed Stay Cables	A	1969. 8.
18. Tension-Compression Plastic Fatigue Tests of Wide-Flange Steel	A	1969. 8.